

Université de Montréal

**Analyse des nanoparticules de dioxyde de cérium à l'aide de
l'ICP-MS en mode particule unique**

Par

Ibrahim Jreije

Département de chimie, Faculté des arts et sciences

Thèse présentée en vue de l'obtention du grade de Philosophiae Doctor (Ph. D)

en chimie

Décembre 2021

© Ibrahim Jreije, 2021

Université de Montréal

Département de chimie, Faculté des arts et sciences

Cette thèse intitulée

**Analyse des nanoparticules de dioxyde de cérium à l'aide de
l'ICP-MS en mode particule unique**

Présenté par

Ibrahim Jreije

A été évalué(e) par un jury composé des personnes suivantes

Alexis Vallée-Bélisle
Président-rapporteur

Kevin James Wilkinson
Directeur de recherche

Patrick Hayes
Membre du jury

Diane Beauchemin
Examineur externe

Résumé

En raison de leurs propriétés uniques, les nanomatériaux manufacturés sont maintenant largement utilisés dans de nombreux produits commerciaux. Les nanoparticules (NPs) de dioxyde de cérium (CeO_2) sont parmi les NPs manufacturées les plus couramment utilisées, avec des applications dans les revêtements de surface, la catalyse, la fabrication de semi-conducteurs, la biomédecine et l'agriculture. Avec l'augmentation significative de la production et l'utilisation des NPs de CeO_2 , l'inquiétude grandit quant à leur rejet dans l'environnement et à leur devenir et toxicité subséquente. Afin d'évaluer leur risque environnemental, il est nécessaire de détecter, quantifier et caractériser les NPs dans tous les compartiments environnementaux. Malheureusement, les analyses des NPs dans les systèmes naturels sont difficiles en raison de leurs petites tailles, de leurs faibles concentrations ($\sim \text{ng L}^{-1}$) et de la complexité des matrices environnementales, qui contiennent également des colloïdes naturels.

La spectrométrie de masse à plasma à couplage inductif en mode particule unique (SP-ICP-MS) est une technique spécifique et sensible qui permet la détection de très faibles concentrations ($\sim \text{ng L}^{-1}$) de NPs en fournissant des informations sur leurs concentrations en nombre, leurs tailles et leurs distributions de taille. Cette technique est souvent limitée par des limites de détection de taille (SDL) élevées. Cependant, il est particulièrement important d'obtenir des données précises sur la taille, la concentration et le devenir des plus petites NPs, qui présentent un plus grand risque environnemental. À cette fin, l'objectif spécifique de cette thèse était de développer une méthode améliorée pour la détection, la quantification et la caractérisation des NPs de CeO_2 dans les eaux naturelles complexes à l'aide de SP-ICP-MS. Le projet a ensuite été divisé en plusieurs parties : (1) diminuer la SDL pour les NPs de CeO_2 ; (2) optimiser la méthode de préparation des échantillons d'eau naturelle; (3) appliquer les méthodes de préparation et d'analyse pour détecter, quantifier et caractériser les NPs de CeO_2 dans plusieurs échantillons d'eau naturelle et produits commerciaux, telles qu'une peinture et une teinture; (4) identifier l'origine (naturelle ou manufacturée) des NPs de CeO_2 détectées; (5) quantifier et caractériser le relargage des NPs de CeO_2 de la peinture et de la teinture sous différents scénarios météorologiques; et (6) Évaluer l'effet des différentes conditions

physicochimiques (pH, force ionique, et la présence de la matière organique naturelle) sur le devenir des NPs de CeO₂ après le relargage.

Un ICP-MS à secteur magnétique (SF-ICP-MS) à haute sensibilité avec des temps d'acquisition (i.e. 'dwell times') à l'échelle de microsecondes (50 μ s) a été utilisé pour diminuer la SDL des NPs de CeO₂ à moins de 4.0 nm. Alors que la filtration est souvent utilisée comme méthode de préparation pour le SP-ICP-MS, son effet sur les concentrations et les tailles des NPs est inconnu. Pour cela, les interactions entre six filtres avec des membranes différentes et les NPs de CeO₂ dans des échantillons aqueux ont été examinées. Les recouvrements les plus élevés ont été observés pour la membrane de polypropylène, où 60% des NPs de pré-filtration ont été trouvées dans l'eau de pluie et 75% dans les eaux de rivière. Les recouvrements pourraient être augmentés à plus de 80% en préconditionnant les membranes des filtres avec une solution multi-éléments. Des recouvrements similaires ont été obtenus lorsque les échantillons ont été centrifugés à une faible vitesse de rotation ($\leq 1000xg$). Le SF-ICP-MS a ensuite été utilisé pour détecter des NPs de CeO₂ dans une eau de pluie de Montréal, une eau du fleuve St. Laurent, une peinture et une teinture. En se basant sur le rapport de cérium/lanthane (Ce/La), les NPs de CeO₂ détectées dans la pluie sont majoritairement d'origine naturelle alors que celles dans la peinture et la teinture sont manufacturées. Une diminution significative des concentrations des NPs de CeO₂, originaires contenues dans la peinture et la teinture, a été mesurée avec le temps, sous l'effet de différentes conditions, ce qui a été attribué à l'agglomération et/ou la dissolution. Finalement, lorsque des panneaux peints et teints ont été placés à l'extérieur, le Ce relargué était principalement sous la forme dissoute, sans relargage significatif des NPs de CeO₂.

Mots-clés : Nanoparticules, ICP-MS, particule unique, oxyde de cérium, secteur magnétique, eau naturelle, revêtement de surface, relargage, méthode de préparation.

Abstract

Due to their unique properties, engineered nanomaterials are now widely used in numerous commercial products. Cerium oxide (CeO_2) nanoparticles (NPs) are among the most commonly used engineered NPs, with applications in surface coatings, catalysis, the manufacturing of semiconductors, biomedicine and agriculture. With the significant increase in the production and use of CeO_2 NPs, concern is increasing over their release into the environment and their subsequent fate and toxicity. In order to evaluate their environmental risk, it is necessary to detect, quantify and characterize the NPs in all environmental compartments. Unfortunately, analyses of NPs in natural systems are challenging due to their small sizes, their low concentrations ($\sim \text{ng L}^{-1}$) and the complexity of environmental matrices, which also contain natural colloids.

Single particle inductively coupled plasma mass spectrometry (SP-ICP-MS) is a specific and sensitive technique that enables the detection of very low concentrations ($\sim \text{ng L}^{-1}$) of NPs and it can provide information on their number concentrations, sizes, and size distributions. This technique is often limited by high size detection limits (SDL). However, it is especially important to obtain rigorous size, concentration, and fate data for the smallest NPs, since they are expected to have the greatest environmental risk. To that end, the specific objective of this thesis was to develop an improved method for the detection, quantification, and characterization of CeO_2 NPs in complex natural waters using SP-ICP-MS. The project was then divided into several objectives: (1) decrease the SDL for CeO_2 NPs; (2) optimize the preparation method for natural water samples; (3) apply the preparation and the analysis methods to detect, quantify, and characterize CeO_2 NPs in several natural water samples and commercial products, such as a paint and a stain; (4) identify the origin (natural or engineered) of the detected CeO_2 NPs; (5) quantify and characterize the release of CeO_2 NPs from paint and stain under natural weathering scenarios; and (6) evaluate the effect of different physicochemical conditions (pH, ionic strength, and NOM) on the fate of CeO_2 NPs after their release.

A high sensitivity sector field ICP-MS (SF-ICP-MS) with microsecond dwell times (50 μs) was used to lower the SDL of CeO_2 NPs to below 4.0 nm. While filtration is often used as a preparation method for SP-ICP-MS, its effect on the concentrations and sizes of NPs is unknown.

For this purpose, the interactions between six different membrane filters and CeO₂ NPs in aqueous samples were examined. The highest recoveries were observed for polypropylene membranes, where 60% of the pre-filtration NPs were found in a rainwater and 75% were found in a river water. Recoveries could be increased to over 80% by pre-conditioning the filtration membranes with a multi-element solution. Similar recoveries were obtained when samples were centrifuged at low centrifugal forces ($\leq 1000xg$). SF-ICP-MS was then used to detect CeO₂ NPs in Montreal rainwater, St. Lawrence River water, a paint, and a stain. A significant decrease in the concentrations of CeO₂ NPs, initially contained in paint and stain, was measured over time under different conditions, which was attributed to agglomeration and/or dissolution. Finally, when painted and stained panels were placed outside, the released Ce in the precipitation was mainly in the dissolved form with no significant release of CeO₂ NPs.

Keywords: Nanoparticles, ICP-MS, single particle, cerium oxide, sector field, natural water, surface coating, release, sample preparation

Table des matières

Résumé	v
Abstract	vii
Table des matières	ix
Liste des tableaux	xv
Liste des figures.....	xvii
Liste des sigles et abréviations	xxiii
Remerciements	xxix
Chapitre 1 – Introduction	1
1.1. Nanomatériaux et nanoparticules	1
1.1.1. Définition.....	1
1.1.2. Classification	1
1.1.2.1. L'origine	1
1.1.2.2. La composition chimique.....	2
1.1.3. Propriétés	3
1.1.4. Production et applications.....	4
1.1.5. Les nanoparticules dans l'environnement.....	5
1.1.5.1. Sources de relargage	5
1.1.5.2. Devenir.....	6
Transformations physiques.....	7
Transformations chimiques	9
Transformations biologiques	10
1.2. Cérium	10
1.2.1. L'élément Ce.....	10

1.2.2.	L'oxyde de cérium.....	11
1.2.3.	Les nanoparticules d'oxydes de cérium.....	12
1.2.3.1.	Propriétés.....	12
1.2.3.2.	Applications.....	13
1.2.3.3.	Voies de relargage.....	13
1.2.3.4.	Toxicité.....	14
1.3.	Analyse et caractérisation des nanoparticules.....	15
1.3.1.	Microscopie.....	15
1.3.2.	Diffusion de la lumière.....	15
1.3.3.	Techniques de séparation.....	16
1.4.	Spectrométrie de masse à plasma à couplage inductif.....	19
1.4.1.	Le système d'introduction.....	19
1.4.2.	Le système d'ionisation.....	20
1.4.3.	L'interface.....	21
1.4.4.	Le filtre de masse.....	21
1.4.4.1.	Quadripôle.....	21
1.4.4.2.	Secteur magnétique.....	21
1.4.4.3.	Temps-de-vol.....	22
1.4.5.	Le détecteur.....	22
1.5.	Spectrométrie de masse à plasma à couplage inductif en mode particule unique	23
1.5.1.	Principes.....	23
1.5.2.	Acquisition et traitement des données.....	24
1.5.3.	Bruit de fond et stratégies de résolution.....	27
1.5.3.1.	Analyte dissous.....	27
1.5.3.2.	Interférences.....	28

1.6. Objectifs de la thèse.....	31
1.7. Contribution des auteurs.....	33
Chapitre 2 – Measurement of CeO ₂ nanoparticles in natural waters using high sensitivity, single particle ICP-MS	35
2.1. Abstract	35
2.2. Introduction	35
2.3. Results and Discussion.....	37
2.3.1. Optimization of SP-ICP-MS for CeO ₂ NPs.....	37
2.3.2. Ce-Containing NPs in Natural Waters: Rainwater.....	42
2.3.3. Ce-Containing NPs in Natural Waters: Riverwater.....	44
2.3.4. Effect of Sample Filtration	45
2.3.5. Ce-containing NPs in natural waters: temporal variations.....	46
2.3.6. Engineered or Natural CeO ₂ NPs?	47
2.4. Materials and Methods	50
2.4.1. Engineered NPs	50
2.4.2. Sampling and Sample preparation.....	51
2.4.3. Instrumentation.....	52
2.4.4. SP-ICP-MS data acquisition.....	52
2.4.5. SP-ICP-MS data processing	53
2.5. Conclusions	54
2.6. Supplementary Information.....	55
Chapitre 3 – Sample preparation for the analysis of nanoparticles in natural waters by single particle ICP-MS	65
3.1. Abstract	65
3.2. Introduction	65
3.3. Materials and methods.....	67

3.3.1. Nanoparticles, chemicals reagents, and filters	67
3.3.2. Sampling and sample preparation	67
3.3.3. ICP-MS (single particle and quantitative determinations)	69
3.3.4. SP-ICP-MS data processing	69
3.4. Results and discussion	70
3.5. Conclusions	82
3.6. Supporting Information	83
Chapitre 4 –Stability of CeO ₂ nanoparticles derived from nano-enabled surface coatings: insights under controlled and environmental scenarios	97
4.1. Abstract	97
4.2. Introduction	97
4.3. Materials and Methods	99
4.3.1. Nanoparticles, chemical reagents, and surface coatings	99
4.3.2. Coating procedure and experimental design	100
4.3.3. Sampling and sample preparation for SP-ICP-MS.....	100
4.3.4. ICP-MS analyses	101
4.3.5. SP-ICP-MS data processing	101
4.4. Results and Discussion.....	102
4.4.1. Ce containing NP in the precipitation, paint and stain	102
4.4.2. Fate of Ce NP contained in the surface coatings.....	105
4.4.2.1. Effect of ionic strength	105
4.4.2.2. Effect of natural organic matter.....	108
4.4.2.3. Effect of pH	111
4.4.2.4. Stability in precipitation	113
4.4.3. Release of CeO ₂ NP from the painted and stained surfaces.....	114

4.5. Conclusions	116
4.6. Supporting Information	117
4.6.1 Effect of sample filtration.....	117
Chapitre 5 – Conclusions et recommandations	133
5.1. Recommandations	135
Références bibliographiques	137

Liste des tableaux

Tableau 1-1 Résumé des informations fournies au sujet des différentes techniques d'analyse des NPs. N.A. signifie «non applicable». (Les données et les informations ont été collectées de Modena <i>et al.</i> ⁸⁸ et Laborda <i>et al.</i> ⁸⁹)	18
Table 2-1 Sensitivity for Ag, Au and Ce and corresponding size detection limits for Ag, Au and CeO ₂ NPs in Milli-Q water obtained using a quadrupole (Q-) or sector field (SF-) ICP-MS running with (dry) or without a desolvator (wet). A 50 µs dwell time was used. Means and standard deviations are obtained from analysis on three different dates.....	39
Table 2-2 Average particle sizes, number concentrations and SDL in 10 ng L ⁻¹ suspensions of Ag, Au and CeO ₂ NPs. Means and standard deviations are obtained from the analysis of triplicate samples.....	42
Table 2-3 Concentration of dissolved Ce, number and mass concentrations of CeO ₂ NPs and SDL in the rainwater and in the St. Lawrence River. Means and standard deviations are obtained from the analysis of triplicate samples.	45
Table 2-4 Ratios of Ce to La determined in the Montreal rainwater, obtained using the SF-ICP-MS run in single particle mode with a dwell time of 50 µs. Means and standard deviations were obtained from triplicate samples.	49
Table 2-S1 Mean particle sizes, NPs number concentrations, mass concentration of dissolved Ce and SDL for Ce containing NPs in St. Lawrence River water, with or without filtration. Measurements were obtained using the wet-SF-ICP-MS with a 50 µs dwell time. Means and standard deviations are obtained from triplicate samples.	60
Table 2-S2 Mean particle sizes, NPs number concentrations and mass concentration of dissolved and nanoparticulate Ce and La in Montreal rainwater. Measurements were obtained using the wet-SF-ICP-MS with a 50 µs dwell time. Means and standard deviations are obtained from triplicate samples.	63
Table 3-1 Average particle sizes, concentrations of NPs and dissolved metal and SDL determined by SP-ICP-MS (Magnetic sector ICP-MS) in addition to total digested metal and DL determined by quadrupole ICP-MS. Means and standard deviations are obtained from the analysis of triplicate samples of rain or river water samples.	75

Table 3-S1 Concentrations of the multi-element solution (QC-21) used to precondition the membranes.....	84
Table 3-S2 pH and concentrations of major elements, including total organic carbon (TOC), in an unfiltered rainwater and river water.	88
Table 3-S3 Recoveries of Ag and Ce, corresponding to the fraction of total (mass) concentration of the metal determined by SP-ICP-MS with respect to concentrations determined by quantitative ICP-MS (digested samples). Means and standard deviations are obtained from the analysis of triplicate samples. ND: not determined.....	94
Table 4-1 Mean and mode particle sizes, polydispersity indices, concentrations of nanoparticulate and dissolved Ce determined by SP-ICP-MS in addition to total digested metal determined by quadrupole ICP-MS. Note that errors correspond to standard deviations obtained from the analysis of triplicate samples and which were systematically smaller than the polydispersities obtained from the PSD.	103
Table 4-S1 Ratios of Ce to La in precipitation, paint, and stain, determined with SP-ICP-MS with a dwell time of 50 μ s. Paint and stain were diluted 2500x. Means and standard deviations were obtained from triplicate samples.	120
Table 4-S2 pH and concentrations of major elements, including total organic carbon (TOC), in an unfiltered rainwater.....	129

Liste des figures

Figure 1-1 Estimation globale (en Tg an ⁻¹) des NPs naturelles (nombres en noir), accidentelles (nombres en bleu) et manufacturées (nombres en violet) dans l'environnement. Tiré de Hochella <i>et al.</i> ⁶).....	2
Figure 1-2 Pourcentage d'atomes en surface des NPs de gallium arsenic (GaAs) avec différentes tailles (nm). (Reproduit à partir des données de Ju-Nam <i>et al.</i> ¹³).....	3
Figure 1-3 L'effet de la taille allant de l'échelle atomique à l'échelle macroscopique sur le changement de réactivité. (Tiré de Wigginton <i>et al.</i> ¹⁵).	4
Figure 1-4 Les processus régissant la formation, la transformation, la distribution et le devenir des NPs dans les différents compartiments environnementaux. (Tiré de Lespes <i>et al.</i> ⁷)....	6
Figure 1-5 Diagramme représentant les sources du relargage et les transformations des NPMs dans l'environnement. Les NPMs peuvent subir des transformations physiques, chimiques ou biologiques. (Tiré de Abbas <i>et al.</i> ³⁵).	7
Figure 1-6 Structure de dioxyde de cérium (CeO ₂). (Modifié de Perullini <i>et al.</i> ⁵⁶).....	11
Figure 1-7 Les différentes applications et sources de rejet des NPs de CeO ₂ dans l'environnement. (Tiré de Dahle <i>et al.</i> ⁵²).	12
Figure 1-8 Schéma des composants principaux de l'ICP-MS : système d'introduction, système d'ionisation, interface, filtre de masse et détecteur. (Modifié de Telgmann <i>et al.</i> ⁹⁶).....	19
Figure 1-9 Les étapes de traitement des données pour la détermination de la taille et de concentration en nombre des NPs en utilisant l'ICP-MS en mode particule unique. (Modifié de Pace <i>et al.</i> ¹²⁷).....	24
Figure 2-1 Signal/noise (blue) and size detection limits (red) as a function of dwell time for: (A) a 10 ng L ⁻¹ suspension of CeO ₂ NPs (1–10 nm) in Milli-Q water; (B) a 10 ng L ⁻¹ suspension of CeO ₂ NPs (1–10 nm) in a Milli-Q water containing 10 ng L ⁻¹ of ionic Ce.	38
Figure 2-2 Particle size distributions as measured by wet-SF-ICP-MS (blue) and dry-SF-ICP-MS (red) for 3 suspensions of a small NP: (A) Ag; (B) Au; (C) CeO ₂	41
Figure 2-3 Particle size distribution of a suspension of CeO ₂ NPs with a nominal size of 1–10 nm. NP were spiked into (A) Milli-Q water or (B) rainwater. (C) Particle size distribution for Ce-containing NPs in rainwater.....	43

Figure 2-4 Particle size distributions of Ce containing NPs in a sample taken from the St. Lawrence River.....	45
Figure 2-5 (A) Number concentrations and (B) mean particle sizes for CeO ₂ NPs measured on different dates in rainwater (blue) and St. Lawrence River water (green).....	47
Figure 2-6 Particle size distributions of Ce- (blue) and La- (red) containing NPs found in a Montreal rainwater.	49
Figure 2-7 Detected proportion of Ce in Ce-containing particles measured in a Montreal rainwater. A Ce fraction of 1 indicates a pure Ce NP, while a fraction < 1 indicates the presence of other elements in the particles.....	50
Figure 2-S1 Time resolved signal of ¹⁴⁰ Ce in a suspension of 10 ng L ⁻¹ CeO ₂ NPs spiked with 10 ng L ⁻¹ of ionic Ce measured at different dwell times.	55
Figure 2-S2 Particle size distributions of a 10 ng L ⁻¹ suspension of CeO ₂ NPs with a nominal size range 1-10 nm spiked with ionic Ce at a mass concentration of (A) 10 ng L ⁻¹ ; (B) 50 ng L ⁻¹ as measured by Wet-SF-ICPMS (blue) and Dry-SF-ICPMS (red).	56
Figure 2-S3 Time-resolved signal for ¹⁴⁰ Ce in a 10 ng L ⁻¹ suspension of CeO ₂ NPs with a nominal size range 1-10 nm spiked with ionic Ce at a mass concentration of (A) 10 ng L ⁻¹ ; (B) 50 ng L ⁻¹ as measured by Wet-SF-ICPMS (blue) and Dry-SF-ICPMS (red).	57
Figure 2-S4 Size detection limit as a function of mass concentration of dissolved Ce as measured by wet-SF-ICP-MS (blue) and dry-SF-ICP-MS (red).	58
Figure 2-S5 Time-resolved signal for ¹⁴⁰ Ce in (A) unfiltered rainwater and (B) unfiltered St. Lawrence River water. For better readability, only 5 s of data collection were shown, the total acquisition time was 50 s.	59
Figure 2-S6 Particle size distributions of Ce containing NPs in St. Lawrence River water with (blue) or without (red) filtration. Samples were filtered using syringe filters with a PVDF membrane with a 0.45 μm pore size.	60
Figure 2-S7 Sampling locations on the St. Lawrence River.	61
Figure 2-S8 Time-resolved signal for (A) ¹⁴⁰ Ce and (B) ¹³⁹ La in Montreal rainwater...62	62
Figure 2-S9 Time-resolved signal for ¹³⁹ La (red) and ¹⁴⁰ Ce (blue) in Montreal rainwater analyzed by TOF-SP-ICPMS showing (A) a pure Ce NP and (B) a NP that contains Ce and La.64	64
Figure 3-1 Recoveries of (a) ionic metals and (b) NPs in a solution/suspension of 50 ng L ⁻¹ of Ag (grey) or Ce (green) in ultrapure water.	71

Figure 3-2 (a) Ag and (b) CeO ₂ NPs recoveries based on their number concentrations, in a rainwater (purple) and in a river water (orange).	73
Figure 3-3 Recoveries of total Ce in rainwater (purple) and river water (orange).	75
Figure 3-4 Recoveries of (a) Ag and (b) CeO ₂ NPs, based on the NP number concentrations, for successive fractions of rainwater (purple) and river water (orange) filtered through PP filters with a pore size of 0.45 μm.	77
Figure 3-5 Recoveries of (a) Ag and (b) CeO ₂ NPs, based on NP number concentrations, in rainwater (purple) and river water (orange), when filtered through polypropylene filters with a pore size of 0.45 μm, preconditioned with different solutions.	78
Figure 3-6 Recoveries of (a) Ag and (b) CeO ₂ NPs, based on NP number concentrations, in rain and river waters when filtered over polypropylene filters with a pore size of 0.22 (brown) or 0.45 (yellow) μm.	79
Figure 3-7 Recoveries of (a) Ag and (b) CeO ₂ NPs, based on NP number concentrations, in rainwater (purple) and river water (orange) when centrifuged at different rotation speeds.	81
Figure 3-S1 Schematic diagram of the (a) filtration protocol and (b) filtration protocols for membrane conditioning. Total metal represents the sum of particulate and dissolved metal. .	83
Figure 3-S2 Particle size distributions of (a) Ag and (b) CeO ₂ NPs in a 50 ng L ⁻¹ suspension in ultrapure water.	84
Figure 3-S3 Recoveries of total Ag (grey) or Ce (green) in a 50 ng L ⁻¹ (a) solution of dissolved metal and (b) suspensions of the NP in ultrapure water.	85
Figure 3-S4 Recoveries of (a) Ag and (b) CeO ₂ NPs, based on the NP mass concentrations, in a rainwater (purple) and a river water (orange).	86
Figure 3-S5 Particle size distributions of (a) Ag and (b) CeO ₂ NPs in an unfiltered rainwater (purple) and river water (orange).	87
Figure 3-S6 Particle size distributions in an unfiltered (a) rainwater and (b) river water. Measurements were determined using Dynamic Light Scattering (DLS) (Möbiuζ, Wyatt Instruments, 532 laser).	89
Figure 3-S7 Particle size distributions of Ag NPs in rainwater.	90
Figure 3-S8 Particle size distributions of Ag NPs in river water.	91
Figure 3-S9 Particle size distributions of CeO ₂ NPs in rainwater.	92

Figure 3-S10	Particle size distributions of CeO ₂ NPs in river water.....	93
Figure 3-S11	Retention of Ce from rainwater (purple) and river water (orange).	94
Figure 3-S12	Recoveries of Ag (grey) and CeO ₂ (green) NPs, based on NP number concentrations, from a suspension of 50 ng L ⁻¹ of the NP in ultrapure water, when centrifuged at different centrifugal forces.	95
Figure 3-S13	Particle size distributions of CeO ₂ NPs in (a) rainwater and (b) river water. Samples were filtered through polypropylene filters that were preconditioned with a multi-element solution (QC-21), centrifuged at 70 x g, or unfiltered/uncentrifuged.	96
Figure 4-1	Mass distributions of Ce NPs in (a) precipitation, (b) diluted (2500 x) paint and (c) diluted (2500 x) stain.	104
Figure 4-2	Mass concentration of the Ce-containing NPs in solutions containing: (a) engineered CeO ₂ NPs in Milli-Q water; (b) Ce NPs in diluted (2500 x) paint and (c) Ce NPs in diluted (2500 x) stain with three different ionic strengths as a function of time.	107
Figure 4-3	Mass concentration of the Ce containing NP as a function of time for: (a) engineered CeO ₂ NPs; (b) paint and (c) stain spiked into Milli-Q water with three different contents of natural organic matter. The paint and stain were diluted 2500x.	109
Figure 4-4	Mass concentrations of dissolved Ce as a function of time for: (a) an engineered CeO ₂ NPs, (b) paint and (c) stain spiked into Milli-Q water with three different concentrations of natural organic matter (0, 2 and 10 mg L ⁻¹).	110
Figure 4-5	Mass concentration of Ce containing NP as a function of time in (a) a suspension of engineered CeO ₂ NPs; (b) a paint and (c) a stain. In order to reduce variability of the pH, NP concentrates were spiked into acetate buffer at pH = 4.0 and bicarbonate buffer at pH = 7.0.....	112
Figure 4-6	Mass concentration of (a) Ce-containing NPs and (b) dissolved Ce as a function of time in: (i) a suspension of CeO ₂ NPs; (ii) a paint and (iii) a stain spiked into a rainwater.....	114
Figure 4-7	Cumulative concentrations of Ce determined by ICP-MS (total concentration), dissolved and Ce-containing NPs as determined by SP-ICP-MS. Measurements were made on precipitation that came into contact with (a) painted and (b) stained surfaces during fall 2018 and winter 2019.....	116

Figure 4-S1 Mass distributions of Ce NPs in a precipitation sample with or without filtration on a 0.45 μm PVDF membrane.....117

Figure 4-S2 Time resolved signal (raw data) for ^{140}Ce in (a) Milli-Q water; (b) precipitation, (c) paint and (d) stain.118

Figure 4-S3 Calculated particle size distributions of Ce NPs in (a) precipitation, (b) paint and (c) stain. Paint and stain were diluted 2500x.....119

Figure 4-S4 Calibration curves performed using Ce standards with three different concentrations of NaNO_3120

Figure 4-S5 Particle size distribution of CeO_2 NPs in a suspension of engineered CeO_2 NPs spiked into Milli-Q water with three different ionic strengths.121

Figure 4-S6 Mass concentration of (a) dissolved and (b) total Ce in a suspension of engineered CeO_2 NPs, spiked into Milli-Q water with three different ionic strength, as a function of time.122

Figure 4-S7 Average CeO_2 NPs sizes in (a) engineered CeO_2 NPs, (b) paint and (c) stain spiked into Milli-Q water with three different ionic strength, as a function of time.123

Figure 4-S8 Particle size distributions of CeO_2 NPs in a suspension of engineered CeO_2 NPs spiked into Milli-Q water with 100 mM of NaNO_3124

Figure 4-S9 (a) Concentration of dissolved Ce measured in a solution of almost 60 ng L^{-1} ionic Ce prepared in Milli-Q water without acidification. Adsorptive losses to the ICP-MS and sample tube were evaluated by measuring Ce in: (i) a Milli-Q water rinse; (ii) Successive (triplicate) rinses in 2% HNO_3 (Figure S9b) (iii) Milli-Q water rinse of the sample tube; (iv) 2% HNO_3 rinse of the sample tube.....125

Figure 4-S10 Average CeO_2 NP sizes in (a) engineered CeO_2 NPs, (b) paint and (c) stain spiked into Milli-Q water with three different contents of natural organic matter, as a function of time.....126

Figure 4-S11 Mass concentration of dissolved Ce in (a) engineered CeO_2 NPs, (b) paint and (c) stain spiked into acetate buffer with $\text{pH} = 4.0$ or bicarbonate buffer with $\text{pH} = 7.0$, as a function of time.127

Figure 4-S12 Time resolved signal for ^{140}Ce in the precipitation (a) unspiked; or spiked with (b) engineered CeO_2 NPs, (c) paint and (d) stain.128

Figure 4-S13 Concentration of dissolved Ce measured in a successive (triplicate) rinses in 2% HNO₃ following the analysis of an unfiltered precipitation sample.129

Figure 4-S14 (A) Daily temperatures (maxima, minima and meant), (B) total precipitation (total liquid equivalent of rain and snow), (C) rain precipitation and (D) snow on ground data for the fall of 2018 and winter of 2019. (Adapted from Azimzada *et al.*¹⁹⁰)130

Figure 4-S15 Time resolved signal for ¹⁴⁰Ce in a filtered precipitation (a) without, or with contact with a (b) painted panel, and (c) stained panel.131

Liste des sigles et abréviations

Dans le cas où l'abréviation provienne du nom en anglais, celui-ci sera donnée entre parenthèses.

AFM : la microscopie à force atomique (Atomic force microscopy)

CA : Acétate de cellulose (Cellulose acetate)

C_{diss} : Concentration massique de la forme dissoute de l'élément en suspension

C_m : Concentration massique des nanoparticules

C_{NP} : Concentration en nombre des nanoparticules

Cps : Comptes par secondes

D : Débit

DL : Limite de détection (Detection limit)

DLS : Diffusion dynamique de la lumière (Dynamic light scattering)

EC : Commission européenne (European Commission)

EDS : Spectroscopie à dispersion d'énergie (Energy-dispersive spectroscopy)

ERO : Espèces réactives d'oxygène

FFF : Fractionnement par couplage flux-force (Field flow fractionation)

GFAAS : Spectroscopie d'absorption atomique par four de graphite (Graphite furnace atomic absorption spectroscopy)

HDC : Chromatographie hydrodynamique (Hydrodynamic chromatography)

ICP-MS : Spectrométrie (ou spectromètre) de masse à plasma à couplage inductif (Inductively coupled plasma mass spectrometry)

ICP-OES : Spectrométrie (ou spectromètre) d'émission optique à plasma à couplage inductif (Inductively

coupled plasma optical emission spectrometry)

I_{NP} : Intensité du signal correspondant à une nanoparticule

I_s : Intensité du seuil

IS : Force ionique (Ionic strength)

ISO : Organisation internationale de normalisation (International organization for standardization)

m/z : Masse sur charge

m_{NP} : Masse d'une nanoparticule

N_a : Nombre aspiré de particules

N_d : Nombre détecté de particules

NM : Nanomatériau

NOM : Matière organique dissoute (Natural organic matter)

NP : Nanoparticule

NPA : Nanoparticule accidentelle

NPM : Nanoparticule manufacturée

NPN : Nanoparticule naturelle

NTA : Analyse du suivi de nanoparticule (Nanoparticle tracking analysis)

PES : Polyethersulfone

PP : Polypropylène

PTFE : Polytétrafluoroéthylène

PVC : Polychlorure de vinyle

PVDF : Polyfluorure de vinylidène (Polyvinylidene fluoride)

PVP : Polyvinylpyrrolidone

PZC : Point de charge zéro (Point of zero charge)

S : Sensibilité

SDL : Limite de détection de taille (Size detection limit)

SEM : Microscopie électronique à balayage (Scanning electron microscopy)

SF : Secteur magnétique (Sector field)

S_m : Sensibilité massique

SP-ICP-MS : Spectrométrie (ou spectromètre) de masse à plasma à couplage inductif en mode particule unique (Single particle Inductively coupled plasma mass spectrometry)

t : Temps d'analyse

TE : Efficacité de transport (Transport efficiency)

TEM : Microscopie électronique à transmission (Transmission electron microscopy)

TOF : Temps-de-vol (Time of flight)

Q : Quadripôle

QD : Points quantiques (Quantum dots)

V_{NP} : Volume d'une nanoparticule

ρ_{NP} : Densité d'une nanoparticule

χ_m : Fraction de masse molaire élément/nanoparticule

"J'ai combattu le bon combat, j'ai achevé la course, j'ai gardé la foi" (2 Timothée 4:7)

À mes parents, mes frères, ma femme et mes enfants.

Remerciements

Pr. Kevin J. Wilkinson, je tiens à vous adresser mes sincères remerciements pour la chance que vous m'avez offerte de pouvoir faire un doctorat dans votre laboratoire. Je vous suis très reconnaissant pour tous les conseils et les commentaires constructifs, tout le soutien et tout le temps que vous m'avez accordé lors de ma thèse. Je vous remercie aussi pour votre patience et votre compréhension durant les moments très difficiles que j'ai vécus.

Je remercie également les membres de mon comité de thèse : Pr. Patrick Hayes et Pr. Alexis Vallée-Bélisle et Pr. Diane Beauchemin. Vos commentaires lors de mon examen de doctorat, du séminaire et des réunions m'ont été très utiles.

Madjid Hadioui, je te remercie de tout cœur pour l'aide précieuse que tu m'as apportée tout le long de mes études supérieures. Merci pour ta patience, ta gentillesse et tes conseils académiques et sur la vie en général. J'ai beaucoup appris de toi, et je ne manquerai pas de passer te voir à l'occasion. Un grand merci à Élise Morel et Agil Azimzada pour tous les conseils, les moments de rire et les discussions lors des journées de travail (lorsqu'on faisait semblant de travailler). Merci également à tous les collègues de labo : Laurie, Juliana, Faraz, ZhiZhong, Nesrine et Lei, pour toutes les discussions toujours intéressantes. Merci aussi à mon cousin Hamid pour toutes les belles soirées qui m'ont aidées à oublier le stress.

Je remercie aussi de tout cœur mes parents et mes frères pour tout le soutien moral. Je vous dois beaucoup, et je ne sais pas comment vous rendre la pareille. Je suis aussi extrêmement reconnaissant à ma belle-famille pour tout le soutien et l'aide. Sara, je te remercie du fond du cœur pour ta présence dans ma vie, ton soutien, ton amour, tes petites attentions, et le fait que tu as supporté mes sautes d'humeur durant le doctorat. À mes deux petits monstres, vous êtes la source de mon bonheur, la cause de ma persévérance et la raison principale pourquoi cette thèse a duré six ans.

Je termine par remercier le Seigneur, merci pour toutes tes bénédictions envers ma famille et envers moi. Sans toi, tout ceci n'aurait pas été possible!

Chapitre 1 – Introduction

1.1. Nanomatériaux et nanoparticules

1.1.1. Définition

L'organisation internationale de normalisation (ISO) a défini un nanomatériau (NM) comme un matériau avec une dimension externe, une structure interne ou une structure de surface à l'échelle nanométrique, et une nanoparticule comme un nano-objet avec les trois dimensions entre 1 et 100 nm.¹ Toutefois, ces définitions, basées uniquement sur la taille, peuvent être insuffisantes de point de vue réglementation et évaluation de risques. Par conséquent, de nombreuses définitions de NM ont été proposées par des gouvernements, des industries et des organismes de normalisation, incluant d'autres éléments tels que les agrégats et les agglomérats, le seuil des distributions (de taille ou de masse) et la solubilité.² Par exemple, la commission européenne (EC) a défini un NM comme : « un matériau naturel, accidentel ou manufacturé contenant des particules à l'état liées ou sous forme d'agrégat ou d'agglomérat, et dont, pour 50% ou plus des particules dans la distribution de taille, une ou plusieurs dimensions externes se situent entre 1 – 100 nm ».³

1.1.2. Classification

Les NPs peuvent être classées selon l'origine ou la composition chimique.^{4, 5}

1.1.2.1. L'origine

Basées sur leur origine, les NPs peuvent d'abord être divisées en deux catégories : Les NPs naturelles (NPNs) et les NPs anthropiques.^{6, 7} Par la suite, les NPs anthropiques peuvent aussi être divisées en deux sous-groupes : les NPs accidentelles (NPAs) et les NPs manufacturées (NPMs).^{6, 7} Les NPNs sont produites par les activités volcaniques, les feux de forêts, ou par érosion.⁸ Les NPAs sont des NPs produites par l'Homme de façon non intentionnelle. Ces NPs sont émises principalement par la combustion des carburants fossiles⁹ et les différents procédés de soudage.¹⁰ En raison de leurs propriétés intéressantes, les NPMs sont conçues et produites par l'Homme de façon intentionnelle. Depuis le discours du physicien et lauréat du prix Nobel Richard P. Feynman en 1959 : « *There's plenty of room at the bottom* »¹¹, les nanotechnologies

connaissent un essor important à l'échelle internationale, et les NPMs sont utilisées dans différents domaines incluant l'agriculture, la chimie, l'électronique, les cosmétiques et la biomédecine. Il est estimé que > 1000 Tg de NPNs et 1 – 10 Tg de NPAs sont produits annuellement (Figure 1-1).⁶ En revanche, 0.3 Tg de NPMs sont estimés de pénétrer chaque année dans les différents compartiments environnementaux.^{6, 12}

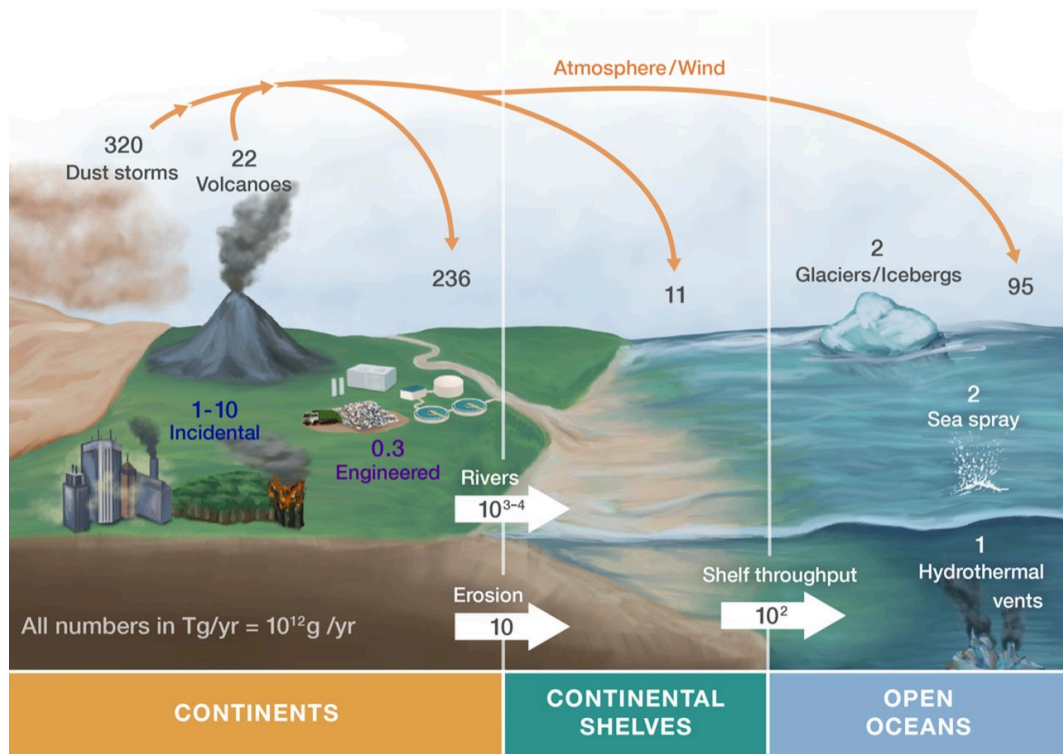


Figure 1-1 Estimation globale (en Tg an⁻¹) des NPs naturelles (nombres en noir), accidentelles (nombres en bleu) et manufacturées (nombres en violet) dans l'environnement. Tiré de Hochella *et al.*⁶)

1.1.2.2. La composition chimique

Basées sur leur composition chimique, les NPs peuvent être divisées en cinq catégories⁴ :

- 1) Les nanostructures à base de carbone : constituées de carbone pur, les nanostructures à base de carbone sont divisées en deux groupes principaux : les fullerènes et les nanotubes de carbone.
- 2) Les NPs inorganiques métalliques : constituées majoritairement d'éléments nobles (e.g. Au, Ag) mais aussi des éléments de transition (Fe, Zn).

- 3) Les NPs d'oxydes de métaux : incluant une variété d'oxydes de métaux de transition (TiO_2 , ZnO , CuO , Fe_2O_3 , et CeO_2) ainsi que d'autres oxydes (SiO_2 , Al_2O_3).
- 4) Les NPs organiques : constituées de nanolipides et d'autres polymères organiques.
- 5) Les points quantiques (QD) : sont des nanocristaux semi-conducteurs auto-fluorescents. Les QD sont constitués de complexes métalliques binaires (CdSe , CdS , CdZn).

1.1.3. Propriétés

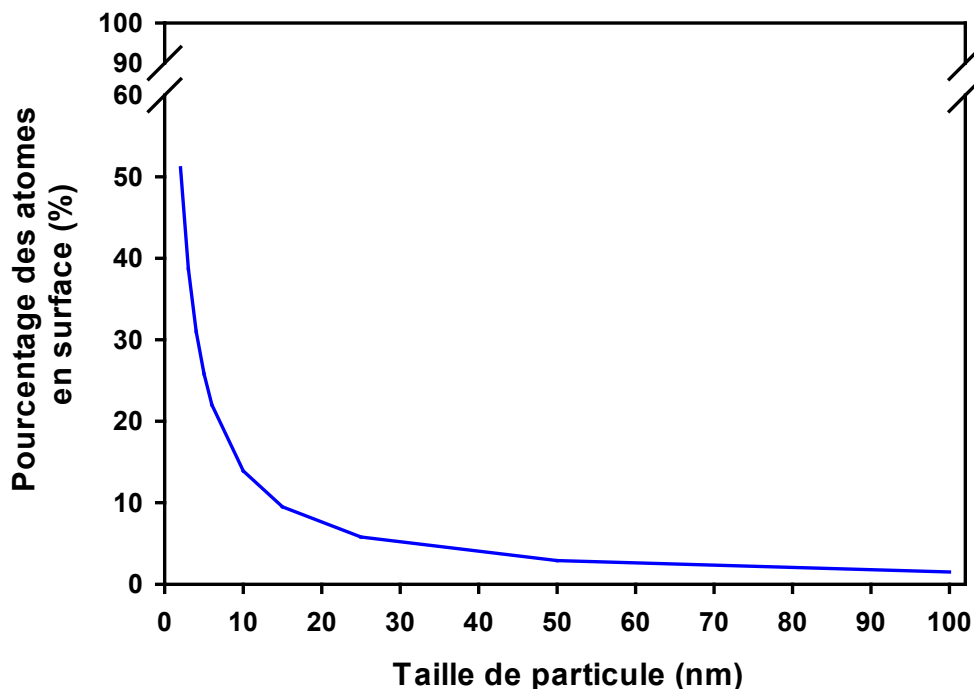


Figure 1-2 Pourcentage d'atomes en surface des NPs de gallium arsenic (GaAs) avec différentes tailles (nm). (Reproduit à partir des données de Ju-Nam *et al.*¹³)

En raison de leur petite taille, les NPs possèdent des propriétés physico-chimiques uniques qui diffèrent du même matériau à l'échelle micro- ou macroscopique. Le changement des propriétés découle de deux effets principaux : l'effet surface et l'effet du confinement quantique. Le rapport surface/volume des atomes d'un matériau est beaucoup plus grand à l'échelle nanométrique. De plus, le pourcentage des atomes en surface augmente exponentiellement en

diminuant la taille des particules en deçà de 10 nm (Figure 1-2).¹³ Cette augmentation de rapport surface/volume est connue sous le nom d'effet surface, et cause une amélioration de la réactivité d'une molécule (Figure 1-3).^{4, 15} De même, en diminuant la taille d'une particule, l'énergie nécessaire pour déplacer un électron entre la bande de valence et la bande de conduction augmente.¹⁶ Cet effet constitue l'effet de confinement quantique qui devient plus important pour des tailles <10 nm. Par conséquent et à cause des effets surface et confinement quantique, les NPs présentent des propriétés électroniques, optiques, catalytiques, magnétiques, mécaniques et thermiques qui peuvent différer grandement des atomes et du matériau en vrac.^{4, 14, 16}

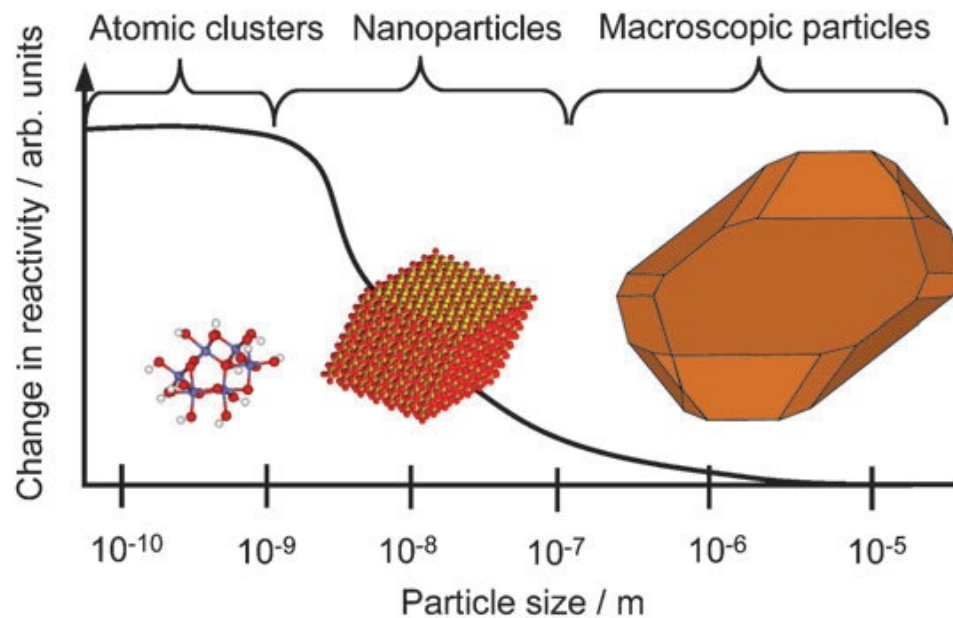


Figure 1-3 L'effet de la taille allant de l'échelle atomique à l'échelle macroscopique sur le changement de réactivité. (Tiré de Wigginton *et al.*¹⁵).

1.1.4. Production et applications

Les données précises des volumes de production des NPs à l'échelle mondiale ne sont pas encore disponibles. Toutefois, une étude¹⁷, effectuée en 2011, a démontré que les NPs de TiO₂ et de SiO₂ sont les NPs les plus produites, avec une production annuelle de >10000 tonnes, suivies par les NPs de CeO₂, FeO_x, Al₂O₃ et ZnO avec une production annuelle de 100 – 1000 tonnes. En 2015, 175 entreprises, qui produisent ou utilisent des NPs, ont été repérées à Québec.¹⁸

Grâce à leurs propriétés mécaniques, les NPs sont utilisées dans de nombreuses applications dans les industries mécaniques, en particulier dans les applications de revêtement, d'adhésif et de lubrifiants.⁵ Les propriétés optiques et électriques des NPs ont conduit à l'utilisation de ces dernières dans les capteurs chimiques et les biocapteurs, ainsi que dans les industries cosmétiques, pharmaceutiques, microélectroniques et aérospatiales.¹⁹ Les NPs sont également utilisées dans le domaine médical, principalement dans l'imagerie cellulaire²⁰ et l'administration des médicaments²¹. À cause de leur grand rapport surface/volume, les NPs sont utilisées en catalyse²² et en environnement dans des processus de purification, aussi connu sous le nom de nano-remédiation²³.

1.1.5. Les nanoparticules dans l'environnement

1.1.5.1. Sources de relargage

Les NPNs et les NPAs sont générées dans les différents compartiments environnementaux par des processus biologiques, physiques ou chimiques, tel qu'illustré par la figure 1-4.^{4, 7} Cependant, l'augmentation exponentielle de la production des NPMs et leur utilisation dans différents domaines, a conduit à la création de différentes sources d'émission potentielle de ces NPs dans l'environnement. Les NPMs peuvent être relarguées dans l'environnement tout au long de leur cycle de vie, i.e. pendant leur production; pendant leur utilisation; et durant la destruction des produits renforcés par des NPMs (gestion des déchets).²⁴⁻²⁶ Les NPs peuvent pénétrer directement dans l'environnement ou indirectement via les stations de traitement des eaux usées ou les décharges.²⁴

Jusqu'à présent, les niveaux d'émission des NPMs dans l'environnement ont été estimés en utilisant des modèles qui se basent sur leur cycle de vie.^{6, 12, 27-30} Toutefois, les niveaux d'émission dépendent du type de la NP, ses propriétés intrinsèques, et son application. Une estimation mondiale des émissions indique que la grande majorité des NPMs finissent dans les décharges (63 – 91%), suivi des sols (8 – 28%), des eaux (7%) et finalement de l'atmosphère (1.5%).³¹ De plus, les revêtements, les peintures, les additifs catalytiques et les cosmétiques sont estimés d'être les sources principales de l'émission des NPMs dans l'environnement.³²

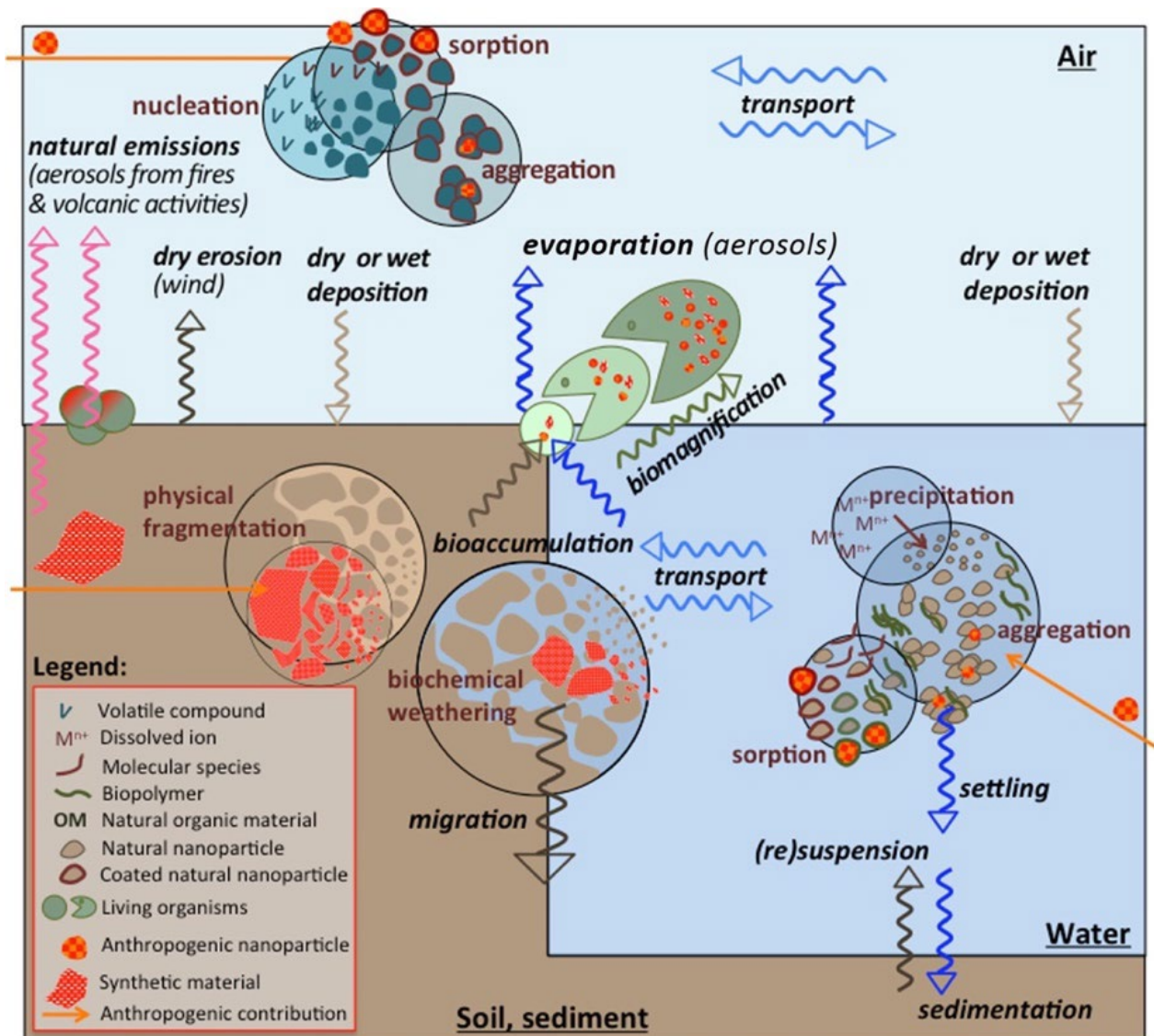


Figure 1-4 Les processus régissant la formation, la transformation, la distribution et le devenir des NPs dans les différents compartiments environnementaux. (Tiré de Lespes *et al.*⁷).

1.1.5.2. Devenir des NPs dans l'environnement

Indépendamment de leur origine, les NPs dans l'environnement peuvent subir des transformations via des processus biologiques, chimiques ou physiques qui affecteront leur comportement, leur devenir, leur mobilité, et leur biodisponibilité.³³ Des processus tels que la dissolution, l'homo- ou l'hétéro-agglomération, la sédimentation, l'adsorption, l'oxydation, la réduction, et la sulfuration sont courantes pour les NPs naturelles et anthropiques dans

l'environnement.^{34, 35} Ces processus sont gouvernés par les propriétés intrinsèques des NPs, tels que leur taille, leur composition, leur forme, leur enrobage et leur charge de surface, ainsi que les conditions environnementales tels que le pH, la force ionique, la température, les conditions rédox et la présence des colloïdes organiques ou inorganiques.^{33, 35} Les processus de transformation des NPMs dans l'environnement, illustrés dans la figure 1-5, peuvent être classés en trois principales catégories : physique, chimique, et biologique.

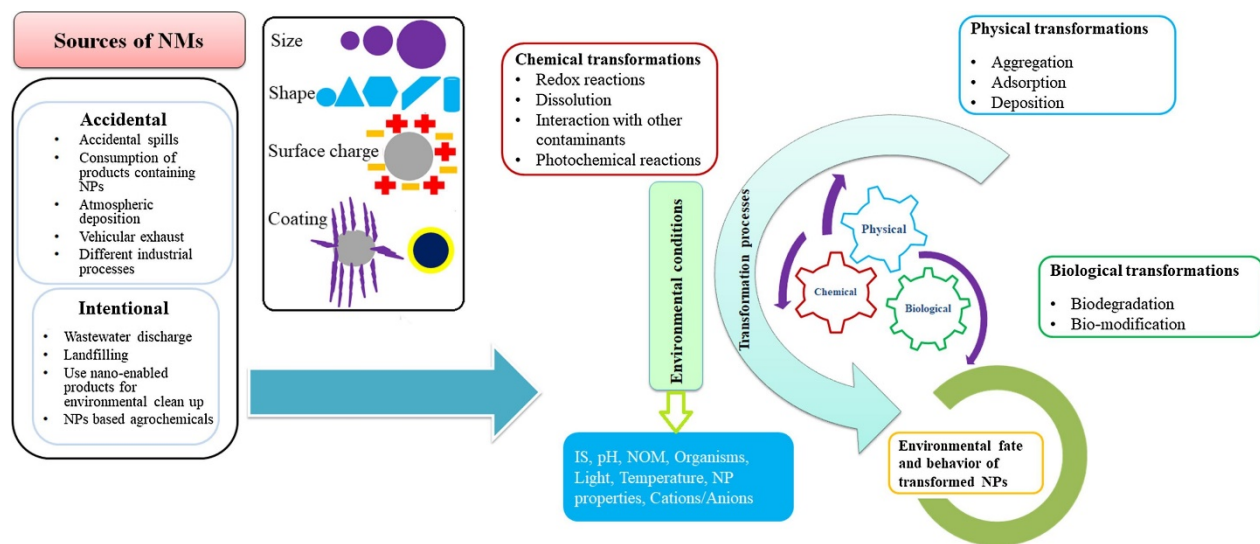


Figure 1-5 Diagramme représentant les sources du relargage et les transformations des NPMs dans l'environnement. Les NPMs peuvent subir des transformations physiques, chimiques ou biologiques. Ces transformations dépendent des propriétés intrinsèques des NPMs et des conditions environnementales. (Tiré de Abbas *et al.*³⁵).

Transformations physiques

À cause des mouvements aléatoires des eaux et de l'air, et en raison du mouvement brownien, les particules sont en mouvement continu et entrent en collision les unes avec les autres. Elles s'agglomèrent lorsque la force attractive de van der Waals surmonte la force électrostatique répulsive. L'agglomération/l'agrégation et la sédimentation constituent donc les principales transformations physiques des NPMs dans les différents compartiments environnementaux.³⁵ Un agglomérat est donc un mélange de particules faiblement liés (forces de

van der Waals) avec une aire de surface similaire à la somme des aires de surfaces des composants individuels.³⁵ Le processus d'agglomération augmente la taille des particules au fil du temps, accompagnée d'une réduction de la concentration en nombre des NPMs en raison de la sédimentation de grosses particules agglomérées.³⁶ En revanche, l'agrégation correspond à un mélange de particules fortement liés et dont l'aire de surface peut être significativement plus petit que la somme des aires de surface des particules distinctes.³⁵ Une fois relarguées dans l'environnement, les NPMs subissent une homo-agglomération (entre NPMs de même type) ou une hétéro-agglomération (entre NPMs de différent type et/ou les NPMs et les colloïdes inorganiques ou organiques).³⁷ Dans les matrices environnementales, l'hétéro-agglomération domine en raison de la présence en grande concentration des différents colloïdes naturels tels que les minéraux argileux, les oxydes de Fe et de Mn, la matière organique et les biopolymères produits par les micro-organismes.³⁵

Les conditions environnementales tels que le pH, la force ionique (IS) et la présence de la matière organique naturelle (NOM) influencent grandement le taux d'agglomération des NPs. Le pH de la solution définit le potentiel de surface de la particule, qui peut être estimé par son potentiel zêta (potentiel- ζ). Lorsque le pH d'une suspension colloïdale s'approche du point de charge zéro (PZC), la charge de surface des NPs est nulle ce qui conduit à une diminution de la stabilité du système colloïdal, et par la suite une agglomération plus importante.³⁸

La force ionique est un autre paramètre clé qui influence le degré d'agglomération et la stabilité des NPs dans les échantillons naturels et qui dépend de la nature et la concentration des ions. En augmentant l'IS, la double couche électrique des NPs se comprime et le potentiel de surface se réduit.³⁵ Par conséquent, la répulsion entre les particules est surmontée par la force attractive, ce qui favorise l'agglomération des NPs. De plus, l'agglomération est particulièrement favorisée en présence d'ions divalents (ex. Ca^{2+} , Mg^{2+}) par rapport aux ions monovalents (ex. Na^+ , K^+).³⁹ En effet, les cations polyvalents sont plus efficaces pour neutraliser la charge de surface (négative), et peuvent aussi servir de pont entre les particules.

La NOM correspond à un large mélange hétérogène de composés organiques allant de macromolécules (acides humiques, acides fulviques, et biopolymères) aux ligands à base de carbone de faible masse moléculaire tels que les amines et les thiols.³⁵ Ces composés organiques sont présents dans les sols et les eaux, et sont dérivés de la décomposition des plantes, des

microbes et des résidus d'animaux dans les écosystèmes naturels.³³ En raison de leur caractéristiques physico-chimiques (différents sites actifs et groupes fonctionnels), la NOM peut s'adsorber sur les NPMs ce qui va modifier la chimie de leur surface (charge et effet stérique). Typiquement, l'adsorption d'acides humiques et fulviques est connue pour réduire le taux d'agglomération et améliorer la stabilité des particules en suspension,⁴⁰ en raison de leur charge négative (au pH des eaux naturelles) et de leur grande taille. Toutefois, l'adsorption de macromolécules, avec des tailles plus grandes que la double couche électrique des particules, est connue pour déstabiliser les systèmes colloïdaux.⁴¹

Transformations chimiques

Les NPMs peuvent subir différentes transformations chimiques telles que les réactions d'oxydoréduction, de dissolution, de sulfuration et de complexation lors de l'interaction avec des ligands organiques ou inorganiques ainsi que d'autres constituants présents dans l'environnement.³⁵ Les réactions rédox, dans lesquelles un transfert d'électron (gain ou perte) se produit entre les différents composés chimiques, sont contrôlées par les conditions environnementales tels que le pH et la présence des accepteurs ou des donneurs d'électrons.⁴² Dans les eaux naturelles et les sols bien aérés, l'oxydation est le processus dominant, tandis que les milieux pauvres en oxygène tels que les sédiments et les eaux souterraines constituent des milieux réducteurs.³⁵ L'oxydation des atomes de surface favorise la dissolution des NPs. Par exemple, l'oxydation des atomes de surface des NPs d'Ag dans les sols et les eaux de surface transforme l'Ag (0) en Ag⁺, favorisant ainsi la dissolution de ces NPs.⁴³ D'autres NPs métalliques (Cu) et d'oxydes métalliques (oxydes de Fe, de Zn et de Ce) peuvent aussi subir des processus d'oxydo-réduction.⁴⁴⁻⁴⁷

La dissolution est un processus chimique qui consiste à la libération des ions ou des molécules des NPMs. Les NPs peuvent être classées en particules hautement solubles (Ag, ZnO, CuO, Fe₂O₃, QD), peu solubles (CeO₂, TiO₂) et insolubles (nanotubes de carbone, fullerènes). La vitesse et le taux de la dissolution des NPMs dépendent de leurs propriétés intrinsèques (taille, composition, forme, chimie de surface, aire de surface et enrobage) ainsi que des paramètres du milieu (pH, IS, NOM, conditions redox, et température). Par exemple, Bian *et al.*⁴⁸ ont démontré que la diminution de la taille des NPs de ZnO, conduit à l'augmentation du taux de dissolution. De même, la chimie de surface et le type d'enrobage affecte aussi le taux de dissolution. Par

exemple, les NPs d'Ag stabilisées par du citrate ont présenté une plus grande dissolution que celles stabilisées par de la polyvinylpyrrolidone (PVP).⁴⁹ Le pH et la présence de ligands comme la NOM influencent aussi le processus de la dissolution. La diminution du pH et la présence de la NOM à de faibles concentrations favorisent la dissolution des NPMs.⁴⁸

Transformations biologiques

Une variété d'organismes, tels que les microbes, les plantes et les animaux sécrètent des biomolécules dans l'environnement. Ces biomolécules ont une nature chimique complexe et sont principalement composées de polysaccharides, protéines, lipides, acide nucléiques, etc.³⁵ Les biomolécules peuvent s'adsorber à la surface d'une NP, en formant une couche, connue sous le nom de «couronne».⁵⁰ Cette couche de biomolécules naturelles peut affecter le comportement et la réactivité des NPs et par conséquent le transport, la biodisponibilité et la toxicité.³³ Les interactions entre les NPMs et les différentes biomolécules sont analogues aux interactions avec la NOM, qui ont fait l'objet de plusieurs recherches aboutissant à des conclusions similaires : les interactions dépendent des propriétés physico-chimiques des NPs ainsi que des conditions environnementales.⁵¹ Les sources du relargage des NPs ainsi que leurs transformations dans l'environnement sont résumées dans la figure 1-2.³⁵

1.2. Cérium

1.2.1. L'élément Ce

Le cérium (Ce) ($z = 58$) possède une configuration électronique $[\text{Xe}] 4f^1 5d^1 6s^2$ et fait partie de la série des métaux des lanthanides du tableau périodique. Parmi les éléments de terres rares (les lanthanides, le scandium (Sc) et l'yttrium (Y)), le Ce constitue l'élément le plus abondant dans la croûte terrestre (0.005% en masse).⁵² Presque 89% du Ce naturel se compose de quatre isotopes stables (^{136}Ce , ^{138}Ce , ^{140}Ce , et ^{142}Ce), où le ^{140}Ce constitue l'isotope le plus abondant à 88.5%.⁵² Le Ce est présent naturellement, avec d'autres métaux des lanthanides, dans une gamme de minéraux dans l'environnement telles que la bastnaésite $((\text{Ce},\text{La})(\text{CO}_3)\text{F})$, l'allanite $((\text{Ca},\text{Ce})(\text{Al}_2\text{Fe}^{2+})(\text{SiO}_4)\text{O}(\text{OH}))$, la cerite $((\text{Ce},\text{Ca})_9(\text{Fe},\text{Mg})(\text{SiO}_4)_3(\text{HSiO}_4)_4(\text{OH})_3)$, la monazite $((\text{Ce},\text{La},\text{Nd},\text{Th})(\text{PO}_4))$ et l'euxenite $((\text{Y},\text{Ca},\text{Ce},\text{U},\text{Th})(\text{Nb},\text{Ti},\text{Ta})_2\text{O}_6)$.⁵³ Le Ce se distingue des autres lanthanides par le fait d'avoir deux états d'oxydation stables : l'ion «céreux» Ce^{3+} et l'ion «cérique» Ce^{4+} , avec des rayons de 114 pm et 97 pm, respectivement.⁵³ Les

composés de Ce sont utilisés dans différentes applications pharmaceutiques, médicales, électroniques et catalytiques, où le Ce serait présent sous forme d'oxyde ou de sel (nitrate, chlorure, bromure, phosphate, oxalate, acétate).⁵²⁻⁵⁵ Parmi ces composés, l'oxyde de cérium est le plus exploité.

1.2.2. L'oxyde de cérium

Les oxydes de cérium peuvent se composer du dioxyde de cérium (CeO_2) pur, ou d'un mélange de CeO_2 et du sesquioxyde de cérium (Ce_2O_3), dépendamment de la température et la pression partielle de l'oxygène.⁵⁶ Le CeO_2 présente une structure cristalline de type fluorite (CaF_2), dans laquelle chaque cation de Ce est coordonné par huit anions d'O au coin d'un cube (Figure 1-6). L'atome de Ce a la capacité d'ajuster facilement sa configuration électronique pour s'adapter à son environnement.⁵⁷ Ainsi, le passage de CeO_2 en Ce_2O_3 résulte de la perte de O^{2-} , ce qui crée un site vacant d'O dans la structure.⁵⁶ Les propriétés rédox du Ce et la structure de l'oxyde de Ce confèrent à ce dernier une capacité élevée de stockage d'oxygène, et par la suite fait de l'oxyde de cérium un candidat idéal pour des applications catalytiques.

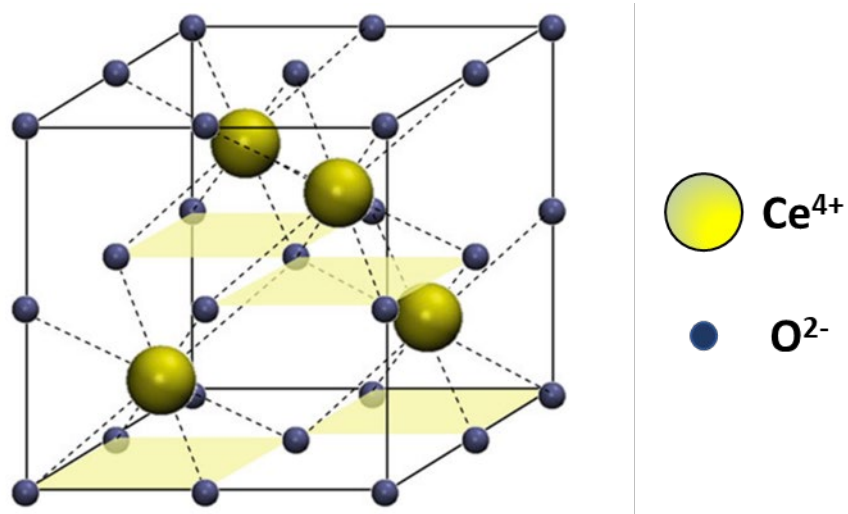


Figure 1-6 Structure de dioxyde de cérium (CeO_2). (Modifié de Perullini *et al.*⁵⁶)

1.2.3. Les nanoparticules d'oxydes de cérium

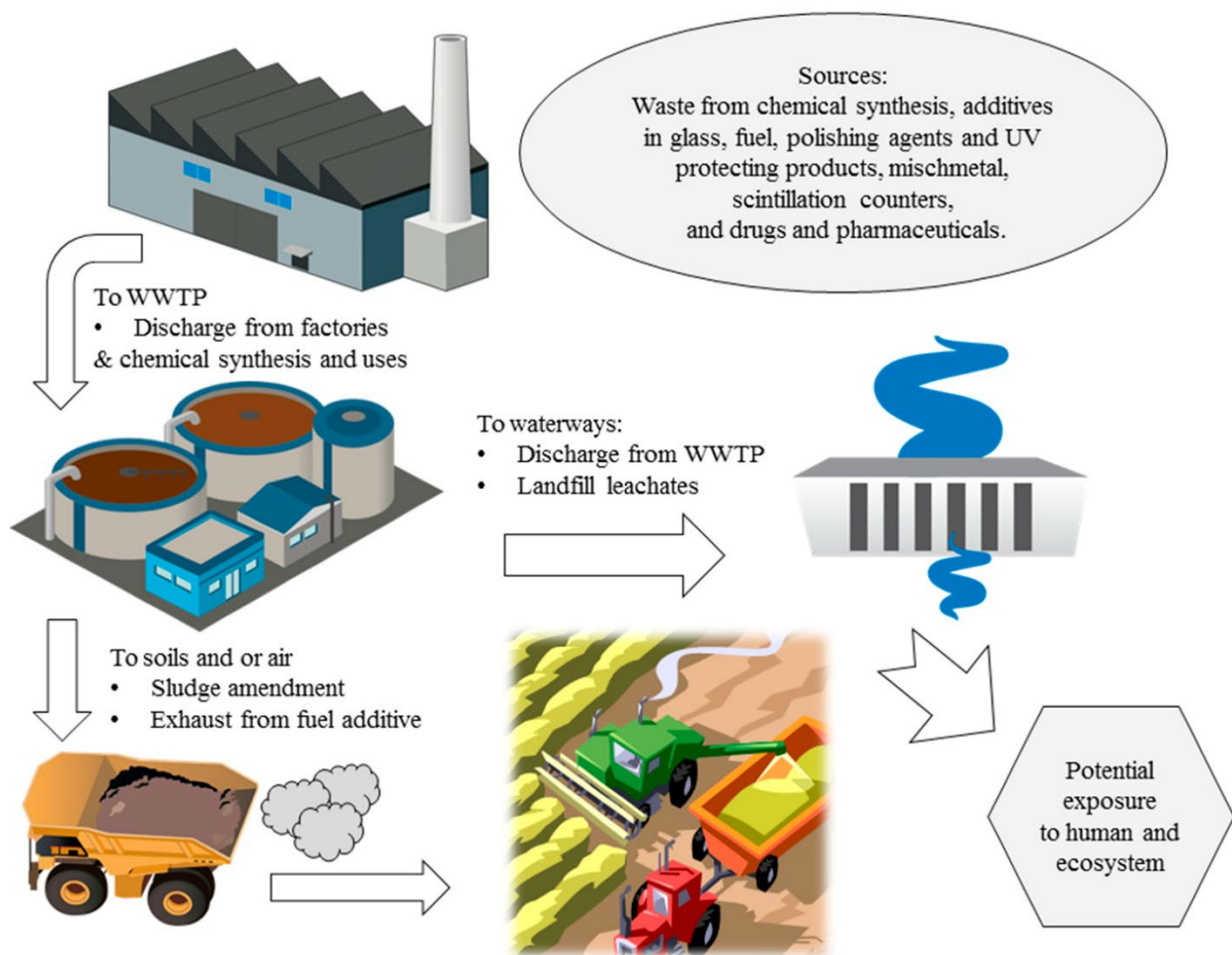


Figure 1-7 Les différentes applications et sources de rejet des NPs de CeO₂ dans l'environnement. (Tiré de Dahle et al.⁵²).

1.2.3.1. Propriétés

En raison de l'effet surface et l'effet quantique, les propriétés de l'oxyde de cérium sont améliorées davantage à l'échelle nanométrique. En diminuant la taille, la constante du réseau cristallin augmente ce qui conduit à un nombre plus grand de sites vacants d'oxygène.⁵² Par conséquent les NPs d'oxydes de cérium ont une capacité de stockage d'oxygène particulièrement élevée, ce qui fait de ces NPs un excellent catalyseur pour différents processus chimiques. Les NPs d'oxydes de Ce peuvent aussi être composées d'un mélange d'ions tri- et tétravalent du Ce, avec un rapport Ce³⁺/Ce⁴⁺ qui augmente en diminuant la taille de la particule.⁵⁸ En plus de la

taille, le rapport Ce^{3+}/Ce^{4+} dépend aussi de la méthode de synthèse des NPs. Le diamètre critique des NPs d'oxydes de Ce est défini par le diamètre en dessous duquel la constante de réseau reste constante, et correspond au passage de tous les atomes de Ce en état d'oxydation +3. Des valeurs de diamètre critique entre 1.1 – 1.2 nm ont été déterminés.^{59, 60} Malgré le fait que les NPs d'oxydes de Ce peuvent contenir des ions de Ce^{3+} , elles sont souvent commercialisées et citées dans la littérature sous le nom de NPs de CeO_2 . Par conséquent, cette abréviation sera utilisée pour la suite de cette thèse.

1.2.3.2. Applications

Les NPs de CeO_2 sont utilisées dans diverses applications industrielles et biologiques, telles que les piles à combustible à oxydes solides⁶¹, les cellules solaires⁶², le polissage de verre⁶³, et les produits de revêtements résistants à l'oxydation⁶⁴. Cependant, le domaine de la catalyse constitue la principale application des NPs de CeO_2 . Les NPs de CeO_2 sont souvent utilisées dans les convertisseurs catalytiques des automobiles, parce qu'elles peuvent absorber ou libérer de l'oxygène en fonction de sa pression partielle.⁵² Grâce à ce mécanisme, les NPs de CeO_2 agissent comme un co-catalyseur (avec le platine) et réduisent les émissions des NO_x et les autres produits de combustion incomplète.^{52, 63} Ainsi, la combustion du diesel est plus « propre » si des NPs d'oxydes de Ce y sont ajoutées entraînant moins de pollution de l'air. Elles sont aussi utilisées comme catalyseur dans l'oxydation du carbone organique volatil⁶⁵ et du toluène⁶⁶, l'ozonation des composés organiques⁶⁷ et les réactions de gaz avec l'eau⁶⁸. À cause de leur propriété d'absorption de l'UV, les NPs de CeO_2 sont aussi ajoutées aux écrans solaires⁶⁹ et aux produits de revêtement⁷⁰. Récemment, il a été démontré que les NPs de CeO_2 possédaient des propriétés enzymatiques intéressantes, en imitant des enzymes connus pour la protection des cellules.^{71, 72} En plus de les propriétés enzymatiques, les NPs de CeO_2 possèdent des activités antibactériennes, antioxydantes et anticancéreuses⁷³, ce qui a conduit à l'utilisation de ces NPs dans les différents domaines biologiques tels que la bioanalyse⁷⁴, la biomédecine⁷⁵ et l'administration de médicaments^{76, 77}.

1.2.3.3. Voies de relargage

Avec l'augmentation importante de la production et l'utilisation des NPs de CeO_2 , l'inquiétude grandit quant à leur rejet dans l'environnement ainsi qu'à leur devenir et toxicité. Parmi leurs voies de rejet dans l'environnement, les NPs de CeO_2 peuvent être relarguées dans

l'air par les émissions de diesel, dans les sols à partir des déchets solides et du recyclage, et dans les systèmes aquatiques à partir des effluents des stations de traitement des eaux usées.⁵² La grande majorité des données sur les concentrations, le devenir et les transformations des NPs de CeO₂ dans l'environnement ont été générées par modélisation.^{12, 27, 78} Par exemple, les concentrations des NPs de CeO₂ prévues dans les eaux naturelles vont de 1 pg L⁻¹ en 2017 à quelques centaines de ng L⁻¹ en 2050.²⁷ L'analyse directe des NPs de CeO₂ dans l'environnement est extrêmement difficile en raison de leurs petites tailles, de leurs faibles concentrations (dans l'ordre de ng L⁻¹) et de la complexité des matrices environnementales qui contiennent également des colloïdes naturels.

1.2.3.4. Toxicité

Au cours de la dernière décennie, une grande partie de la recherche sur les NPs de CeO₂ s'est concentrée sur leur toxicité et leurs interactions avec les cellules, compte tenu de leur application en biomédecine. En général, trois mécanismes principaux ont été évalués (1) l'internalisation des NPs dans la cellule, en raison de leur petite taille; (2) la capacité des NPs de relarguer des ions métalliques, via dissolution; et (3) la production des espèces réactives d'oxygène (ERO).^{52, 56} Il a été démontré, pour une grande variété de NP, que les plus petites particules entraîne une plus grande toxicité dans les systèmes biologiques, en raison de leur capacité de traverser les membranes cellulaires, et de leur dissolution plus rapide. Par exemple, Singh *et al.*⁷⁹ ont démontré que les NPs de CeO₂ de 3 – 5 nm ont été internalisées et distribuées dans les différents compartiments cellulaire. Cependant, l'internalisation des NPs dépend de leurs propriétés, tels que la taille, la forme, la composition, la charge de surface et l'enrobage. Safi *et al.*⁸⁰ ont étudié des NPs de CeO₂ (de taille similaire) avec deux enrobages différents (citrate et acide polyacrylique) et ils ont démontré que seulement les NPs de CeO₂ enrobées de citrate ont été internalisées dans les cellules. Les études ont rapporté des résultats contradictoires concernant les effets toxiques des NPs de CeO₂: il a été démontré que les NPs de CeO₂ agissent à la fois comme un antioxydant et un producteur (ou induit la production) des ERO à travers de multiples voies biologiques.⁵² Plusieurs chercheurs ont signalé que les NPs de CeO₂ agissent comme un antioxydant en réduisant la production et les dommages causées par les ERO aux cellules de mammifères en transformant le superoxyde en oxygène et en peroxyde d'hydrogène.⁸¹⁻⁸³ Toutefois, de nombreux chercheurs ont rapportés des effets complètement opposés des NPs de CeO₂ qui ont induit ou catalysé la génération des ERO dans plusieurs systèmes biologiques.⁸⁴⁻⁸⁶

Bien que des recherches récentes^{56, 57, 87} aient indiqué que les comportements antagonistes des NPs de CeO₂ sont attribués aux différences dans la taille des particules ainsi que la valeur du rapport Ce³⁺/Ce⁴⁺, des recherches supplémentaires sont nécessaires avant de pouvoir tirer des conclusions sur les effets nocifs ou bénéfiques des NPs de CeO₂.

1.3. Analyse et caractérisation des nanoparticules

Afin d'évaluer leur risque environnemental, il est nécessaire de détecter, quantifier et caractériser les NPs dans tous les compartiments environnementaux. Dans ce but, plusieurs techniques analytiques ont été développées et utilisées. L'identification de différentes propriétés, telles que la taille, la forme, la composition, et la chimie de surface, est nécessaire pour une caractérisation complète des NPs pour l'analyse des NPs. Les techniques analytiques les plus utilisées pour l'analyse des NPs sont résumées dans cette section.

1.3.1. Microscopie

La microscopie est parmi les techniques de caractérisation les plus utilisées pour l'évaluation de la taille et la forme des NPs. Les techniques de microscopie les plus utilisées sont : (i) la microscopie à force atomique (AFM) qui fournit des informations qualitatives et quantitatives sur plusieurs propriétés telles que la taille, la morphologie et la texture de la surface⁴; (ii) la microscopie électronique à transmission (TEM) qui permet l'évaluation de la taille, la forme et la structure cristalline avec une résolution au niveau atomique.⁸⁸ La composition élémentaire peut aussi être obtenue par la TEM couplée à la spectroscopie à dispersion d'énergie (EDS) ; et (iii) la microscopie électronique à balayage (SEM) qui fournit les mêmes informations que la TEM plus la possibilité d'analyser des particules à l'échelle micrométrique (ce qui n'est pas vraiment le cas de l'AFM et la TEM)⁸⁸. Cependant, malgré les différents avantages, la préparation (séchage, revêtement) et l'analyse (sous vide) de l'échantillon par les techniques de microscopie peuvent conduire à des artefacts.⁸⁹

1.3.2. Diffusion de la lumière

Parmi les différentes techniques basées sur la diffusion de la lumière, la diffusion dynamique de la lumière (DLS) est la technique la plus utilisée pour la caractérisation des NPs dans les échantillons aqueux. La DLS mesure les fluctuations temporelles de l'intensité de la lumière diffusée par les NPs en mouvement brownien.⁹⁰ Ce mouvement est ensuite relié à un

diamètre hydrodynamique équivalent. Cette technique présente trois limitations majeures : (1) une concentration élevée des NPs (souvent $> 1 \text{ mg L}^{-1}$) est nécessaire; (2) la difficulté de détecter les plus petites particules parmi les plus grandes dans une suspension polydispense. Ceci est dû au fait que l'intensité de diffusion dépend du diamètre des particules à la puissance six; et (3) le manque de spécificité chimique.^{89, 90}

L'analyse du suivi de nanoparticule (NTA) est une technique émergente, qui est basée aussi sur la diffusion de la lumière. La diffusion de la lumière est utilisée pour détecter la distance parcourue, en deux dimensions, par chaque nanoparticule. Comme les petites nanoparticules ont des coefficients de diffusion plus grands, la quantification de la distance parcourue dans un intervalle de temps donné peut être reliée au diamètre hydrodynamique de la nanoparticule.⁹¹ Ensuite, en utilisant une technique de microscopie vidéo, des informations telles que la concentration en nombre et la distribution de taille peuvent être obtenues. En raison des limitations liées à la puissance du laser et au détecteur de la caméra, des NPs avec une taille inférieure à 20 nm sont difficilement analysées.⁸⁹

1.3.3. Techniques de séparation

Les échantillons polydispenses constituent une limitation pour plusieurs techniques de caractérisation des NPs. Dans ce cas, il est utile d'utiliser une méthode de séparation, tels que la chromatographie hydrodynamique (HDC) ou le fractionnement par couplage flux-force (FFF) afin de faciliter la mesure des différentes populations présentes dans l'échantillon. En FFF, la séparation d'un mélange de composés, avec une large gamme de taille (1 nm jusqu'à 100 μm), peut être réalisé par l'interaction des composants de l'échantillon avec un champ externe qui est appliqué perpendiculairement à la direction du flux de la phase mobile.^{4, 89} En HDC, la phase stationnaire est constituée de billes non poreuses, et la séparation est effectuée par les différences de parcours des petites et grandes particules, semblable à la chromatographie par exclusion de taille.⁹² Ainsi les grandes particules sont éluées plus rapidement que les plus petites qui passent plus de temps entre les billes. Ces techniques de séparation peuvent être couplées en ligne ou hors ligne à une variété de détecteurs tels que l'UV-vis⁹³, DLS⁹⁴ et la spectrométrie de masse à plasma à couplage inductif (ICP-MS)⁹⁵. Toutefois, le processus d'optimisation peut être long et difficile, et dépend des propriétés des NPs (chimie de surface) et de la matrice. Les meilleures limites de

détection sont obtenues en couplant le HDC et le FFF à ICP-MS, sauf que dans les deux cas les échantillons sont dilués ce qui conduit à une augmentation des LDs.

Malgré les nombreux avantages des différentes techniques de caractérisation et de séparation, leur application pour l'analyse des NPs dans des échantillons naturels est limité par un manque de spécificité et de sensibilité (faibles concentrations et petites tailles des NPs) et par la complexité des matrices environnementales qui contiennent des colloïdes inorganiques et organiques avec une large gamme de taille. Dans ce but, l'ICP-MS en mode particule unique (SP-ICP-MS) semble être une technique avantageuse pour l'analyse des NPs parce qu'elle combine la spécificité et la sensibilité de la spectrométrie de masse avec l'analyse « particule par particule ». De plus, avec cette technique, les échantillons ne nécessitent pas de préparation préalable. Le principe de la SP-ICP-MS sera discuté en détail dans les prochains paragraphes. Le tableau suivant résume les informations fournies au sujet des différentes techniques discutées.

Tableau 1-1 Résumé des informations fournies au sujet des différentes techniques d'analyse des NPs.

N.A. signifie «non applicable». (Les données et les informations ont été collectées de Modena *et al.*⁸⁸ et Laborda *et al.*⁸⁹)

Technique	Limite de détection de taille (SDL) (nm)	Limite de détection (ng L ⁻¹)	Limite de détection (NP L ⁻¹)	Informations fournies
AFM	10 – 20	N.A.	N.A.	- Taille (moyenne et distribution) - Forme
TEM	<1	N.A.	N.A.	- Taille (moyenne et distribution) - Forme - Composition élémentaire (+EDS)
SEM	30	N.A.	10 ¹²	- Taille (moyenne et distribution) - Forme
DLS	5 – 10	N.A.	N.A.	- Taille (moyenne et distribution)
NTA	20	N.A.	10 ⁹	- Taille (moyenne et distribution) - Concentration en nombre
FFF-UV-vis	1 – 5	0.1 mg L ⁻¹	N.A.	- Taille (moyenne et distribution)
FFF-DLS	1 – 5	1 mg L ⁻¹	N.A.	- Concentration massique
FFF-ICP-MS	1 – 5	1 – 10 µg L ⁻¹	N.A.	- Concentration massique
HDC-ICP-MS	5	1 µg L ⁻¹	N.A.	- Concentration du dissous - Taille (moyenne et distribution) - Concentration en masse
SP-ICP-MS	10 – 20	ng L ⁻¹	10 ⁶	- Concentration du dissous - Taille (moyenne et distribution) - Concentration en masse et en nombre des NPs - Composition chimique

1.4. Spectrométrie de masse à plasma à couplage inductif

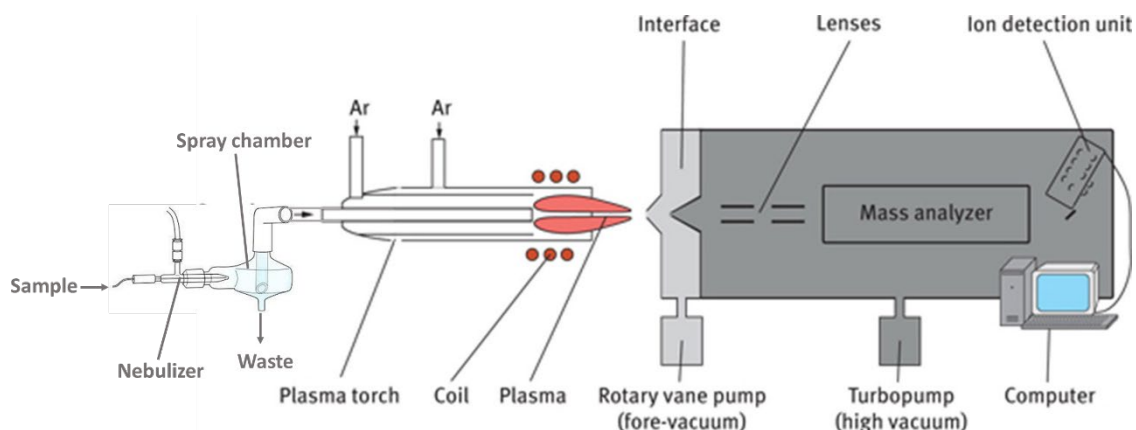


Figure 1-8 Schéma des composants principaux de l'ICP-MS : système d'introduction, système d'ionisation, interface, filtre de masse et détecteur. (Modifié de Telgmann *et al.*⁹⁶).

Depuis sa commercialisation en 1983, la spectrométrie de masse à plasma à couplage inductif (ICP-MS) est devenue la technique la plus utilisée dans le domaine de l'analyse élémentaire des métaux et métalloïdes en traces et ultra-traces.⁹⁷⁻⁹⁹ Comparé aux autres techniques d'analyse élémentaires, tels que la spectrométrie d'émission optique à plasma à couplage inductif (ICP-OES) et la spectroscopie d'absorption atomique par four de graphite (GFAAS), l'ICP-MS présente de nombreux avantages uniques telles qu'une : (i) haute sensibilité (basses limites de détection), (ii) haute spécificité (capacité de distinction isotopique), et (iii) large gamme linéaire (pg L^{-1} – mg L^{-1}).^{97, 99} L'ICP-MS est couramment utilisée par les institutions gouvernementales et les industries privées dans différents domaines tels que géochimie, l'environnemental, biomédical, et nucléaire. La configuration des instruments diffère d'un modèle à l'autre, mais, en général, la structure de l'ICP-MS peut être divisée en cinq composants principaux :

1.4.1. Le système d'introduction

La majorité des échantillons analysés par l'ICP-MS sont des liquides. Le rôle du système d'introduction est de transformer ces solutions en un aérosol de fines gouttelettes avant de les introduire dans le plasma. Cela est effectué à l'aide d'une pompe péristaltique, des tubes, un nébuliseur et une chambre de nébulisation. D'abord le liquide est aspiré par la pompe

péristaltique, qui assure un flux constant, et des tubes souvent en polychlorure de vinyle (PVC), qui sont compatibles avec une large gamme d'acide. Les déterminations des métaux et métalloïdes en solution s'effectuent à bas pH afin d'assurer une plus grande stabilité ainsi que de réduire l'adsorption des analytes sur les différents composants du système d'introduction.⁹⁹⁻¹⁰¹ Le liquide est ensuite acheminé vers le nébuliseur qui va produire un aérosol de fines gouttelettes. Il existe différents types de nébuliseurs et le type utilisé dépend des propriétés de la solution analysée (viscosité, volume disponible).¹⁰² Dans le nébuliseur, un gaz (l'argon) est poussé perpendiculairement au trajet du liquide ce qui va conduire au fractionnement de ce dernier en fines gouttelettes. L'aérosol passe ensuite par une chambre de nébulisation qui joue le rôle d'un filtre de gouttelettes ne permettant qu'aux plus petites d'entrer dans le plasma. Les fines gouttelettes, introduites au plasma, constituent 1 – 2 % de l'aérosol.^{99, 100} Il existe également différents types (verre, quartz, polymères) et modèles (cycloniques, Scott) de chambre de nébulisation. Le modèle cyclonique est le modèle le plus utilisé. La chambre de nébulisation cyclonique possède une plus grande efficacité de transmission ce qui se traduit par une sensibilité plus élevée et des limites de détection plus basses. Cependant, la distribution de tailles des gouttelettes est plus large et moins précise que celle obtenue avec le modèle Scott.⁹⁹ La chambre de nébulisation peut aussi être refroidie par un système Peltier qui va augmenter la stabilité en réduisant la quantité de vapeur (par condensation).

1.4.2. Le système d'ionisation

Le système d'ionisation est constitué d'une torche et d'une bobine. Pour créer le plasma, une bobine d'induction métallique, entourant une torche, est parcourue par un courant électrique de grande puissance (700 – 1500 W) à très haute fréquence (27 ou 40 MHz), ce qui génère un champ magnétique.⁹⁸ Le gaz (généralement l'argon) est introduit dans ce champ via une torche en quartz. Une décharge électrique déclenche l'ionisation de l'Ar. Un plasma, à très haute température (6000 – 1000 K), est alors généré puis entretenu par la circulation des électrons et des cations d'Ar, prises dans le champ magnétique.¹⁰³ Suite à leur introduction dans le plasma, les molécules contenues dans les gouttelettes passent par une série de changements physiques : désolvatation, sublimation, atomisation et ionisation.⁹⁸ Les cations monovalents générés sont par la suite acheminés vers le spectromètre de masse à travers l'interface.

1.4.3. L'interface

La température et la pression (760 torr) dans le plasma sont beaucoup plus grande que celles requises pour les différents composants du spectromètre de masse (pression de $10^{-4} - 10^{-5}$ torr).¹⁰³ Ainsi, le rôle principal de l'interface consiste à extraire les ions du plasma et de les introduire au spectromètre de masse. L'interface se compose de deux cônes métalliques (nickel ou platine) avec de très petits orifices (diamètre entre 0.4 et 1.1 mm).^{99, 101}

1.4.4. Le filtre de masse

Le filtre de masse, ou analyseur, sert à séparer les ions selon leur rapport masse sur charge (m/z). Les premiers instruments ICP-MS utilisaient des filtres quadripolaires en raison de leur grande robustesse et de leur faible coût.⁹⁹ Cependant, d'autres filtres ont été commercialisés, par la suite, tels que le secteur magnétique et le temps-de-vol qui offrent des avantages additionnels comme une meilleure sensibilité et une possibilité d'analyse multi-élément.

1.4.4.1. Quadripôle

Un filtre quadripolaire est constitué de quatre barres parallèles entre elles. Une tension continue et une tension alternative sont appliquées de façon que les barres opposées soient de même signe et les barres adjacentes de signes opposés.¹⁰⁴ Pour une combinaison donnée de tensions, seules les espèces ayant un m/z spécifique peuvent avoir une trajectoire stable à travers les barres et par la suite atteindre le détecteur.¹⁰⁵ Toutefois, ce type de filtre est limité par sa faible résolution ($m/\Delta m = 300$), ce qui le rend vulnérable aux interférences. La résolution indique la capacité d'un spectromètre de masse à différencier entre deux masses et est défini par le rapport $m/\Delta m$ où Δm correspond à la différence de masse entre deux pics adjacents et m à la masse du premier pic. Généralement les appareils d'ICP-MS utilisant un filtre quadripolaire (Q-ICP-MS) sont munis d'une cellule de collision et/ou d'une cellule de réaction qui ont pour but de réduire les interférences. Le fonctionnement de ces cellules sera expliqué plus tard dans ce chapitre.

1.4.4.2. Secteur magnétique

L'ICP-MS à secteur magnétique (SF-ICP-MS), aussi connu sous le nom d'ICP-MS à haute résolution ($m/\Delta m$ jusqu'à ~ 13000), permet de résoudre de nombreuses interférences. Comparé à Q-ICP-MS, le SF-ICP-MS offre une meilleure sensibilité et par la suite des limites de

détection (LD) plus petites. Les ions sont d'abord accélérés par un potentiel et ensuite soumis à un champ magnétique perpendiculaire. Par la suite, en effectuant un balayage du potentiel ou du champ magnétique, un ion avec un m/z spécifique empruntera la courbure désirée vers le détecteur.¹⁰⁶ Le secteur magnétique est souvent couplé à un secteur électrostatique, d'où le nom système à double focalisation. Dans ce système, le secteur électrostatique agit comme un filtre d'énergie de telle façon qu'il laisse passer les ions ayant la même énergie, quelle que soit leur masse, et le secteur magnétique permet de focaliser les ions de même masse et les faire converger vers le détecteur.¹⁰⁴

1.4.4.3. Temps-de-vol

Un appareil d'ICP-MS équipé d'un filtre de masse à temps-de-vol (TOF-ICP-MS) permet la détection quasi-simultanée de tout le spectre de masse.¹⁰⁰ Le principe est basé sur la mesure du temps mis par les ions pour traverser une distance fixe. Les ions sont d'abord accélérés par une haute tension à l'entrée d'un tube sans champ. Ayant une énergie cinétique de départ identique, le temps de vol des ions dans le tube est proportionnel à la racine carrée de leur masse. Ainsi, les ions les plus légers (plus petits m/z) arrivent plus tôt au détecteur que les ions les plus lourds. Les isotopes sont ensuite identifiés par le fait que chaque m/z correspond à un temps de vol unique. L'appareil de TOF-ICP-MS peut aussi être équipé d'un miroir à ions (*reflectron*) qui a le rôle d'allonger le parcours des ions, ce qui améliore davantage la résolution ($m/\Delta m \sim 1800$).^{100, 104}

1.4.5. Le détecteur

Deux types de détecteurs sont utilisés dans les instruments d'ICP-MS : le multiplicateur d'électrons à dynodes discrètes et le collecteur de Faraday.¹⁰⁴ L'ion sortant du filtre de masse frappe la première dynode qui libère des électrons qui frappent une deuxième dynode où plus d'électrons sont libérés. Cette cascade d'électrons se poursuit jusqu'à ce qu'une impulsion mesurable soit créée.¹⁰² Le multiplicateur à dynodes discrètes peut fonctionner en deux modes : mode pulsé (jusqu'à $\sim 10^7$ comptes par secondes (cps)) qui permet de mesurer les faibles signaux et mode atténué pour les fortes intensités (jusqu'à $\sim 10^{10}$ cps). Le collecteur de Faraday est généralement utilisé pour les plus fortes intensités (jusqu'à $\sim 10^{12}$ cps).¹⁰⁷

1.5. Spectrométrie de masse à plasma à couplage inductif en mode particule unique

La première utilisation du mode particule unique remonte à 1986, où un ICP-OES en mode SP a été utilisé pour analyser des particules en suspension dans l'air.¹⁰⁸ Toutefois, ce n'est qu'au début des années 2000, que la spectrométrie de masse à plasma à couplage inductif en mode particule unique (SP-ICP-MS) a été développée dans le but d'analyser des colloïdes et des microparticules en suspension.¹⁰⁹⁻¹¹² Plus récemment, l'augmentation de la production et l'utilisation des NPMs, a augmenté l'intérêt pour la SP-ICP-MS comme alternative aux autres techniques disponibles pour la détection, caractérisation et quantification des NPs. Cette méthode profite des avantages de l'ICP-MS, telles que la haute sensibilité et spécificité. De plus, telles que les techniques de comptage des particules, la SP-ICP-MS est basée sur l'analyse d'une particule à la fois. La SP-ICP-MS permet de différencier entre la forme dissoute et particulaire d'un élément en suspension en déterminant leurs concentrations massiques séparément. Pour la fraction particulaire, la SP-ICP-MS fournit des informations sur la taille, la distribution de taille et la concentration en nombre.^{89, 113} Tous ces avantages ont fait de cette méthode l'une des plus utilisées pour l'analyse des NPs dans les échantillons environnementaux. La SP-ICP-MS a été utilisée pour l'analyse des NPs de thorium (Th),¹¹⁰ d'or (Au),¹¹² d'oxyde de zinc (ZnO),¹¹⁴⁻¹¹⁶ de dioxyde de titane (TiO₂),^{3, 117, 118} d'argent (Ag),^{3, 119, 120}, de CeO₂^{114, 121-123}, etc.

1.5.1. Principes

Une suspension de nanoparticules peut être constituée de la forme dissoute et la forme particulaire de l'élément. La forme dissoute est distribuée d'une façon homogène dans la solution, ainsi la masse d'élément entrant dans le plasma et arrivant au détecteur est constant, ce qui va produire un signal continu (bruit de fond ou *background*).¹¹³ Lorsqu'une nanoparticule est introduite dans le plasma, sa vaporisation, son atomisation et son ionisation vont générer un paquet d'ions qui sera détecté par un signal transitoire au-dessus du signal continu.¹¹³ L'intensité du signal est reliée à la masse de l'élément dans la particule alors que le nombre de signaux transitoires (i.e. pics) est relié à la concentration en nombre. En SP-ICP-MS, le temps d'acquisition (*dwell time*) est défini par le temps d'analyse de chaque point du signal et contrôle la fréquence d'acquisition. Les premières mesures^{110, 112} de SP-ICP-MS utilisaient des temps d'acquisition de l'ordre de millisecondes (3 – 10 ms); toutefois, avec l'avancement des

instruments, des temps d'acquisition à l'échelle des microsecondes peuvent être atteints (10 – 200 μ s).¹²⁴ L'utilisation de courts temps d'acquisition (hautes fréquences d'acquisition) permet d'augmenter le rapport signal / bruit de fond, de mieux définir le signal mesuré et de diminuer le risque de coïncidence.^{125, 126} Ce dernier est défini par la détection simultanée de deux ou plusieurs NPs.

1.5.2. Acquisition et traitement des données

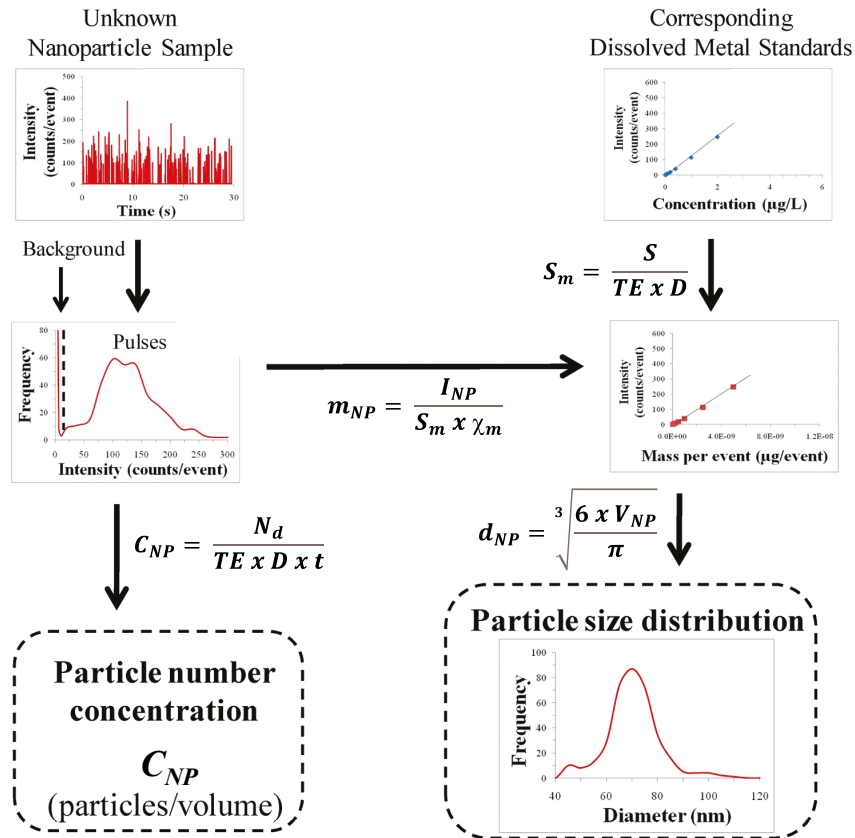


Figure 1-9 Les étapes de traitement des données pour la détermination de la taille et de concentration en nombre des NPs en utilisant l'ICP-MS en mode particule unique. La sensibilité massique (S_m) est calculée à partir de l'efficacité de transport (TE), le débit (D) et la sensibilité (S). La S_m est ensuite utilisée pour convertir l'intensité d'un pic (I_{NP}) en masse de la NP (m_{NP}) en tenant compte de la fraction massique (χ_m). Le diamètre de la NP (d_{NP}) est obtenu à partir de son volume (V_{NP}). La concentration en nombre des NPs (C_{NP}) est calculée à partir du nombre de pics détectés (N_d) pendant un certain temps d'analyse (t). (Modifié de Pace *et al.*¹²⁷).

La première étape de l'analyse des NPs par SP-ICP-MS consiste à créer une droite de calibration en utilisant des étalons ioniques de l'élément à déterminer avec une concentration connue (ng L^{-1}). La sensibilité (S , cps ng L^{-1}) correspond à la pente de la droite de calibration et permet de relier le signal d'intensité (comptes par seconde) à la concentration de l'analyte. Afin de convertir la sensibilité en sensibilité massique (S_m , compte fg^{-1}), l'efficacité de transport (TE) doit être mesurée. La TE est définie comme la fraction de l'échantillon qui atteint le détecteur par rapport à celle qui a été aspirée et tient compte des pertes lors de la nébulisation, ionisation et extraction des ions. Tel qu'expliqué précédemment, lors de la nébulisation de la solution, seules les gouttelettes les plus fines (1 – 2%) sont introduites au plasma et cette perte est exprimée en efficacité de nébulisation. Une fois dans le plasma, les atomes ne seront pas tous ionisés à cause de leur énergie d'ionisation ou la présence en grande concentration d'autres éléments facilement ionisables. Cette perte est exprimée comme l'efficacité d'ionisation. D'autres pertes peuvent se produire lors de l'extraction des ions par l'interface et de leur voyage vers le détecteur. Ces pertes sont résumées en l'efficacité d'extraction. Plusieurs méthodes sont utilisées pour déterminer la TE, la plus commune étant l'utilisation d'une suspension standard de NPs avec une concentration en nombre connue (C_{NP} , μL^{-1}).¹²⁷ Ainsi la TE pourrait être déterminée à partir du nombre détecté de particules (N_d , μL^{-1}) par rapport à celui aspiré (N_a , μL^{-1}) en tenant compte du débit (D , $\mu\text{L s}^{-1}$) et du temps d'analyse (t , s), selon l'équation suivante :¹¹⁸

$$TE = \frac{N_d}{N_a} = \frac{N_d}{C_{NP} \times D \times t} \quad \text{Équation 1.1}$$

Par la suite la sensibilité massique peut être calculée selon l'équation suivante :

$$S_m = \frac{S}{TE \times D} \quad \text{Équation 1.2}$$

Suite à la détection d'un signal correspondant à une NP, son intégration y compris la soustraction de bruit de fond donnera l'intensité nette du pic (I_{NP} , comptes). Celle-ci peut être utilisée pour calculer la masse de la NP (m_{NP} , fg) selon l'équation suivante :

$$m_{NP} = \frac{I_{NP}}{S_m \times \chi_m} \quad \text{Équation 1.3}$$

où χ_m correspond à la fraction de masse molaire élément/NP.

Connaissant la densité (ρ_{NP} , g cm⁻³), le volume de la NP (V_{NP} , nm³) peut être calculé selon l'équation suivante :

$$V_{NP} = \frac{m_{NP} \times 10^6}{\rho_{NP}} \quad \text{Équation 1.4}$$

Sous l'hypothèse qu'il s'agit d'une NP sphérique, le diamètre (d_{NP} , nm) peut être calculé selon l'équation suivante :

$$d_{NP} = \sqrt[3]{\frac{6 \times V_{NP}}{\pi}} \quad \text{Équation 1.5}$$

La concentration en nombre des NPs (C_{NP} , µL⁻¹) peut être déterminée selon l'équation suivante :

$$C_{NP} = \frac{N_d}{TE \times D \times t} \quad \text{Équation 1.6}$$

Alors que la concentration massique des NPs (C_m , ng L⁻¹) peut être déterminée par l'équation suivante :

$$C_m = \frac{\sum_{i=1}^{i=N_d} I_{NP}}{S_m \times TE \times D \times t} \quad \text{Équation 1.7}$$

La concentration massique (C_{diss} , ng L⁻¹) de la forme dissoute de l'élément est calculée à partir de l'intensité moyenne du signal continu (I_{bruit} , compte) qui constitue le bruit de fond :

$$C_{diss} = \frac{I_{bruit}}{S_m \times TE \times D \times t} \quad \text{Équation 1.8}$$

Et finalement, la limite de détection de taille (SDL, nm) peut être déterminée de la même façon que le diamètre d'une NP (équations 1.3 – 1.6) mais en remplaçant l'intensité de la NP (I_{NP}) par l'intensité du seuil (I_S , compte) qui sépare le bruit de fond des pics correspondants aux NPs :

$$SDL = \sqrt[3]{\frac{6 \times I_S}{\pi \times 10^6 \times \rho_{NP} \times S_m \times \lambda_m}} \quad \text{Équation 1.9}$$

Afin qu'un signal soit attribué à une NP, il faut que son intensité dépasse celui du bruit de fond. Ce dernier est dû à la présence de l'analyte dissout, aux interférences et/ou les petites NPs (< SDL). Plusieurs approches statistiques¹²⁸⁻¹³⁰ sont utilisées afin de définir le seuil qui sépare le bruit de fond des signaux attribués aux NPs. L'approche la plus commune définie I_{bruit} par l'intensité moyenne du bruit de fond + n x l'écart-type (SD) (généralement n = 3). Toutefois,

dans le cas où le SD est faible, des artefacts du bruit de fond peuvent être comptés comme des NPs, menant à la surestimation de leur concentration en nombre.¹¹⁸ Récemment, un algorithme est développé qui identifie les signaux des NPs par leurs points d'inflexion et détermine un signal de bruit de fond local (pour chaque NP).¹³¹ Les données SP-ICP-MS présentées dans cette thèse ont été traitées par un logiciel *Nu Quant* utilisant cet algorithme. Dans cette méthode, les données sont d'abord lissées afin de définir la ligne de base de fond. L'algorithme recherche ensuite dans une fenêtre définie un signal avec une intensité maximale qui dépasse le bruit de fond lissé. Par la suite, les données entre les points de pré- et post-inflexion du maximum sont intégrées et soustraites d'un signal de bruit de fond local. Le logiciel permet la vérification de chaque pic, ce qui permet d'identifier les artefacts incluant la coïncidence des particules.¹¹⁸

1.5.3. Bruit de fond et stratégies de résolution

Tel que discuté précédemment, le bruit de fond en SP-ICP-MS est attribué à l'analyte dissous, aux interférences, aux petites NPs et/ou au bruit électronique instrumental. Réduire ce bruit a fait l'objet de nombreuses études de recherche, parce qu'il conduit à la diminution de la SDL et par la suite à la détection des plus petites NPs qui sont susceptibles d'être plus pertinentes pour des systèmes biologiques ou environnementaux, i.e. interagir plus avec les membranes biologiques ou avoir une plus grande mobilité dans l'environnement. Dans les prochains paragraphes, les deux causes majeures du bruit de fond (analyte dissous et interférences) seront discutées en plus des différentes stratégies employées pour les réduire.

1.5.3.1. Analyte dissous

La forme dissoute d'un élément inclut sa forme ionique et les différents complexes organiques et inorganiques solubles. Lorsque la fraction dissoute dans la suspension est importante, surtout dans le cas des NPs très solubles (ZnO, CuO, Ag), le signal du bruit de fond peut être problématique pour la détection des petites NPs. Une méthode simple de diminuer le bruit de fond consiste à diluer l'échantillon.¹³² En diluant, l'intensité du bruit de fond diminue alors que celles des pics des NPs restent inchangées. Ceci va donc améliorer la SDL et permet de détecter les plus petites NPs. Cependant, la dilution peut être problématique lors de l'analyse des échantillons avec de faibles concentrations de NPs, tels que les échantillons environnementaux. Il a aussi été démontré que la dilution favorise la dissolution des NPs.¹³³

Une autre méthode de réduction du bruit de fond, consiste à faire passer la solution à analyser dans une résine échangeuse d'ions avant l'analyse par SP-ICP-MS.^{115, 134} Cette technique peut aussi être liée directement à l'ICP-MS. Ainsi, les cations métalliques se lient aux sites chargés négativement de la résine (forces électrostatiques), en échange avec d'autres cations. En revanche, les NPs sont peu retenues par la résine, sauf si elles possèdent une charge de surface positive.¹³⁴ Cependant, cette technique se limite seulement à l'élimination (ou la réduction) des ions métalliques de la solution alors que les complexes, qui peuvent être neutres ou chargés négativement, ne sont pas nécessairement retenus par la résine.

1.5.3.2. Interférences

Les interférences en ICP-MS peuvent être spectrales et non spectrales.¹³⁵ Les interférences non spectrales sont attribuées aux effets de matrice. Ce type d'interférence ne contribue pas nécessairement au signal du bruit de fond mais induit une diminution ou une augmentation du signal de l'ion de l'analyte. Les interférences non spectrales incluent la présence de certaines ions facilement ionisable tel que le sodium qui est connu pour conduire à une suppression du signal des autres ions présents en solution. Les interférences non spectrales peuvent être résolues par l'utilisation d'un étalon interne ou par simple dilution des échantillons. L'utilisation de l'étalon interne peut aussi être utile pour corriger pour des différences de viscosité parmi les échantillons ou entre l'échantillon et les étalons.¹⁰³

Les interférences spectrales se manifestent par la superposition du signal de l'ion de l'analyte avec celui d'un autre ion mono- ou polyatomique ayant un rapport m/z très proche.¹³⁵ Les interférences spectrales sont de trois types :^{98, 103, 135, 136}

- Les interférences isobariques monoatomiques observées lorsque deux isotopes de deux éléments distincts possèdent des rapports m/z très proches de façon que la résolution du spectromètre de masse ne permet pas de les discriminer. C'est le cas, par exemple, pour $^{40}\text{Ca}^+$ et $^{40}\text{Ar}^+$; $^{76}\text{Se}^+$ et $^{76}\text{Ge}^+$; ou $^{116}\text{Cd}^+$ et $^{116}\text{Sn}^+$.
- Les interférences isobariques polyatomiques résultent lorsque la combinaison de deux ou plusieurs ions donne un rapport m/z similaire à celui de l'analyte. Ces ions proviennent généralement du plasma (Ar) ou de la matrice de l'échantillon (H, C, N, O...). Parmi les exemples des interférences polyatomiques les plus

communes, on retrouve le $^{12}\text{C}^{16}\text{O}^+$ qui interfère avec le $^{28}\text{Si}^+$ et $^{140}\text{Ar}^{16}\text{O}^+$ qui interfère avec le $^{56}\text{Fe}^+$.

- Les interférences dues aux ions doublement chargés observées dans le cas où un ion doublement chargé possède un rapport m/z identique à celui de l'ion de l'analyte. En raison de leur abondance et/ou leur seconde énergie d'ionisation, certains éléments forment des ions doublement chargés dans le plasma, comme c'est le cas pour le $^{88}\text{Sr}^{2+}$ et le $^{136}\text{Ba}^{2+}$ qui interfèrent avec le $^{44}\text{Ca}^+$ et le $^{68}\text{Zn}^+$, respectivement.

Plusieurs stratégies ont été développées dans le but de réduire l'effet des interférences spectrales.

Isotope. Une méthode simple consiste à choisir un autre isotope, lorsque possible, de l'analyte qui présente moins d'interférences. Cependant, l'autre isotope choisi est généralement moins abondant ce qui entraîne une baisse de sensibilité.

Équations de correction. La plupart des interférences mono- ou polyatomiques a été identifiée. Des équations mathématiques peuvent être introduites dans le logiciel de l'ICP-MS pour corriger certains cas. En tenant compte de l'abondance des isotopes et en mesurant un autre isotope qui n'interfère pas, la contribution de l'isotope interférent peut être estimée et soustraite du signal de l'analyte.¹³⁷ Toutefois, l'utilisation de cette stratégie n'est pas possible lors d'une analyse en mode particule unique.

Cellules de réaction et de collision. L'utilisation d'une cellule de réaction ou de collision est très commune lors de la détermination de certains éléments afin de réduire les interférences. Dans la cellule de réaction, un gaz est introduit afin de réagir avec l'ion interférent. Deux mécanismes sont possibles pour la réaction entre le gaz et l'ion interférent: (1) donner lieu à un nouvel ion polyatomique avec une masse différente de celle de l'analyte; (2) neutraliser l'ion interférent via un échange de charge avec le gaz.¹⁰² De nombreux gaz ont été utilisés incluant le NH_3 , H_2 , CH_4 , O_2 , CO_2 , SF_6 , NO , CH_3F , et CS_2 .¹³⁷ Toutefois, les gaz ne sont pas spécifiques et même si seulement l'interférent est ciblé, ces gaz peuvent aussi réagir avec l'analyte.

Le principe de la cellule de collision est basé sur le fait que l'ion polyatomique interférent est plus grand de taille que l'ion analysé. Ainsi en traversant une cellule contenant un gaz inerte,

l'ion interférent va subir plus de collision avec le gaz que l'analyte. Chaque collision entraîne une perte d'une certaine quantité d'énergie cinétique. Une barrière d'énergie est placée à la sortie de la cellule, ainsi seulement les ions d'analyte qui possèdent une plus haute énergie peuvent traverser.¹⁰² Les inconvénients de cette méthode sont que la sensibilité de l'analyte va aussi diminuer, en raison de la fraction perdue par collision, et les interférences monoatomiques et doublement chargés ne sont pas éliminées.¹³⁷

Récemment, les instruments d'ICP-MS sont équipés d'une cellule dite universelle, qui peut agir comme une cellule de collision ou de réaction. Toutefois, l'utilisation de cette stratégie n'est pas possible lors d'une analyse en mode particule unique. Dans le cas des travaux effectués dans cette thèse, nous avons aussi eu la possibilité d'augmenter la résolution de l'analyse afin de séparer l'analyte et son interférence spectrale.

ICP-MS à haute résolution. Les instruments d'ICP-MS à haute résolution tel que la SF-ICP-MS sont capables de séparer la plupart des interférences spectrales. Tel que discuté précédemment, la résolution par SF-ICP-MS peut atteindre $m/\Delta m \sim 13000$, ce qui est suffisant pour résoudre de nombreuses interférences isobariques. Par exemple, lorsque le $^{56}\text{Fe}^+$ est déterminé par Q-ICP-MS (sans la cellule universelle), son signal ne peut être séparé de celui de l'ion interférent $^{40}\text{Ar}^{16}\text{O}^+$. Pour que la séparation ait lieu, une résolution de 2504 est requise, ce qui est facilement obtenu par SF-ICP-MS.⁹⁸ Cependant, la haute résolution est obtenue en réduisant la largeur de la fente d'entrée ce qui diminuera la transmission des ions. Cette diminution entraîne une diminution de la sensibilité. L'augmentation de résolution de 300 à 2504, diminuera la transmission des ions de 100% à 18%.⁹⁸ De même, la transmission des ions sera $< 2\%$ pour des résolutions > 10000 . Ainsi, bien que l'augmentation de la résolution permette de résoudre les interférences isobariques et diminuer le bruit de fond, elle réduit en parallèle la sensibilité ce qui conduit à une augmentation de la SDL.

D'autres méthodes ne sont pas reliées directement à la réduction des interférences, mais sont aussi utilisées dans le but d'augmenter le rapport signal / bruit, surtout en mode particule unique.

Désolvateur. Un désolvateur peut être couplé à l'ICP-MS et agit comme un système d'introduction. L'échantillon est nébulisé dans une chambre de nébulisation chauffée ($\sim 140^\circ\text{C}$) ce qui va conduire à l'évaporation du solvant. L'aérosol est ensuite acheminé vers une membrane

de désolvation chauffée à une plus haute température (~160 °C) où un flux d'Ar à contre-courant est balayé dans le but d'éliminer toutes traces de solvant.¹¹⁸ Par la suite, l'aérosol sec, constitué principalement des espèces non volatiles, est envoyé au plasma. En diminuant la quantité qui se rend au plasma, la sensibilité, l'efficacité de transport et l'extraction des ions augmentent. Par conséquent, la SDL diminue et les plus petites NPs peuvent être détectées.

Temps d'acquisition. Tel que discuté précédemment, l'utilisation de courts temps d'acquisition (de l'ordre de μ s) permet de mieux définir le signal mesuré et de diminuer le risque de coïncidence. Alors que la réduction des temps d'acquisition diminue l'intensité des pics des NPs et le signal du bruit de fond, le rapport signal/bruit augmente aux courts temps d'acquisition.¹³⁸
¹³⁹ Cette augmentation mènera à l'amélioration de la SDL.

Générateur de microgouttelettes. Ce dispositif produit des gouttelettes monodisperses à l'échelle de μ m. En raison de leurs petites tailles, les microgouttelettes sont acheminées au plasma avec une efficacité de transport de 100%.^{140, 141} L'augmentation de la TE se traduit par des SDLs inférieures à celles pouvant être atteintes avec un nébuliseur et une chambre de nébulisation conventionnels.

1.6. Objectifs de la thèse

L'objectif principal de la thèse est de développer une méthode analytique pour la détection, la quantification et la caractérisation des NPs de CeO₂ dans les eaux naturelles complexes. La SP-ICP-MS présente de nombreux avantages bien adaptés à l'analyse des NPs dans les matrices environnementales. Cependant, comparée à d'autres techniques d'analyse des NPs, le SP-ICP-MS est limité par des SDLs élevées, souvent causées par les interférences et/ou la présence du métal dissous. À cette fin, le **chapitre 2** vise à diminuer la SDL pour différents types de NPs (Ag, Au, et CeO₂) en utilisant un SF-ICP-MS à haute résolution et de courts temps d'acquisition (< 100 μ s). L'utilisation d'un SF-ICP-MS a augmenté la sensibilité de ~100 – 200 x par rapport au Q-ICP-MS ce qui a conduit à une diminution de SDL de ~5 x pour les trois types de NPs. Le SF-ICP-MS a ensuite été couplé à un désolvateur ce qui a conduit à une augmentation supplémentaire de sensibilité de ~5 x. Cette augmentation a permis de détecter des NPs d'Ag, d'Au et de CeO₂ aussi petites que 2 – 3 nm. Par la suite, la méthode optimisée a été utilisée pour détecter, caractériser et quantifier des NPs de CeO₂ dans deux échantillons d'eau naturelle : pluie

et rivière (collectées à Montréal). Suite à la détection, la nature des NPs de CeO₂ (manufacturés ou naturelles) a été évalué à l'aide de TOF-ICP-MS en mode particule unique.

En raison de ses nombreux avantages, le SP-ICP-MS est de plus en plus utilisé pour l'analyse des NPs dans les échantillons environnementaux. Cependant, il n'existe pas de protocole unifié pour la préparation d'échantillons d'eau naturelle pour l'analyse par SP-ICP-MS. Afin de minimiser le blocage du nébuliseur, la filtration est souvent utilisée dans l'espoir que les membranes de 0.45 µm n'élimineront pas les NPs de 1 – 100 nm. Néanmoins, il existe des données limitées sur l'effet de la filtration sur les concentrations et les distributions de taille des NPs. Ainsi, l'objectif principal du **chapitre 3** est de développer une méthode de préparation d'un échantillon d'eau naturelle pour l'analyse par SP-ICP-MS. À cette fin, des filtres de différents types de membrane (polyfluorure de vinilydène, polyéthersulfone, polypropylène, polytétrafluoroéthylène, nylon et acétate de cellulose) ont été testés pour évaluer l'effet de filtration sur l'analyse des NPs d'Ag et de CeO₂ dans des échantillons aqueux. La centrifugation a aussi été évaluée comme une méthode alternative pour la préparation d'échantillons avec moins de potentiel de pertes d'adsorption.

La peinture constitue l'une des applications les plus importantes des NPs de CeO₂ en raison de leur propriété de protection contre l'UV. Récemment, quelques chercheurs ont mesuré le relargage des NPs de CeO₂ par la peinture. Cependant, ces études ont été réalisées dans des conditions contrôlées au laboratoire. Ainsi, les informations quantitatives sur le relargage des NPs de CeO₂ des produits de peinture sous les conditions météorologiques naturelles ne sont pas encore disponibles. À la suite du relargage, une compréhension détaillée du devenir et du comportement des NPs dans l'environnement est essentiel pour l'évaluation de leur risque. Ainsi, bien que le devenir des NPMs de CeO₂ dans des milieux présentant différentes conditions (pH, force ionique, présence de la matière organique naturelle) a bien été étudié, les études ont généralement examiné des suspensions des NPMs dans des échantillons d'eau naturelle simulée. Ainsi, les données sur le devenir et le comportement des NPs de CeO₂ originellement présents dans des produits commerciaux ne sont pas encore disponibles. Considérant le manque d'information, les objectifs du **chapitre 4** sont : (i) d'examiner l'effet des différentes propriétés physicochimiques sur les NPs de CeO₂ contenues dans la peinture et la teinture; (ii) évaluer leur

stabilité dans un échantillon de précipitation; et (iii) quantifier et caractériser leur relargage dans des scénarios météorologiques naturels.

1.7. Contribution des auteurs

Chapitre 2. *Publié dans le journal Molecules.* Ma contribution dans ce chapitre consiste d'abord en la conception et la planification des expériences (choix des nanoparticules et des caractéristiques de l'ICP-MS). De même, j'ai collecté, préparé et analysé les échantillons par Q- et SF-ICP-MS. Avec l'aide de Madjid Hadioui, j'ai traité les données de Q- et SF-ICP-MS. Agil Azimzada a participé à la collection des échantillons naturels, a effectué les analyses et a traité les données du TOF-ICP-MS. J'ai rédigé la première version du manuscrit qui a été commenté et révisé par Madjid Hadioui et Pr. Kevin J. Wilkinson, qui m'a aussi supervisé tout le long de l'étude.

Chapitre 3. *Publié dans le journal Talanta.* Dans ce chapitre, j'ai conçu et planifié les expériences. J'ai choisi les différents types de filtres et de NPs à investiguer ainsi que les différentes conditions des expériences (nature de solution de pré-conditionnement, vitesse de centrifugation). J'ai également collecté, préparé et analysé les échantillons par SF-ICP-MS. Après le traitement des données, j'ai rédigé le manuscrit qui a été commenté et révisé par Madjid Hadioui et Pr. Kevin J. Wilkinson.

Chapitre 4. *Soumis au journal ES Nano.* Ce chapitre peut être divisé en deux expériences : (1) Devenir et stabilité des NPs dans la peinture et la teinture; et (2) Relargage des NPs de la peinture et la teinture. J'ai conçu et planifié la première expérience en choisissant les différentes conditions : grandeur de pH, concentration des sels, et type et quantité de NOM. J'ai également collecté, préparé et analysé les échantillons par SF-ICP-MS. Agil Azimzada a conçu et planifié la deuxième expérience et on a collecté les échantillons ensemble. Carolyn Liu-Kang a préparé les échantillons et a effectué l'analyse sur Q-ICP-MS. Après le traitement des données, j'ai rédigé le manuscrit qui a été commenté et révisé par Madjid Hadioui et Pr. Kevin J. Wilkinson.

Pendant mon doctorat j'ai aussi participé aux analyses, traitements de données et rédaction de cinq autres publications :

- 1- Morel, E.; Jreije, I.; Tetreault, V.; Hauser, C.; Zerges, W.; Wilkinson, K. J., Biological impacts of Ce nanoparticles with different surface coatings as revealed by RNA-Seq in *Chlamydomonas reinhardtii*. *NanoImpact* **2020**, *19*, 100228.
- 2- Azimzada, A.; Jreije, I.; Hadioui, M.; Shaw, P.; Farner, J. M.; Wilkinson, K. J., Quantification and Characterization of Ti-, Ce-, and Ag-Nanoparticles in Global Surface Waters and Precipitation. *Environmental Science & Technology* **2021**, *55* (14), 9836-9844.
- 3- Hadioui, M.; Knapp, G.; Azimzada, A.; Jreije, I.; Frechette-Viens, L.; Wilkinson, K. J., Lowering the Size Detection Limits of Ag and TiO₂ Nanoparticles by Single Particle ICP-MS. *Analytical Chemistry* **2019**, *91* (20), 13275-13284.
- 4- Azimzada, A.; Farner, J. M.; Jreije, I.; Hadioui, M.; Liu-Kang, C.; Tufenkji, N.; Shaw, P.; Wilkinson, K. J., Single- and Multi-Element Quantification and Characterization of TiO₂ Nanoparticles Released from Outdoor Stains and Paints. *Frontiers in Environmental Science* **2020**, *8* (91).
- 5- Azimzada, A.; Farner, J. M.; Hadioui, M.; Liu-Kang, C.; Jreije, I.; Tufenkji, N.; Wilkinson, K. J., Release of TiO₂ nanoparticles from painted surfaces in cold climates: characterization using a high sensitivity single-particle ICP-MS. *Environmental Science: Nano* **2020**, *7* (1), 139-148.

Chapitre 2 – Measurement of CeO₂ nanoparticles in natural waters using high sensitivity, single particle ICP-MS

2.1. Abstract

As the production and use of cerium oxide nanoparticles (CeO₂ NPs) increases, so does the concern of the scientific community over their release into the environment. Single particle inductively coupled plasma mass spectrometry is emerging as one of the best techniques for NP detection and quantification; however, it is often limited by high size detection limits (SDL). To that end, a high sensitivity sector field ICP-MS (SF-ICP-MS) with microsecond dwell times (50 μs) was used to lower the SDL of CeO₂ NPs to below 4.0 nm. Ag and Au NPs were also analyzed for reference. SF-ICP-MS was then used to detect CeO₂ NPs in a Montreal rainwater at a concentration of $(2.2 \pm 0.1) \times 10^8 \text{ L}^{-1}$ with a mean diameter of $10.8 \pm 0.2 \text{ nm}$; and in a St. Lawrence River water at a concentration of $((1.6 \pm 0.3) \times 10^9 \text{ L}^{-1})$ with a higher mean diameter ($21.9 \pm 0.8 \text{ nm}$). SF-ICP-MS and single particle time of flight ICP-MS on Ce and La indicated that 36% of the Ce-containing NPs detected in Montreal rainwater were engineered Ce NPs.

2.2. Introduction

Due to their unique properties, engineered nanomaterials are now widely used in numerous commercial products. Cerium oxide (CeO₂) nanoparticles (NPs) are among the most commonly used engineered NPs, with applications in catalysis,^{52, 142, 143} the manufacturing of semiconductors,¹⁴² biomedicine¹⁴⁴ and agriculture,¹⁴⁵ among other fields. For example, they are commonly found as UV filters in sunscreens, additives in diesel fuels and as a component of paints and stains.^{121, 146} With the significant increase in the production and use of CeO₂ NPs, concern is increasing over their release into the environment and their subsequent fate and toxicity. Among their important environmental pathways, CeO₂ NPs can be released into the air by diesel emissions; into soils from solid waste and recycling and into aquatic systems from the effluents of wastewater treatment plants.⁵² Furthermore, a number of recent papers^{117, 147, 148} have measured the release of CeO₂ NP from surface coatings such as paints and stains. Nonetheless, the vast majority of data on the concentrations, fate and transformations of CeO₂ NP in the environment have been generated by modelling,^{28, 149} or extrapolated from release studies

performed under controlled laboratory conditions. This is mainly because the direct analysis of CeO₂ NPs in the environment is extremely challenging due to their small sizes (often below 20 nm), their low concentrations (on the order of ng L⁻¹) and the complexity of environmental matrices, which also contain natural colloids.

Techniques based upon inductively coupled plasma mass spectrometry (ICP-MS) are likely to be the most promising for detecting and quantifying inorganic NP in biological and environmental samples. Particle size distributions can be obtained either by coupling a separation technique such as field flow fractionation (FFF)¹⁵⁰ or hydrodynamic chromatography (HDC)¹⁵¹ upstream of the ICP-MS or by performing ultrafast measurements on single particles (single particle (SP) ICP-MS). SP-ICP-MS combines the specificity and sensitivity of mass spectrometry with a particle-by-particle analysis, enabling quantification of very low NP concentrations (ng L⁻¹) and information on their number concentrations, sizes, and size distributions. Transient ion clouds that are created from the NP in the plasma (typically 300–500 μs) are directly related to the particle number concentrations, while the signal intensity is related to particle (elemental) mass.¹⁵² For a given NP composition, density and geometry, particle size can be calculated.

The very small NPs are expected to have a greater environmental risk, due to their increased propensity to cross biological membranes.^{153, 154} Therefore, it is especially important to obtain rigorous size, concentration, and fate data for the smallest NP. The minimal particle size (size detection limit = SDL) that can be measured by SP-ICP-MS depends largely upon the signal to noise ratio. A number of approaches have been employed to decrease the SDL¹¹⁸ including: sample dilution, judicious choice of isotopes, interference removal strategies,^{115, 155} shorter dwell times,¹⁵⁶ etc.

The first objective of this study was to decrease the SDL for CeO₂ NPs using a high sensitivity sector field ICP-MS (SF-ICP-MS), very short dwell times (<100 μs) and the introduction of a dry aerosol. The optimized method was then used to detect, quantify, and characterize CeO₂ NPs in several natural water samples.

2.3. Results and Discussion

2.3.1. Optimization of SP-ICP-MS for CeO₂ NPs

In single particle ICP-MS, size detection limits (SDL) are minimized for Ce NPs by optimizing the signal/noise (S/N) for ¹⁴⁰Ce⁺. In this case, noise includes both electronic noise and background concentrations, comprised of isobaric and polyatomic interferences, dissolved Ce and Ce NPs that are smaller than the SDL. The impact of dwell times on the SDL¹⁵⁶ was first tested on a suspension of CeO₂ NPs in Milli-Q water, with or without dissolved Ce. While both spike intensity and background signal decreased as dwell time was decreased from 500 to 20 μs (Figure 2-S1), S/N was clearly improved at the shorter dwell times (Figure 2-1). For example, for a decrease in dwell time from 500 μs to 20 μs, the SDL decreased from 4 nm to 2.2 nm in Milli-Q water (Figure 2-1A) and from 6.2 nm to 3.8 nm when the data were acquired in the presence of 10 ng L⁻¹ of dissolved Ce (Figure 2-1B). Although the lowest SDL was measured with a 20 μs dwell time, it was not used further here since analysis was limited to one million datapoints per run (and thus an overall analysis time of 20 s). For environmental samples, longer acquisition times better ensure representativity by better taking into account sample polydispersity and low particle numbers. Given the slight difference in SDL between dwell times of 20 and 50 μs (Figure 2-1), a dwell time of 50 μs and a corresponding 50 s acquisition time were used in a majority of subsequent experiments.

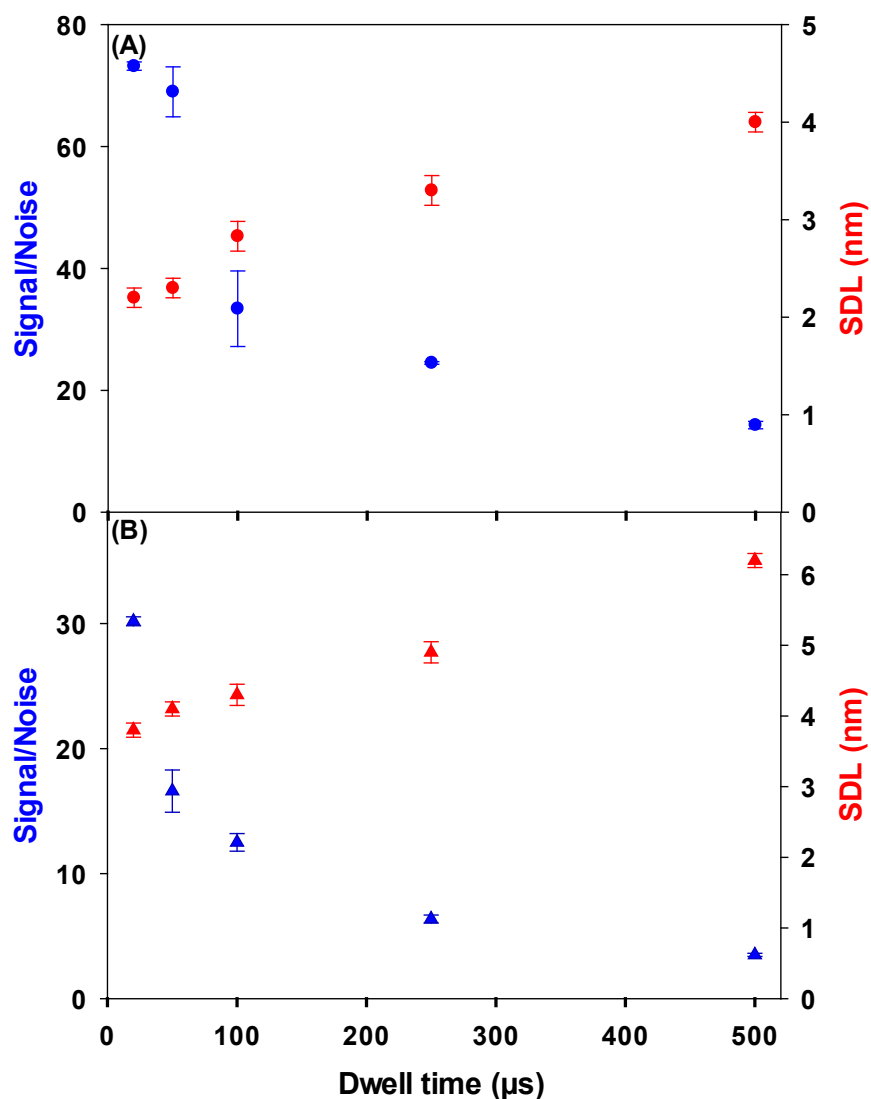


Figure 2-1 Signal/noise (blue) and size detection limits (red) as a function of dwell time for: (A) a 10 ng L⁻¹ suspension of CeO₂ NPs (1–10 nm) in Milli-Q water; (B) a 10 ng L⁻¹ suspension of CeO₂ NPs (1–10 nm) in a Milli-Q water containing 10 ng L⁻¹ of ionic Ce. Signal/Noise was determined by dividing the average intensity of a well resolved peak of a 9 nm CeO₂ NP by the average intensity of the continuous background. All measurements were obtained using SF-ICP-MS and sample introduction via a desolvator.

Sensitivity and transport efficiency were determined for gold, silver and CeO₂ NPs using a quadrupole based ICP-MS (Q-ICP-MS) and a SF-ICP-MS, using wet or dry (i.e., desolvator) sample introduction. Sensitivity increased about 100× for Ag and 200× for Au and Ce when

using the SF-ICP-MS as compared to the Q-ICP-MS (Table 2-1). This increase of sensitivity led to a lowering of the SDL from 16.3 to 4.7 nm for Ag; from 19.0 to 4.4 nm for Au and from 16.8 to 4.0 nm for CeO₂. For the Q-ICP-MS, similar SDL have previously been reported for CeO₂ in the literature.^{114, 146} When the sample was introduced as a dry aerosol, sensitivity increased a further 5× for Ag and Au and 3× for Ce, resulting in a lowering of the SDLs to 3.1 nm (Ag), 2.8 nm (Au) and 2.3 nm (CeO₂) (Table 2-1).

Table 2-1 Sensitivity for Ag, Au and Ce and corresponding size detection limits for Ag, Au and CeO₂ NPs in Milli-Q water obtained using a quadrupole (Q-) or sector field (SF-) ICP-MS running with (dry) or without a desolvator (wet). A 50 μs dwell time was used. Means and standard deviations are obtained from analysis on three different dates.

Analyte	Sensitivity (Counts fg ⁻¹)			Nanoparticle	Size detection limit (nm)		
	Q-ICP-MS	SF-ICP-MS			Q-ICP-MS	SF-ICP-MS	
		Wet	Dry			Wet	Dry
Ag	50 ± 19	4750 ± 1200	22300 ± 2400	Ag	16.3 ± 2.1	4.7 ± 0.2	3.1 ± 0.3
Au	15 ± 3	2900 ± 800	13700 ± 1200	Au	19.0 ± 1.0	4.4 ± 0.1	2.8 ± 0.1
Ce	72 ± 15	14800 ± 700	47900 ± 8600	CeO ₂	16.8 ± 1.1	4.0 ± 0.2	2.3 ± 0.2

The role of membrane desolvation was further evaluated by comparing size distributions and particle number concentrations for small Ag, Au and CeO₂ NPs (nominally 10 nm Ag, 10 nm Au and 1–10 nm CeO₂), using both dry and wet aerosol introduction (Table 2-2). Some smaller NPs were detected using the dry-SP-ICP-MS due to the lower SDL, consequently leading to higher particle number concentrations (approximately 1.5× more NPs when compared to wet aerosol injection) and a lower average particle size (Figure 2-2).

The difference between the two setups became more significant for an increasing proportion of dissolved metal in the suspensions, which reversed the impact of the desolvator. For example, when a 10 ng L⁻¹ suspension of CeO₂ NPs was spiked with 10 ng L⁻¹ of dissolved Ce, particle size distributions were similar, with similar average sizes (8.1 ± 0.1 nm for dry-SF-ICP-MS and 8.3 ± 0.1 nm for wet-SF-ICP-MS) (Figure 2-S2A), however, nearly 1.6× more CeO₂ NPs were detected using wet-SF-ICP-MS as compared to dry-SF-ICP-MS. Moreover, when a 10 ng L⁻¹ suspension of CeO₂ NPs was spiked with 50 ng L⁻¹ of dissolved Ce, significantly different

particle number concentrations were measured with the two introduction systems with nearly 5× more CeO₂ NPs detected by wet-SF-ICP-MS (Figure 2-S2B). It would appear that when using the desolvator, both the background signal and the NP signal increased, however, background increased to a greater proportion. Therefore, in the presence of significant dissolved metal, the S/N decreased when using dry-SF-ICP-MS as compared to the wet-SF-ICP-MS (Figure 2-S3). For example, for a 9.0 nm CeO₂ NP combined with 50 ng L⁻¹ of dissolved Ce, the S/N was 2.8 ± 0.3 when using dry-SF-ICP-MS and 6.8 ± 0.1 when using wet-SF-ICP-MS. When NP suspensions containing increasing dissolved Ce were analyzed in single particle SF-ICP-MS, results clearly showed that the desolvator was more sensitive to the presence of the dissolved fraction with higher SDLs as compared to the wet-SF-ICP-MS (Figure 2-S4). Therefore, although smaller SDLs could be determined by dry-SF-ICP-MS for very low concentrations of dissolved Ce; due to an unknown and variable proportion of dissolved Ce, the introduction of a wet aerosol was prioritized for natural samples.

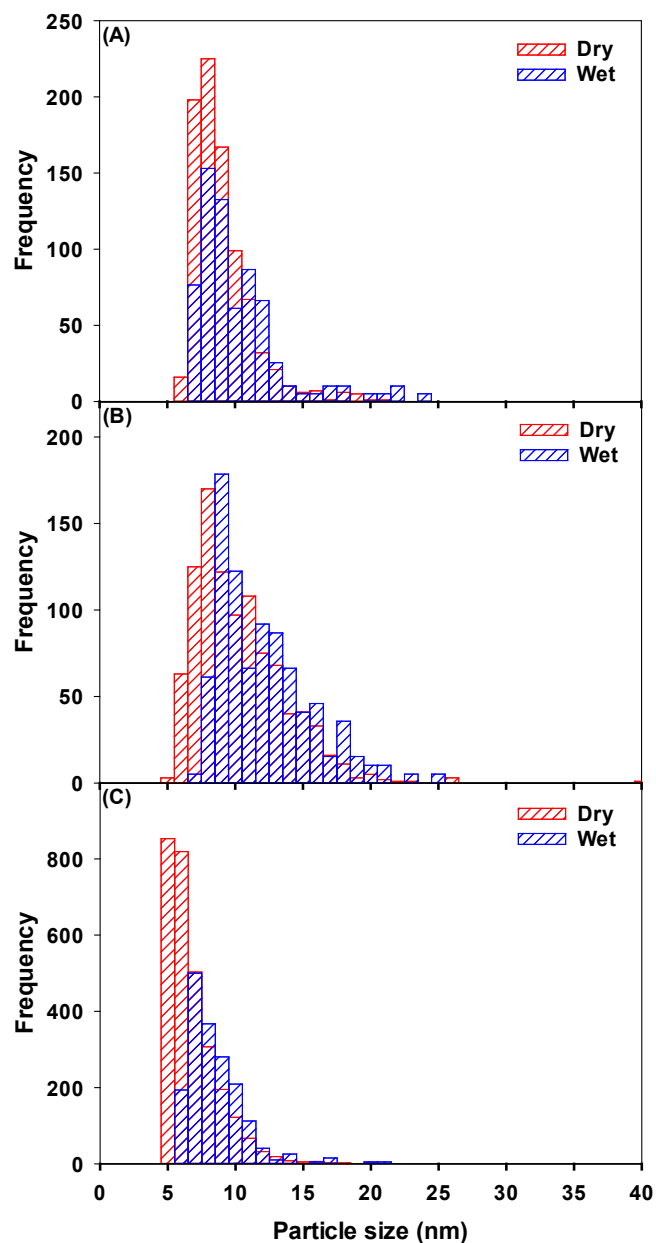


Figure 2-2 Particle size distributions as measured by wet-SF-ICP-MS (blue) and dry-SF-ICP-MS (red) for 3 suspensions of a small NP: **(A)** Ag: the mean particle size \pm polydispersity of the suspension was 8.5 ± 2.2 with dry introduction and 9.8 ± 3.3 with wet introduction; **(B)** Au: the mean particle size \pm polydispersity of the suspension was 9.8 ± 3.4 with dry introduction and 11.8 ± 3.6 with wet introduction; **(C)** CeO₂: the mean particle size \pm polydispersity of the distribution in the suspension was 6.3 ± 2.0 with dry introduction and 8.0 ± 2.1 with wet introduction.

Table 2-2 Average particle sizes, number concentrations and SDL in 10 ng L⁻¹ suspensions of Ag, Au and CeO₂ NPs. Means and standard deviations are obtained from the analysis of triplicate samples.

NP Suspension	Average Particle Size (nm)		NP Number Concentration ($\times 10^7$ L ⁻¹)		SDL (nm)	
	Wet	Dry	Wet	Dry	Wet	Dry
Ag	9.3 ± 0.4	8.5 ± 0.1	5.5 ± 0.6	7.7 ± 0.2	4.6 ± 0.1	3.1 ± 0.1
Au	11.8 ± 0.1	9.7 ± 0.1	6.6 ± 0.8	8.9 ± 0.1	4.2 ± 0.1	3.1 ± 0.1
CeO ₂	8.0 ± 0.1	6.3 ± 0.0	20.9 ± 0.4	26.3 ± 1.5	4.1 ± 0.1	2.8 ± 0.1

2.3.2. Ce-Containing NPs in Natural Waters: Rainwater

The wet-SF-ICP-MS was first used to determine whether Ce NP could be detected in rain. In the rainwater matrix alone, significant numbers of Ce-containing NPs were found, with a mean particle diameter of 10.8 ± 0.2 nm (Figure 2-3C, calculated under the assumption that the particles were spherical CeO₂ NPs). Subsequently, 10 ng L⁻¹ of 1–10 nm CeO₂ NPs were spiked into the rainwater and compared with observations performed in Milli-Q water. An average particle diameter of 7.9 ± 0.2 nm was determined in Milli-Q water (Figure 2-3A), which was smaller than the size obtained for the NP spiked into rainwater (9.5 ± 0.4 nm, Figure 2-3B). About three times more CeO₂ NPs were detected in the spiked rainwater (5.1×10^8 NPs L⁻¹) as compared to the spiked Milli-Q water (1.6×10^8 NPs L⁻¹), which was reasonable given the initial NP numbers found in the unspiked rainwater (3.8×10^8 NPs L⁻¹). These values corresponded to a recovery for the spike of $84 \pm 16\%$. The slightly smaller than expected recovery could be attributed to an increased aggregation of CeO₂ NPs in the natural precipitation (increased ionic strength), as compared to the Milli-Q water. Note that recovery of total Ce in the rainwater, determined on acidified samples, was $78 \pm 24\%$.

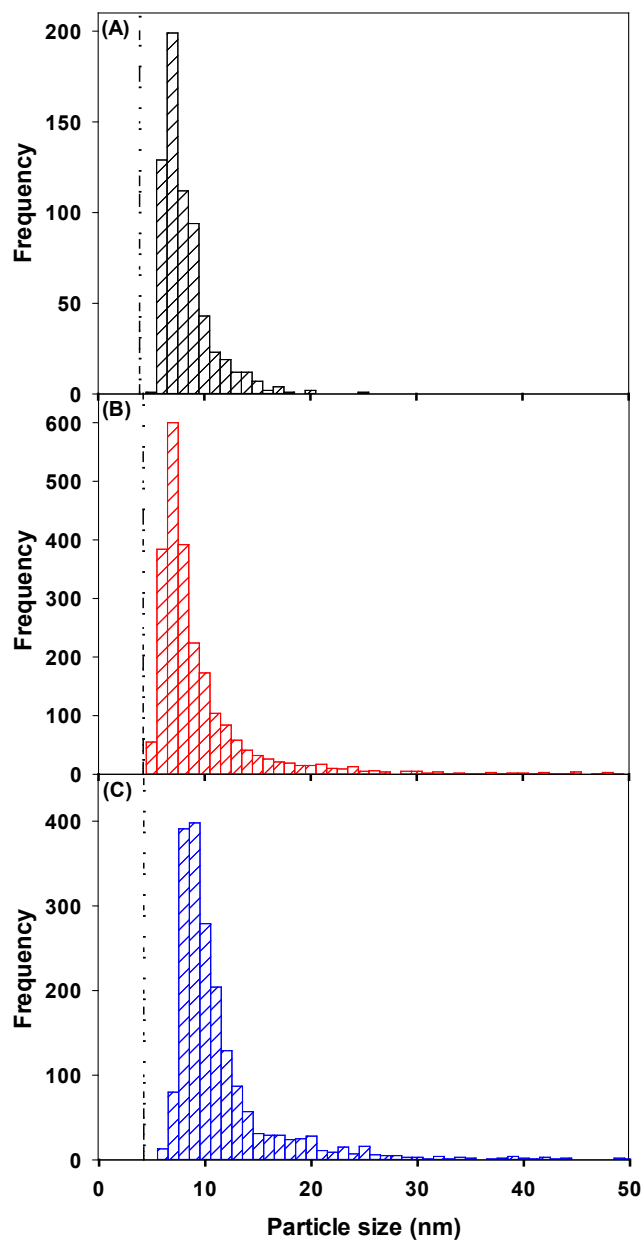


Figure 2-3 Particle size distribution of a suspension of CeO₂ NPs with a nominal size of 1–10 nm. NP were spiked into (A) Milli-Q water or (B) rainwater. (C) Particle size distribution for Ce-containing NPs in rainwater, determined under the assumption that they were spherical CeO₂ NPs with a density of 7.13 kg dm⁻³.¹⁵⁷ The dashed line corresponds to the SDL. The mean particle size ± polydispersity of the CeO₂ NPs was (A) 11.0 ± 5.8 nm; (B) 7.7 ± 2.4 nm and (C) 9.2 ± 6.1 nm. Measurements were obtained using the wet-SF-ICP-MS with a 50 μs dwell time.

2.3.3. Ce-Containing NPs in Natural Waters: Riverwater

When unspiked, unfiltered and undiluted St. Lawrence River water samples were analyzed by SP-ICP-MS for ^{140}Ce , the raw data clearly showed the presence of spikes, strongly indicating the presence of Ce containing NPs or, alternatively, larger particles with a minor Ce component (Figure 2-S5). Under the assumption that the detected particles correspond to spherical CeO_2 NPs, particle size distributions could be estimated (Figure 2-4). An average particle size of 21.9 ± 0.8 nm was determined for particles sampled from the Saint Lawrence River (means and errors correspond to triplicate samples) (Table 2-3). The larger particle size, as compared to the rainwater sample could be attributed to both analytical and geochemical differences, i.e., (i) the hardness ions in the St. Lawrence River ($\sim 130 \text{ mg L}^{-1}$)¹⁵⁸ are expected to induce some agglomeration of the NPs; (ii) the lower pH of the rainwater (pH = 5.4), with respect to St. Lawrence River (pH = 6.8), could facilitate greater particle dissolution and (iii) the higher dissolved (background) Ce in the river water sample resulted in a higher SDL (6.2 nm, Table 2-3), which could slightly increase the overall average particle size. Note that $\sim 7\times$ more NPs and $\sim 60\times$ more particle mass was determined in the river water with respect to the rainwater. Ce NP concentrations in the river water were $107 \pm 26 \text{ ng L}^{-1}$ (Table 2-3), in line with concentrations predicted by modelling (24 ng L^{-1} ,¹⁵⁹; $0.6\text{--}100 \text{ ng L}^{-1}$,¹⁶⁰) and the limited available experimental data ($0.4\text{--}5.2 \text{ ng L}^{-1}$,¹⁶¹). While it might be tempting to attribute the slightly higher concentrations of Ce NP to greater emissions in the St. Lawrence, it is more likely that additional NPs were detected due to the lower detection limits in this study. Nonetheless, for the majority of detected NPs, similar particle size distributions were determined in the St. Lawrence River (mean diameter ~ 19 nm; Figure 2-4), as were observed in the Meuse and IJssel Rivers in the Netherlands ($14\text{--}21$ nm, mean 19 nm).¹⁶¹ Such a narrow distribution of NP in such geographically different samples suggests either a similar source for the NPs or similar removal processes such as agglomeration leading to removal of the larger particles.^{162, 163}

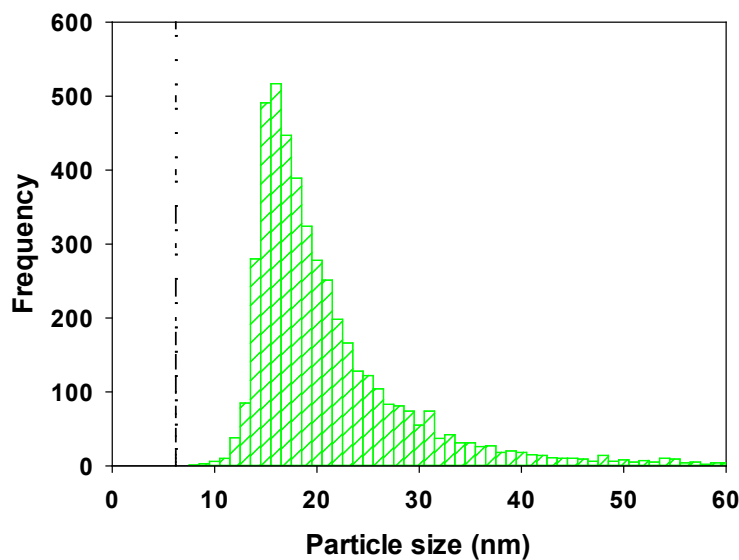


Figure 2-4 Particle size distributions of Ce containing NPs in a sample taken from the St. Lawrence River. The mean particle size \pm polydispersity corresponded to 21.0 ± 9.2 nm. The dashed line corresponds to the SDL. Measurements were obtained using the wet-SF-ICP-MS with a $50 \mu\text{s}$ dwell time. NP sizes were calculated by assuming that the particles were spherical CeO_2 particles with a density of 7.13 kg dm^{-3} .¹⁵⁷

Table 2-3 Concentration of dissolved Ce, number and mass concentrations of CeO_2 NPs and SDL in the rainwater and in the St. Lawrence River. Means and standard deviations are obtained from the analysis of triplicate samples.

Water natural sample	Mass concentration of dissolved Ce (ng L^{-1})	Number concentration ($\times 10^9 \text{ CeO}_2 \text{ NPs L}^{-1}$)	Mass concentration of CeO_2 NPs (ng L^{-1})	SDL (nm)
Montreal rainwater	4.0 ± 0.1	0.22 ± 0.01	1.9 ± 0.1	4.6 ± 0.1
St. Lawrence River	53 ± 17	1.6 ± 0.3	107 ± 26	6.2 ± 0.6

2.3.4. Effect of Sample Filtration

Although the natural samples can be analyzed unfiltered, some of the larger particles can block the nebulizer. Given that we were interested in quantifying the smallest (nano) particles, the effect of $0.45 \mu\text{m}$ membrane filtration was examined for a natural sample. For a St. Lawrence

River water sample examined before or after filtration, filtration decreased background Ce concentrations by 30%, which was attributed to an adsorption of dissolved Ce on the filters. The decrease of dissolved Ce led to a decrease in the SDL, which may explain the small shift of the particle size distribution to lower sizes (Table 2-S1 and Figure 2-S6). Nonetheless, in spite of having a lower SDL, NP numbers decreased almost by 30% after filtration, which was attributed mainly to the removal of large particles (i.e., $>0.45 \mu\text{m}$) with some minor losses of Ce and/or small Ce-containing NPs to the filters via adsorption.

2.3.5. Ce-containing NPs in natural waters: temporal variations

Temporal variations of the Ce NPs were examined by collecting rainwater samples between October 2018 and December 2018 and river water samples between August 2019 and September 2019. In the rainwater, the concentration of CeO₂ NPs varied from $(0.1\text{--}3.8) \times 10^8 \text{ L}^{-1}$, while they varied from $(1.1\text{--}7.2) \times 10^8 \text{ L}^{-1}$ in the river water (Figure 2-5A). Although particle number variations were more important in the rainwater (38 \times), as compared to the river water (7 \times), particle sizes were fairly similar in all samples (Figure 2-5B). In contrast, NP sizes in the river water were smaller than those detected previously in the same water catchment (St. Lawrence), but much further downstream stream (Figure 2-4). This result can be explained by the difference in sampling locations, which would indicate that the Ce-containing NPs are both time and geographically dependent (Figure 2-S7).

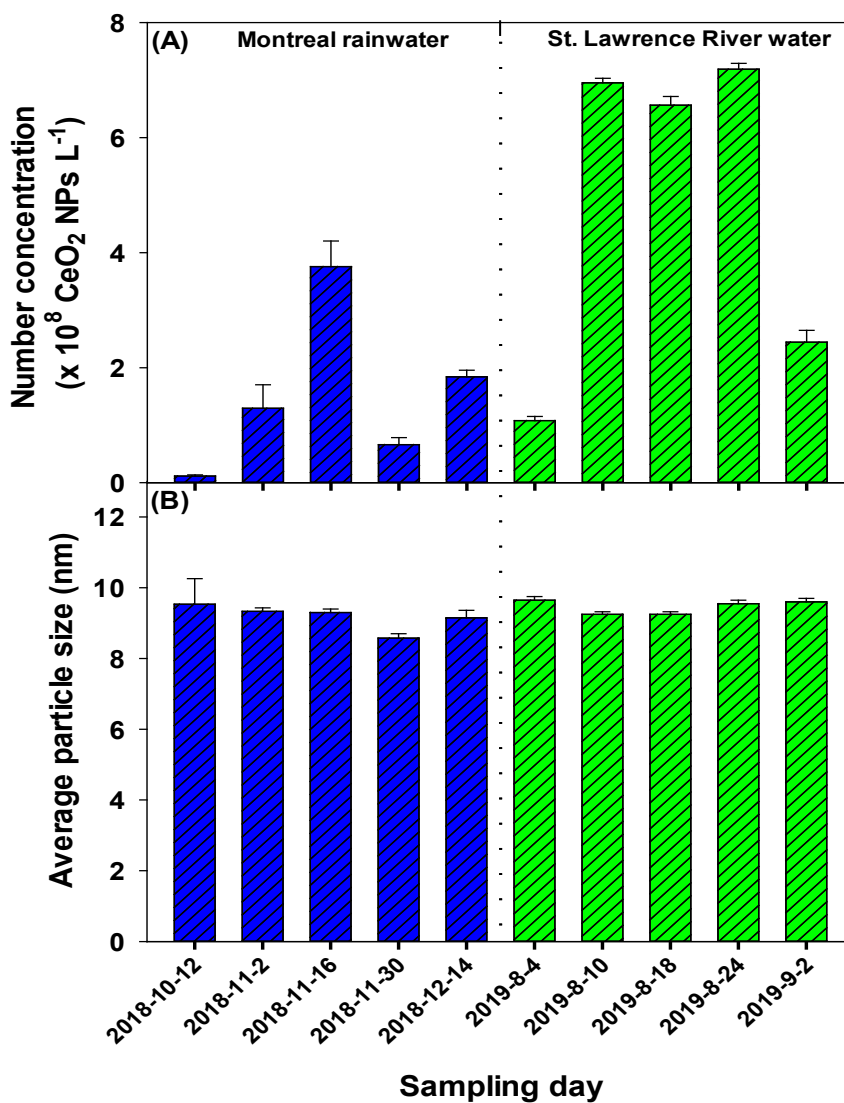


Figure 2-5 (A) Number concentrations and (B) mean particle sizes for CeO₂ NPs measured on different dates in rainwater (blue) and St. Lawrence River water (green). Error bars correspond to standard deviations obtained from triplicate analysis. Measurements were performed using wet-SF-ICP-MS and a dwell time of 50 μ s.

2.3.6. Engineered or Natural CeO₂ NPs?

It is very difficult to non-ambiguously distinguish between engineered and natural NPs in the environment. Most commonly, it is assumed that engineered NPs (including metal oxides) contain a single metal, while natural NPs are often multi-element.¹⁶⁴ For Ce NPs, the Ce/La ratio has been used to differentiate the two types of NPs^{165, 166} since the rare earth elements are

naturally nearly always found as mixtures. Natural NPs can be formed by mechanical erosion, weathering or precipitation¹⁶⁷ in which case, they are likely to have a similar composition as the minerals in sediments and soils. For example, Ce is found with La in minerals such as bastnasite with a Ce/La ratio of 1.5^{52, 168} and in monazite with a Ce/La ratio of 1.8.^{52, 168} In the earth's crust, a Ce/La ratio of 2.1¹⁶⁹ has been documented. In that light, Montañó et al.¹⁶⁴ compared Ce/La ratios of nearly 100 surface water samples collected from three European countries to the Ce/La ratios of 807 water samples collected across a wide geographical range in Europe. In those samples, a fairly stable Ce/La ratio of 1.7 was measured.

In order to determine whether the NP contained only Ce or several metals, SF-ICP-MS was first used to measure individual particles for their Ce and La contents, albeit in different particles. Results were later validated with TOF-ICP-MS, run in single particle mode, which measures multiple elements in a single nanoparticle. The TOF-ICP-MS that was employed had a sensitivity for Ce (1720 counts fg^{-1}) that was about 24 \times higher than the Q-ICP-MS (72 counts fg^{-1}) but lower than the SF-ICP-MS (14,800 counts fg^{-1}) and was necessarily limited to larger nanoparticles (SDL \sim 11 nm).

The rainwater was analyzed for its Ce and La contents by SF-ICP-MS. Similar sensitivities were measured for La (14,600 \pm 1700 counts fg^{-1}) and Ce (13,600 \pm 500 counts fg^{-1}), which led to similar SDLs in the rainwater of 4.4 \pm 0.1 nm for La₂O₃ and 4.6 \pm 0.1 nm for CeO₂. The raw data clearly indicated the presence of both Ce and La NPs or indeed composite NPs (Figure 2-S8). As a control, no La (dissolved or NP) was detected in the suspension of 1–10 nm CeO₂ NPs. Detected Ce and La NPs showed similar mean sizes and size distributions (Table 2-S2, Figure 2-6). Concentrations of both the dissolved and particulate forms of Ce were almost 2 \times those of La with a Ce/La NP ratio of 2.2 \pm 0.6 and a total Ce/La ratio of 2.4 \pm 2.2 (Table 2-4). The slightly higher values, when compared to the expected global natural ratio of 1.7, was suggestive of the presence of engineered (single element) CeO₂ NPs in the rainwater.

Table 2-4 Ratios of Ce to La determined in the Montreal rainwater, obtained using the SF-ICP-MS run in single particle mode with a dwell time of 50 μs . Means and standard deviations were obtained from triplicate samples.

Water natural sample	Fraction of Ce NPs (%)	Fraction of La NPs (%)	Ce NPs / La NPs	Dissolved Ce / Dissolved La	Total Ce / Total La
Montreal rainwater	46.3 \pm 8.8	50.6 \pm 3.9	2.2 \pm 0.6	2.6 \pm 1.8	2.4 \pm 2.2

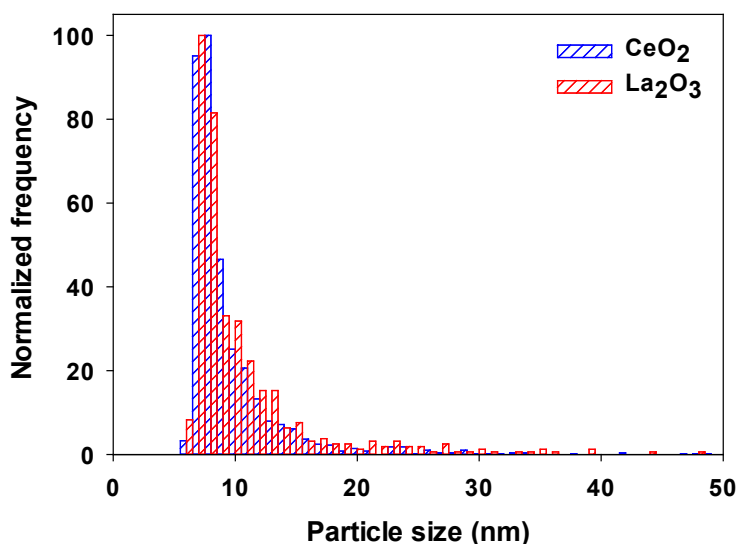


Figure 2-6 Particle size distributions of Ce- (blue) and La- (red) containing NPs found in a Montreal rainwater. Particle size distributions were calculated by assuming spherical particles of pure CeO_2 (density= 7.13 kg dm^{-3})¹⁵⁷ and La_2O_3 (density= 6.51 kg dm^{-3}).¹⁷⁰ Measurements were obtained using the wet-SF-ICP-MS with a 50 μs dwell time.

The rainwater sample was re-analyzed by TOF-ICP-MS in single particle mode. Given the size quantification limits (SQLs of $\sim 16 \text{ nm}$ for Ce and for La), only few Ce-containing particles were detected in the rainwater ($1.5 \times 10^6 \text{ L}^{-1}$). Nonetheless, for 36% of the Ce-containing nanoparticles in the rainwater, no second element was detected (Figure 2-7 and Figure 2-S9).

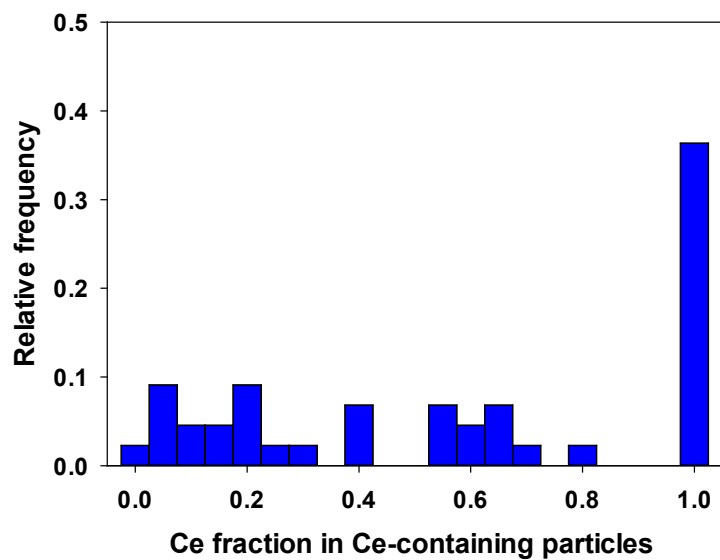


Figure 2-7 Detected proportion of Ce in Ce-containing particles measured in a Montreal rainwater. A Ce fraction of 1 indicates a pure Ce NP, while a fraction < 1 indicates the presence of other elements in the particles. Measurements were obtained using the TOF-ICP-MS with a 76.5 μ s dwell time; SDL (Ce) = 11 nm and SQL (Ce) = 16 nm.

2.4. Materials and Methods

2.4.1. Engineered NPs

The cerium oxide NPs used in this study were purchased as an aqueous dispersion of citrate stabilized CeO₂ NPs with a nominal size range of 1–10 nm (Nanobyk[®]-3810, Byk, Germany). Silver and gold NPs were used to determine transport efficiency and validate instrumental sensitivity and precision. Ag NPs were purchased from NanoComposix (San Diego, CA, USA) as a citrate stabilized suspension with nominal sizes of either 10 nm (NanoXact, AGCN10) or 20 nm (NanoXact, AGCN20). Three Au NPs were used. One was purchased as citrate stabilized suspension from NanoComposix (10 nm, NanoXact, AUCN10), a second was a monodisperse poly(ethylene glycol) carboxylated Au NP (30 nm, UltraUniform, AUXU30, NanoComposix) and a third was acquired from the National Institute of Standards and Technology (60 nm, NIST, SRM 8013, Gaithersburg, MD, USA).

NP stock suspensions were stored in the dark at 4 °C until use. Prior to analysis, the stock suspensions were vortexed for one minute, sonicated for 10 min (Branson Ultrasonic Cleaner, 5510R-DTH Model, 135 W), diluted to adequate concentrations in Milli-Q water ($R > 18.2 \text{ M}\Omega \text{ cm}$; total organic carbon $< 1 \mu\text{g L}^{-1}$), and then re-vortexed for one minute. Final suspensions had a mass concentration between 10–50 ng L^{-1} , depending on the NP size. Concentrations were optimized in order to ensure a statistically significant number of events, while reducing the probability for the concurrent atomization and ionization of more than one NP (which would lead to an overestimation of particle size and underestimation of particle number). To evaluate the impact of background noise on NP size and concentration determinations, a 10 ng L^{-1} suspension of the Nanobyk[®] CeO₂ NPs was spiked with 5–100 ng L^{-1} of ionic Ce purchased from Inorganic Ventures (CGCE1, Christianburg, VA, USA).

The total Ce concentration was determined by adding 400 μL of HNO₃ (67–70%) and 300 μL of H₂O₂ (30%) to 1 mL of the sample, prior to heating the mixture at 80 °C for 5 h (DigiPREP, SCP science, Montreal, Can.). Samples were then diluted to 2% v/v HNO₃ prior to their analysis by ICP-MS, using the ionic Ce (CGCE1) for calibration and indium (CGIN1) as an internal standard. Ce and In standards were purchased from Inorganic Ventures.

2.4.2. Sampling and Sample preparation

Rainwater samples were collected, between October and December 2018, using wide-mouth polypropylene containers (500 mL, Fisher Scientific), which were placed on the 7th floor roof of the Roger-Gaudry Pavillon of the University of Montreal (coordinates: 45.502639, -73.615822, Montreal, QC, Canada). St. Lawrence River water samples were collected from two different locations (Figure 2-S7), between August and September 2019, using polypropylene tubes (50 mL, Fisher Scientific), at a depth of 20–30 cm, 1 m from the shore. In total, 10 – 15 samples were collected for each type of water. The exact dates are presented in figure 2-5. All samples were stored at 4 °C in the dark. Prior to their analysis, water samples were first shaken manually, sonicated for 10 min, vortexed for one minute and then filtered through a 0.45 μm , 33 mm diameter PVDF syringe filter. Filters were pre-rinsed with Milli-Q water and 5 mL of sample.

2.4.3. Instrumentation

Single particle ICP-MS data were acquired in fast scan mode using a quadrupole ICP-MS (Q-ICP-MS; Perkin Elmer NexION 300×, Woodbridge, Ont., Canada) or a double focusing magnetic sector field ICP-MS (SF-ICP-MS; Nu AttoM ES, Nu Instruments, Wrexham, UK). The introduction system for the Q-ICP-MS consisted of a quartz cyclonic spray chamber, a type C0.5 concentric glass nebulizer (0.5 mL min^{-1}) and a quartz 2 mm bore injector. In the case of the SF-ICP-MS, two introduction systems were used: (i) A micro-flow concentric glass nebulizer (self-aspiration rate of $200 \mu\text{L/min}$ for 1 L min^{-1} argon gas) with a quartz cyclonic spray chamber cooled to $4 \text{ }^\circ\text{C}$ (wet-SF-ICP-MS); or (ii) an Apex Omega desolvator (Elemental Scientific, Omaha, NE, USA). When using the desolvator (dry-SF-ICP-MS), the sample was nebulized, with a PFA (perfluoroalkoxy) concentric micro-flow nebulizer (self-aspiration rate of $200 \mu\text{L min}^{-1}$) in a quartz cyclonic spray chamber that was heated to $140 \text{ }^\circ\text{C}$ before condensation at $3 \text{ }^\circ\text{C}$ and passage through a porous PFA membrane heated at $160 \text{ }^\circ\text{C}$. Argon was used as the membrane sweep gas ($6\text{--}8 \text{ L min}^{-1}$) and as the nebulizer gas ($0.7\text{--}1.0 \text{ L min}^{-1}$). In both introduction systems, the aerosol was injected into the plasma through a 1.5 mm internal diameter quartz injector. The argon was also used as a coolant gas with a flow rate of 13.0 L min^{-1} .

Time of flight ICP-MS (TOF-ICP-MS) measurements were performed on a time-of-flight ICP-MS (Vitesse, Nu Instruments, Wrexham, UK) that allowed for multi-element characterization of individual nanoparticles. The instrument used a segmented reaction cell in which $4\text{--}6 \text{ cm}^3 \text{ min}^{-1}$ of He and ca. $4 \text{ cm}^3 \text{ min}^{-1}$ of H_2 gas was introduced in order to eliminate argon and nitrogen-based interferences for elements such as Si, K, Ca, Cr and Fe ¹⁷¹. Time of flight mass spectra ($23\text{--}238 \text{ amu}$) were acquired with a dwell time of $76.5 \mu\text{s}$ ¹⁷¹. Total sample acquisition time was 32 s. In some experiments, the instrument was coupled to an Aridus II desolvator (Teledyne Cetac Technologies, Omaha, NE, USA) (Argon was used as the membrane sweep gas ($5\text{--}6 \text{ L min}^{-1}$) and as the nebulizer gas ($0.9\text{--}1.0 \text{ L min}^{-1}$). Calibrations were performed using different custom-prepared standards (CLMS-1, CLMS-2, CLMS-3 and CLMS-4, SPEX CertiPrep, Metuchen, NJ, USA) that included all of the metals and metalloids.

2.4.4. SP-ICP-MS data acquisition

Triplicate samples were each analyzed three times- means and standard deviations were determined from the triplicate samples and triplicate measurements. In addition, in some cases,

the breadth of the particle size distributions was indicated by calculating polydispersities. The isotopes ^{107}Ag , ^{197}Au , ^{139}La and ^{140}Ce were measured using a resolution of 300 and a dwell time of 50 μs . Data were acquired for 50 s at a sample flow rate of 100–200 $\mu\text{L min}^{-1}$. External calibrations (0.05 to 1.0 $\mu\text{g L}^{-1}$) were performed using ionic standards (Ag, La and Ce: Inorganic Ventures; IV-ICP-MS-71A; Au: Inorganic Ventures; MSAU-100PPM, Christianburg, VA, USA). Sensitivities were validated with an ionic quality control standard provided by High-Purity Standards (QCS-27). Transport efficiency (TE) was determined¹⁷² by measuring the instrument sensitivity for ionic Au standards and the particle number concentration of a standard suspension of Au NPs. For analysis with the Q-ICP-MS, a 50 ng L^{-1} suspension of 60 nm Au NPs (NIST) was used for TE determinations, while for SF- and TOF-ICP-MS, a suspension of ultra-uniform 30 nm Au NPs (NanoComposix) was prepared daily at 20 ng L^{-1} . Furthermore, TE was validated by verifying the sizes of Ag NPs (NanoComposix) with a nominal size of 20 nm. TE values for the Q-ICP-MS were between 3–5%. With SF-ICP-MS, they were between 4–7%, except when using the desolvator (15–20%). For the TOF-ICP-MS, TE values ranged between 10–15%.

2.4.5. SP-ICP-MS data processing

Q-ICP-MS data were processed using the Syngistix Nano Module (Perkin Elmer, Woodbridge, Ont., Canada). Peaks were considered if their intensity was greater than the average background + three times the standard deviation of the background. SF-ICP-MS data were processed using Nu Quant software (version 2.2, Nu Instruments, Wrexham, UK^{118, 173}). A built-in algorithm searches in a fixed window (3–15 ms) for a peak maximum that is greater than the signal of the smoothed background. When a maximum is found, the algorithm searches for the pre- and post-inflection points, integrates the data between these points and subtracts local peak background. Local peak background is determined from smoothed data prior to the pre-inflection point of the peak. The script also calculates the full width at half maximum (FWHM) for each peak, which was used on several occasions to identify artifacts and coincidence (overly large FWHM). A major difference between the programs is that the Syngistix module identifies peaks with respect to the average signal background, whereas Nu Quant employs the local background. In both cases, the concentration of dissolved metal is determined from the average background signal, obtained from the entire data set.

Size detection limits (nm) are determined from the threshold intensity (I_s) (counts) used to discriminate between NPs and the background according to Equation (2.1) ^{118, 152}.

$$SDL = \sqrt[3]{\frac{6 \times I_s}{\pi \times 10^6 \times \rho_{NP} \times S_m \times \chi_m}} \quad \text{Equation 2.1}$$

where ρ_{NP} is the particle density (kg dm^{-3}), S_m is the sensitivity (counts fg^{-1}) and χ_m is the fraction of measured element in the NP. Similarly, the size quantification limit (SQL) can be defined as the smallest diameters that can be detected with confidence. Thus, SDL is a mean value that is calculated from the sum of the threshold intensity (I_s) and 3 times its standard deviation (SD), whereas the SQL was determined from $I_s + 10SD$.

A modified version of NuQuant (Nu Instruments, UK) was used for the treatment of the TOF-ICP-MS data. In that case, the algorithm searched for a target isotope, i.e. ^{140}Ce , using similar smoothing and peak detection parameters as with SF-ICP-MS. Following detection of the Ce-containing peaks, each particle event was assigned start and end timestamps, which were used to integrate peaks for all other isotopes ¹⁷¹. As above, the criteria to report peak events as NPs were based on the FWHM values as well as the standard deviation of the background (for each isotope), which were used to estimate threshold values. Artefacts were flagged based upon abnormally large or small FWHM values. For the TOF-ICP-MS, thresholds were typically based upon 5-7 multiples of the standard deviation of the background, which were selected to remove most background artifacts, while optimizing the detection of the real NP peaks ¹⁷¹.

2.5. Conclusions

In conclusion, the use of a high sensitivity sector field ICP-MS with very short dwell times (50 μs) improved sensitivity (200x more) and decreased SDL (4x less) for Ce, when compared to the use of a Q-ICP-MS. The sensitivity and SDL were further improved when the SF-ICP-MS was coupled to a desolvator; however, this setup was shown to be much more sensitive to the presence of the dissolved analyte. SF-ICP-MS was shown to be useful to detect and characterize Ce-containing NPs in natural samples such as rain and river waters. The use of a TOF-SP-ICP-MS allowed us to show that some of the nanoparticles in the Montreal rainwater were engineered CeO_2 NPs.

2.6. Supplementary Information

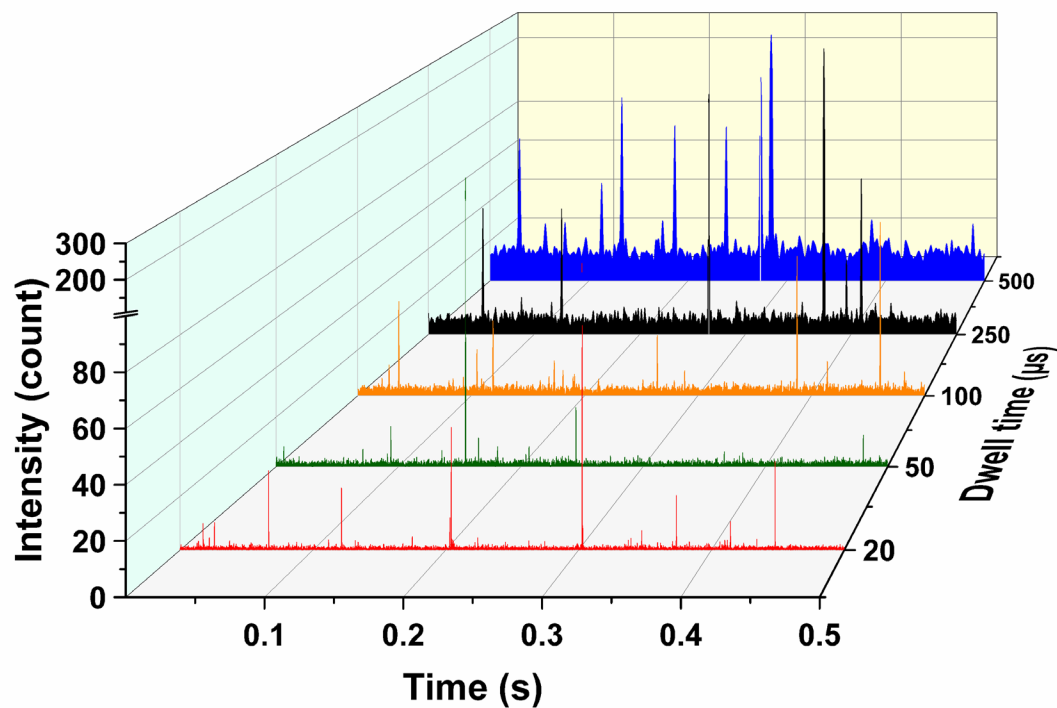


Figure 2-S1 Time resolved signal of ^{140}Ce in a suspension of 10 ng L^{-1} CeO_2 NPs spiked with 10 ng L^{-1} of ionic Ce measured at different dwell times. Measurements were obtained using the dry-SF-ICP-MS.

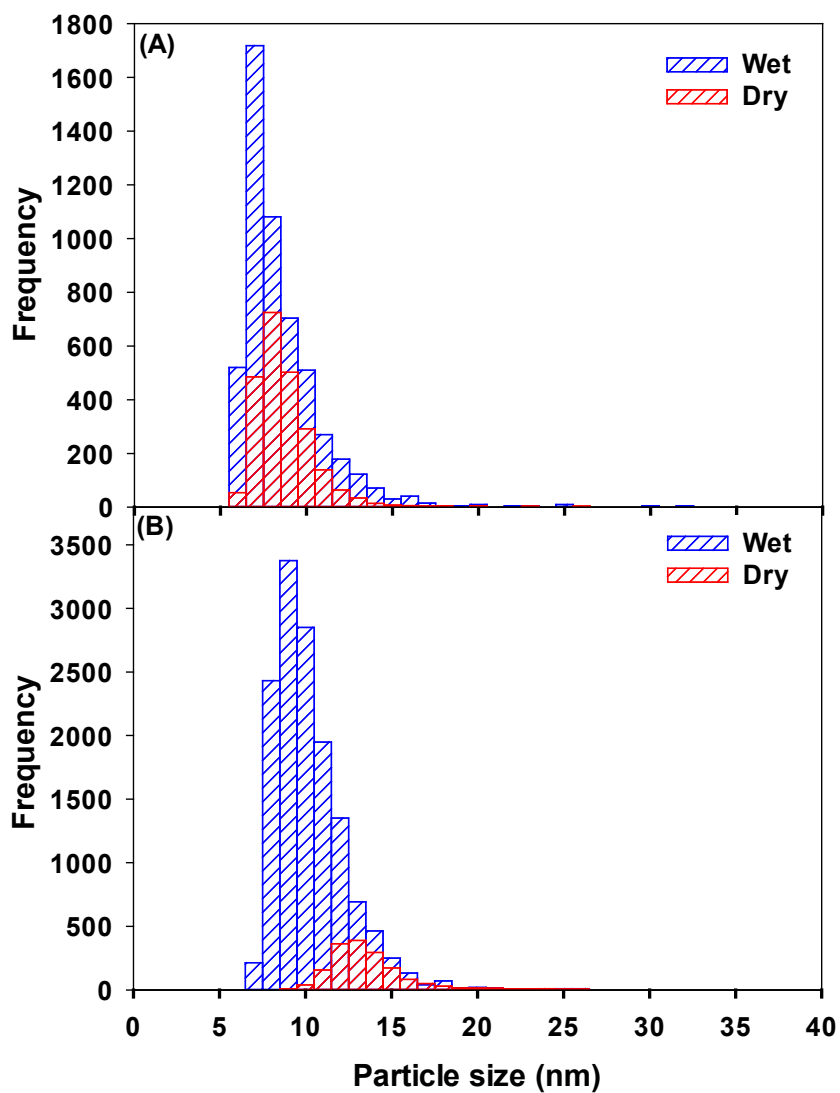


Figure 2-S2 Particle size distributions of a 10 ng L⁻¹ suspension of CeO₂ NPs with a nominal size range 1-10 nm spiked with ionic Ce at a mass concentration of **(A)** 10 ng L⁻¹; **(B)** 50 ng L⁻¹ as measured by Wet-SF-ICPMS (blue) and Dry-SF-ICPMS (red). The mean particle size ± the standard deviation on the distribution in the suspension in **(A)** is 8.3 ± 2.3 with dry introduction and 8.1 ± 1.8 with wet introduction; **(B)** is 11.2 ± 2.3 with dry introduction and 9.7 ± 3.2 with wet introduction.

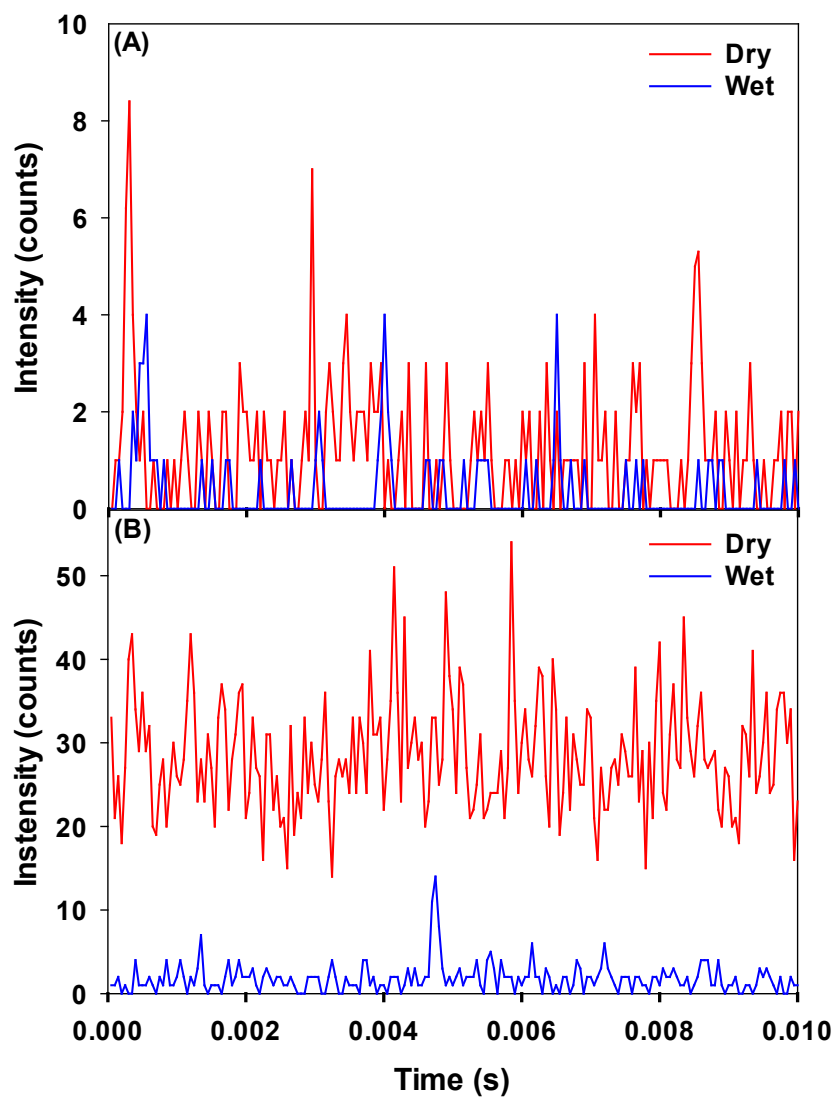


Figure 2-S3 Time-resolved signal for ^{140}Ce in a 10 ng L^{-1} suspension of CeO_2 NPs with a nominal size range 1-10 nm spiked with ionic Ce at a mass concentration of **(A)** 10 ng L^{-1} ; **(B)** 50 ng L^{-1} as measured by Wet-SF-ICPMS (blue) and Dry-SF-ICPMS (red). For better readability, only 0.01 s of data collection were shown, the total acquisition time was 50 s. A dwell time of $50 \mu\text{s}$ was used with both introduction systems.

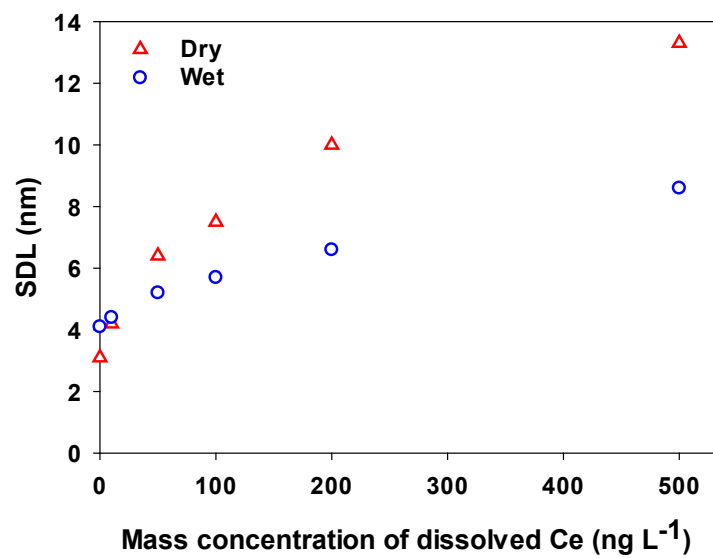


Figure 2-S4 Size detection limit as a function of mass concentration of dissolved Ce as measured by wet-SF-ICP-MS (blue) and dry-SF-ICP-MS (red). A dwell time of 50 μ s was used with the two introduction systems.

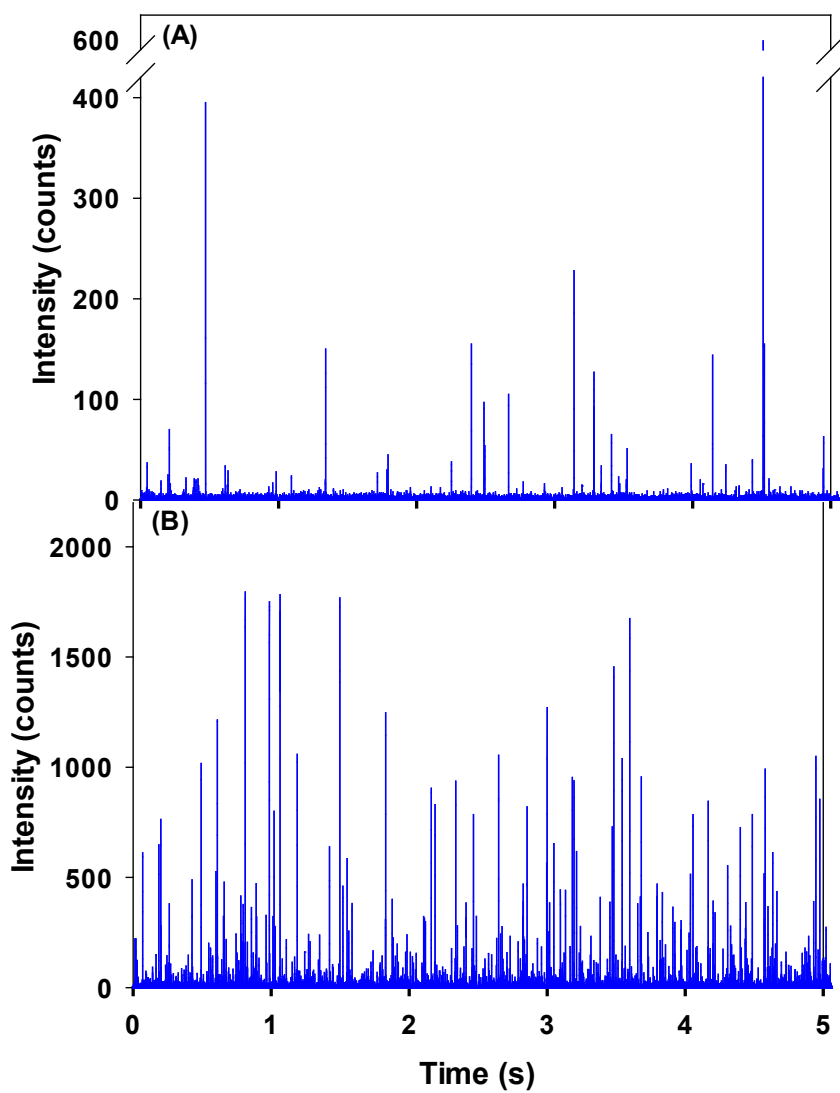


Figure 2-S5 Time-resolved signal for ^{140}Ce in (A) unfiltered rainwater and (B) unfiltered St. Lawrence River water. For better readability, only 5 s of data collection were shown, the total acquisition time was 50 s. Measurements were obtained using the wet-SF-ICP-MS with a 50 μs dwell time.

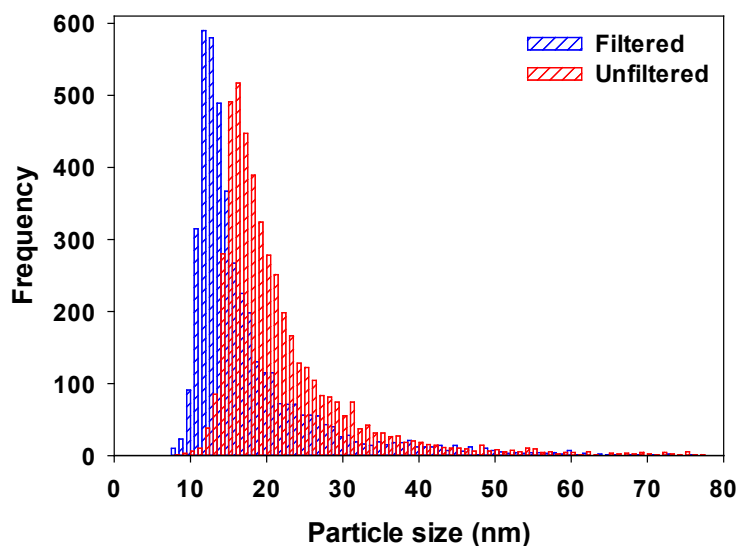


Figure 2-S6 Particle size distributions of Ce containing NPs in St. Lawrence River water with (blue) or without (red) filtration. Samples were filtered using syringe filters with a PVDF membrane with a 0.45 μm pore size. NP sizes were calculated by assuming that the particles were spherical CeO_2 particles with a density of 7.13 kg dm^{-3} . Measurements were obtained using the wet-SF-ICP-MS with a 50 μs dwell time.

Table 2-S1 Mean particle sizes, NPs number concentrations, mass concentration of dissolved Ce and SDL for Ce containing NPs in St. Lawrence River water, with or without filtration. Measurements were obtained using the wet-SF-ICP-MS with a 50 μs dwell time. Means and standard deviations are obtained from triplicate samples.

St. Lawrence River	Mean particle size (nm)	Number concentration ($\times 10^9 \text{ CeO}_2 \text{ NPs L}^{-1}$)	Mass concentration of dissolved Ce (ng L^{-1})	SDL (nm)
Filtered	17.2 ± 0.0	1.13 ± 0.02	36.0 ± 0.6	5.2 ± 0.1
Unfiltered	21.9 ± 0.9	1.60 ± 0.32	52.7 ± 17.0	6.2 ± 0.6

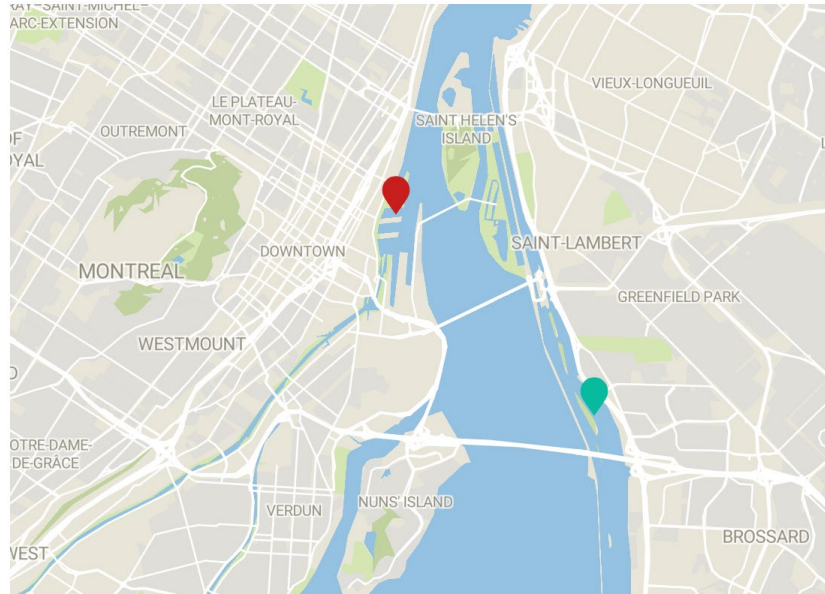


Figure 2-S7 Sampling locations on the St. Lawrence River. The green mark corresponds to the location (coordinates: 45.477473, -73.504144) where the results of the sample were presented in **Figure 2-4, S4 & S5**; the red mark corresponds to the location (coordinates: 45.5090203, -73.5485275) of the samples used for the temporal variability experiments (**Figure 2-5**).

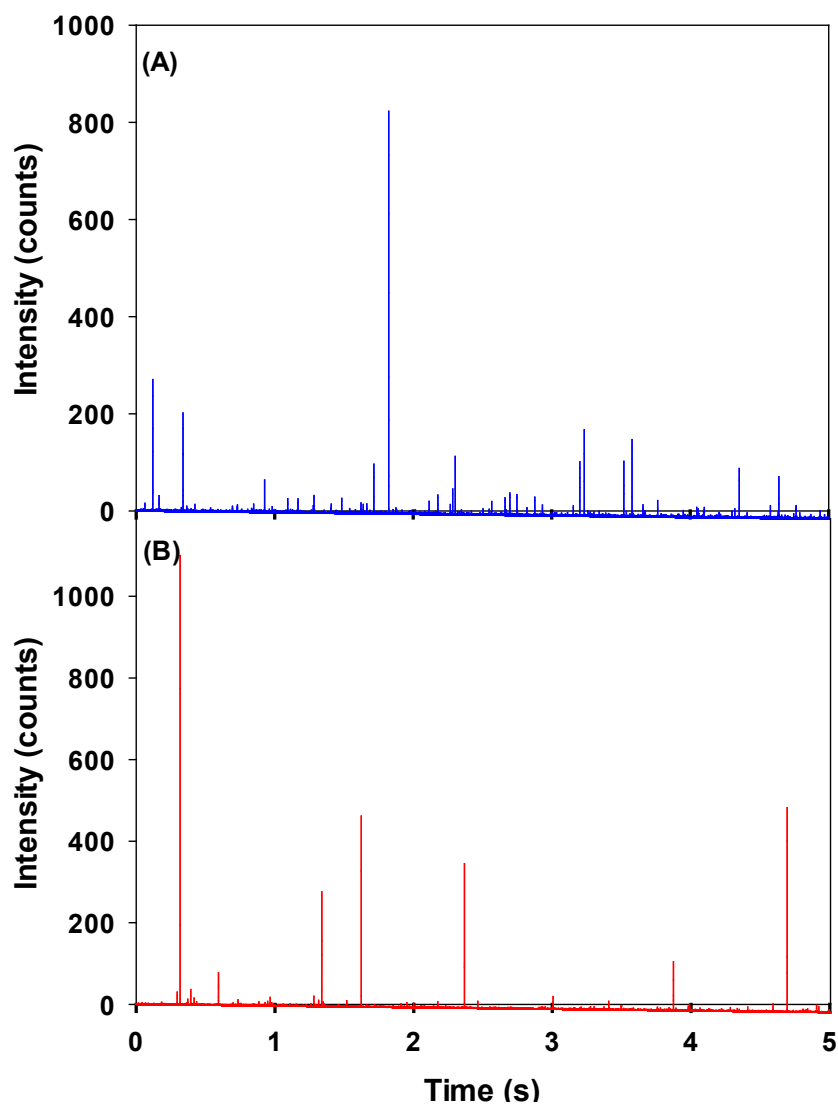


Figure 2-S8 Time-resolved signal for (A) ^{140}Ce and (B) ^{139}La in Montreal rainwater. For better readability, only 5 s of data collection were shown, the total acquisition time was 50 s. Measurements were obtained using the wet-SF-ICP-MS with a 50 μs dwell time.

Table 2-S2 Mean particle sizes, NPs number concentrations and mass concentration of dissolved and nanoparticulate Ce and La in Montreal rainwater. Measurements were obtained using the wet-SF-ICP-MS with a 50 μ s dwell time. Means and standard deviations are obtained from triplicate samples.

Water natural sample	Mean particle size (nm)		Number concentration ($\times 10^8 \text{ L}^{-1}$)		Mass concentration of dissolved (ng L^{-1})		NPs mass concentration (ng L^{-1})	
	CeO ₂	La ₂ O ₃	Ce	La	Ce	La	Ce	La
Montreal rainwater	10.0 \pm 1.1	9.9 \pm 0.4	3.9 \pm 0.5	1.6 \pm 0.6	2.4 \pm 0.8	1.0 \pm 0.4	2.0 \pm 0.1	1.0 \pm 0.2

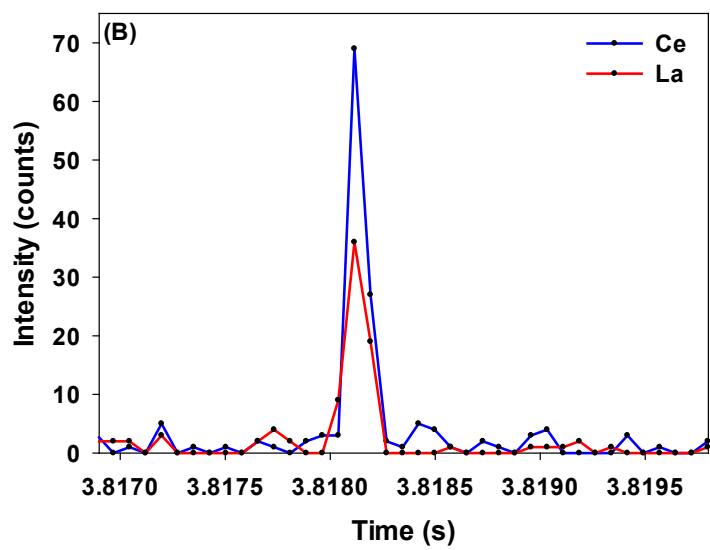
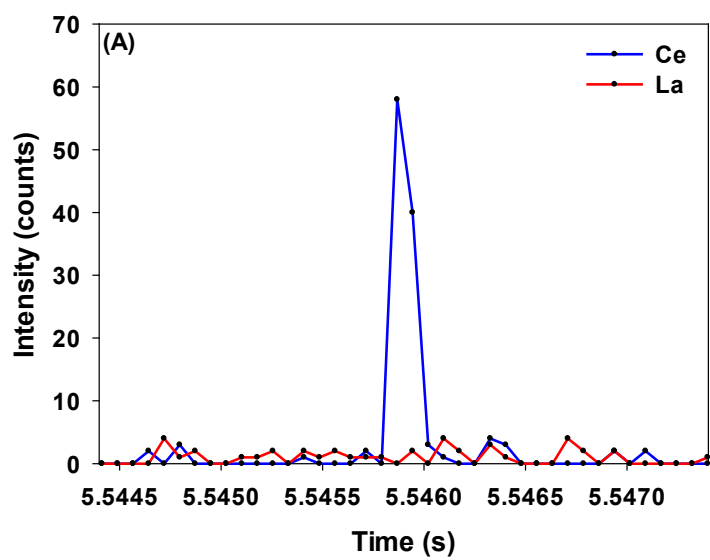


Figure 2-S9 Time-resolved signal for ^{139}La (red) and ^{140}Ce (blue) in Montreal rainwater analyzed by TOF-SP-ICPMS showing (A) a pure Ce NP and (B) a NP that contains Ce and La.

Chapitre 3 – Sample preparation for the analysis of nanoparticles in natural waters by single particle ICP-MS

3.1. Abstract

With the significant increase in the production and use of nanoparticles (NPs), concern is increasing over their release into their environment. Single particle inductively coupled plasma mass spectrometry (SP-ICP-MS) is emerging as one of the best techniques for detecting the very small NPs at very low concentrations in natural waters. However, there is no unified protocol for the preparation of natural water samples for SP-ICP-MS analysis. In order to minimize nebulizer blockage, filtration is often used with the expectation that 0.45 μm membranes will not remove significant quantities of 1-100 nm NP. Nonetheless, there are limited data on its effect on the concentrations or size distributions of the NPs. To that end, we examined the interactions between six different membrane filters and silver (Ag) and cerium oxide (CeO_2) NPs in aqueous samples. For Ag NPs, the highest recoveries were observed for polypropylene membranes, where 55% of the pre-filtration NPs were found in rainwater and 75% were found in river waters. For CeO_2 NP, recoveries for the polypropylene membrane attained 60% in rainwater and 75% in river water. Recoveries could be increased to over 80% by pre-conditioning the filtration membranes with a multi-element solution. Similar recoveries were obtained when samples were centrifuged at low centrifugal forces ($\leq 1000xg$).

3.2. Introduction

The production and uses of engineered nanoparticles (NPs) are continuously increasing. With their widespread use in commercial products, serious concerns are being raised over their release to the environment and their subsequent fate and toxicity. In order to evaluate their environmental risk, it is necessary to detect, quantify and characterize the NPs in all environmental compartments. Unfortunately, analyses of NPs in natural systems are challenging due to their small sizes, their low concentrations ($\sim \text{ng L}^{-1}$) and the complexity of environmental

matrices, which also contain natural colloids. Thus, the vast majority of published concentrations of NPs in the environment have been obtained from modelling studies.^{12, 27, 29, 30, 78}

Single particle inductively coupled plasma mass spectrometry (SP-ICP-MS) is a specific and sensitive technique that enables the detection of very low concentrations ($\sim \text{ng L}^{-1}$) of NPs and it can provide information on their number concentrations, sizes and size distributions.¹¹³ Although several groups have used SP-ICP-MS to measure NPs in surface waters,^{116, 139, 161, 174, 175} different methods have been used to prepare the samples, which could lead to variations in the results. While several protocols for the preparation of NPs suspensions have been proposed,¹⁷⁶⁻¹⁸¹ guidance is lacking on the best ways to prepare natural water and wastewater samples for SP-ICP-MS analysis. For example, filtration is often used because it removes microbial contamination and suspended particles in addition to aggregates that may cause blockages in the ICP-MS introduction system.^{179, 182} Nonetheless, different pore sizes (0.2 – 0.45 μm) and membrane types have been used, including nylon,^{174, 183} cellulose acetate,^{184, 185} regenerated cellulose,¹⁸⁶ polyethersulfone,^{187, 188} polytetrafluoroethylene,¹⁸⁹ and polyvinylidene difluoride^{117, 119, 190}. Only a few papers¹⁹¹⁻¹⁹³ have examined the effect of filtration on NP suspensions. Despite the use of filters with pore sizes substantially exceeding the nanoscale (1 – 100 nm), particle retention can occur, leading to inaccurate quantification of NPs concentrations in natural systems. Indeed, NP number concentrations are generally thought to be underestimated due to losses caused by adsorption to the filter or by retention of NPs within agglomerates.

The main objective of this study was to evaluate the interactions between different membrane filters and silver (Ag) and cerium oxide (CeO_2) NPs in aqueous samples. Ag and CeO_2 are among the most commonly used NPs,^{52, 194} with applications in electronics,^{143, 194} catalysis^{142, 194}, agriculture¹⁴⁶ and medicine^{52, 195}. For example, Ag NPs are commonly used as antibacterial agents,¹⁹⁴ for food storage¹⁹⁶ and in textiles¹⁹⁷ while CeO_2 NPs are used as UV filters in sunscreens, diesel fuel additives and components in paints.^{146, 198} Membranes made of different materials (polyvinylidene difluoride, polyethersulfone, polypropylene, polytetrafluoroethylene, nylon and cellulose acetate) were first tested to evaluate the impact of filtration on the analysis of engineered Ag and CeO_2 NPs in deionised water **and** on Ag- and Ce-containing NPs in natural waters (rain and rivers). For the polypropylene membranes, which showed the lowest adsorptive losses, subsequent experiments were carried out to examine the effect of filter pre-conditioning

and successive filtrations. Finally, centrifugation was compared to filtration for some natural waters.

3.3. Materials and methods

3.3.1. Nanoparticles, chemicals reagents, and filters

Citrate stabilized cerium oxide nanoparticles, with a nominal size range of 1-10 nm, were purchased as an aqueous dispersion from Nanobyk (Byk; Nanobyk®-3810). Aqueous suspensions of citrate stabilized silver nanoparticles with nominal sizes of either 10 (NanoXact, AGCN10) or 20 nm (NanoXact, AGCN20) were purchased from NanoComposix. Monodisperse Au NPs, with a nominal size of 30 nm and a poly(ethylene glycol) carboxylic acid coating were purchased from NanoComposix (UltraUniform, AUXU30).

Analytical grade nitric acid (67–70%) and hydrogen peroxide (30%) were purchased from SCP Science and VWR, respectively. Ionic cerium (Ce; CGCE1), silver (Ag; AAAG1), potassium (K; CGK1), magnesium (Mg; CGMG1), lanthanum (La; CGLA1) and Indium (In; CGIN1) were all purchased from Inorganic Ventures. Multi-element quality control standards QC-21, IV-ICPMS-71A and QCS-27 were purchased from Perkin Elmer, Inorganic Ventures, and High Purity Standards, respectively.

Syringes were purchased from ThermoFisher Scientific (Luer-Slip Syringes, 10 mL capacity, polypropylene and polyethylene material). Six types of syringe filters (25 mm diameter, 0.45 µm pore size) were purchased from ThermoFisher Scientific: polyvinylidene difluoride (PVDF; CH4525-PVH), polyethersulfone (PES; CH4525-PES), polypropylene (PP; CH4525-PP), polytetrafluoroethylene (PTFE; CH4525-NP), nylon (CH4525-NN) and cellulose acetate (CA; CH4525-CA). A second polypropylene filter with a pore size of 0.22 µm (CH2225-PP) was also used in some experiments.

3.3.2. Sampling and sample preparation

Rain and river water samples were collected, between October 2020 and February 2021, using wide-mouth polypropylene containers (500 mL, ThermoFisher Scientific). Rainwater samples were collected in Brossard, Canada (coordinates: 45.47329, -73.47789). River water

samples were collected from the St. Lawrence River (Montreal, Canada) at a depth of 20 – 30 cm, ~ 1 m from the shore (coordinates: 45.416323. -73.610577).

Four different types of samples were considered in this study: (i) deionized water (Milli-Q, $R > 18.2 \text{ M}\Omega \text{ cm}$; total organic carbon $< 1 \mu\text{g L}^{-1}$) spiked with ionic Ag or Ce; (ii) deionized water spiked with engineered Ag or CeO_2 NPs; (iii) non-spiked rainwater; (iv) non-spiked river water. Immediately after collection, the rain and river water samples were transferred (without filtration) into polypropylene centrifuge tubes and stored in the dark at 4°C until use. Nanoparticle suspensions and ionic solutions (50 ng L^{-1} of Ag or Ce in Milli-Q water) were also prepared in polypropylene centrifuge tubes and handled under the same conditions as the natural water samples. To study the impact of filtration, triplicate 50 mL sample tubes were prepared for each of the 6 membrane filters. Each tube contained a sufficient volume to accomplish the following procedures (Figure 3-S1): 5 mL were analyzed by SP-ICP-MS without filtration; 10 mL were used for filter conditioning; 10 mL were filtered of which 5 mL were digested and analyzed by ICP-MS for total metal content and 5 mL was analysed by SP-ICP-MS. Prior to use, samples were vortexed for one minute, sonicated for 10 minutes (Branson Ultrasonic Cleaner, 5510R-DTH Model, 135W) and then vortexed for another minute. Prior to the filter conditioning step (above), filters were pre-rinsed with 10 mL of Milli-Q water.

Several experiments were performed to evaluate the effect of the filter conditioning step. In those cases, polypropylene filters were preconditioned with 10 mL of 10^{-6} M solutions containing K^+ , Mg^{2+} or La^{3+} (Inorganic Ventures) or a multi-element mixture (Perkin Elmer Quality Control Standard 21, Table 3-S1) that contained neither Ag nor Ce.

Finally, twelve 15 mL PP tubes containing rainwater, river water or deionized water spiked with engineered Ag or CeO_2 NPs were used to study the effect of sample centrifugation (Heraeus Multifuge 1 S-R centrifuge, ThermoFisher Scientific). In that case, samples were placed in swinging bucket rotor (TTH 400, 75002000) and centrifuged for 5 minutes at 4 different rotational forces: 70, 270, 1000 and 6000 x g. Following centrifugation, the top 5 mL were carefully removed for analysis by SP-ICP-MS.

Dynamic Light Scattering (DLS) (Möbiuζ, Wyatt Instruments, 532 laser) measurements were performed on the rainwater and river water samples. Total organic carbon in the natural water samples was measured using a Sievers M5310C analyzer (Suez).

3.3.3. ICP-MS (single particle and quantitative determinations)

A double focusing magnetic sector field ICP-MS (Nu AttoM ES, Nu Instruments, UK) was used in fast scan mode for the acquisition of single particle data. The introduction system consisted of a micro-flow concentric glass nebulizer (self-aspiration rate of $\sim 200 \mu\text{L}/\text{min}$ for 1 L min^{-1} argon gas), a 1.5 mm internal diameter quartz injector and a quartz cyclonic spray chamber, cooled to 4°C . The argon was also used as a coolant gas with a flow rate of 13.0 L min^{-1} . Isotopes (^{107}Ag , ^{140}Ce , ^{197}Au) were measured for 50 s using a dwell time of $50 \mu\text{s}$ (one million datapoints). Calibrations were performed using ionic standards and transport efficiency (TE) was determined by measuring the particle number concentration of a standard suspension of ultra-uniform 30 nm Au NP.¹²⁷ Sensitivities and TE were validated with a multi-element standard (QCS-27) and a suspension of 20 nm Ag NP, respectively.^{115, 139}

Acid-extractable metal concentrations were determined by adding 200 μL of HNO_3 (67–70%) and 100 μL of H_2O_2 (30%) to 5 mL of sample and then heating the mixture at 80°C for 5 h (DigiPREP, SCP Science). In order to quantify the metal fraction that was retained on the different filters, they were rinsed with 2 mL of 10% (v/v) HNO_3 . All solutions were diluted to 2% v/v HNO_3 prior to their analysis by ICP-MS. Metal concentrations in the digested samples were measured using a quadrupole ICP-MS (Perkin Elmer NexIon 300x). Ionic Ag and Ce standards and a multi-element IV-ICPMS-71-A were used for calibration. Indium was employed as the internal standard.

3.3.4. SP-ICP-MS data processing

SP-ICP-MS data were processed using Nu Quant software (version 2.2, Nu Instruments, UK). The operating mode of this software has been described in detail elsewhere.^{118, 131} Briefly, the data is first smoothed in order to define the background baseline. The algorithm then searches a defined window for the maximum intensity that exceeds the smoothed background. The data between the pre- and post-inflection points of the maximum are then integrated with a threshold based upon the local peak background. The local peak backgrounds are used to calculate the average background for the whole data set, which is converted to the concentration of dissolved metal in the sample. The software allows the verification of each peak, which helps in the identification of artefacts, including particle coincidence. Size detection limits (SDL) are calculated from the average value of the threshold.

3.4. Results and discussion

Solutions of ionic Ag and Ce and suspensions of Ag and Ce NPs, suspended in Milli-Q water, were filtered through the different 0.45 μm membrane filters, in order to better understand interactions between the different membranes and the two forms of metals in aqueous samples. Fifty ng L^{-1} solutions of the ionic metals (prepared in Milli-Q water) were analyzed by SP-ICP-MS, with or without filtration. When compared to the unfiltered solution, nylon showed the least retention of the ionic metals (Figure 3-1a), however, results for Ag^+ and Ce^{3+} were very different ($p < 0.01$). Indeed, recoveries for Ce^{3+} were extremely low ($\sim 0\%$) for the PVDF, PES, PTFE and CA membranes, while 87 – 96% of the Ag^+ passed through the same filters (Figure 3-1a), suggesting that adsorption was likely due to electrostatic interactions between the cations and the negatively charged filtration membranes. While showing more adsorption than the nylon, recoveries for the polypropylene membranes exceeded 60%. Fr chet-Viens et al. previously demonstrated that the adsorptive losses of La^{3+} were smaller for PP tubes and bottles when compared to PVC (polyvinyl chloride) and PFA (polyfluoroalkoxy alkane) surfaces.¹⁹⁹

In contrast, fewer differences were observed when comparing the different membranes for their retention of Ag and CeO_2 NPs. In spite of their small sizes (~ 10 nm; particle size distributions are given in Figure 3-S2), about 90% of the NP were removed by all the filters, with the exception of the PP membrane, which showed a retention of 20% for the Ag NPs and 30% for the CeO_2 NP (Figure 3-1b). Generally speaking, the retention of the NPs by the different membranes can be attributed to three main interaction mechanisms: (i) size exclusion for particles (agglomerates) larger than the pore size; (ii) adsorption on the membrane; (iii) concentration polarization in which agglomeration is promoted by the high concentrations of particles found in the microlayers immediately above the filtration membrane.^{78, 191-193}

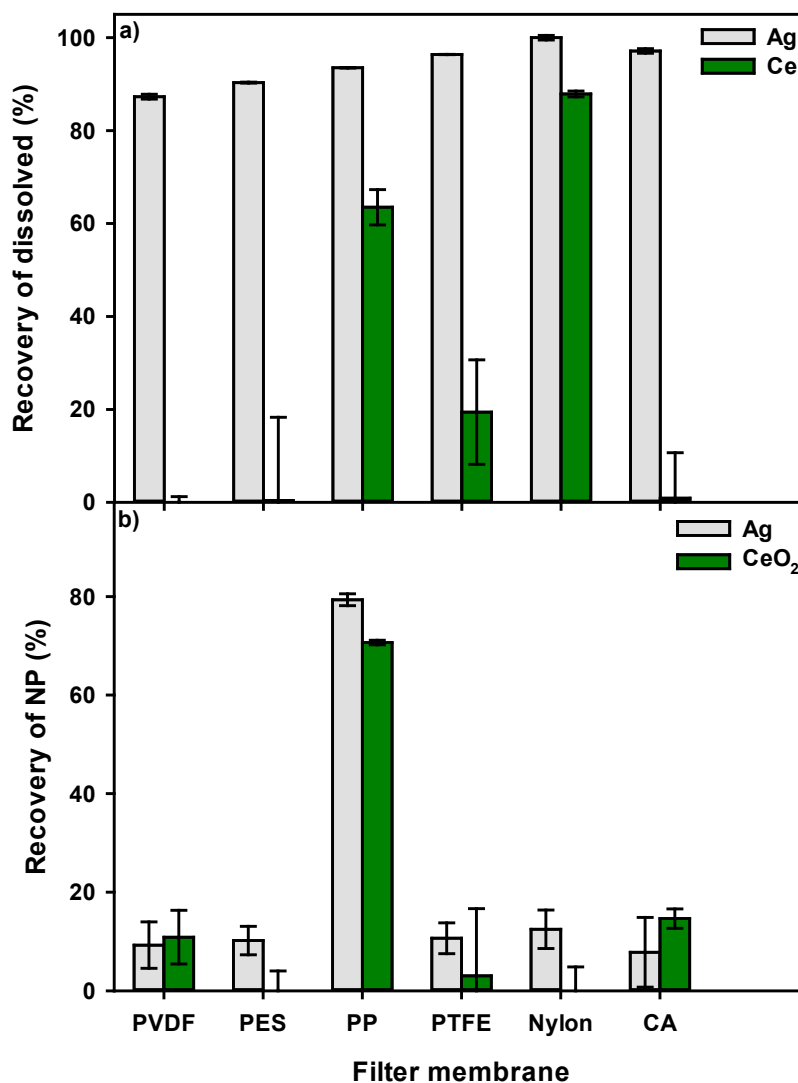


Figure 3-1 Recoveries of (a) ionic metals and (b) NPs in a solution/suspension of 50 ng L⁻¹ of Ag (grey) or Ce (green) in ultrapure water. Samples were filtered over different membranes: PVDF: polyvinylidene fluoride; PES: polyethersulfone; PP: polypropylene; PTFE: polytetrafluoroethylene; CA: cellulose acetate, all with a nominal pore size of 0.45 μm. Recoveries were calculated by dividing concentrations in the filtered samples by concentrations determined in the unfiltered samples. All measurements were performed using SP-ICP-MS and a dwell time of 50 μs. Error bars correspond to standard deviations obtained from triplicate analyses.

Samples were digested and analyzed for total (extractable) metal content using quantitative mode ICP-MS. Results obtained (Figure 3-S3) were similar to those obtained by SP-ICP-MS (Figure 3-1). For the analysis of 50 ng L⁻¹ of *dissolved* metal, the highest concentrations of Ag and Ce were measured following filtration through the nylon and PP membranes (Figure 3-S3a), whereas the highest recoveries for the NPs were determined for suspensions filtered over the PP membrane (Figure 3-S3b).

Unspiked rain and river waters were also filtered over the different 0.45 μm membrane filters prior to their analysis by SP-ICP-MS for Ag- and Ce-containing particles. When compared to the unfiltered samples, >50% of the Ag NPs were removed from both matrices, for all of the filter membranes except polypropylene (Figure 3-2a), which showed a recovery of 55% for the rainwater and 75% for the river water. Similarly, for the CeO₂ NPs, the highest recoveries were observed for the PP membrane: 60% in the rainwater and 75% in the river water (Figure 3-2b). The membranes generally showed less removal of the NPs from the river water than the rainwater, which can be attributed to its greater chemical complexity,²⁰⁰ including the presence of natural organic matter (Table 3-S2), which is known to stabilize colloidal suspensions.⁴¹ Similar results were obtained when recoveries were calculated based on the mass concentration of the NPs (Figure 3-S4). However, because of the low concentration of Ag in the rain and the river waters, higher variability was measured when recoveries were calculated using mass concentrations. Particle size distributions (Figure 3-S5) were consistent with those determined previously from the same sampling site.²⁰¹ Sizes determined by SP-ICP-MS are based only on the mass of the analyte of interest (i.e., Ag and Ce in our case). Therefore, if Ag and Ce containing particles in the natural water samples are very large but their metal (Ag or Ce) fraction is small, SP-ICP-MS analysis will invariably give small NP sizes. Indeed, DLS measurements indicated that particles larger than 450 nm and some exceeding 1 μm, were present in both (unfiltered) natural waters (Figure 3-S6). If these large particles contained Ag and Ce, their retention by the filter would greatly impact the results by reducing apparent recoveries. This was likely the case since both filtered and unfiltered samples gave size distributions that were well below the pore size of the filters. In addition, particles smaller than the pore size could homo-aggregate or adsorb on other inorganic or organic particles (heteroaggregation), resulting in their retention by the filter. All of these scenarios are plausible, and we admit that it is very difficult, based on the above analytical data, to identify a dominant mechanism.

Filtration clearly decreased particle number concentrations measured by SP-ICP-MS. However, for both the rain and river waters and for both NPs, no apparent differences were seen when comparing the particle size distributions before and after filtration, over any of the different membranes (Figures 3-S7, 3-S8, 3-S9 & 3-S10). This suggests that filtration might be an acceptable preparative technique for determining particle size distributions of nanoparticles in natural waters, but that it is likely less suitable for particle number determinations.

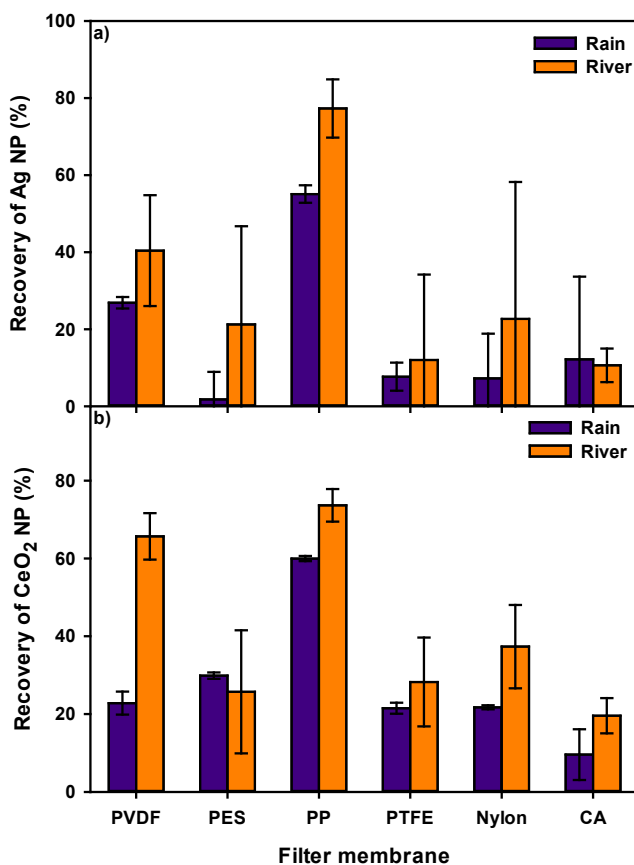


Figure 3-2 (a) Ag and (b) CeO₂ NPs recoveries based on their number concentrations, in a rainwater (purple) and in a river water (orange). Samples were filtered over different membranes: PVDF: polyvinylidene fluoride; PES: polyethersulfone; PP: polypropylene; PTFE: polytetrafluoroethylene; CA: cellulose acetate, all with a pore size of 0.45 μm . Recoveries are calculated by dividing NP concentrations in filtered samples by the concentrations in unfiltered samples. Measurements were performed using SP-ICP-MS and a dwell time of 50 μs . Error bars correspond to standard deviations obtained from triplicate measurements.

Mass balances were performed by digesting samples and rinsing syringes and syringe filters with a solution of 10% HNO₃ prior to analysis by quantitative ICP-MS for total metal content. The effect of filtration on total Ag in the natural waters could not be evaluated because of its low concentration. Even in the unfiltered rain and river waters, Ag levels were close to or lower than instrumental detection limits (DL) (Table 3-1). In filtered samples, they were below DL. Ce concentrations were higher than Ag in both waters. Nanoparticle losses to the filters (and recoveries) were evaluated by comparing ICP-MS determinations of metal concentrations in the acidified filtrate with those in the acidified sample prior to filtration (Figure 3-3).

Like SP-ICP-MS, results for the digested samples from the natural waters showed that PP membranes retained the least Ce (Figure 3-3). Indeed, recoveries of 45% for the rainwater and 78% for the river water were obtained for the PP membrane. While losses were significant, they were much less important than those observed for the PVDF, PES, PTFE and CA membranes, where ~10% of the Ce was recovered from the rainwaters when compared to digested, unfiltered samples. For the syringes, no Ce was detected in the rinse solutions (Ag was below DL), indicating that there were negligible adsorptive losses to the walls of the syringes.

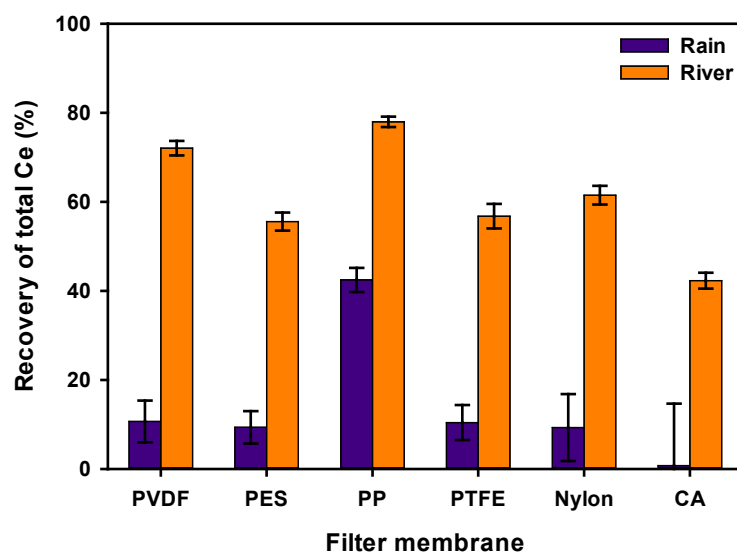


Figure 3-3 Recoveries of total Ce in rainwater (purple) and river water (orange). Samples were filtered over different membranes: PVDF: polyvinylidene fluoride; PES: polyethersulfone; PP: polypropylene; PTFE: polytetrafluoroethylene; CA: cellulose acetate, all with a pore size of 0.45 μm . Recoveries were calculated by dividing the total Ce concentrations in filtered samples by the concentrations in unfiltered samples. Measurements were performed on digested solutions using ICP-MS in quantitative mode. Error bars corresponds to standard deviations obtained from triplicate analysis.

Table 3-1 Average particle sizes, concentrations of NPs and dissolved metal and SDL determined by SP-ICP-MS (Magnetic sector ICP-MS) in addition to total digested metal and DL determined by quadrupole ICP-MS. Means and standard deviations are obtained from the analysis of triplicate samples of rain or river water samples.

Sample	Element	Average particle size (nm)	NP number concentration ($\times 10^8 \text{ L}^{-1}$)	Mass concentration of dissolved (ng L^{-1})	Mass concentration of NPs (ng L^{-1})	SDL (nm)	Total mass concentration (ng L^{-1})	DL (ng L^{-1})
Rain	Ag	9.9 ± 0.1	1.5 ± 0.0	2.8 ± 0.1	1.0 ± 0.0	5.3 ± 0.1	6.0 ± 1.2	5.5
	Ce	9.3 ± 0.1	12.0 ± 0.2	8.0 ± 0.1	8.4 ± 0.12	4.6 ± 0.0	126.0 ± 2.6	2.1
River	Ag	9.7 ± 0.3	0.1 ± 0.0	1.6 ± 0.3	0.3 ± 0.1	5.2 ± 0.1	<DL	5.5
	Ce	23.1 ± 0.6	11.5 ± 1.8	382.4 ± 3.1	66.2 ± 4.1	10.3 ± 0.1	553.4 ± 16.0	2.1

For the Ce in the rain and river waters, fractions retained by the different syringe filters were quantified by rinsing the membranes with acid. As seen above, the PP membrane showed the smallest retention of Ce from the natural water (Figure 3-S11), and results were comparable to the recoveries obtained by subtracting filtered from non-filtered samples (Figure 3-3).

In addition to the recovery determinations for the filtration components, it should be noted that adsorptive losses are also occurring to the introduction system of the ICP-MS, especially when measurements are performed in single particle mode (i.e. fast transient measurements with no acid added to samples) (Table 3-S3). Therefore, recovery determinations were also performed with respect to all parts of the analysis by comparing data with the total mass concentration of metal (dissolved and NP) using quantitative ICP-MS (digested samples). For example, 8% of dissolved Ag and 35% of dissolved Ce were adsorbed to the introduction system when the ionic solutions were analyzed by SP-ICP-MS (Table 3-S3). The higher adsorption (lower recovery) of ionic Ce with respect to ionic Ag can again be explained by its higher charge. For the NPs suspensions, the results were the opposite- a lower recovery was determined for Ag NPs as compared to the CeO₂ NPs. For Ce in the natural water samples, a higher recovery of the NPs was measured for the river water, which was again attributed to the presence of humic substances and their ability to stabilize colloidal suspensions.⁴¹ In natural water samples, the relationships between adsorption and detection are complex since adsorptive losses of dissolved metal will actually improve size detection limits by driving down the background, potentially leading to improved detection of the NPs (in contrast, adsorptive losses of NPs will lead to reduced NPs detection). Indeed, while a low size detection limit of 4.6 nm was determined for the Ce NPs in rain (8 ng L⁻¹ of dissolved Ce), a much higher SDL of 10.3 nm was obtained in the river water where the dissolved Ce was much higher (382.4 ng L⁻¹).

Given that they had the least significant interactions with the Ag and CeO₂ NP in the Milli-Q water, rainwater and river water, PP filter membranes were used for several complementary experiments in order to gain further insight on the removal mechanisms of the metal NP. For example, for a 25 mL sample, subsequent 5 mL sub-samples of the filtrate were collected for a single filter (Figure 3-S1b). In this case, no sample pre-conditioning of the filter was performed. Our hypothesis was that with increased cumulative sample volume, adsorptive losses (mechanism ii) would decrease due to saturation of active sites. In contrast, we would

expect recoveries of the NP to decrease as the membrane pores became clogged (mechanisms iii). For both metals, NP losses were the greatest in the first two fractions (Figure 3-4), consistent with the ideas that: particle losses were mainly occurring due to adsorption and losses could be reduced (though apparently not eliminated) by prefiltering the sample through the filter membrane.

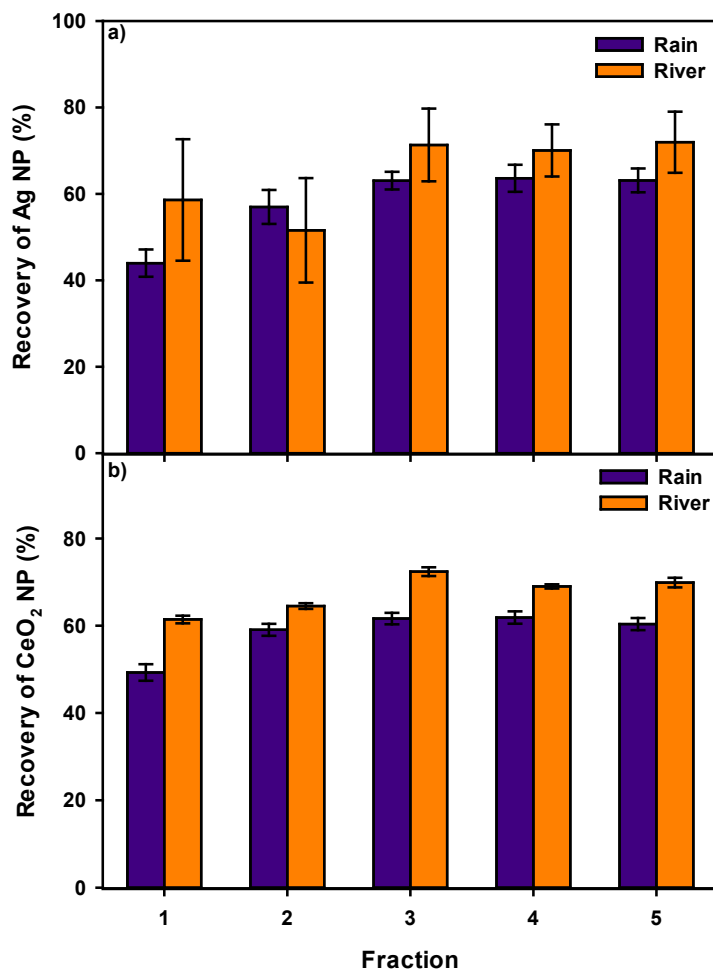


Figure 3-4 Recoveries of (a) Ag and (b) CeO₂ NPs, based on the NP number concentrations, for successive fractions of rainwater (purple) and river water (orange) filtered through PP filters with a pore size of 0.45 μm . Twenty-five mL of samples were filtered, and five 5 mL sub-samples were collected over the same filter. Recoveries are calculated by dividing NP concentrations in the filtered samples by the concentrations in unfiltered samples. Measurements were performed using SP-ICP-MS with a dwell time of 50 μs . Error bars corresponds to standard deviations obtained from triplicate analysis.

Several other solutions were used to pre-condition the membranes including (10^{-6} M) salts of: a monovalent (K), divalent (Mg) or trivalent ion (La) or a multi-element solution (QC-21) (Table 3-S1). In general, the higher ionic strengths of the salt solutions were more efficient than the natural waters in reducing the adsorptive losses of the NPs, with the trivalent salt and the mixed ions, being the most efficient (Figure 3-5). While these results confirm the importance of adsorption, it should be noted that there was nonetheless ~ 1.5 x more NP losses when a $0.22 \mu\text{m}$ PP membrane was substituted for a $0.45 \mu\text{m}$ membrane (Figure 3-6), suggesting that filtration could not be entirely excluded as a mechanism for the retention of the NP.

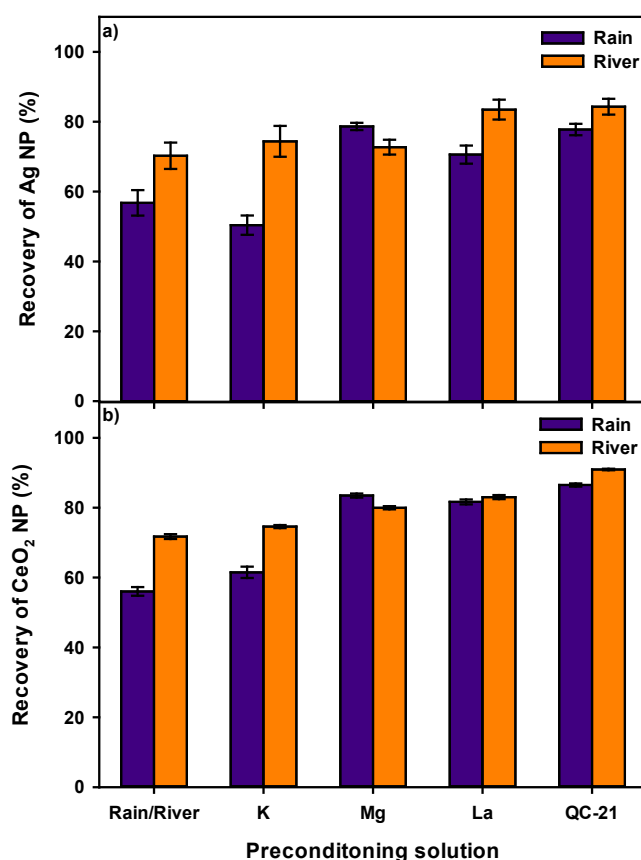


Figure 3-5 Recoveries of (a) Ag and (b) CeO₂ NPs, based on NP number concentrations, in rainwater (purple) and river water (orange), when filtered through polypropylene filters with a pore size of $0.45 \mu\text{m}$, preconditioned with different solutions. Recoveries are calculated by dividing NP concentrations in filtered samples by the concentrations in unfiltered samples. Measurements were performed using SP-ICP-MS with a dwell time of $50 \mu\text{s}$. Error bars correspond to standard deviations obtained from triplicate analysis.

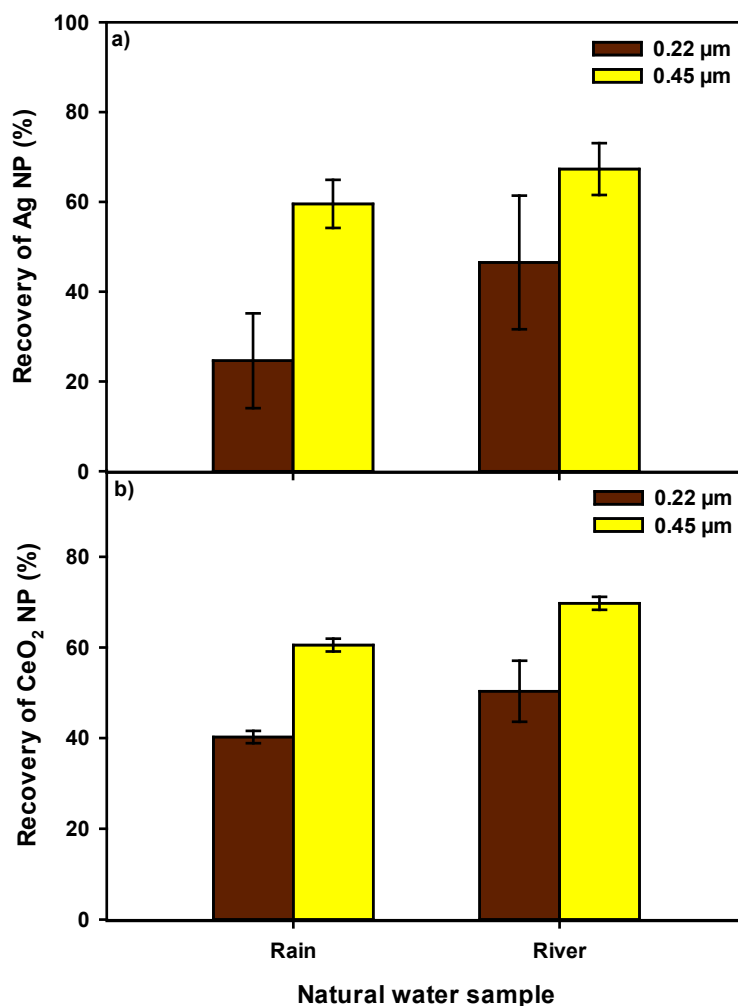


Figure 3-6 Recoveries of (a) Ag and (b) CeO₂ NPs, based on NP number concentrations, in rain and river waters when filtered over polypropylene filters with a pore size of 0.22 (brown) or 0.45 (yellow) μm. Measurements were performed using SP-ICP-MS and a dwell time of 50 μs. Error bars corresponds to standard deviations obtained from triplicate analysis.

Finally, centrifugation (5 min.) was examined as an alternative technique for sample preparation with less potential for adsorptive losses. First, suspensions of Ag and CeO₂ NPs in Milli-Q water were centrifuged and analyzed by SP-ICP-MS. When compared to the unfiltered sample, recoveries of >90% were measured for the two types of NP at centrifugal forces <1000xg (Figure 3-S12). Even for centrifugal forces of 6000xg, recoveries were >80% in Milli-Q water, indicating that the centrifugation alone was not sufficient to remove the NPs. Rain and river

waters were also centrifuged and then analyzed by SP-ICP-MS for Ag and Ce containing particles. For low centrifugal forces (i.e. 50xg, initial points in Figure 3-7), NP losses were minimal. These losses were attributed to adsorption to the centrifuge tubes. An increase of the centrifugal force increased removal for both NP types and for centrifugal forces from 1000-6000xg, there appeared to be little difference in NP losses (Figure 3-7). Based upon Stokes' law calculations, centrifuging at 1000xg will remove particles $>0.6 \mu\text{m}$ for Ag and $>0.7 \mu\text{m}$ for CeO_2 , which explains the similarity with the filtration results when using the $0.45 \mu\text{m}$ PP membrane. The slightly lower recovery that was observed for filters can likely be attributed to adsorption on the membrane, as discussed above. Note that NPs recoveries following centrifugation were higher in Milli-Q, once again, indicating the importance of adsorptive processes since it is assumed that adsorption to natural colloidal particles (i.e. heteroagglomeration²⁰²) might be the dominant process here. For example, about 27% less Ag NP and 47% less CeO_2 were removed from Milli-Q water (Figure 3-S12) as compared to the river water (Figure 3-7), when the samples were centrifuged at 1000xg. Given the similarity in recoveries for the natural water samples when comparing filtration using pre-conditioned PP membranes and centrifugation, we conclude that the losses at low centrifugal forces could be attributed to adsorption (centrifugation tubes), whereas those observed at the higher centrifugal forces could be attributed to adsorption and sedimentation of the larger colloidal sized particles and aggregates (Figure 3-7). Particle size distributions for Ce-containing NPs are shown for the rainwater and the river water following filtration using a preconditioning step (multi-element mixture) and after centrifugation (Figure 3-S13). In the case of the rainwater, both filtration and centrifugation led to quite similar results, suggesting that in the less complex matrix neither pre-treatment procedure would significantly alter the results of the SP-ICP-MS analysis. In the case of river water, however, centrifugation appeared to be preferable to filtration, since a significant shift towards smaller sizes was observed following filtration (likely due particle losses to the filter) and centrifugation results more closely resembled the untreated sample.

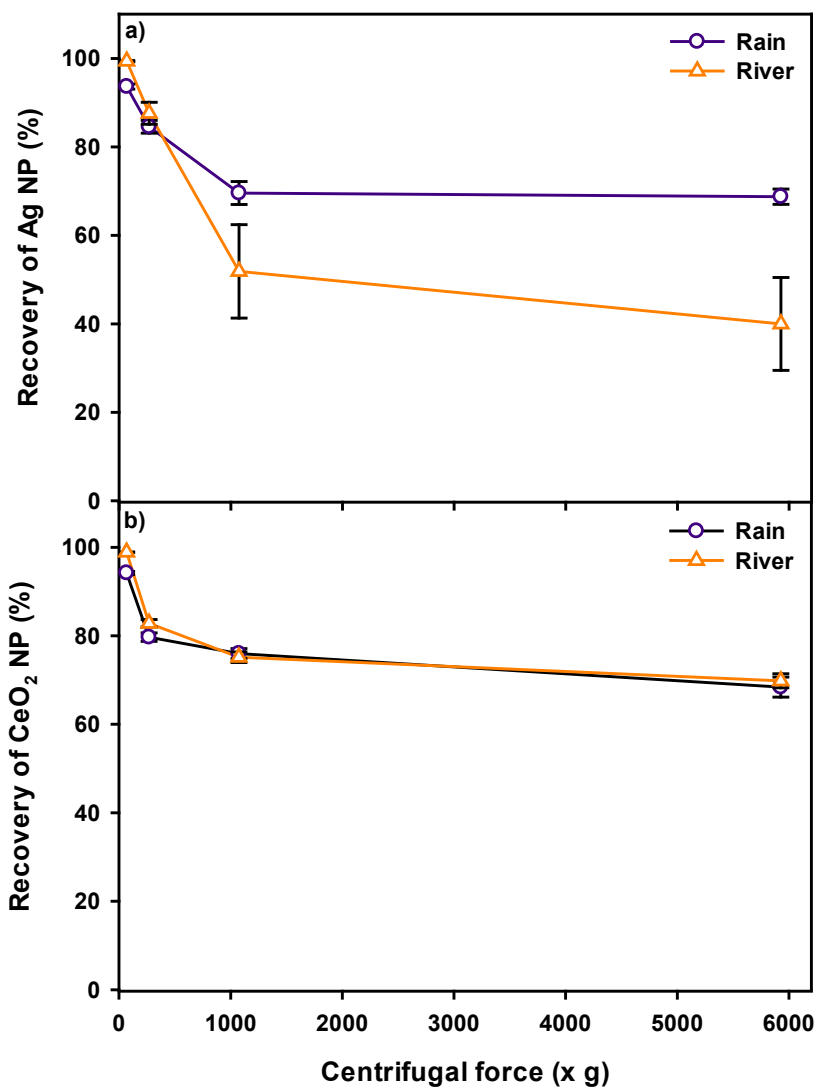


Figure 3-7 Recoveries of (a) Ag and (b) CeO₂ NPs, based on NP number concentrations, in rainwater (purple) and river water (orange) when centrifuged at different rotation speeds. Recoveries are calculated by dividing NP concentrations in centrifuged samples by the concentrations in uncentrifuged samples. Measurements were performed using SP-ICP-MS and a dwell time of 50 μ s. Error bars corresponds to standard deviations obtained from triplicate analysis.

3.5. Conclusions

When analyzing aqueous samples by single particle ICP-MS, sample preparation techniques can lead to very important losses of NPs. While the nylon membrane showed the lowest retention of ionic Ag^+ and Ce^{3+} , the highest recoveries for Ag and CeO_2 NPs were obtained in Milli-Q, rainwater and river waters when filtration occurred over a PP membrane. Furthermore, preconditioning the PP membrane with a multi-ion solution increased the recoveries for Ag and Ce containing particles to >80%. The retained fraction was mainly attributed to heteroaggregates or particles larger than the pore sizes. Similar results were obtained when the natural samples were centrifuged at 1000xg. dans (~1000xg). Finally, some care should be undertaken when extrapolating these ‘best practices’ to NPs in natural systems, which can vary greatly in both ionic and colloidal composition and concentrations.²⁰³ When working with natural dynamic colloidal systems, best practice will always include the use of numerous mass balances to account for potential NP losses.^{199, 204}

3.6. Supporting Information

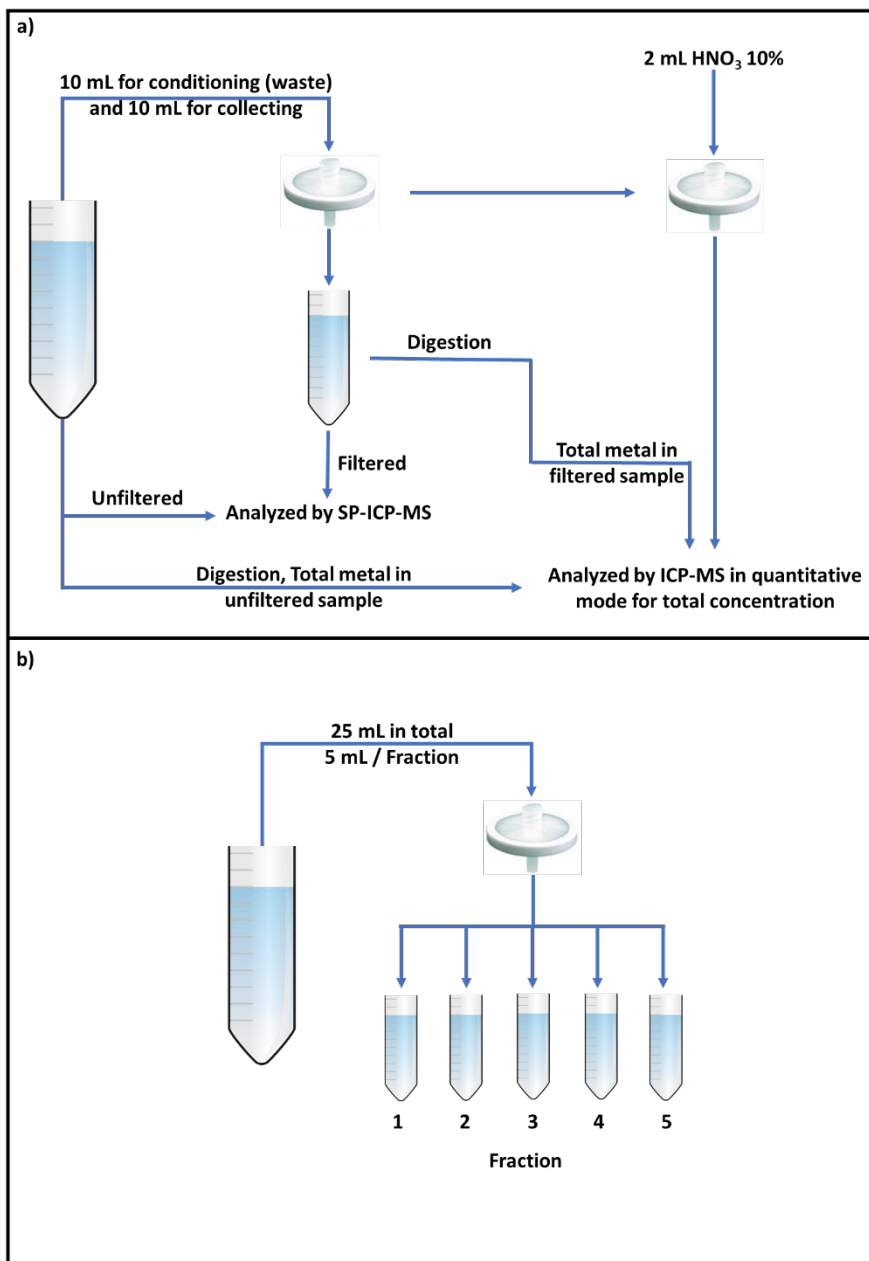


Figure 3-S1 Schematic diagram of the (a) filtration protocol and (b) filtration protocols for membrane conditioning. Total metal represents the sum of particulate and dissolved metal.

Table 3-S1 Concentrations of the multi-element solution (QC-21) used to precondition the membranes.

Element	As	Be	Ca	Cd	Co	Cr	Cu	Fe	Li	Mg	Mn	Mo	Ni	Pb	Sb	Se	Sr	Ti	Tl	V	Zn
Concentration (μM)	1.3	11.1	2.5	0.9	1.7	1.9	1.6	1.8	14.4	4.1	1.8	1.0	1.7	0.5	0.8	1.3	1.1	2.1	0.5	2.0	1.5

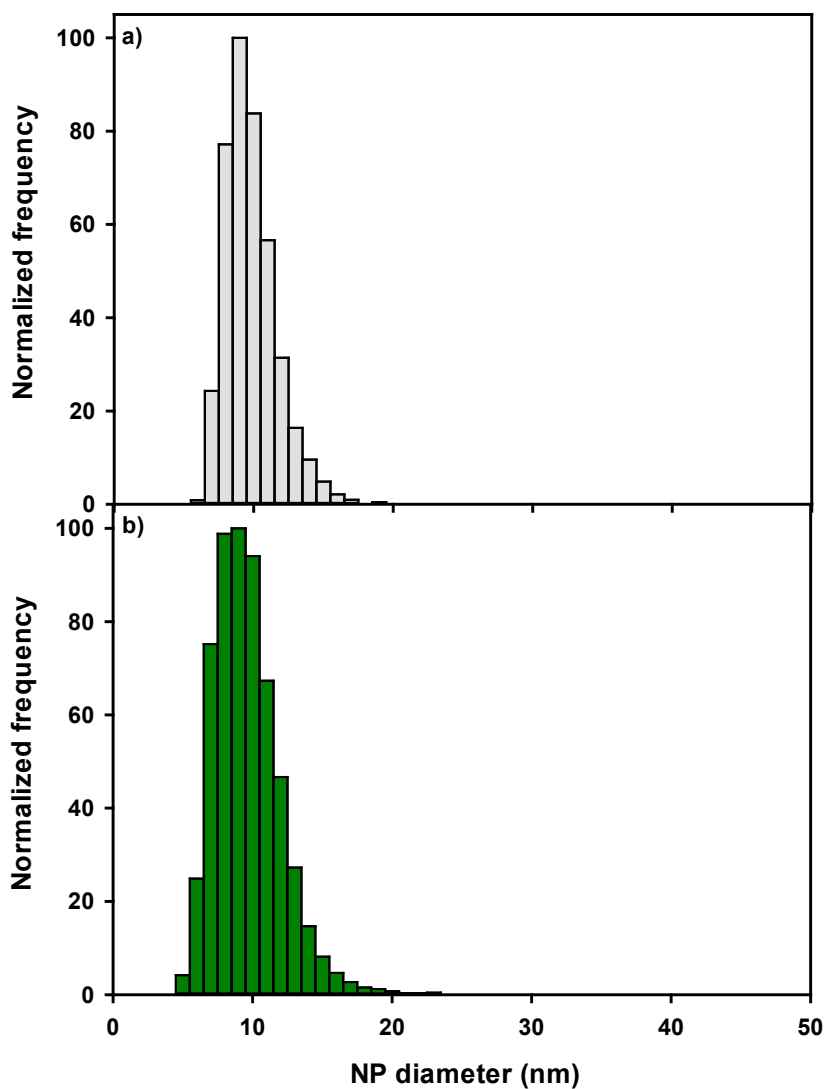


Figure 3-S2 Particle size distributions of (a) Ag and (b) CeO₂ NPs in a 50 ng L⁻¹ suspension in ultrapure water. Measurements were performed using SP-ICP-MS and a dwell time of 50 μs . NP sizes were calculated by assuming that the particles were spherical with a density of 10.5 kg dm⁻³ for Ag and 7.13 kg dm⁻³ for CeO₂.

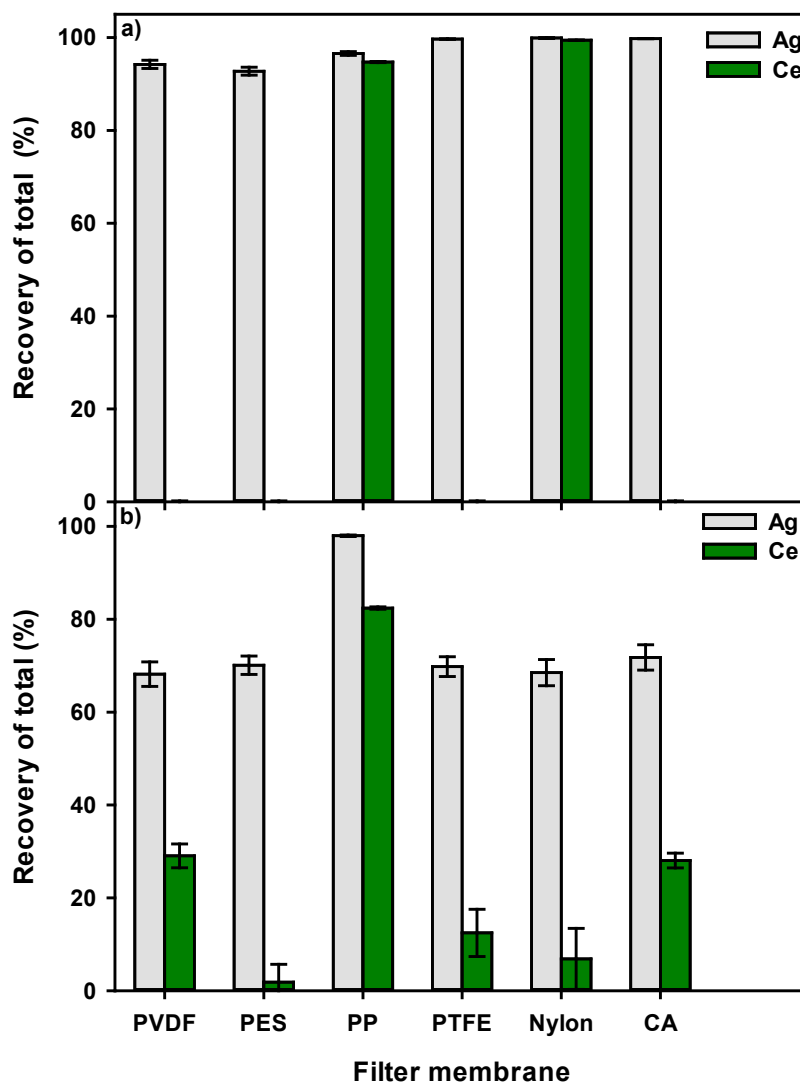


Figure 3-S3 Recoveries of total Ag (grey) or Ce (green) in a 50 ng L⁻¹ **(a)** solution of dissolved metal and **(b)** suspensions of the NP in ultrapure water. Samples were filtered over different membranes: PVDF: polyvinylidene fluoride; PES: polyethersulfone; PP: polypropylene; PTFE: polytetrafluoroethylene; CA: cellulose acetate, all with a pore size of 0.45 μm. In contrast to Figure 1, recoveries are calculated by dividing the total (acid-extractable) metal concentrations in the filtered samples by the concentrations in unfiltered samples. Measurements were performed on digested particle suspensions using ICP-MS in quantitative mode. Error bars correspond to standard deviations obtained from triplicate analyses.

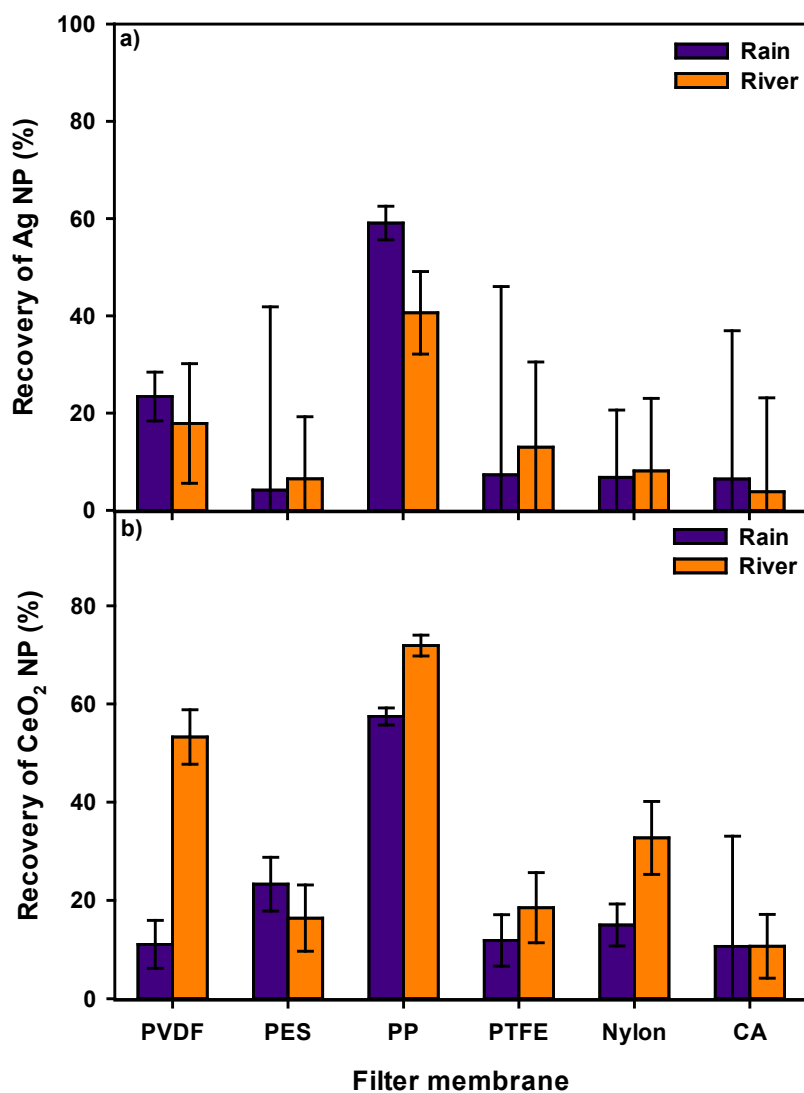


Figure 3-S4 Recoveries of (a) Ag and (b) CeO₂ NPs, based on the NP mass concentrations, in a rainwater (purple) and a river water (orange). Samples were filtered over different membranes: PVDF: polyvinylidene fluoride; PES: polyethersulfone; PP: polypropylene; PTFE: polytetrafluoroethylene; CA: cellulose acetate, all with nominal pore sizes of 0.45 μm . Recoveries are calculated by dividing (a) Ag and (b) CeO₂ NPs mass concentrations in filtered samples by the concentrations in unfiltered samples. Measurements were performed using SP-ICP-MS and a dwell time of 50 μs . Error bars correspond to standard deviations obtained from triplicate analyses.

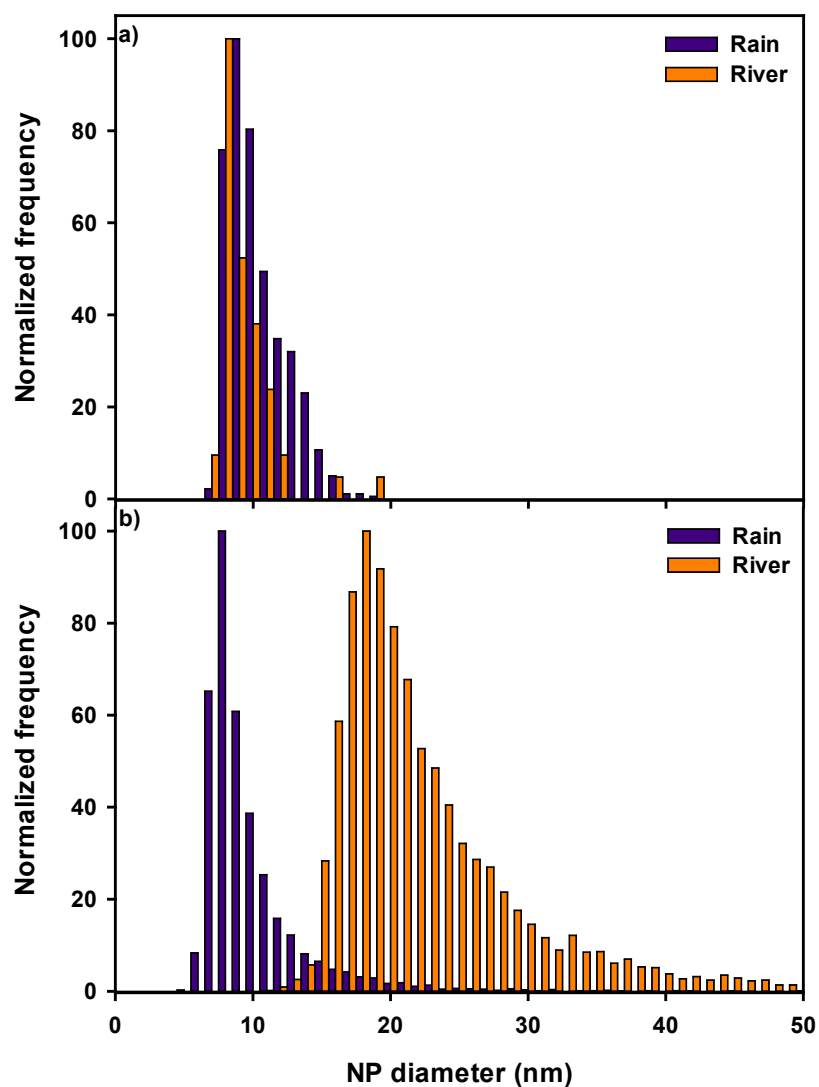


Figure 3-S5 Particle size distributions of **(a)** Ag and **(b)** CeO₂ NPs in an unfiltered rainwater (purple) and river water (orange). Measurements were performed using SP-ICP-MS and a dwell time of 50 μ s. NP sizes were calculated by assuming that the particles were spherical particles with a density of 10.5 kg dm⁻³ for Ag and 7.13 kg dm⁻³ for CeO₂.

Table 3-S2 pH and concentrations of major elements, including total organic carbon (TOC), in an unfiltered rainwater and river water.

Element	Concentration ($\mu\text{g L}^{-1}$)									pH	
	Al	Ca	Cu	Fe	K	Mg	Mn	Na	Zn		TOC
Rain	4.9 \pm 0.3	3784 \pm 170	0.4 \pm 0.0	5.1 \pm 0.1	221 \pm 11	914 \pm 38	0.5 \pm 0.0	1747 \pm 79	<DL	3040 \pm 46	5.4
River	39.3 \pm 0.7	33715 \pm 270	1.3 \pm 0.1	50.1 \pm 0.7	1796 \pm 5	8017 \pm 48	4.0 \pm 0.1	14650 \pm 132	0.3 \pm 0.0	1490 \pm 49	7.6

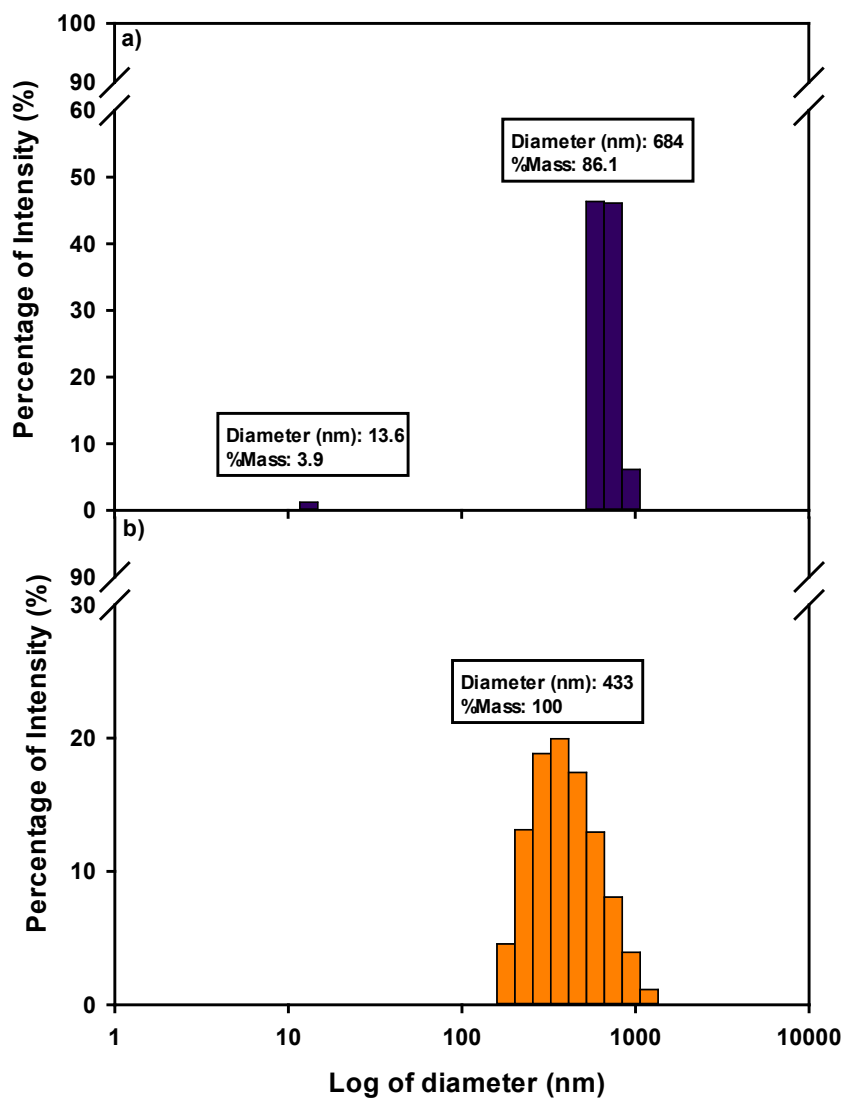


Figure 3-S6 Particle size distributions in an unfiltered (a) rainwater and (b) river water. Measurements were determined using Dynamic Light Scattering (DLS) (Möbiuζ, Wyatt Instruments, 532 laser).

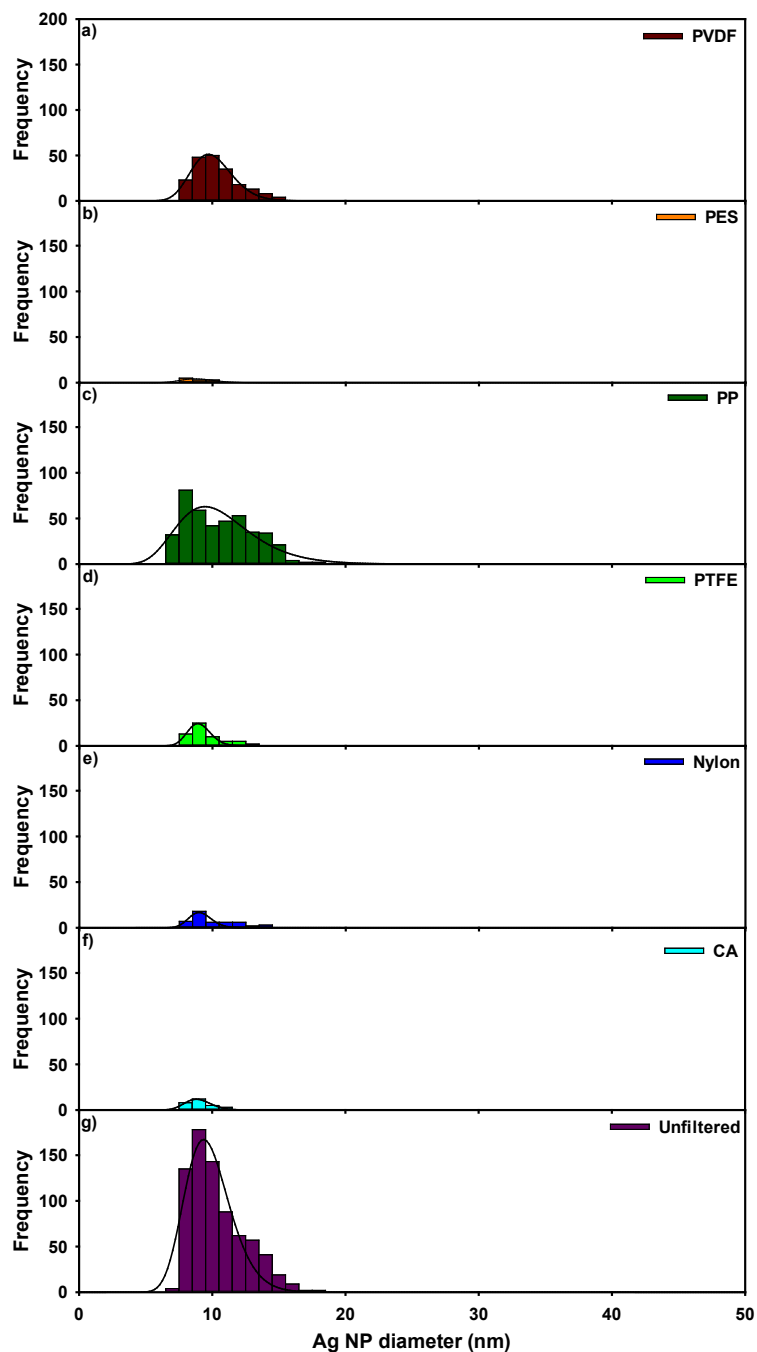


Figure 3-S7 Particle size distributions of Ag NPs in rainwater. Samples were filtered over different membranes: **(a)** PVDF: polyvinylidene fluoride; **(b)** PES: polyethersulfone; **(c)** PP: polypropylene; **(d)** PTFE: polytetrafluoroethylene; **(e)** Nylon; **(f)** CA: cellulose acetate, all with a pore size of 0.45 μm or **(g)** unfiltered. Lines in the graphs represent the log normal fit. Measurements were performed using SP-ICP-MS and a dwell time of 50 μs .

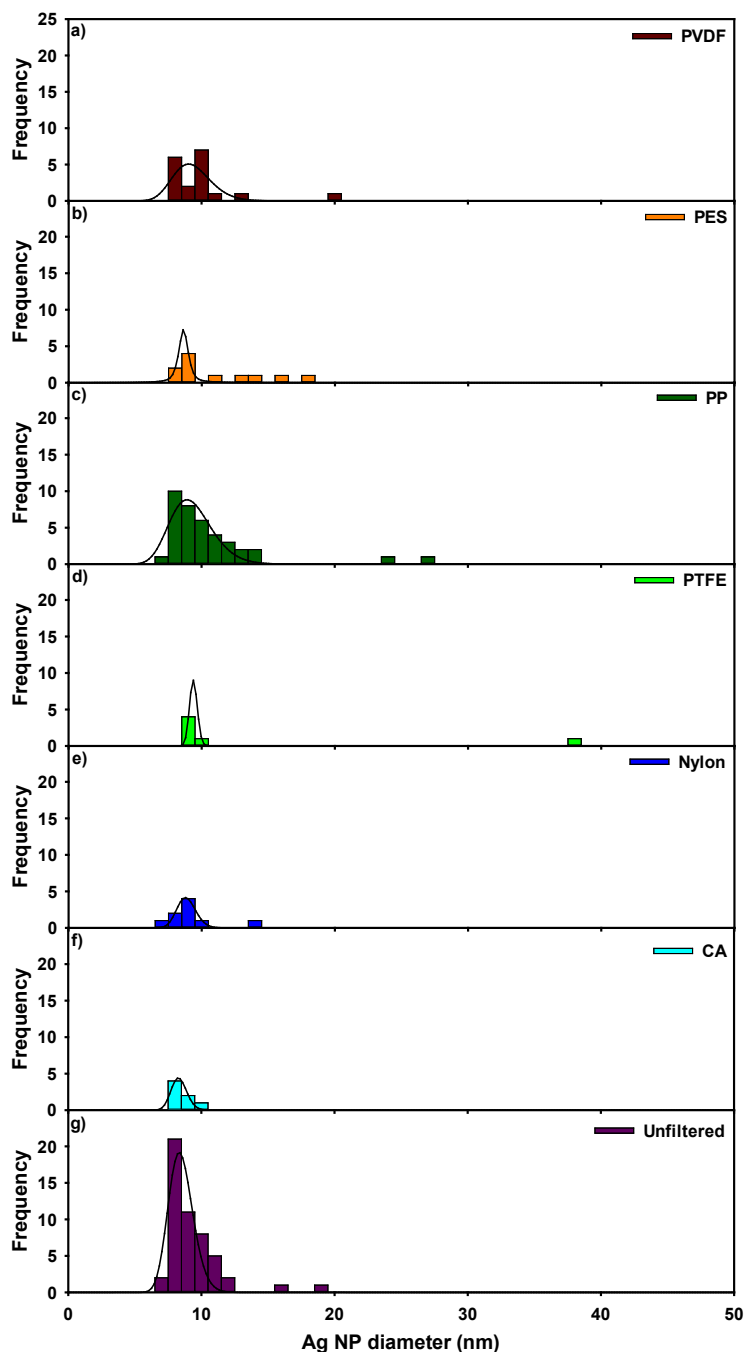


Figure 3-S8 Particle size distributions of Ag NPs in river water. Samples were filtered over different membranes: **(a)** PVDF: polyvinylidene fluoride; **(b)** PES: polyethersulfone; **(c)** PP: polypropylene; **(d)** PTFE: polytetrafluoroethylene; **(e)** Nylon; **(f)** CA: cellulose acetate, all with a pore size of 0.45 μm or **(g)** unfiltered. Lines in the graphs represent the log normal fit. Measurements were performed using SP-ICP-MS and a dwell time of 50 μs .

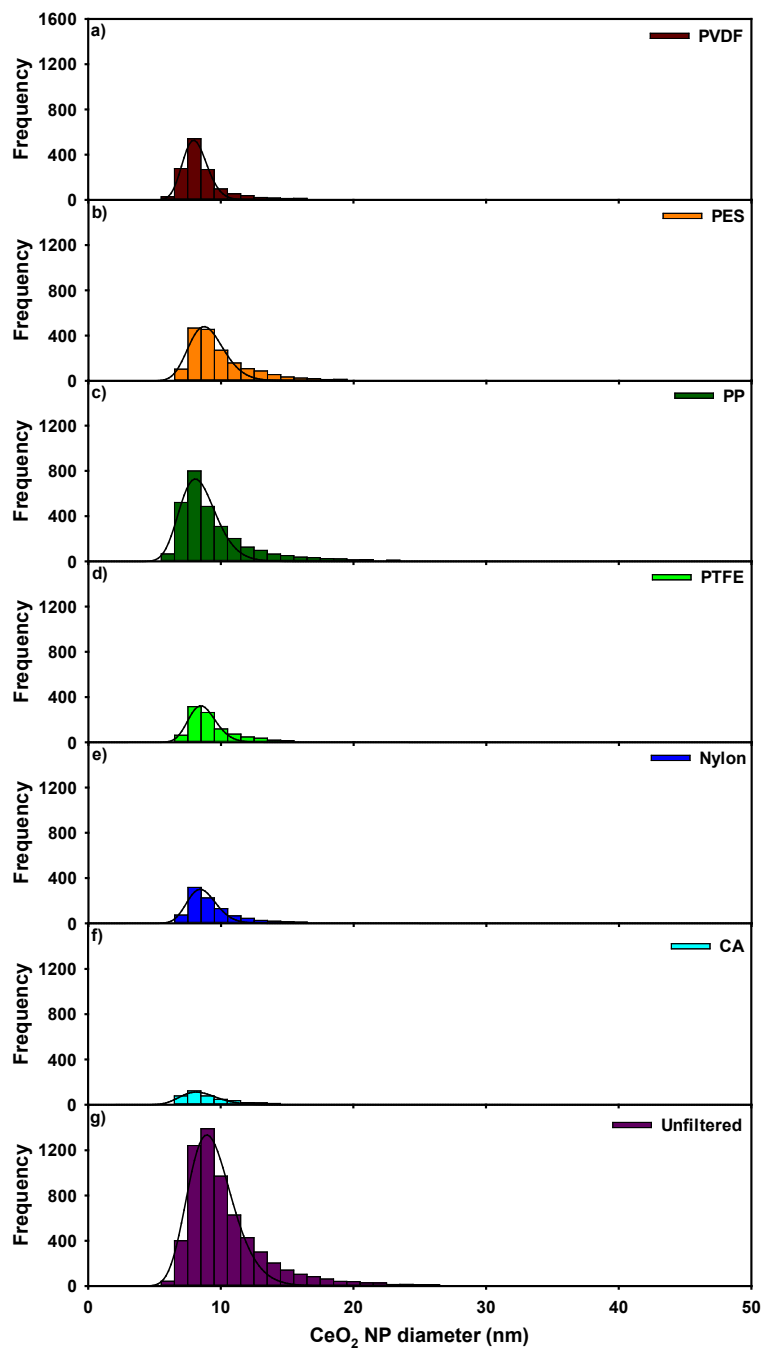


Figure 3-S9 Particle size distributions of CeO₂ NPs in rainwater. Samples were filtered over different membranes: **(a)** PVDF: polyvinylidene fluoride; **(b)** PES: polyethersulfone; **(c)** PP: polypropylene; **(d)** PTFE: polytetrafluoroethylene; **(e)** Nylon; **(f)** CA: cellulose acetate, all with a pore size of 0.45 μm or **(g)** unfiltered. Lines in the graphs represent the log normal fit. Measurements were performed using SP-ICP-MS and a dwell time of 50 μs .

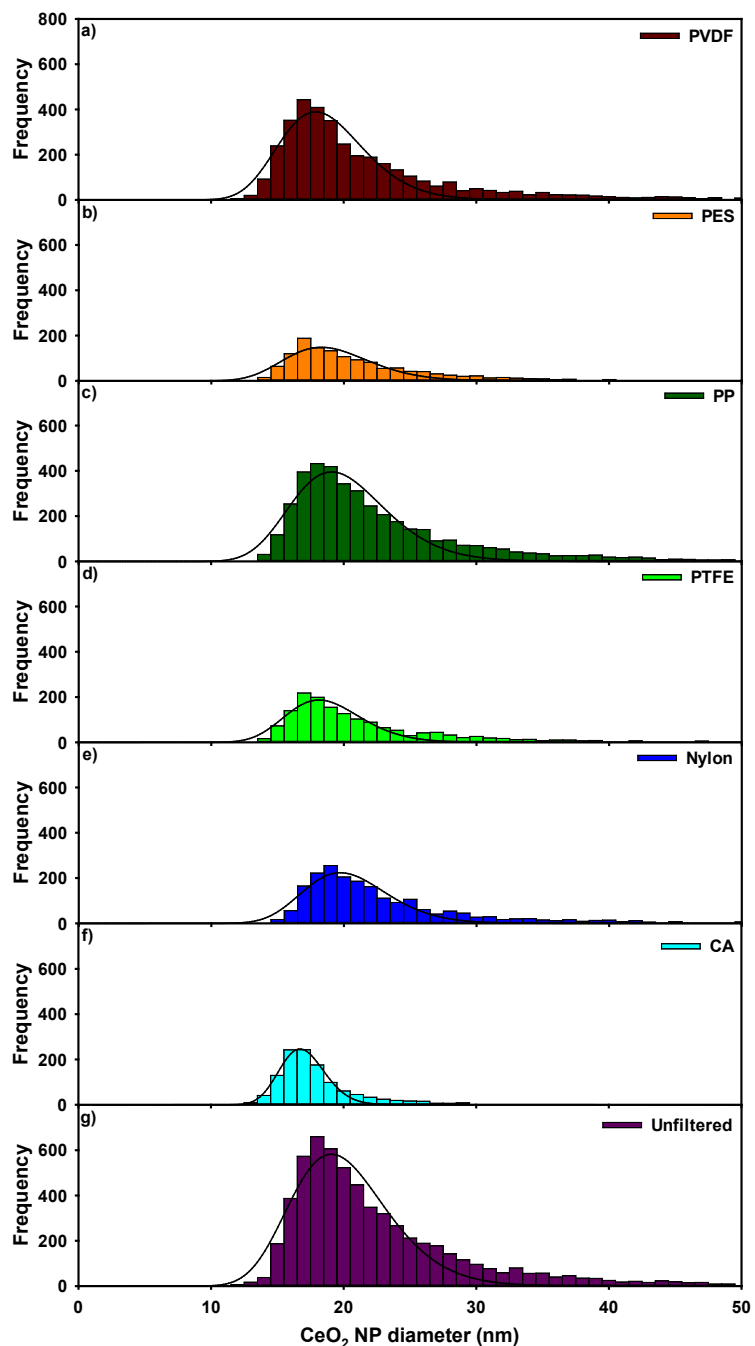


Figure 3-S10 Particle size distributions of CeO₂ NPs in river water. Samples were filtered over different membranes: **(a)** PVDF: polyvinylidene fluoride; **(b)** PES: polyethersulfone; **(c)** PP: polypropylene; **(d)** PTFE: polytetrafluoroethylene; **(e)** Nylon; **(f)** CA: cellulose acetate, all with a pore size of 0.45 μm or **(g)** unfiltered. Lines in the graphs represent the log normal fit. Measurements were performed using SP-ICP-MS and a dwell time of 50 μs.

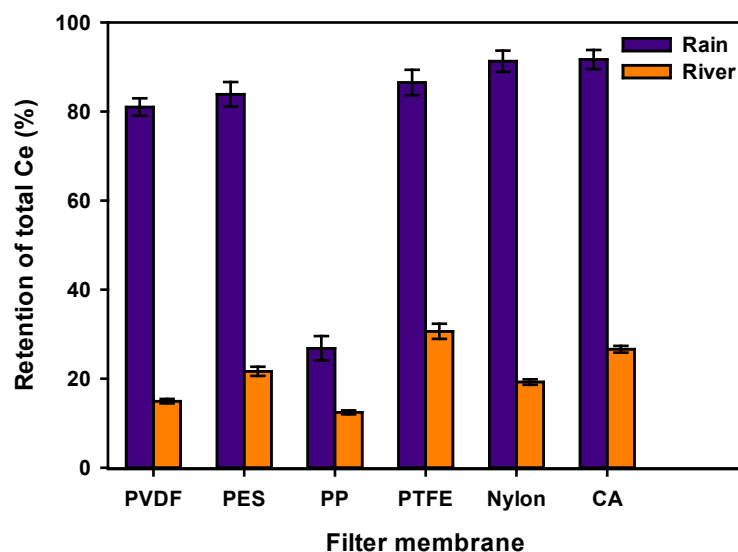


Figure 3-S11 Retention of Ce from rainwater (purple) and river water (orange). Samples were filtered over different membranes: PVDF: polyvinylidene fluoride; PES: polyethersulfone; PP: polypropylene; PTFE: polytetrafluoroethylene; CA: cellulose acetate, all with nominal pore sizes of 0.45 μm . Syringe filters were rinsed with a solution of 10% HNO_3 , which was then analyzed (after dilution) using ICP-MS in quantitative mode. Error bars correspond to standard deviations obtained from triplicate analysis.

Table 3-S3 Recoveries of Ag and Ce, corresponding to the fraction of total (mass) concentration of the metal determined by SP-ICP-MS with respect to concentrations determined by quantitative ICP-MS (digested samples). Means and standard deviations are obtained from the analysis of triplicate samples. ND: not determined.

Unfiltered sample	Recovery (SP/quantitative ICP-MS) (%)	
	Ag	Ce
Ionic solution	92 ± 1	65 ± 1
NP suspension	30 ± 7	51 ± 1
Rain	63 ± 1	27 ± 1
River	ND	81 ± 5

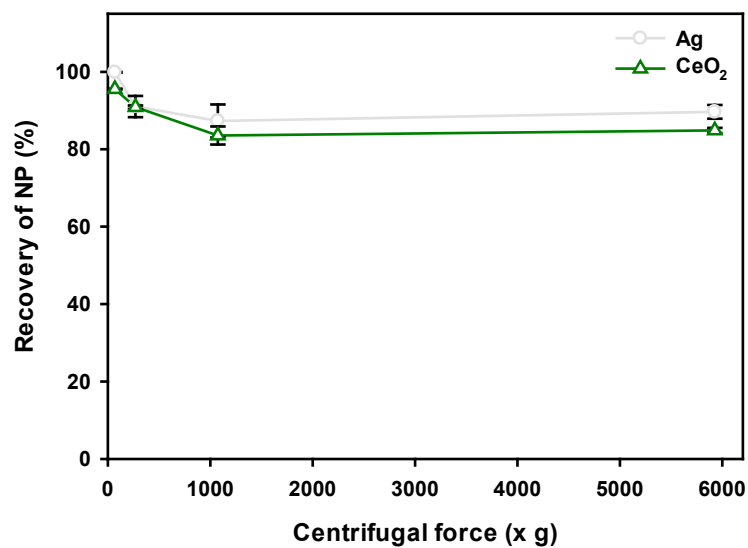


Figure 3-S12 Recoveries of Ag (grey) and CeO₂ (green) NPs, based on NP number concentrations, from a suspension of 50 ng L⁻¹ of the NP in ultrapure water, when centrifuged at different centrifugal forces. Recoveries are calculated by dividing Ag and CeO₂ NP concentrations in centrifuged samples by the concentrations in uncentrifuged samples. Measurements were performed using SP-ICP-MS and a dwell time of 50 μs. Error bars corresponds to standard deviations obtained from triplicate analysis.

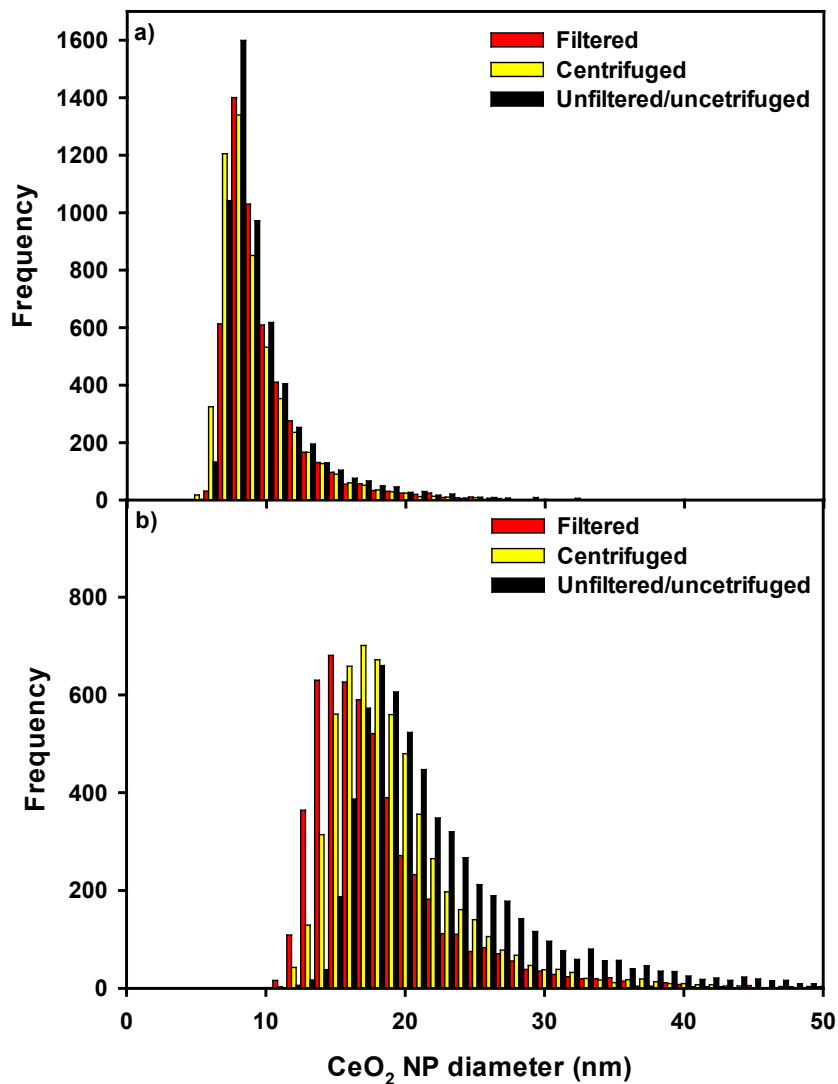


Figure 3-S13 Particle size distributions of CeO₂ NPs in **(a)** rainwater and **(b)** river water. Samples were filtered through polypropylene filters that were preconditioned with a multi-element solution (QC-21), centrifuged at 70 x g, or unfiltered/uncentrifuged. Measurements were performed using SP-ICP-MS and a dwell time of 50 μ s. NP sizes were calculated by assuming that the particles were spherical particles with a density of 10.5 kg dm⁻³ for Ag and 7.13 kg dm⁻³ for CeO₂.

Chapitre 4 –Stability of CeO₂ nanoparticles derived from nano-enabled surface coatings: insights under controlled and environmental scenarios

4.1. Abstract

Due largely to their ability to absorb UV light, cerium oxide (CeO₂) nanoparticles (NPs) are now widely used in numerous surface coatings. CeO₂ NPs release from the surface coatings and their subsequent fate in the environment is difficult to evaluate, and to-date, has either been modelled, based upon elemental mass balances or measured under controlled laboratory conditions. Single particle inductively coupled plasma mass spectrometry (SP-ICP-MS) is emerging as one of the best techniques for detecting very small NPs at very low concentrations in complex media such as natural waters. In this study, we first examined the role of different physicochemical properties (e.g., pH, ionic strength, and concentration of natural organic matter) on CeO₂ NPs contained in a paint and a stain. Their stability was then evaluated in rainwater over 30 days. Finally, we quantified and characterized the release of both dissolved and particulate Ce from the surface coatings under natural weathering conditions. Depending on the media, Ce NPs concentrations in the paint and the stain decreased by 65 – 90%, and 15 – 35%, respectively after 30 days. The loss was attributed to either dissolution or agglomeration/sedimentation. On the other hand, Ce released from painted and stained panels could be shown to be mainly in dissolved metal forms. After 23 weeks of exposure, 3 – 15% of the Ce applied to the painted and 5 – 35% of the Ce applied to stained panels was released to the precipitation, however, Ce NPs were only at background levels.

4.2. Introduction

Surface coatings represent one of the major growth areas for nano-enabled products.²⁰⁵⁻²⁰⁸ Nanoparticles (NPs) are added to surface coatings, including paints, stains, and sealants, to give them a variety of beneficial properties. For example, silver (Ag) NPs are often added to improve antimicrobial activity²⁰⁷⁻²⁰⁹, silica (SiO₂) NPs for scratch resistance, self-cleaning and hydrophobic properties^{207, 210}, titanium dioxide (TiO₂), zinc oxide (ZnO), and cerium oxide

(CeO₂) NPs for photocatalytic and UV protection^{207, 211, 212}. Furthermore, there is growing interest in using CeO₂ NPs, over other metal oxides, as an additive to coatings and sunscreens for UV protection.^{207, 208, 213}

With the significant increase in the production and use of CeO₂ NPs, concern is increasing over their release to the environment and their subsequent fate and toxicity.^{84, 85} Based on modelling scenarios of their releases^{17, 31}, surface coatings are estimated to be a main source for NP release into the environment, which make it necessary to be able to detect, quantify, and characterize the NP in environmental matrices. Unfortunately, analyses of NPs in natural systems are challenging due to their small sizes, their low concentrations (\sim ng L⁻¹) and the complexity of environmental matrices, which also contain natural colloids. While a few recent papers^{208, 211, 214} have measured CeO₂ NPs release from surface coatings such as paints and stains, these studies were performed under controlled laboratory conditions and were limited to observations based upon electron microscopy or measurements of total metal content. There is still relatively little data on the fate of CeO₂ NPs once released from surface coatings, especially under natural weathering conditions.

Single particle inductively coupled plasma mass spectrometry (SP-ICP-MS) is a specific and sensitive technique that enables the detection of very low concentrations (\sim ng L⁻¹) of NP. It can provide information on number concentrations, sizes and particle size distributions.¹¹³ Nonetheless, this technique can be limited by the relatively high size detection limits (SDL), when compared to other techniques such as transmission electron microscopy and dynamic light scattering. Recent advances in this technique, in particular the use of a high sensitivity ICP-MS with short dwell times (<100 μ s) have led to lower SDL on the order of 3 nm.^{118, 173}

NPs fate depends on their physicochemical properties (e.g., size, coating, surface charge, etc.), as well as the nature of the environmental media (e.g., pH, ionic strength and natural organic matter (NOM) content).^{215, 216} While several papers^{120, 123, 163, 215-217} have studied the role of pH, ionic strength and NOM on the stability and fate of CeO₂ NPs, these studies have generally examined pristine NP in simulated natural water samples. Due to analytical limitations, most studies have been performed at high, less relevant, concentrations where agglomeration of NP is favored, and dissolution reduced.^{133, 215-217} Few data are available for the environmental fate

and behavior of CeO₂ NPs that were initially embedded in consumer products, once they are in contact with complex natural waters.

Given the above knowledge gaps, the specific objectives of this study were: (i) to examine the effect of the different physicochemical properties (e.g., pH, ionic strength, and NOM) on CeO₂ NPs that were found in a paint and a stain; (ii) to evaluate their stability in precipitation, and (iii) to quantify and characterize their release under natural weathering scenarios.

4.3. Materials and Methods

4.3.1. Nanoparticles, chemical reagents, and surface coatings

Several nanoparticles were used to optimize and validate the techniques used in this study. Aqueous suspensions of citrate stabilized, Ag nanoparticles with a nominal size of 20 nm (NanoXact, AGCN20) and monodisperse Au NPs with a poly(ethylene glycol) carboxylic acid coating and a nominal size of 30 nm (UltraUniform, AUXU30) were purchased from NanoComposix. Cerium oxide nanoparticles were purchased from Nanobyk (Byk; Nanobyk®-3810, Germany), where they had been developed as an additive for paints. They were purchased as a citrate stabilized aqueous suspension ~~dispersion~~ with a nominal size range of 1-10 nm.

Analytical grade nitric acid (67–70%) was purchased from SCP Science. Ionic cerium (Ce; CGCE1), lanthanum (La; CGLA1) and indium (In; CGIN1) were all ICP-MS standards purchased from Inorganic Ventures. A multi-element, quality control standard QCS-27, was purchased from High Purity Standards. Sodium nitrate (NaNO₃) (purity >99.0%) was purchased from Fisher Scientific. Suwannee River humic (3S101H) and fulvic acids (3S101F) were purchased from the International Humic Substances Society. A stock solution of 50:50 mix of humic acid and fulvic acid was prepared at a concentration of 1000 mg L⁻¹. Sodium bicarbonate (purity >99.5%) and sodium acetate (purity >99.0%) were purchased from Sigma Aldrich for use in preparing 10 mM pH buffers at pH 4.0 and 7.0. pH was adjusted with concentrated nitric acid. Based upon their advertised (Nanoguard) technology, nano-sized pigments, and UV absorbers, two surface coatings were selected for this study: a paint from Behr (Behr Premium Plus ultra exterior satin enamel ultra-pure white paint) and a stain from Sico (exterior semi-transparent wood stain).

4.3.2. Coating procedure and experimental design

Untreated oak slats were cut into panels with the following dimensions: 0.64 cm thick x 6.4 cm wide x 8.4 cm long. Panels were painted using a film applicator (Bird Film Applicator, Inc., USA) on each side of the panel. Due to its lower viscosity, the stain was applied to each side of the oak slat using a paintbrush. Panels surfaces were coated twice on each side (paint: $400 \pm 40 \text{ g m}^{-2}$; stain: $360 \pm 3 \text{ g m}^{-2}$).^{117, 190}

The dry coated panels were placed vertically in pre-weighed, wide-mouth polypropylene containers (500 mL, Fisher Scientific). Containers were placed in plastic bins outdoors on a 7th floor roof (Roger-Gaudry building, University of Montreal, Canada). Due to the ubiquitous presence of NP in the precipitation, empty containers were placed alongside exposure samples in order to collect precipitation. Every 2-3 weeks, containers and water were collected. Wood panels were put into new cleaned and pre-weighed containers. Two sets of experiments were performed: one for 11 weeks beginning in October 2018 and another 12-weeks-experiment starting in late January (2019). All exposure and control samples included 4 replicates.

4.3.3. Sampling and sample preparation for SP-ICP-MS

Precipitation collected in this study was either rainwater, sleet or snow. For fate experiments, rainwater was collected in Brossard, Canada (coordinates: 45.47329, -73.47789) between May and July 2021, using wide-mouth polypropylene containers (500 mL, ThermoFisher Scientific). Samples were stored filled in polypropylene centrifuge tubes (15 and 50 mL), in the dark at 4°C until use. Prior to analysis, samples were vortexed for one minute, sonicated for 10 minutes (Branson Ultrasonic Cleaner, 5510R-DTH Model, 135W) and then vortexed for another minute.

For the experiments examining NPs release from the panels, samples were capped and brought inside the lab at each timepoint and snow and ice were allowed to melt. After weighing, samples were gently mixed and sonicated for 10 minutes. In order to avoid blockage of the ICP-MS nebulizers, 8-10 mL of each sample were filtered through a PVDF (Polyvinylidene fluoride) syringe filter with a diameter of 33 mm and a pore size of 0.45 μm (Sigma-Aldrich). Prior to collecting the sample, the filter membrane was pre-rinsed with 12 mL of Milli-Q water and 6 mL of the sample.^{117, 190} The effect of filtration on the nanoparticle concentrations and sizes was examined and is presented in the Supplementary Information where it is shown that $60 \pm 7\%$ of

the dissolved Ce from a precipitation sample was removed by filtration, resulting in slightly better (i.e. lower) size detection limits for the measurements of the Ce NPs. While $55 \pm 15\%$ of the particles were also removed, based upon the particle size distributions (Figure 4-S1), particles lost to the filter appeared to be mainly in the larger class sizes (i.e. $>0.45 \mu\text{m}$). For the NPs fate experiments, precipitation samples were freshly collected and quickly analyzed (short storage time at 4°C) and thus did not require filtration.

4.3.4. ICP-MS analyses

The acquisition of single particle data was performed using a double focusing magnetic sector field ICP-MS in fast scan mode (Nu AttoM ES, Nu Instruments, UK). The introduction system consisted of a micro-flow concentric glass nebulizer (self-aspiration rate of $\sim 200 \mu\text{L}/\text{min}$ for 1 L min^{-1} Ar), a 1.5 mm internal diameter quartz injector and a quartz cyclonic spray chamber, cooled to 4°C . The argon was also used as a coolant gas with a flow rate of 13.0 L min^{-1} . Isotopes (^{107}Ag , ^{139}La , ^{140}Ce , ^{197}Au) were measured for 50 s using a dwell time of $50 \mu\text{s}$ (i.e. one million datapoints). Calibrations were performed using ionic standards. Transport efficiency (TE) was determined by measuring the particle number concentration of a standard suspension of ultra-uniform 30 nm Au NP.¹²⁷ Sensitivities and TE were validated with a multi-element standard (QCS-27) and a suspension of 20 nm Ag NPs, respectively.^{115, 122}

Total metal concentrations were determined by digesting samples by adding 70% ultrapure HNO_3 to aliquots of filtered samples in order to achieve a final acid concentration of 20% v/v. Samples were then heated for 16 h at 85°C using a DigiPREP digestion system (SCP science), followed by dilution to 4% v/v HNO_3 with Milli-Q water. Metal concentrations were measured using a quadrupole ICP-MS (Perkin Elmer NexIon 300x). Ionic Ce was used for calibration and In was employed as the internal standard. Sensitivities were validated using QCS-27.

4.3.5. SP-ICP-MS data processing

Nu Quant software (version 2.2, Nu Instruments, UK) was used to process SP-ICP-MS data. The operating mode of this software has been described in detail elsewhere.^{118, 173} Briefly, the background baseline is first defined by smoothing the data. The algorithm then searches a defined window for intensity maxima that exceed the smoothed background. Pre- and post-

inflection points of the maxima are defined, and the data are integrated between these points using a threshold that is based upon the local peak background. The concentration of dissolved metal in the sample is calculated from the average background for the entire data set.

4.4. Results and Discussion

4.4.1. Ce containing NP in the precipitation, paint and stain

Since the precise particle compositions were not known (especially for the paint and stain samples), results have been given as the masses of Ce in each NP. When precipitation, paint and stain samples were analyzed by SP-ICP-MS for ^{140}Ce , the transient raw data showed the presence of spikes, clearly indicating the presence of Ce-containing NPs (Figure 4-S2). The particles detected in the precipitation had a fraction of Ce with an average mass of 9 ag. On the other hand, a higher fraction of Ce was detected in the particles contained in the paint and the stain, with average masses of 29 and 32 ag, respectively (Figure 4-1). Under the assumption that the detected particles correspond to spherical CeO_2 NPs, particle size distributions (PSD) could be estimated (Figure 4-S3). In all three sample types, particulate and dissolved Ce were clearly detected (Table 4-1). While the nanoparticles in the paint were generally larger, those in the stain were more polydisperse (Table 4-1). Nearly 25% of the Ce in the precipitation was in the form of NP, while the paint and stain samples had 40 and 70%, respectively (Table 4-1).

Samples were also digested and analyzed for total Ce using ICP-MS in quantitative mode. The paint and stain had similar total Ce concentrations (Table 4-1). When concentrations in the digested samples were compared to those obtained by SP-ICP-MS, recoveries of 26%, 97% and 98% were determined for the precipitation, paint and stain, respectively. The low recoveries for the precipitation measured in single particle mode (i.e. no acid added to samples) were mainly attributed to adsorptive losses within the introduction system of the ICP-MS and to the presence of larger particles that could not be analyzed by SP-ICP-MS. We hypothesize that the higher recoveries determined in the paint and stain could have been due to the presence of dispersants that would reduce adsorption.

In order to determine whether the detected particles were engineered or natural NP, ^{139}La was also measured by SP-ICP-MS. For Ce NP, Ce/La ratio has been used to differentiate the two types of NP since the rare earth elements are nearly always found as mixtures in the

environment.^{165, 174} Based on the ratio in the earth's crust, a Ce/La ratio of ~2 is expected for natural NP. In that light, Montañó *et al.*²¹⁸ compared Ce/La ratios of nearly 1000 European surface water samples where they found a fairly stable Ce/La ratio of 1.7. In the precipitation, concentrations of both the dissolved and particulate forms of Ce were almost 2x those of La with a Ce/La NP ratio of 1.6 ± 0.6 and a dissolved Ce/La of 2.7 ± 0.7 (Table 4-S1). However, in the paint and the stain samples, the Ce/La NP ratios were 26.7 ± 0.1 and 80.5 ± 11.1 , respectively, indicating the presence of engineered Ce NPs (Table 4-S1). As a control, no La (dissolved or NP) was detected in the suspension of engineered CeO₂ NP.

Table 4-1 Mean and mode particle sizes, polydispersity indices, concentrations of nanoparticulate and dissolved Ce determined by SP-ICP-MS in addition to total digested metal determined by quadrupole ICP-MS. Note that errors correspond to standard deviations obtained from the analysis of triplicate samples and which were systematically smaller than the polydispersities obtained from the PSD.

Sample	Precipitation	Paint	Stain
Average CeO ₂ NPs size (nm)	11.8 ± 0.1	17.5 ± 0.1	16.6 ± 0.1
Mode CeO ₂ NPs size (nm)	10	14	12
Polydispersity index	0.19 ± 0.01	0.17 ± 0.00	0.30 ± 0.01
Particle number concentration	$(5.9 \pm 0.6) \times 10^8 \text{ (L}^{-1}\text{)}$	$(2.7 \pm 0.1) \times 10^{12} \text{ (kg}^{-1}\text{)}$	$(4.9 \pm 0.1) \times 10^{12} \text{ (kg}^{-1}\text{)}$
Mass concentration of dissolved Ce	$0.016 \pm 0.001 \text{ (}\mu\text{g L}^{-1}\text{)}$	$121.7 \pm 1.5 \text{ (}\mu\text{g kg}^{-1}\text{)}$	$66.6 \pm 0.7 \text{ (}\mu\text{g kg}^{-1}\text{)}$
Mass concentration of Ce NPs	$0.005 \pm 0.002 \text{ (}\mu\text{g L}^{-1}\text{)}$	$79.2 \pm 2.4 \text{ (}\mu\text{g kg}^{-1}\text{)}$	$166.5 \pm 7.7 \text{ (}\mu\text{g kg}^{-1}\text{)}$
Total Ce mass concentration	$0.08 \pm 0.01 \text{ (}\mu\text{g L}^{-1}\text{)}$	$206.0 \pm 1.4 \text{ (}\mu\text{g kg}^{-1}\text{)}$	$238.7 \pm 13.6 \text{ (}\mu\text{g kg}^{-1}\text{)}$

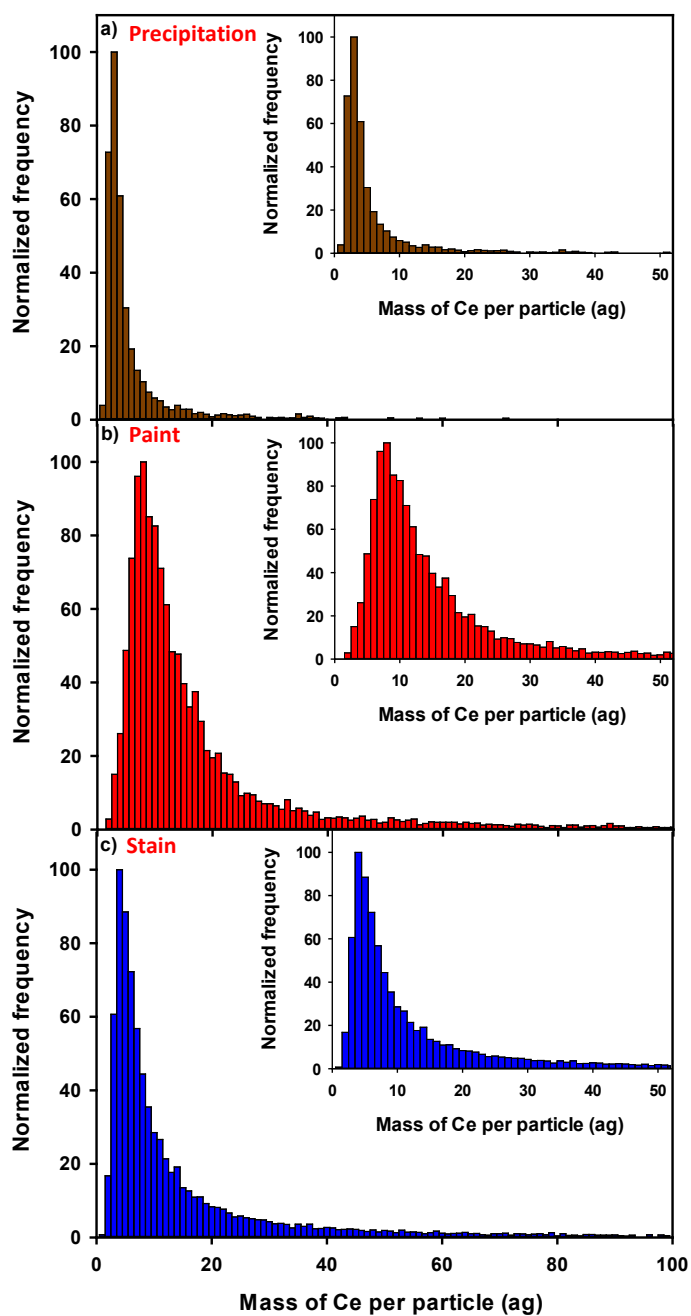


Figure 4-1 Mass distributions of Ce NPs in (a) precipitation, (b) diluted (2500 x) paint and (c) diluted (2500 x) stain. Measurements were performed on a sector field SP-ICP-MS using a dwell time of 50 μ s.

4.4.2. Fate of Ce NPs contained in the surface coatings

Engineered CeO₂ NPs, paint, and stain samples were spiked into different media in order to have a final Ce NPs mass concentration of approx. 50 ng L⁻¹. Samples were monitored for 30 days to evaluate the effect of individual aqueous parameters on the stability of the Ce NP.

4.4.2.1. Effect of ionic strength

The presence of easily ionized elements (e.g. Na) at high concentrations in the matrix can lead to a signal suppression. Thus, in order to study the effect of sodium ions on NP PSD measurements, the impact of their presence on the ¹⁴⁰Ce signal was first evaluated by performing calibrations with or without NaNO₃. The sensitivity for Ce decreased by 3% when 10 mM ~~and~~ of NaNO₃ was added to the standards and by 28% when 100 mM was added (Figure 4-S4). Consequently, when NP stabilities were evaluated as a function of ionic strength, part of the sensitivity reduction, leading to smaller NP sizes, could be attributed to signal suppression. Results were corrected by performing the calibration in the same NaNO₃ concentration as the particle size determinations.

One day after spiking the CeO₂ NPs into Milli-Q water with different concentrations of NaNO₃, a decrease in the NP concentration was observed as a function of ionic strength (Figure 4-2a). Based upon classical DLVO (Derjaguin, Landau, Verwey, Overbeek) theory, the accumulation of Na ions in the electrical double layer, is likely to have masked the particle charge (citrate coating), facilitating the agglomeration (and eventually sedimentation) of the NP. PSD are consistent with this process where shifts to larger particle sizes and lower particle concentrations were measured as a function of increasing ionic strength (Figure 4-S5). Indeed, NP concentrations decreased with time in the three media, even in the absence of ionic strength (> 90% of loss of NP after 30 days) (Figure 4-2a). In order to determine if the loss of NP was primarily due to agglomeration or dissolution, dissolved and total Ce concentrations were monitored with time (Figure 4-S6). While dissolved Ce concentrations did not increase with time (Figure 4-S6a), mean NP sizes appeared to decrease over the first 10 days of the experiment (Figure 4-S7a), indicating that either the cationic Ce (Ce³⁺/Ce⁴⁺) was being lost to the container walls via adsorption or that the largest particles and particle agglomerates were lost through sedimentation, which could have shifted mean NP diameters to smaller sizes (Figure 4-S8). While this second explanation is consistent with the known mechanisms of particle charge

screening and the ionic strength effect observed in Figure 2, both mechanisms are likely to be occurring simultaneously.

Adsorptive losses of ionic lanthanides to the sample tube walls and to the inside of the ICP-MS introduction system have been documented previously.¹⁹⁹ In order to verify whether they were important here, a solution of ionic Ce in Milli-Q water was analyzed by SP-ICP-MS followed by rinses using either Milli-Q water or a solution of 2% HNO₃. When compared to the measurement of an acidified sample, a recovery of 55% was obtained for the unacidified sample (Figure 4-S9a), confirming important adsorptive losses to either the sample tubes or the components of the ICP-MS introduction system. Of the missing 45%, 7.5% of the Ce losses were found on the walls of the sample tube (Figure 4-S9a), while the remaining losses could be recovered through the addition of 2% HNO₃. Negligible Ce was recovered when non-acidified Milli-Q water was injected immediately after the sample (Figure 4-S9a). In fact, not all Ce was recovered in the first replicate of acid wash (Ce continued to be released above detection limits until the third replicate) (Figure 4-S9b).

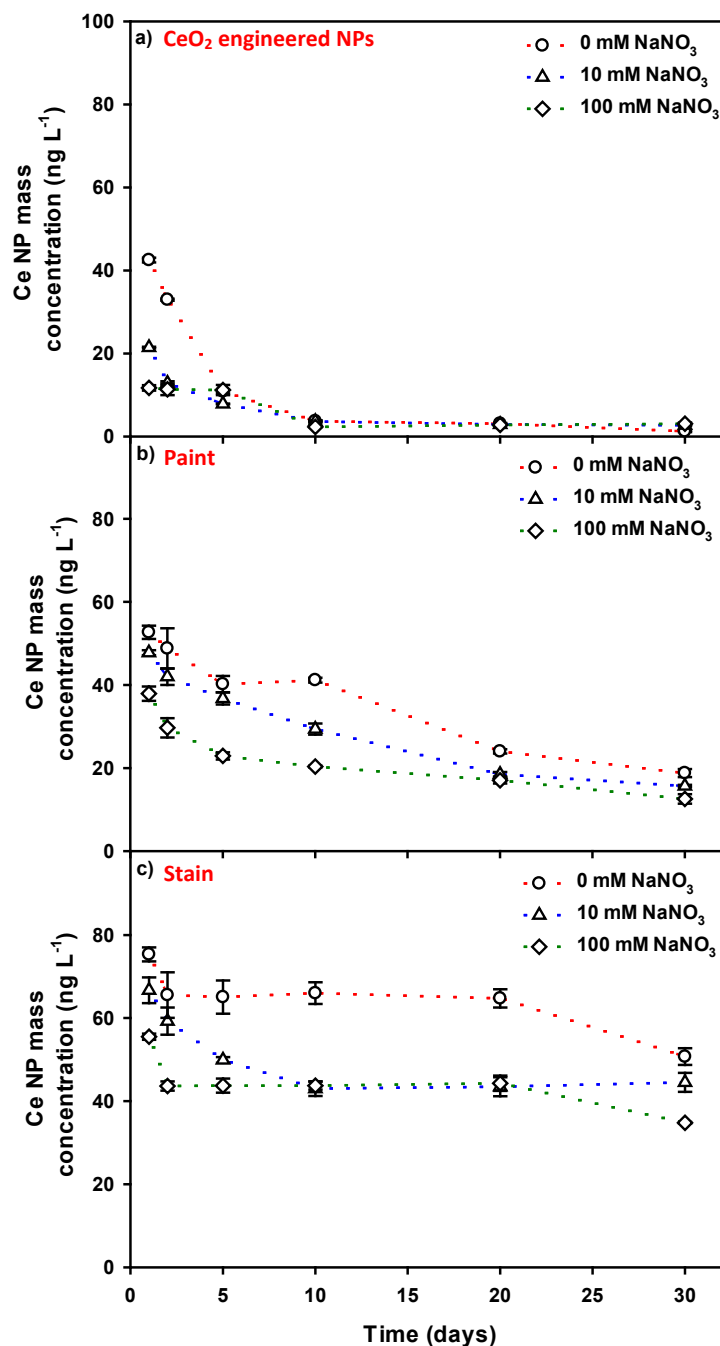


Figure 4-2 Mass concentration of the Ce-containing NPs in solutions containing: **(a)** engineered CeO₂ NPs in Milli-Q water; **(b)** Ce NPs in diluted (2500 x) paint and **(c)** Ce NPs in diluted (2500 x) stain with three different ionic strengths as a function of time. Error bars correspond to standard deviations obtained from triplicate analysis. Measurements were performed using a sector field SP-ICP-MS with dwell times of 50 μ s.

Paint and stain samples were also diluted into Milli-Q water at similar ionic strengths. As was seen for the CeO₂ NPs, the concentration of the Ce-containing NPs in the paint and stain decreased with increasing NaNO₃ (Figure 4-2b & c). For both the paint and stain, decreases in the NP concentrations were consistent with either agglomeration/sedimentation or adsorptive losses of the dissolved Ce. With or without the NaNO₃, the NPs concentrations decreased by almost 65% in the paint and by 35% in the stain after 30 days. However, the mean diameters of the NP in the paint and stain did appear to stabilize after 10 days (Figure 4-S7b & c), suggesting that even in the presence of significant ionic strength, the NPs appear to have some long-term stability. Particle number decreases observed in the stain and paint were substantially smaller than losses observed for the CeO₂ NPs (~99%), which suggests that the dispersants and NP surface coatings in the paint and stain played a long-term role in stabilizing the NPs, mainly by decreasing particle agglomeration.

4.4.2.2. Effect of natural organic matter

The engineered CeO₂ NPs, the paint, and the stain were spiked into Milli-Q water with different NOM contents (0, 2 or 10 mg L⁻¹). Contrary to our expectation that the presence of NOM would lead to a stabilization of the Ce NPs,^{41, 163, 215} no significant differences (ANOVA, $p < 0.05$) were observed when comparing the controls obtained in the absence of NOM with those obtained in the presence of either 2 or 10 mg L⁻¹ of NOM. While the presence of NOM did not appear to reduce agglomeration (Figure 4-3 & Figure 4-S10), it did appear to increase dissolution slightly for the CeO₂ NP (Figure 4-4a). Complexation of the NPs by NOM is thought to increase dissolution by complexing the free Ce in solution, i.e. ligand enhanced dissolution^{219, 220}). After 30 days in the media containing either 2 or 10 mg L⁻¹ of NOM, Ce dissolution accounted for 50% of the decrease in the concentrations of the CeO₂ NPs. Nonetheless, enhanced dissolution was not observed for the NPs from the paint or stain (Figure 4-4b & c), suggesting that once again, chemical composition of the NPs (including surface coatings) or the presence of dispersing agents increased the long-term of the NPs in water. For all three samples, NPs dissolution was not sufficient to explain all of the observed losses of NPs that were observed over 30 days- losses due to agglomeration/sedimentation or adsorptive losses are likely important in all three suspensions.

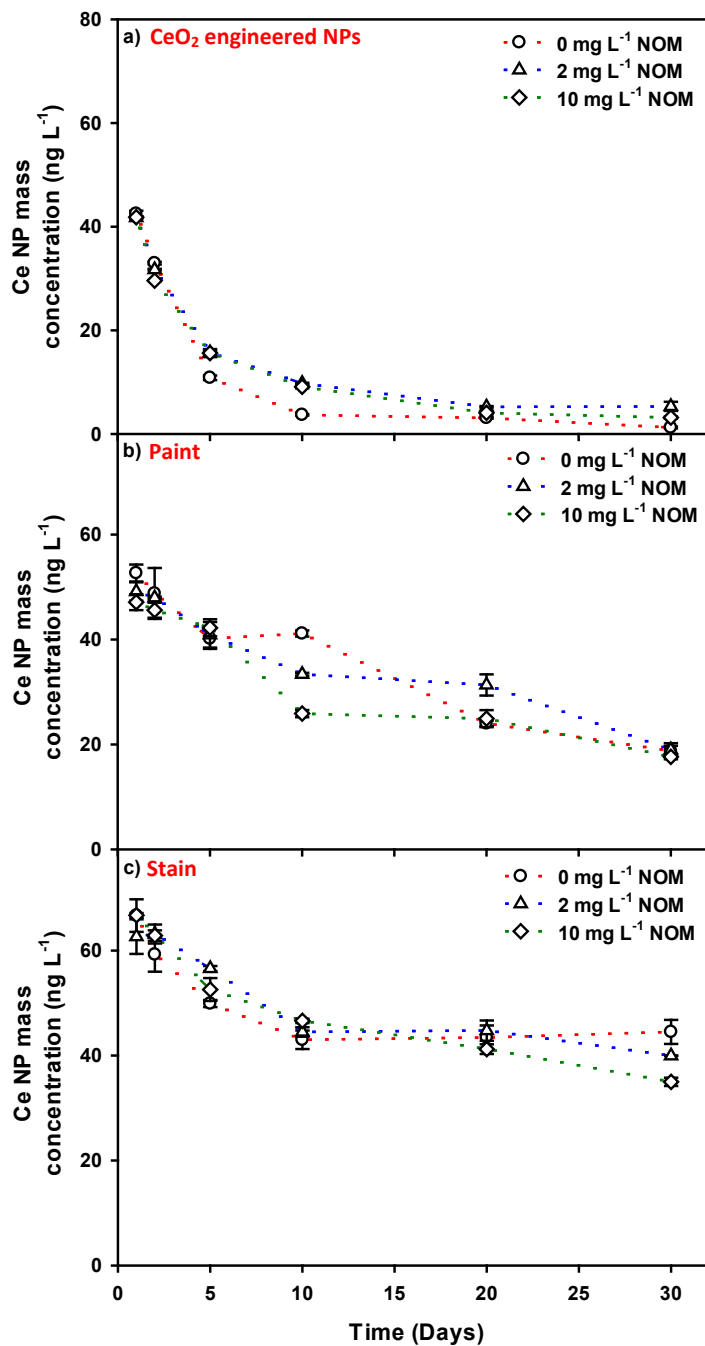


Figure 4-3 Mass concentration of the Ce containing NP as a function of time for: **(a)** engineered CeO₂ NPs; **(b)** paint and **(c)** stain spiked into Milli-Q water with three different contents of natural organic matter. The paint and stain were diluted 2500x. Error bars correspond to standard deviations obtained from triplicate analysis. Measurements were performed using a magnetic sector SP-ICP-MS with a dwell time of 50 μ s.

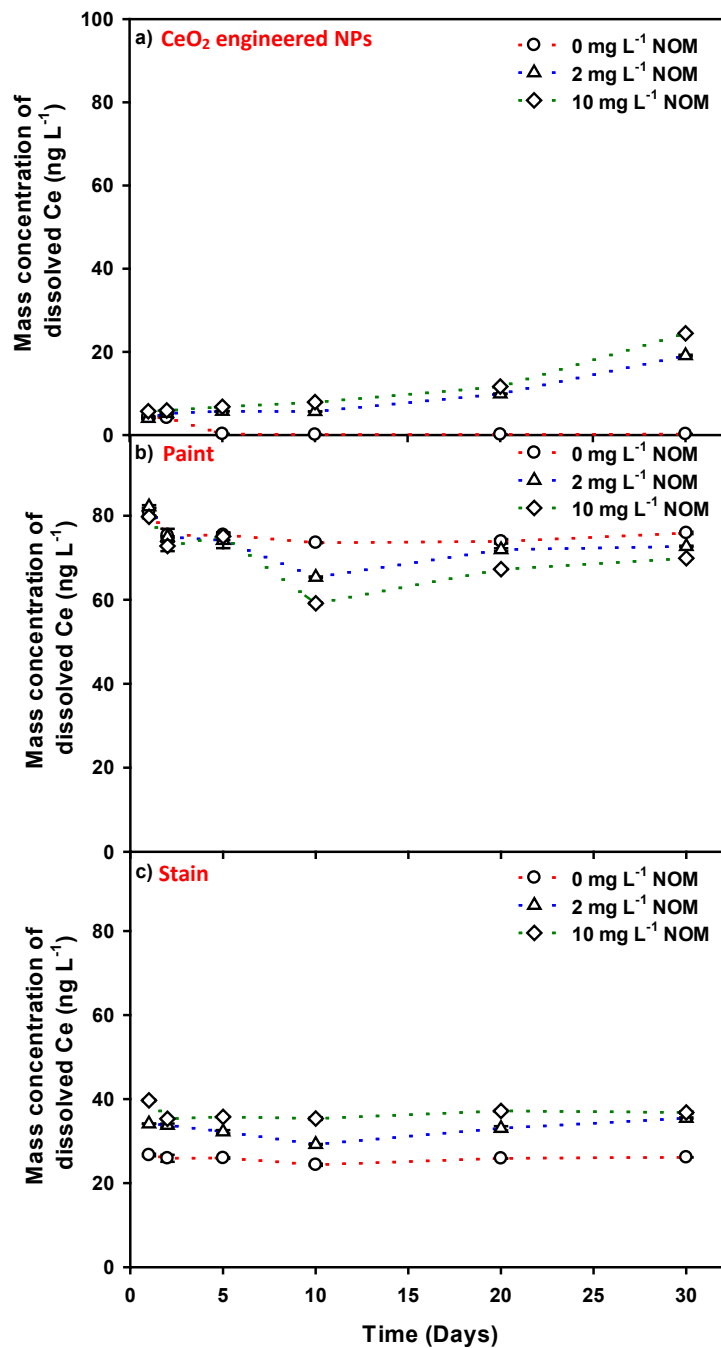


Figure 4-4 Mass concentrations of dissolved Ce as a function of time for: **(a)** an engineered CeO₂ NPs, **(b)** paint and **(c)** stain spiked into Milli-Q water with three different concentrations of natural organic matter (0, 2 and 10 mg L⁻¹). Paint and stain were diluted 2500x. Error bars correspond to standard deviations obtained from triplicate analysis. Measurements were performed using a magnetic sector SP-ICP-MS with a dwell time of 50 μ s.

4.4.2.3. Effect of pH

In order to examine the effect of pH on the NPs, samples were dispersed at either pH 4.0 or pH 7.0. For the engineered CeO₂ NPs, the concentration of NPs decreased with time at both pH (Figure 4-5a). The concentration of dissolved Ce increased with time at pH 4.0 but was stable at pH 7.0, suggesting that NPs dissolution mainly occurred at the lower pH (Figure 4-S11a). Nonetheless, as discussed above, one cannot discount that NPs dissolution was also occurring at pH 7.0, but that dissolved Ce was lost to adsorption. When compared to pH 4.0, adsorption is likely to be more important at pH 7.0, due to less competition with protons for adsorptive sites.

Very different curves were observed for the NPs in the paint and stain. Already on day 1, 9x fewer NPs were measured in the paint at pH 4.0 as compared to pH 7.0 (Figure 4-5b), consistent with the high concentrations of dissolved Ce (Figure 4-S11b). In contrast, pH appeared to have very little effect on the Ce NPs in the stain over the first 5 days of the experiment where no differences were observed when comparing the two pH values (Figure 4-5c). Nonetheless, after 10 days, a greater decrease in the NP concentration could be seen at pH 4.0 (t-test, $p = 0.01$). Indeed, after one month, the concentration of Ce NPs in the (diluted) stain decreased by almost 35% at pH 4.0 and by 15% at pH 7.0. Much of the decrease could be attributed to increased dissolution at the lower pH since the concentration of dissolved Ce increased by 20% at pH 4.0 as compared to 5% at pH 7.0 (Figure 4-S11).

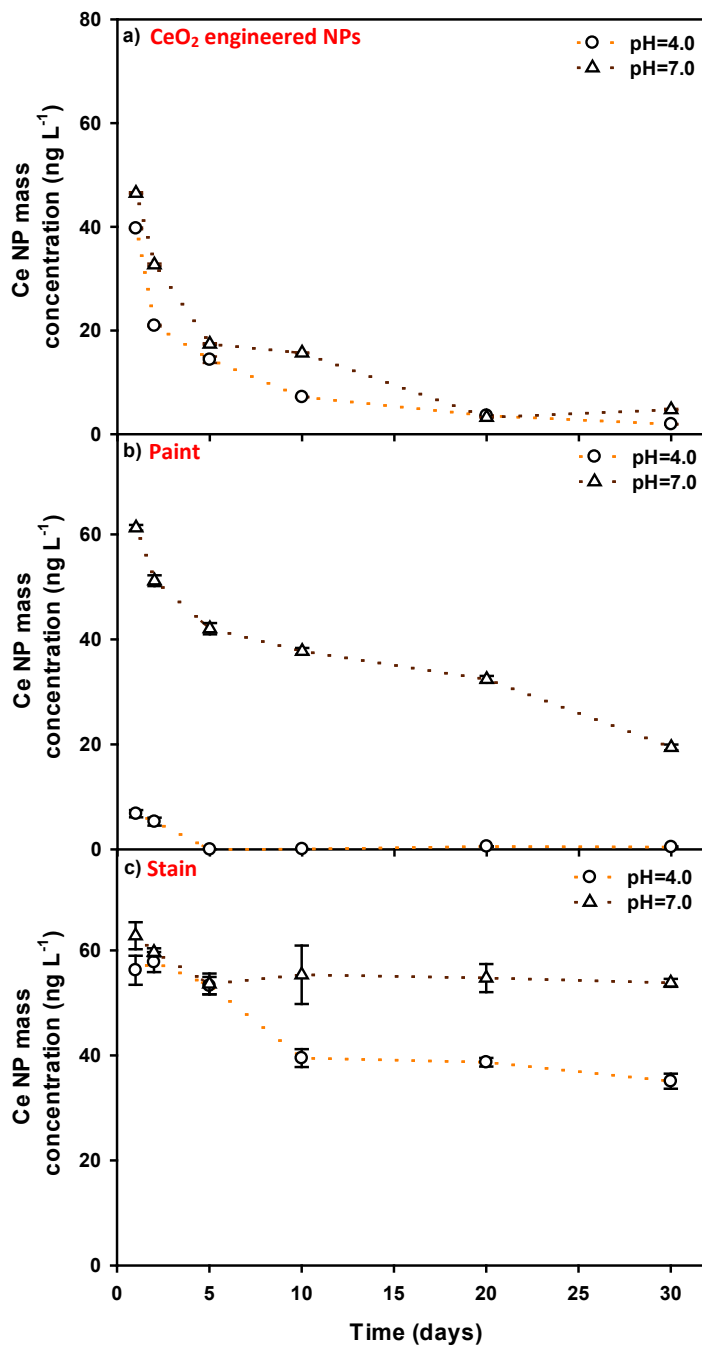


Figure 4-5 Mass concentration of Ce containing NP as a function of time in **(a)** a suspension of engineered CeO₂ NPs; **(b)** a paint and **(c)** a stain. In order to reduce variability of the pH, NP concentrates were spiked into acetate buffer at pH = 4.0 and bicarbonate buffer at pH = 7.0. Paint and stain were diluted 2500x. Error bars correspond to standard deviations obtained from triplicate analysis. Measurements were performed using a magnetic sector SP-ICP-MS with a dwell time of 50 μ s.

4.4.2.4. Stability in precipitation

Finally, all three samples were spiked into a natural precipitation in order to evaluate their stability. In all three samples, concentrations of the NPs decreased with time (Figure 4-6a). Generally, fewer NPs were detected in the precipitation samples as compared to similar samples spiked into Milli-Q water, in spite of the *a priori* presence of NPs in the rain (Figure 4-S12). For example, Ce NPs from the stain decreased by 35% when spiked into Milli-Q water but by 50% when spiked into the rainwater. This lower value in the precipitation is attributed to its greater chemical complexity (Table 4-S2), which can lead to the adsorption of NPs to natural colloidal particles in the rain (i.e. heteroagglomeration) followed by their sedimentation. Although measurements of dissolved Ce were stable for 30 days in all three samples (Figure 4-6b), dissolution could not be entirely excluded due to potential adsorptive losses to the containers and the tubing. In order to verify whether adsorptive losses to the inside of the ICP-MS introduction system is occurring while analyzing the precipitation samples, the system was rinsed with a solution of 2% HNO₃, following the analysis. An important fraction of dissolved Ce was washed off the system with the first replicate of acid rinse and the release of Ce continued even after three replicates, confirming the adsorption of dissolved Ce to the components of the introduction system (Figure 4-S13).

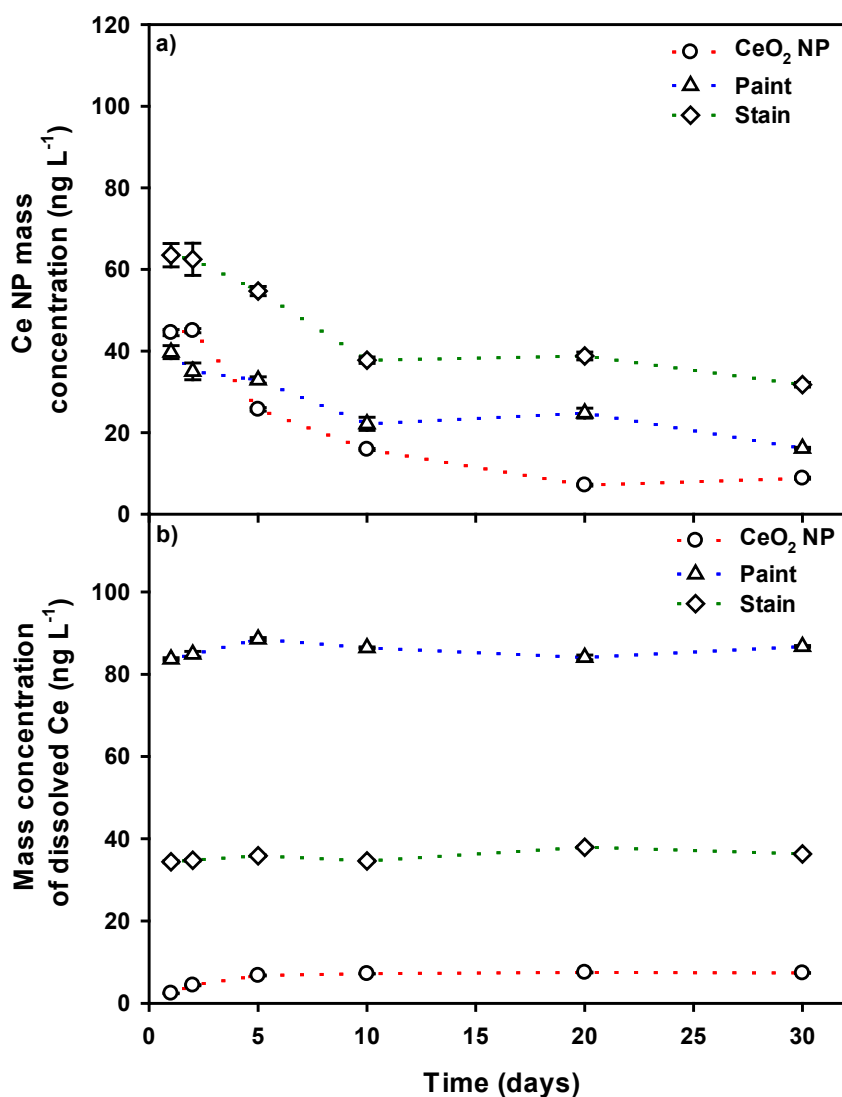


Figure 4-6 Mass concentration of (a) Ce-containing NPs and (b) dissolved Ce as a function of time in: (i) a suspension of CeO₂ NPs; (ii) a paint and (iii) a stain spiked into a rainwater. The paint and stain were diluted 2500x. Error bars correspond to standard deviations obtained from triplicate analysis. Measurements were performed using a magnetic sector SP-ICP-MS with a dwell time of 50 μ s.

4.4.3. Release of CeO₂ NPs from the painted and stained surfaces

The previous experiments allowed us to identify the main parameters that would affect the fate of Ce NPs in natural waters. Clearly, pH and ionic strength, and to a lesser extent NOM content, were key for influencing the fate of the Ce NPs, once in solution. The final set of

experiments looked at whether a similar behaviour could be expected from NPs once they were applied and dried within surface coatings. Painted or stained panels were placed outdoors within washed, plastic containers and exposed to natural weathering (Figure 4-S14). Precipitation samples that had been in contact with the treated panels were analyzed by both SP-ICP-MS (dissolved and Ce NPs) and ICP-MS (total Ce on acidified samples). NPs concentrations were cumulated in order to show long-term release. Note that both dissolved Ce and Ce-containing NPs were found in the natural precipitation at high concentrations (Figure 4-S15). It was thus essential to accurately correct for the background NPs concentrations when analyzing the panels for surface release. Indeed, the concentration of dissolved Ce in the precipitation that had been in contact with the painted panel was slightly higher than for the precipitation blanks (Figure 4-7a). For example, during the 11 weeks of autumn exposure experiments, $1.7 \pm 0.2 \mu\text{g m}^{-2}$ of dissolved Ce was released, which represented 3% of the Ce applied to the wood panels. During the 12 weeks of winter exposure, $7.5 \pm 0.2 \mu\text{g m}^{-2}$ of the dissolved Ce was released, equivalent to a 15% loss of Ce from the panel (Figure 4-7a). In contrast, no significant increase in Ce NPs concentrations could be detected when comparing precipitation that was or was not in contact with the painted panels. This result clearly suggested that Ce release was occurring via the dissolved forms of the metal, in stark contrast with earlier results for TiO_2 .¹⁹⁰ Samples were also digested and analyzed for their total Ce content. Indeed, the concentration of the total Ce in the precipitation that had been in contact with the painted panel was higher than for the precipitation blanks, confirming the release of Ce from painted panels.

Similarly, when precipitation that was in contact with the *stained* panels was analyzed by SP-ICP-MS, only dissolved Ce could be detected (Figure 4-7b). In the autumn exposures, 5% of the Ce per panel was released in the form of dissolved Ce, while 35% of the Ce was released after 12 weeks of winter. Moreover, the concentration of total Ce in the digested samples that were in contact with the stained samples were higher than the blanks, confirming the release of Ce. However, in some cases, the released Ce (measured by SP-ICP-MS) was smaller than the total released Ce (analyzed by ICP-MS) for the same samples. The missing Ce fraction could be attributed to the adsorption to the tube walls and to the components of the introduction system, as was demonstrated above.

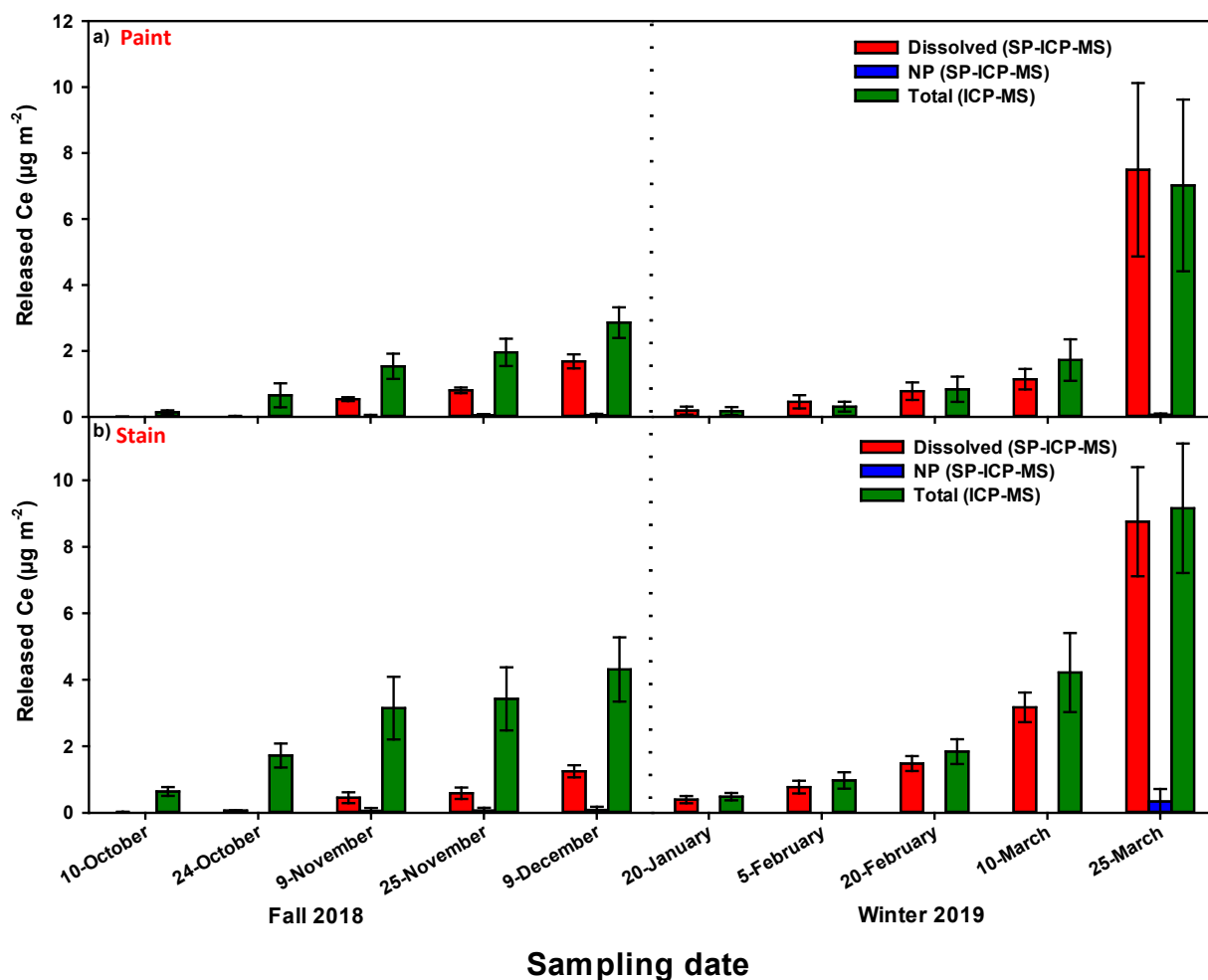


Figure 4-7 Cumulative concentrations of Ce determined by ICP-MS (total concentration), dissolved and Ce-containing NPs as determined by SP-ICP-MS. Measurements were made on precipitation that came into contact with (a) **Painted** and (b) **Stained** surfaces during fall 2018 and winter 2019. Release was normalized by the surface area of the painted/stained panels. Error bars correspond to standard deviations obtained from four replicate samples. Magnetic sector SP-ICP-MS measurements were performed using a dwell time of 50 μs .

4.5. Conclusions

As the production and use of CeO_2 NPs increases, so does the risk of their release into the different environmental compartments. The environmental behaviour and fate after release is critical for reliable risk assessments. In order to study the fate of Ce NPs contained in a paint and a stain once released in the environment, we first evaluated their stability under different

physicochemical conditions (pH, ionic strength, and NOM). Depending on the media, Ce NPs concentrations in the paint and the stain decreased by 65 – 90%, and 15 – 35%, respectively after 30 days. The loss was attributed to either dissolution or agglomeration/sedimentation. However, when painted and stained panels were put outside under natural weathering conditions, the release was largely dissolved Ce, with little evidence for the release of Ce NPs.

4.6. Supporting Information

4.6.1 Effect of sample filtration

Although the precipitation can be analyzed, unfiltered, suspended particles and aggregates may cause blockages in the ICP-MS introduction system. Given that we were mainly interested in quantifying the smaller (nano) particles, the effect of 0.45 μm membrane filtration was examined for a natural sample. For a precipitation sample examined before and after filtration, filtration decreased background Ce concentrations by $(60 \pm 7)\%$, which was attributed to an adsorption of dissolved Ce on the filters. The decrease of dissolved Ce, led to a decrease in the SDL. Which may explain the small shift of the PSD to lower sizes. However, in spite of having a lower SDL after filtration, NPs numbers decreased by $(55 \pm 15)\%$ which was attributed mainly to the removal of large particles (i.e. $>0.45 \mu\text{m}$) with some losses of small Ce-containing NP to the filters via adsorption (Figure 4-S1).

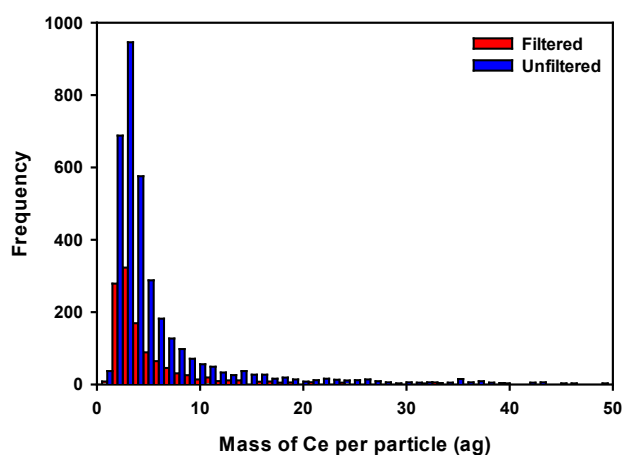


Figure 4-S1 Mass distributions of Ce NPs in a precipitation sample with or without filtration on a 0.45 μm PVDF membrane. Measurements were performed using SP-ICP-MS and a dwell time of 50 μs .

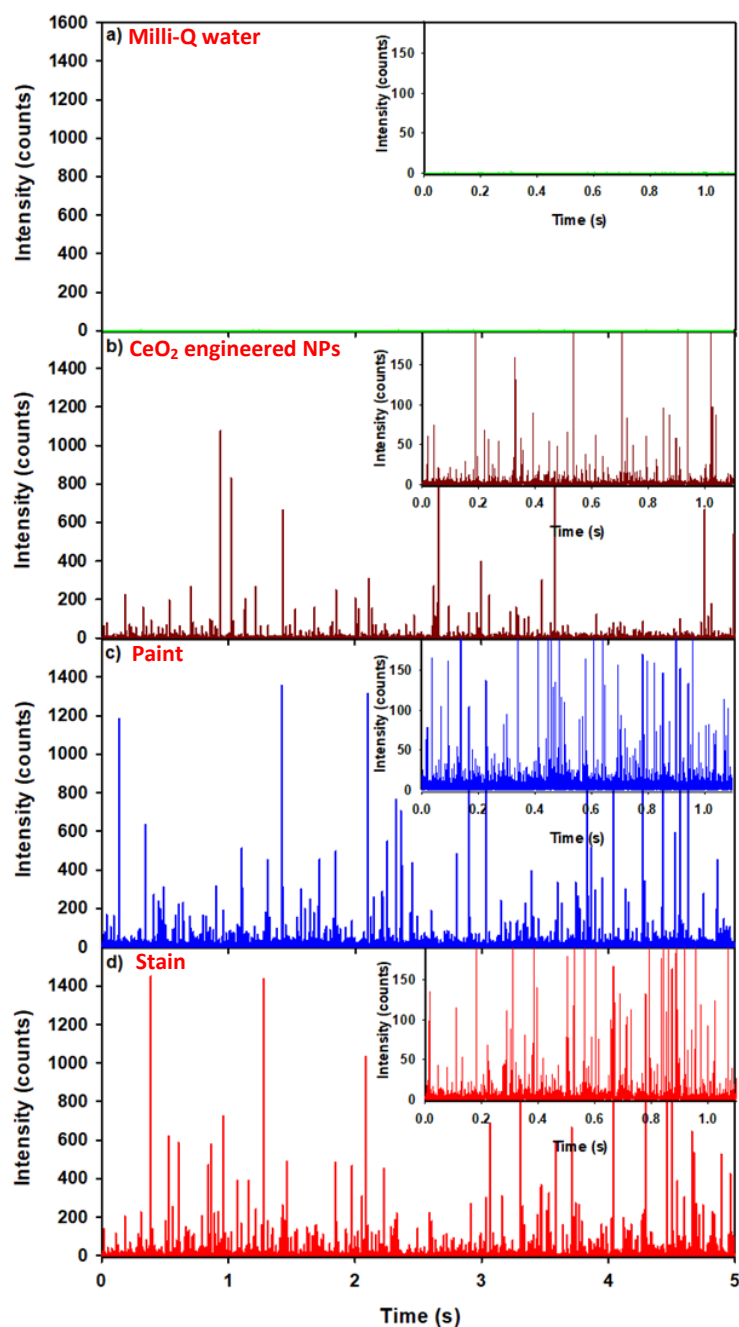


Figure 4-S2 Time resolved signal (raw data) for ^{140}Ce in **(a)** Milli-Q water; **(b)** precipitation, **(c)** paint and **(d)** stain. Paint and stain were diluted 2500x. For better readability, only 5 s of data collection were shown, the total acquisition time was 50 s. Measurements were obtained using SP-ICP-MS with a 50 μs dwell time.

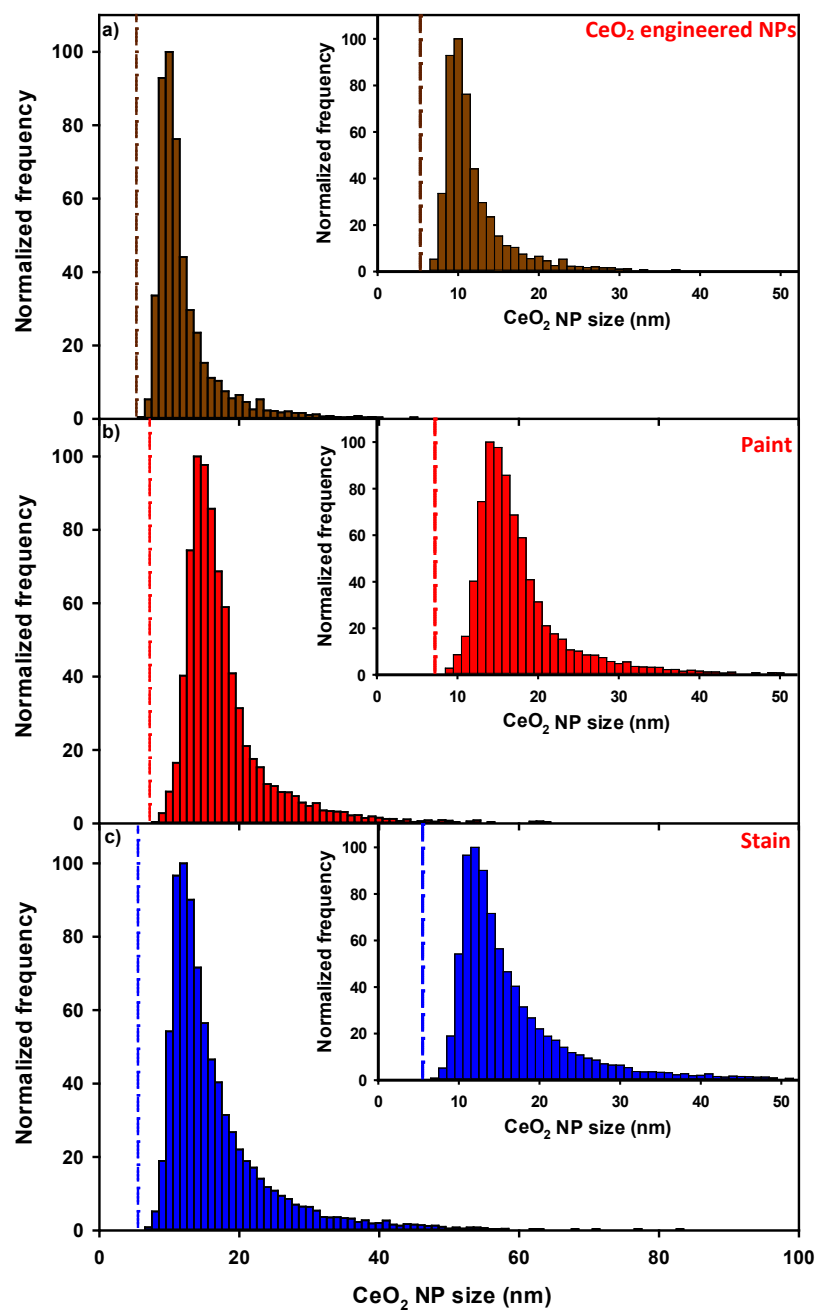


Figure 4-S3 Calculated particle size distributions of Ce NPs in (a) precipitation, (b) paint and (c) stain. Paint and stain were diluted 2500x. NPs sizes were calculated by assuming that the particles were spherical CeO₂ particles with a density of 7.13 kg. dm⁻³. The dashed lines correspond to the calculated size detection limits. Measurements were performed on a sector field SP-ICP-MS using a dwell time of 50 μ s.

Table 4-S1 Ratios of Ce to La in precipitation, paint, and stain, determined with SP-ICP-MS with a dwell time of 50 μ s. Paint and stain were diluted 2500x. Means and standard deviations were obtained from triplicate samples.

Sample	Ce NPs / La NPs	Dissolved Ce / Dissolved La
Precipitation	1.6 ± 0.6	2.7 ± 0.7
Paint	26.7 ± 0.1	2.0 ± 0.3
Stain	80.5 ± 11.1	3.2 ± 0.4

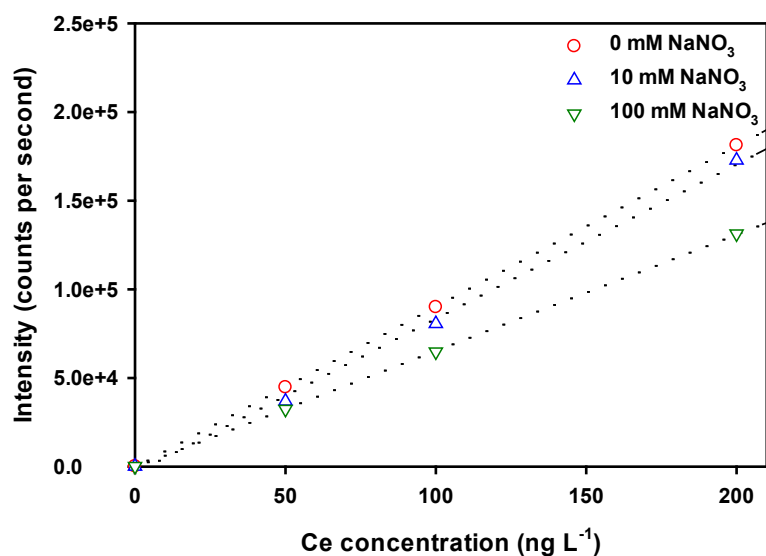


Figure 4-S4 Calibration curves performed using Ce standards with three different concentrations of NaNO₃. The measured sensitivities were 863, 811 and 604 cps ng L⁻¹ for standards with 0, 10 and 100 mM of NaNO₃, respectively. Measurements were performed using SP-ICP-MS and a dwell time of 50 μ s.

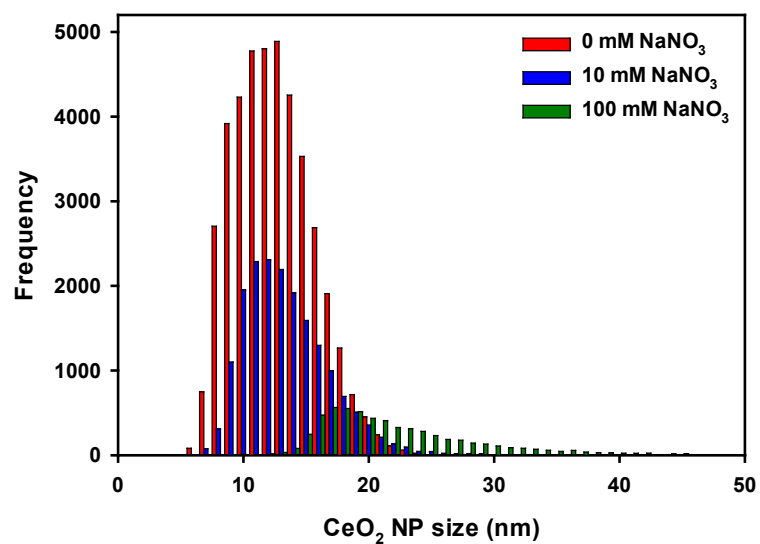


Figure 4-S5 Particle size distribution of CeO₂ NPs in a suspension of engineered CeO₂ NPs spiked into Milli-Q water with three different ionic strengths. Measurements were performed using SP-ICP-MS and a dwell time of 50 μ s.

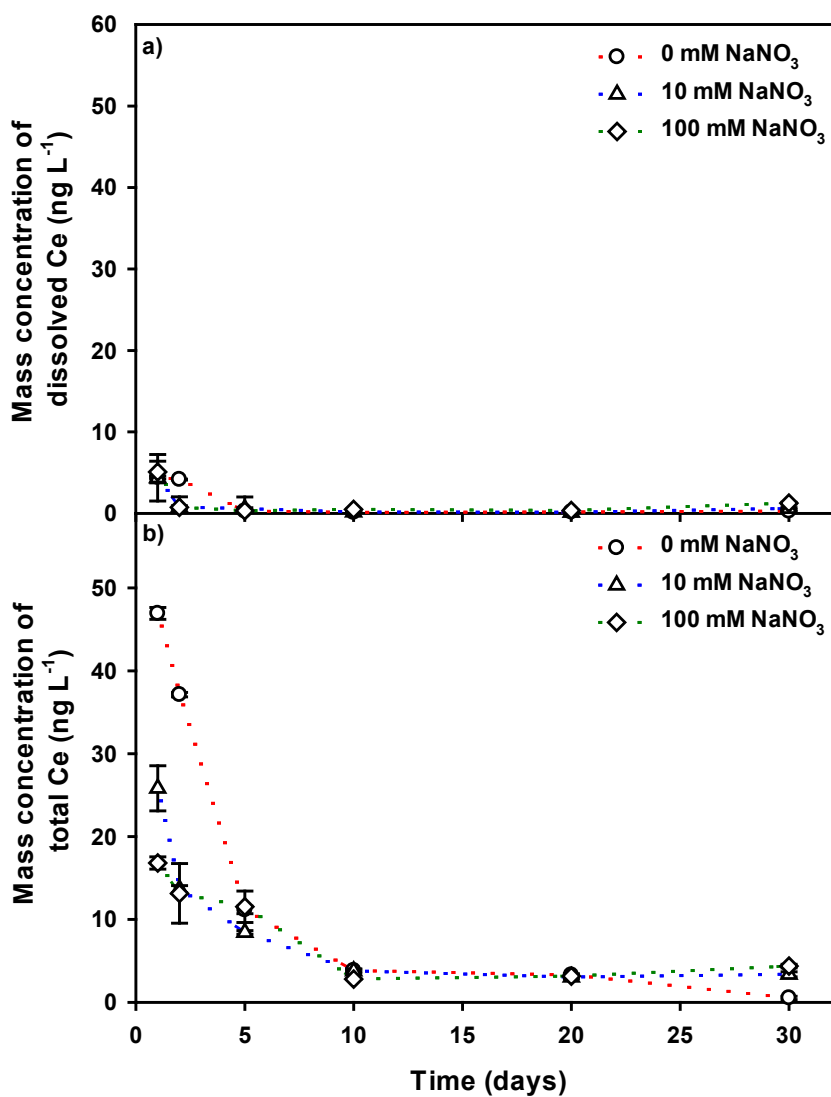


Figure 4-S6 Mass concentration of (a) dissolved and (b) total Ce in a suspension of engineered CeO₂ NPs, spiked into Milli-Q water with three different ionic strength, as a function of time. Error bars correspond to standard deviations obtained from triplicate analysis. Measurements were performed using SP-ICP-MS and a dwell time of 50 μ s.

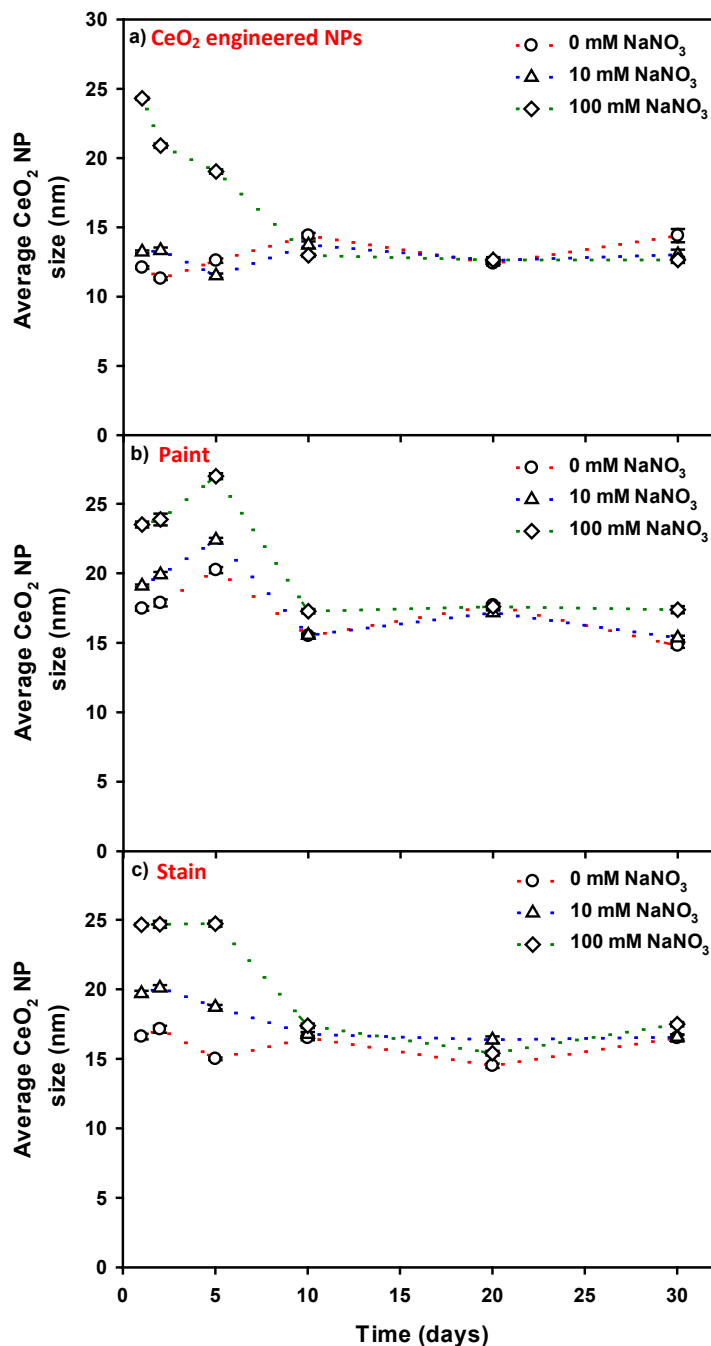


Figure 4-S7 Average CeO₂ NPs sizes in (a) engineered CeO₂ NPs, (b) paint and (c) stain spiked into Milli-Q water with three different ionic strength, as a function of time. Paint and stain were diluted 2500x. NPs sizes were calculated by assuming that the particles were spherical CeO₂ particles with a density of 7.13 kg. dm⁻³. Error bars correspond to standard deviations obtained from triplicate analysis. Measurements were performed using SP-ICP-MS and a dwell time of 50 μs.

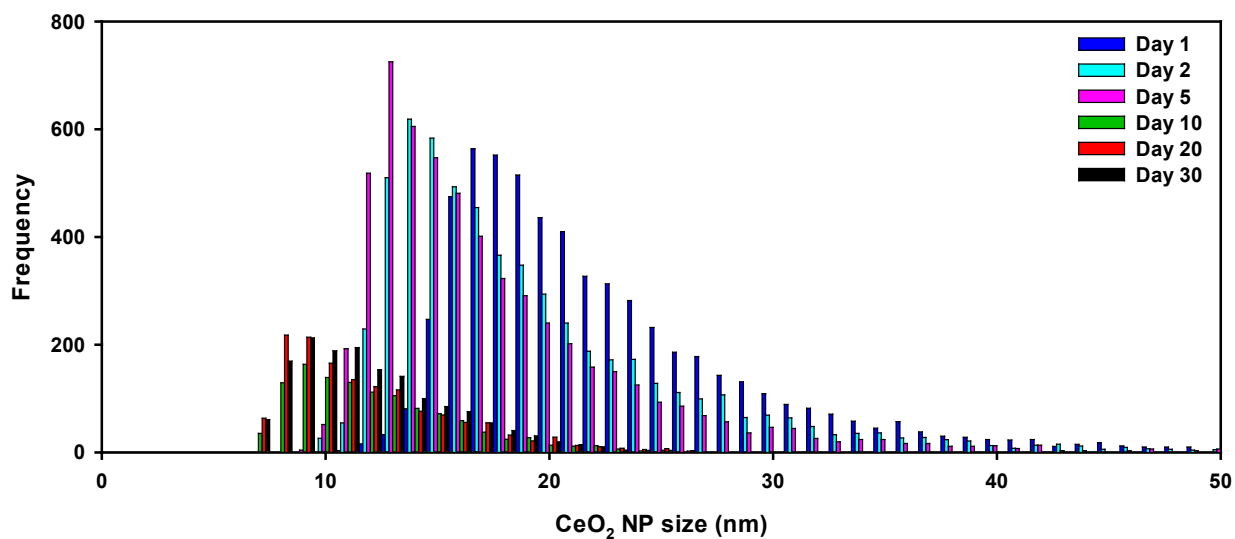


Figure 4-S8 Particle size distributions of CeO₂ NPs in a suspension of engineered CeO₂ NPs spiked into Milli-Q water with 100 mM of NaNO₃. Measurements were performed using SP-ICP-MS and a dwell time of 50 μ s.

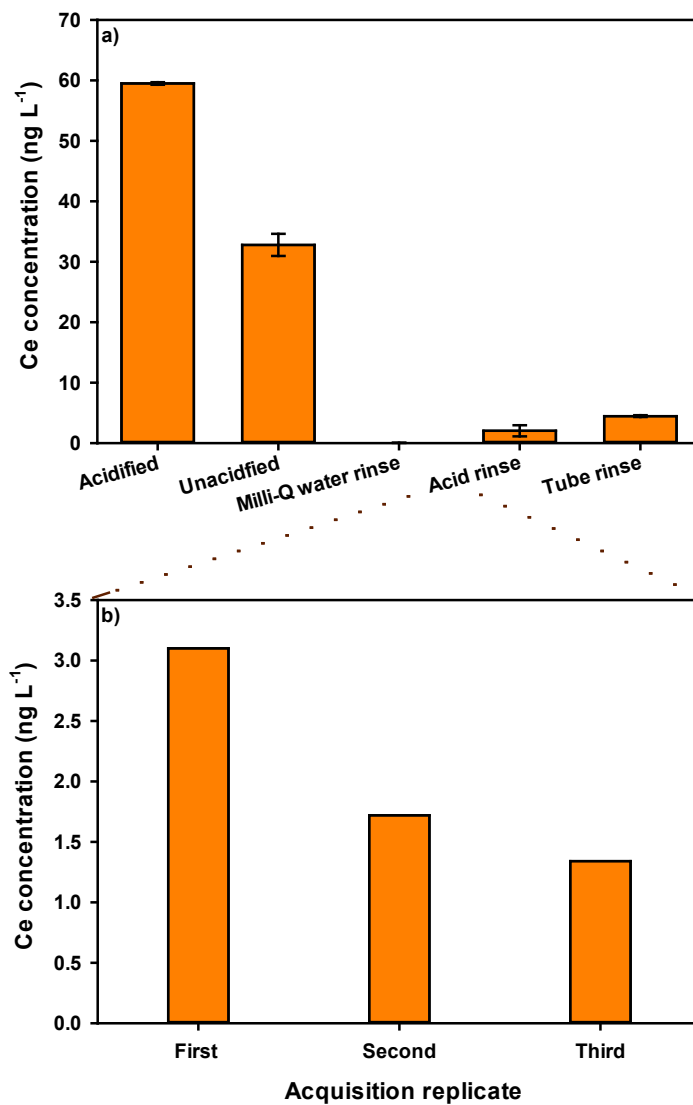


Figure 4-S9 (a) Concentration of dissolved Ce measured in a solution of almost 60 ng L⁻¹ ionic Ce prepared in Milli-Q water without acidification. Adsorptive losses to the ICP-MS and sample tube were evaluated by measuring Ce in: (i) a Milli-Q water rinse; (ii) Successive (triplicate) rinses in 2% HNO₃ (Figure S9b) (iii) Milli-Q water rinse of the sample tube; (iv) 2% HNO₃ rinse of the sample tube. Measurements were performed using SP-ICP-MS and a dwell time of 50 μs.

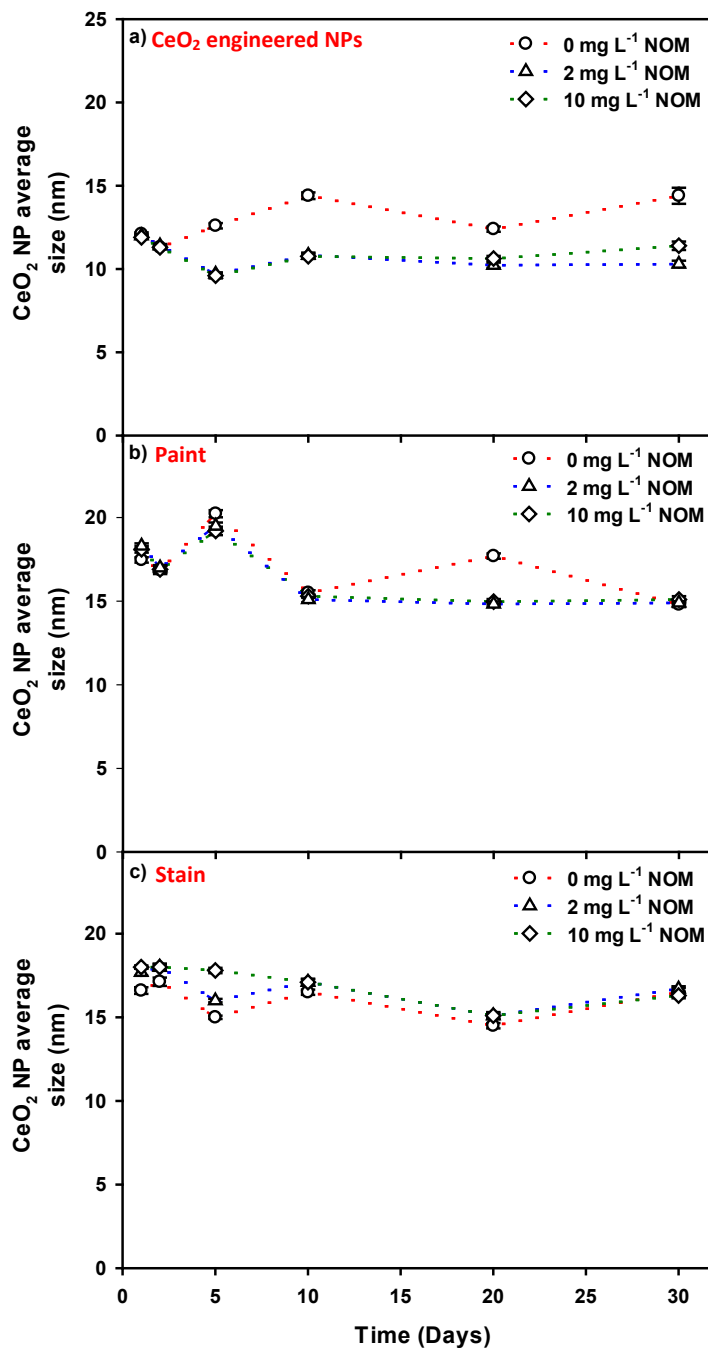


Figure 4-S10 Average CeO₂ NP sizes in (a) engineered CeO₂ NPs, (b) paint and (c) stain spiked into Milli-Q water with three different contents of natural organic matter, as a function of time. Paint and stain were diluted 2500x. NPs sizes were calculated by assuming that the particles were spherical CeO₂ particles with a density of 7.13 kg. dm⁻³. Error bars correspond to standard deviations obtained from triplicate analysis. Measurements were performed using SP-ICP-MS and a dwell time of 50 μs.

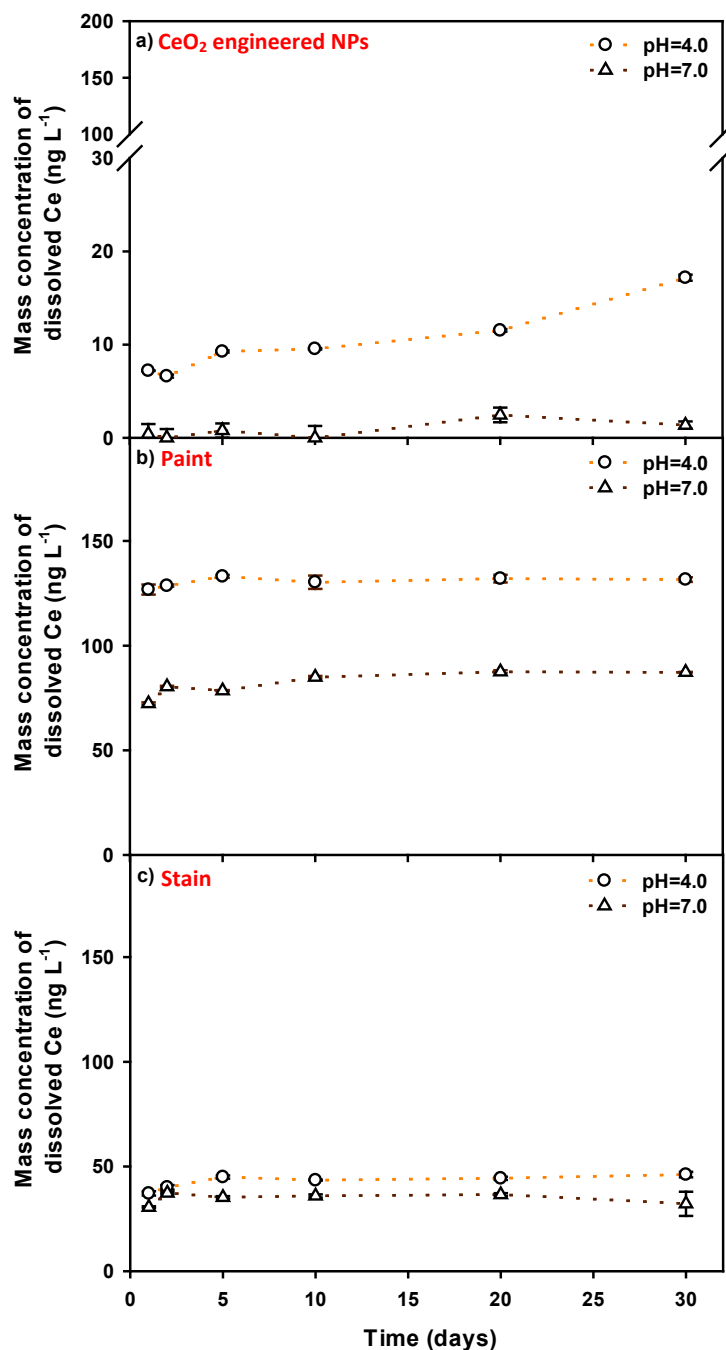


Figure 4-S11 Mass concentration of dissolved Ce in (a) engineered CeO₂ NPs, (b) paint and (c) stain spiked into acetate buffer with pH = 4.0 or bicarbonate buffer with pH = 7.0, as a function of time. Paint and stain were diluted 2500x. Error bars correspond to standard deviations obtained from triplicate analysis. Measurements were performed using SP-ICP-MS and a dwell time of 50 μ s.

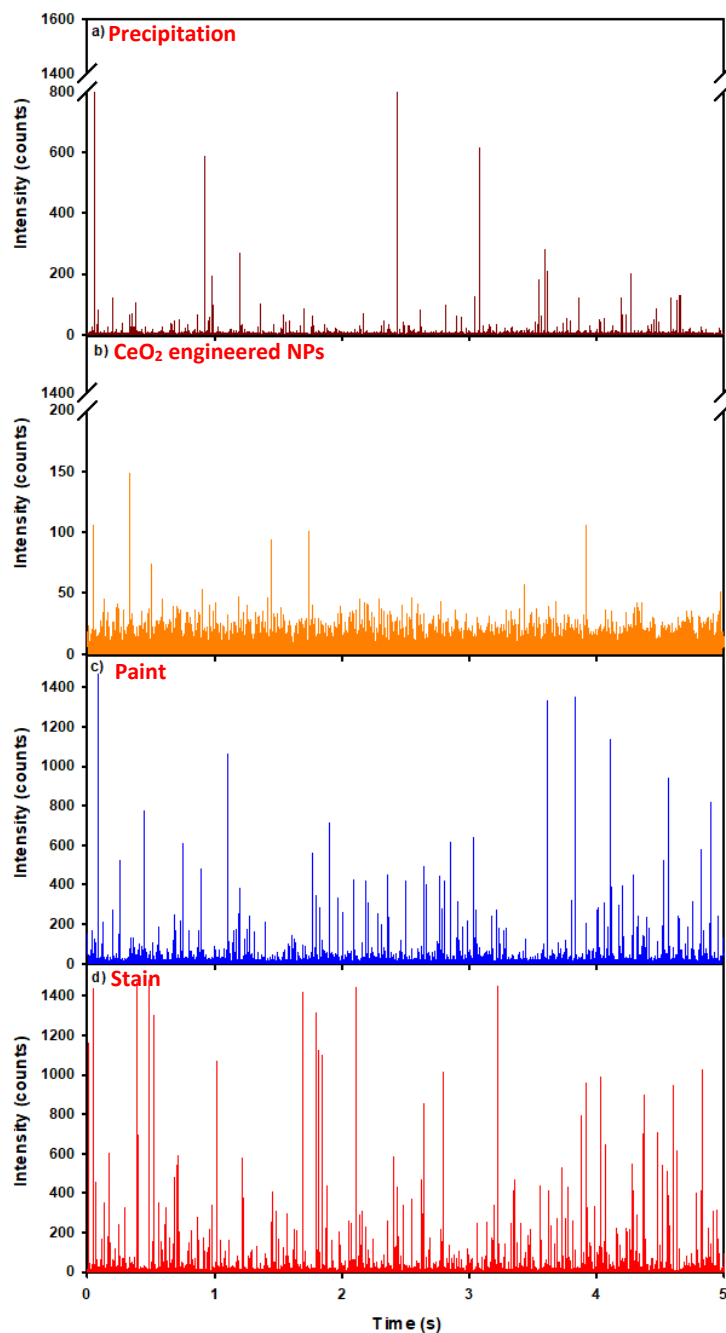


Figure 4-S12 Time resolved signal for ^{140}Ce in the precipitation **(a)** unspiked; or spiked with **(b)** engineered CeO_2 NPs, **(c)** paint and **(d)** stain. CeO_2 NPs, paint and stain were spiked in the precipitation. For better readability, only 5 s of data collection were shown, the total acquisition time was 50 s. Measurements were obtained using SP-ICP-MS with a 50 μs dwell time.

Table 4-S2 pH and concentrations of major elements, including total organic carbon (TOC), in an unfiltered rainwater.

Element	Concentration ($\mu\text{g L}^{-1}$)										pH
	Al	Ca	Cu	Fe	K	Mg	Mn	Na	Zn	TOC	
Rain	4.9 ±	3784 ±	0.4 ±	5.1 ±	221 ±	914 ±	0.5 ±	1747 ±	<DL	3040 ±	5.2
	0.3	170	0.0	0.1	11	38	0.0	79		46	

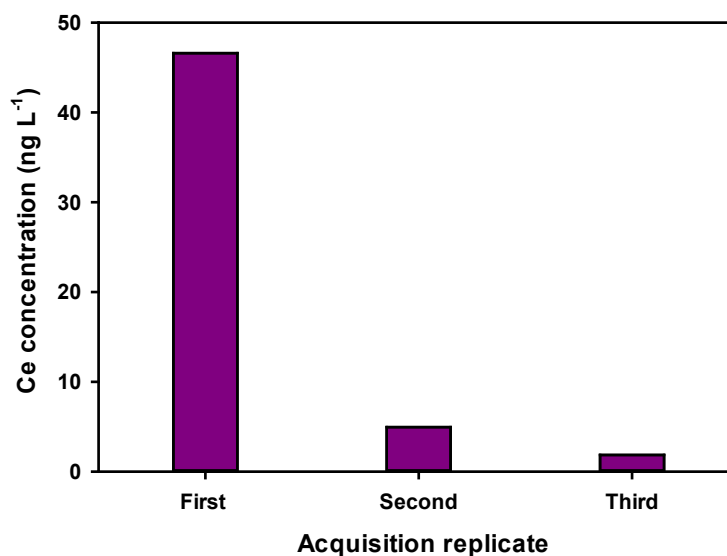


Figure 4-S13 Concentration of dissolved Ce measured in a successive (triplicate) rinses in 2% HNO_3 following the analysis of an unfiltered precipitation sample. Measurements were performed using SP-ICP-MS and a dwell time of 50 μs .

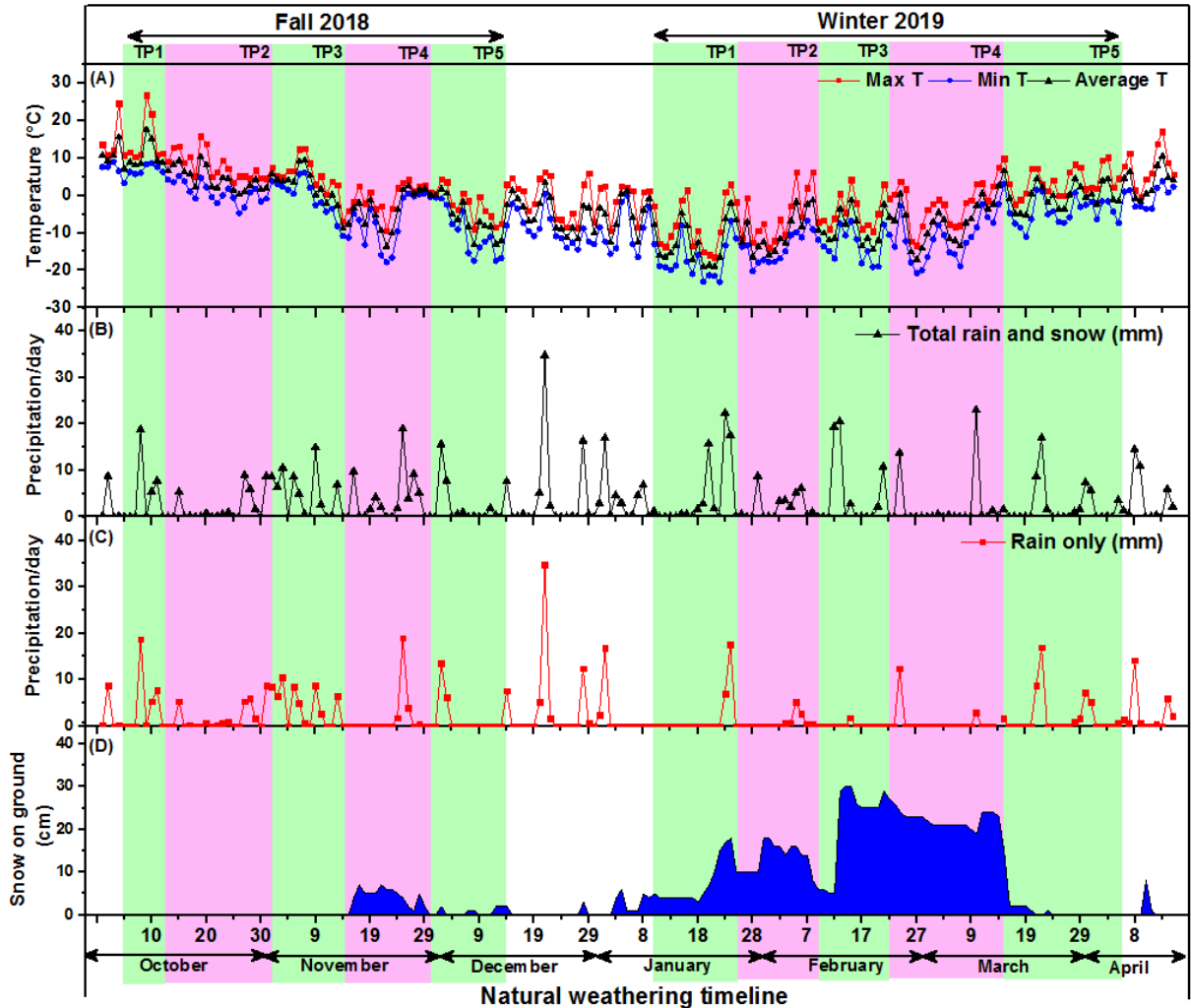


Figure 4-S14 (A) Daily temperatures (maxima, minima and meant), (B) total precipitation (total liquid equivalent of rain and snow), (C) rain precipitation and (D) snow on ground data for the fall of 2018 and winter of 2019, as collected from the Montreal International Airport weather station (coordinates: 45°28'14.000''N, 73°44'27.000'' W) and retrieved from the Environment and Climate Change Canada database. Timepoints (TP) indicate when the respective fall or winter samplings were conducted. (Adapted from Azimzada *et al.*¹⁹⁰).

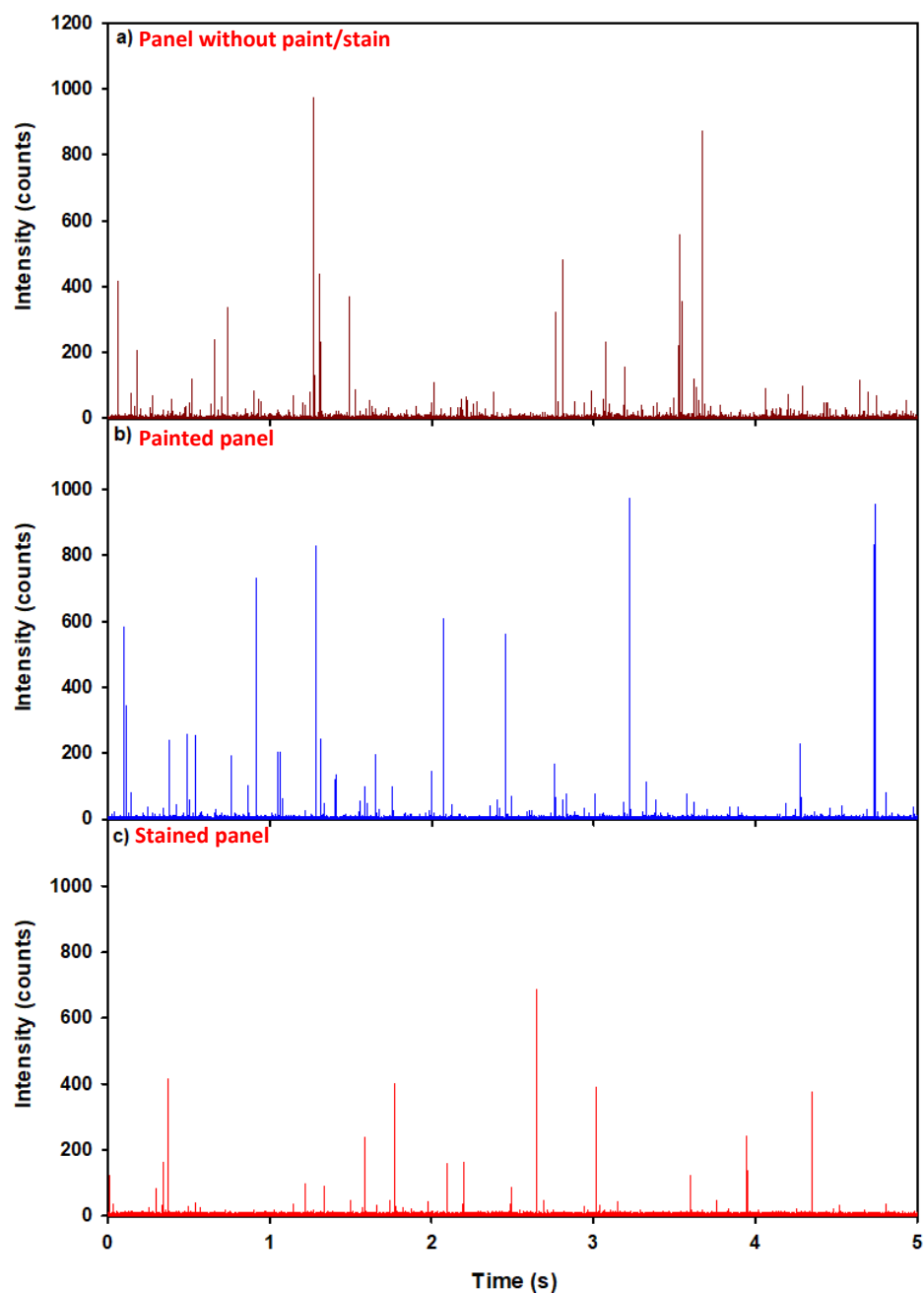


Figure 4-S15 Time resolved signal for ^{140}Ce in a filtered precipitation (a) without, or with contact with a (b) painted panel, and (c) stained panel. For better readability, only 5 s of data collection were shown, the total acquisition time was 50 s. Measurements were obtained using SP-ICP-MS with a 50 μs dwell time.

Chapitre 5 – Conclusions et recommandations

Tout au long de ce travail, des nanoparticules de CeO₂ ont été détectées dans des échantillons de pluie et d'eau de rivière à la suite d'échantillonnages ponctuels sur plusieurs années. Des analyses par, notamment, TOF-SP-ICP-MS ont suggéré la présence des NPs manufacturées de CeO₂. Ceci constitue une autre indication que l'essor que connaissent les nanotechnologies risque d'augmenter les émissions de nanoparticules ou des ions métalliques dans l'environnement. Il s'avère que le manque de données relatives à la détection des nanoparticules dans les matrices environnementales est principalement dû aux limites des techniques analytiques communément utilisées dans ce domaine, notamment la spécificité et la difficulté de mesurer de faibles concentrations. Dans ce contexte, la méthode d'analyse des NPs par SP-ICP-MS est venue au secours avec ses avantages inégalés. En effet, le SP-ICP-MS combine les atouts de la spectrométrie de masse (haute sensibilité et spécificité) à ceux des techniques de comptage de particules (basées sur l'analyse d'une particule à la fois) permettant ainsi des mesures précises de faibles concentrations (en masse et en nombre) de NPs et leur composition. Toutefois, cette technique est limitée par les limites de détection de taille relativement élevées (> 20 nm pour la plupart des éléments), empêchant ainsi la détection des petites NPs qui sont susceptibles d'être plus toxiques (vu qu'elles traversent facilement les membranes cellulaires). Cependant, les récents progrès dans le domaine des instruments analytiques (encouragés par nous les chercheurs) ont conduit à une nette amélioration de la technique SP-ICP-MS. Ainsi, nous avons eu recours à l'utilisation d'un ICP-MS à secteur magnétique (SF-ICP-MS) de haute sensibilité et permettant d'utiliser de courts temps d'acquisition (50 µs), des temps morts quasi-nuls (de l'ordre de 15 ns) afin d'enregistrer le signal de façon ultra-rapide et sans interruption. En outre, nous avons contribué à perfectionner les algorithmes de traitement du signal de données SP-ICP-MS pour une meilleure distinction des pics de nanoparticules du bruit de fond et leur intégration plus précise. Ceci nous a permis de réduire significativement les SDLs des NPs d'Ag, d'Au et de CeO₂ sous 5 nm. Cette amélioration a conduit à la détection des plus petites particules dans les eaux de pluie et de rivière, qui, avant ces exploits, passaient sous le radar, non seulement des autres techniques, mais aussi de la technique SP-ICP-MS elle-même.

L'utilisation de cette technique améliorée de façon simple ne suffisait pas pour garantir la qualité et la justesse des analyses. En effet, la nature complexe des échantillons naturels et les exigences d'échantillonnage de l'instrumentation ICP-MS s'accompagnaient de contraintes analytiques qui risquaient de compromettre la qualité des résultats. Il nous a donc fallu examiner tous les aspects relatifs à la préparation de l'échantillon (notamment la filtration et la centrifugation) et leur impact sur l'analyse par SP-ICP-MS. D'une part, nous avons démontré que les filtres avec une membrane en polypropylène préconditionnée donnent les recouvrements les plus élevés (>80%) pour les NPs d'Ag et de CeO₂ dans les eaux naturelles, tandis que les autres filtres membranaires fluorés (PTFE, PVDF, etc.) sont à éviter à cause des pertes drastiques de matière qu'ils provoquent impactant sérieusement la qualité et la justesse des résultats. D'autre part, des recouvrements similaires ont été obtenus lorsque les échantillons ont été centrifugés à une faible vitesse de rotation de l'ordre de 1000 xg. Il en découle de cette étude que seules la filtration sur une membrane en PP et la centrifugation à ~1000xg sont à considérer pour la préparation des échantillons naturels (non propres) à des fins d'analyse par SP-ICP-MS. Pour arriver à cette conclusion, nous avons méticuleusement analysé la quantité de matière (d'argent et de cérium) sous ses deux formes particulaire et dissoute à différentes étapes, de la préparation de l'échantillon à son injection dans le système ICP-MS. Ainsi, des bilans de masse ont été faits à plusieurs niveaux pour des résultats les plus justes possibles.

Nous avons utilisé le SF-ICP-MS pour détecter, quantifier et caractériser des NPs de CeO₂ dans des échantillons d'eau de pluie, d'eau de rivière, de peinture et de teinture. En plus du cérium, le lanthane a aussi été mesuré pour déterminer le rapport Ce/La. Ceci a permis de conclure que les NPs de CeO₂ détectées dans les eaux naturelles étaient majoritairement d'origine naturelle. Bien que minoritaires, des NPs de CeO₂ manufacturées ont aussi été détectées. La mesure du rapport Ce/La a aussi confirmé l'origine industrielle des NPs de CeO₂ retrouvées dans la peinture et dans la teinture. En effet, ces produits de revêtements de surface constituent une application majeure des NPs de CeO₂, en raison de leur propriété d'absorption UV, constituant ainsi une source potentielle de relargage de NPs dans l'environnement. Par conséquent, et pour une évaluation de risque plus fiable, il est primordial de comprendre de façon détaillée le devenir et le comportement des NPs de CeO₂ relarguées. Dans ce travail nous nous sommes penchés sur le comportement des NPs de CeO₂ contenues dans la peinture et la teinture sous différentes conditions physicochimiques (pH, force ionique et NOM). Dans tous cas, nous avons constaté

une diminution des concentrations des NPs dans la peinture et la teinture avec le temps, lorsqu'elles ont été ajoutées dans l'eau avec différentes conditions. Cette diminution était plus prononcée à un pH relativement acide et a été attribuée à la dissolution et possiblement à l'agglomération/sédimentation à force ionique élevée. Les pluies acides en Amérique du nord ont un pH avoisinant 5 et pouvant attaquer et dégrader les revêtement de surface. En effet, lorsque des morceaux de bois peints et teints ont été placés dehors, le Ce relargué était seulement sous la forme dissoute et/ou particulaire sous la SDL de 4 nm. L'acidité moyenne des précipitations (pH 5.2) aurait initié la dissolution des NPs de CeO₂ en cérium ionique stabilisé par la matière organique (présente dans la précipitation ou provenant de la dégradation de la peinture/teinture). Cette stabilisation aurait contribué à réduire la taille des NPs de CeO₂ sous la SDL.

5.1. Recommandations

Basé sur ces conclusions et considérant la contribution que cette thèse apporte à la communauté scientifique travaillant sur l'analyse par SP-ICP-MS, des recommandations et des développements futurs sont proposés, afin d'évaluer de manière fiable les NPs:

1. Efficacité de transport : ce paramètre est essentiel pour la quantification et la caractérisation des NPs par SP-ICP-MS. Bien que des suspensions standards de NPs sont utilisées pour la détermination de TE, des erreurs peuvent se produire lors de la préparation et l'analyse de cette suspension, ce qui fausse les résultats des suspensions de NPs analysées par la suite. De plus, la détermination de TE est basée sur des hypothèses telles que toutes les NPs de la suspension étalon ont exactement la même taille, qu'elles sont très stables, et qu'elles ne s'adsorbent pas sur le système d'introduction. Or, ces hypothèses ne sont qu'en partie justes et s'accompagnent inévitablement d'une erreur sur la détermination de TE, une erreur relative qui peut atteindre des dizaines de pourcentage. Par exemple, une erreur de 20% sur la TE mène à une surestimation de ~ 20% sur la concentration en nombre et une sous-estimation de ~ 10% sur la taille moyenne des NPs. Ainsi, il est recommandé de valider la valeur de TE par l'analyse d'autres NPs standards (de taille ou concentration en nombre connues).
2. Adsorption : des pertes dues à l'adsorption sur les parois des tubes et les différents composants du système d'introduction ont été démontrées dans les

chapitres 2 – 4 de cette thèse. Ces pertes peuvent se produire lors de la préparation et l'analyse des échantillons par SP-ICP-MS. Ainsi, afin de préparer les échantillons naturels, il est recommandé de les filtrer sur des membranes de polypropylène préalablement conditionnées par une solution multi-élément, ou les centrifuger à des vitesses < 1000 xg. De plus, on recommande la préparation des échantillons dans des tubes en PP et de réduire au maximum les surfaces de contact dans le système d'introduction (i.e., capillaire d'échantillonnage plus court et de petit diamètre interne). Finalement, les meilleures pratiques incluront l'utilisation de bilans de masse pour tenir compte des pertes potentielles de NPs et/ou dissous.

3. Origine des NPs : après la détection des NPs dans l'environnement, la détermination de leur origine (naturelle ou manufacturée) est nécessaire pour la réglementation et l'évaluation des risques des NPMs. Le critère le plus utilisé pour différencier les NPNs des NPMs est la pureté élémentaire. Pour ce but, le TOF-ICP-MS en mode particule unique est la technique idéale qui permet l'analyse de plusieurs éléments dans une particule. Toutefois, des améliorations aux sensibilités obtenues par cette techniques sont requises afin d'améliorer les SDLs.
4. Techniques d'analyse complémentaires : les paramètres importants pour la caractérisation des NPs incluent la concentration, la taille, la distribution de taille, la composition, la charge de surface, l'état d'agglomération, la structure, l'état d'oxydation, la solubilité, la réactivité et la stabilité. Ainsi, il est recommandé d'utiliser plusieurs techniques en parallèle (TEM, DLS, SP-ICP-MS, etc.) afin d'atteindre un haut degré de précision et de fiabilité.

Références bibliographiques

1. ISO, International Organization for Standardization. Nanotechnologies-vocabulary-part1: Core Terms. ISO/TS 80004-1:2015. **2015**.
2. Boverhof, D. R.; Bramante, C. M.; Butala, J. H.; Clancy, S. F.; Lafronconi, M.; West, J.; Gordon, S. C., Comparative assessment of nanomaterial definitions and safety evaluation considerations. *Regulatory Toxicology and Pharmacology* **2015**, *73* (1), 137-150.
3. European Commission. Commission recommendation of 18 October 2011 on the definition of nanomaterial. *Off. J. Eur. Union* **2011**, *275*, 38.
4. López-Serrano, A.; Olivas, R. M.; Landaluze, J. S.; Cámara, C., Nanoparticles: a global vision. Characterization, separation, and quantification methods. Potential environmental and health impact. *Analytical Methods* **2014**, *6* (1), 38-56.
5. Khan, I.; Saeed, K.; Khan, I., Nanoparticles: Properties, applications and toxicities. *Arabian Journal of Chemistry* **2019**, *12* (7), 908-931.
6. Hochella Michael, F.; Mogk David, W.; Ranville, J.; Allen Irving, C.; Luther George, W.; Marr Linsey, C.; McGrail, B. P.; Murayama, M.; Qafoku Nikolla, P.; Rosso Kevin, M.; Sahai, N.; Schroeder Paul, A.; Vikesland, P.; Westerhoff, P.; Yang, Y., Natural, incidental, and engineered nanomaterials and their impacts on the Earth system. *Science* **2019**, *363* (6434), eaau8299.
7. Lespes, G.; Faucher, S.; Slaveykova, V. I., Natural Nanoparticles, Anthropogenic Nanoparticles, Where Is the Frontier? *Front. Environ. Sci.* **2020**, *8* (71).
8. Lanone, S.; Boczkowski, J., Les sources de nanoparticules. *Revue Française d'Allergologie* **2010**, *50* (3), 211-213.
9. Baulig, A.; Poirault, J.-J.; Ausset, P.; Schins, R.; Shi, T.; Baralle, D.; Dorlhene, P.; Meyer, M.; Lefevre, R.; Baeza-Squiban, A.; Marano, F., Physicochemical Characteristics and Biological Activities of Seasonal Atmospheric Particulate Matter Sampling in Two Locations of Paris. *Environmental Science & Technology* **2004**, *38* (22), 5985-5992.
10. Dasch, J.; D'Arcy, J., Physical and Chemical Characterization of Airborne Particles from Welding Operations in Automotive Plants. *Journal of Occupational and Environmental Hygiene* **2008**, *5* (7), 444-454.
11. Feynman, R. P., There's plenty of room at the bottom. *Journal of Microelectromechanical Systems* **1992**, *1* (1), 60-66.
12. Keller, A. A.; Lazareva, A., Predicted Releases of Engineered Nanomaterials: From Global to Regional to Local. *Environmental Science & Technology Letters* **2014**, *1* (1), 65-70.
13. Ju-Nam, Y.; Lead, J. R., Manufactured nanoparticles: An overview of their chemistry, interactions and potential environmental implications. *Science of The Total Environment* **2008**, *400* (1), 396-414.
14. Sudha, P. N.; Sangeetha, K.; Vijayalakshmi, K.; Barhoum, A., Chapter 12 - Nanomaterials history, classification, unique properties, production and market. In *Emerging Applications of Nanoparticles and Architecture Nanostructures*, Elsevier: 2018; pp 341-384.
15. Wigginton, N. S.; Haus, K. L.; Hochella Jr, M. F., Aquatic environmental nanoparticles. *Journal of Environmental Monitoring* **2007**, *9* (12), 1306-1316.
16. Mohan Bhagyaraj, S.; Oluwafemi, O. S., Chapter 1 - Nanotechnology: The Science of the Invisible. In *Synthesis of Inorganic Nanomaterials*, Mohan Bhagyaraj, S.; Oluwafemi, O. S.; Kalarikkal, N.; Thomas, S., Eds. Woodhead Publishing: 2018; pp 1-18.

17. Piccinno, F.; Gottschalk, F.; Seeger, S.; Nowack, B., Industrial production quantities and uses of ten engineered nanomaterials in Europe and the world. *Journal of Nanoparticle Research* **2012**, *14* (9), 1109.
18. Charles-Anica, E.; Claude, O.; N. Inès, D.; Claude, É., Portrait de la nanotechnologie au Québec dans les milieux industriels et de la recherche universitaire et publique. *IRSST* **2015**, 1-104.
19. Weiss, J.; Takhistov, P.; McClements, D. J., Functional Materials in Food Nanotechnology. *Journal of Food Science* **2006**, *71* (9), R107-R116.
20. Jain, P. K.; Lee, K. S.; El-Sayed, I. H.; El-Sayed, M. A., Calculated Absorption and Scattering Properties of Gold Nanoparticles of Different Size, Shape, and Composition: Applications in Biological Imaging and Biomedicine. *The Journal of Physical Chemistry B* **2006**, *110* (14), 7238-7248.
21. Zhang, J.; Saltzman, M., Engineering biodegradable nanoparticles for drug and gene delivery. *Chem Eng Prog* **2013**, *109* (3), 25-30.
22. Walkey, C.; Das, S.; Seal, S.; Erlichman, J.; Heckman, K.; Ghibelli, L.; Traversa, E.; McGinnis, J. F.; Self, W. T., Catalytic properties and biomedical applications of cerium oxide nanoparticles. *Environmental Science: Nano* **2015**, *2* (1), 33-53.
23. Xue, W.; Peng, Z.; Huang, D.; Zeng, G.; Wan, J.; Xu, R.; Cheng, M.; Zhang, C.; Jiang, D.; Hu, Z., Nanoremediation of cadmium contaminated river sediments: Microbial response and organic carbon changes. *Journal of Hazardous Materials* **2018**, *359*, 290-299.
24. Bundschuh, M.; Filser, J.; Lüderwald, S.; McKee, M. S.; Metreveli, G.; Schaumann, G. E.; Schulz, R.; Wagner, S., Nanoparticles in the environment: where do we come from, where do we go to? *Environmental Sciences Europe* **2018**, *30* (1), 6.
25. Gottschalk, F.; Sun, T.; Nowack, B., Environmental concentrations of engineered nanomaterials: Review of modeling and analytical studies. *Environmental Pollution* **2013**, *181*, 287-300.
26. Tolaymat, T.; El Badawy, A.; Genaidy, A.; Abdelraheem, W.; Sequeira, R., Analysis of metallic and metal oxide nanomaterial environmental emissions. *Journal of Cleaner Production* **2017**, *143*, 401-412.
27. Giese, B.; Klaessig, F.; Park, B.; Kaegi, R.; Steinfeldt, M.; Wigger, H.; von Gleich, A.; Gottschalk, F., Risks, Release and Concentrations of Engineered Nanomaterial in the Environment. *Scientific Reports* **2018**, *8* (1), 1565.
28. Limbach, L. K.; Bereiter, R.; Muller, E.; Krebs, R.; Galli, R.; Stark, W. J., Removal of oxide nanoparticles in a model wastewater treatment plant: influence of agglomeration and surfactants on clearing efficiency. *Environ Sci Technol* **2008**, *42* (15), 5828-33.
29. Mueller, N. C.; Nowack, B., Exposure Modeling of Engineered Nanoparticles in the Environment. *Environmental Science & Technology* **2008**, *42* (12), 4447-4453.
30. Simonet, B. M.; Valcárcel, M., Monitoring nanoparticles in the environment. *Analytical and Bioanalytical Chemistry* **2008**, *393* (1), 17.
31. Keller, A. A.; McFerran, S.; Lazareva, A.; Suh, S., Global life cycle releases of engineered nanomaterials. *Journal of Nanoparticle Research* **2013**, *15* (6), 1692.
32. Foss Hansen, S.; Heggelund, L. R.; Revilla Besora, P.; Mackevica, A.; Boldrin, A.; Baun, A., Nanoproducts – what is actually available to European consumers? *Environmental Science: Nano* **2016**, *3* (1), 169-180.
33. Lowry, G. V.; Gregory, K. B.; Apte, S. C.; Lead, J. R., Transformations of Nanomaterials in the Environment. *Environmental Science & Technology* **2012**, *46* (13), 6893-6899.

34. Baalousha, M.; Lead, J.; Ju-Nam, Y.; Wilderer, P. J. T. o. w. s., Natural colloids and manufactured nanoparticles in aquatic and terrestrial systems. **2011**, *3*, 89-129.
35. Abbas, Q.; Yousaf, B.; Amina; Ali, M. U.; Munir, M. A. M.; El-Naggar, A.; Rinklebe, J.; Naushad, M., Transformation pathways and fate of engineered nanoparticles (ENPs) in distinct interactive environmental compartments: A review. *Environment International* **2020**, *138*, 105646.
36. Mitrano, D. M.; Nowack, B., The need for a life-cycle based aging paradigm for nanomaterials: importance of real-world test systems to identify realistic particle transformations. *Nanotechnology* **2017**, *28* (7), 072001.
37. Lei, C.; Sun, Y.; Tsang, D. C. W.; Lin, D., Environmental transformations and ecological effects of iron-based nanoparticles. *Environmental Pollution* **2018**, *232*, 10-30.
38. Zhang, C.; Hu, Z.; Deng, B., Silver nanoparticles in aquatic environments: Physicochemical behavior and antimicrobial mechanisms. *Water Research* **2016**, *88*, 403-427.
39. Baalousha, M.; Nur, Y.; Römer, I.; Tejamaya, M.; Lead, J. R., Effect of monovalent and divalent cations, anions and fulvic acid on aggregation of citrate-coated silver nanoparticles. *Science of The Total Environment* **2013**, *454-455*, 119-131.
40. Domingos, R. F.; Rafiei, Z.; Monteiro, C. E.; Khan, M. A. K.; Wilkinson, K. J., Agglomeration and dissolution of zinc oxide nanoparticles: role of pH, ionic strength and fulvic acid. *Environmental Chemistry* **2013**, *10* (4), 306-312.
41. Buffle, J.; Wilkinson, K. J.; Stoll, S.; Filella, M.; Zhang, J., A Generalized Description of Aquatic Colloidal Interactions: The Three-colloidal Component Approach. *Environmental Science & Technology* **1998**, *32* (19), 2887-2899.
42. Nowack, B.; Ranville, J. F.; Diamond, S.; Gallego-Urrea, J. A.; Metcalfe, C.; Rose, J.; Horne, N.; Koelmans, A. A.; Klaine, S. J., Potential scenarios for nanomaterial release and subsequent alteration in the environment. *Environmental Toxicology and Chemistry* **2012**, *31* (1), 50-59.
43. Dwivedi, A. D.; Dubey, S. P.; Sillanpää, M.; Kwon, Y.-N.; Lee, C.; Varma, R. S., Fate of engineered nanoparticles: Implications in the environment. *Coordination Chemistry Reviews* **2015**, *287*, 64-78.
44. Mitrano, D. M.; Limpiteprakan, P.; Babel, S.; Nowack, B., Durability of nano-enhanced textiles through the life cycle: releases from landfilling after washing. *Environmental Science: Nano* **2016**, *3* (2), 375-387.
45. Mudunkotuwa, I. A.; Pettibone, J. M.; Grassian, V. H., Environmental Implications of Nanoparticle Aging in the Processing and Fate of Copper-Based Nanomaterials. *Environmental Science & Technology* **2012**, *46* (13), 7001-7010.
46. Phenrat, T.; Long, T. C.; Lowry, G. V.; Veronesi, B., Partial Oxidation (“Aging”) and Surface Modification Decrease the Toxicity of Nanosized Zerovalent Iron. *Environmental Science & Technology* **2009**, *43* (1), 195-200.
47. Sayle, T. X. T.; Molinari, M.; Das, S.; Bhatta, U. M.; Möbus, G.; Parker, S. C.; Seal, S.; Sayle, D. C., Environment-mediated structure, surface redox activity and reactivity of ceria nanoparticles. *Nanoscale* **2013**, *5* (13), 6063-6073.
48. Bian, S.-W.; Mudunkotuwa, I. A.; Rupasinghe, T.; Grassian, V. H., Aggregation and Dissolution of 4 nm ZnO Nanoparticles in Aqueous Environments: Influence of pH, Ionic Strength, Size, and Adsorption of Humic Acid. *Langmuir* **2011**, *27* (10), 6059-6068.
49. Angel, B. M.; Batley, G. E.; Jarolimek, C. V.; Rogers, N. J., The impact of size on the fate and toxicity of nanoparticulate silver in aquatic systems. *Chemosphere* **2013**, *93* (2), 359-365.

50. Nasser, F.; Constantinou, J.; Lynch, I., Nanomaterials in the Environment Acquire an “Eco-Corona” Impacting their Toxicity to *Daphnia Magna*—a Call for Updating Toxicity Testing Policies. *PROTEOMICS* **2020**, *20* (9), 1800412.
51. Pulido-Reyes, G.; Leganes, F.; Fernández-Piñas, F.; Rosal, R., Bio-nano interface and environment: A critical review. *Environmental Toxicology and Chemistry* **2017**, *36* (12), 3181-3193.
52. Dahle, J. T.; Arai, Y., Environmental geochemistry of cerium: applications and toxicology of cerium oxide nanoparticles. *Int J Environ Res Public Health* **2015**, *12* (2), 1253-78.
53. Kilbourn, B. T., Cerium and Cerium Compounds. *Kirk-Othmer Encyclopedia of Chemical Technology* **2011**, 1-23.
54. Jakupec, M. A.; Unfried, P.; Keppler, B. K., Pharmacological properties of cerium compounds. In *Reviews of Physiology, Biochemistry and Pharmacology*, Springer Berlin Heidelberg: Berlin, Heidelberg, 2005; pp 101-111.
55. Monafó, W. W.; Tandon, S. N.; Ayvazian, V. H.; Tuchschildt, J.; Skinner, A. M.; Deitz, F., Cerium nitrate: a new topical antiseptic for extensive burns. *Surgery* **1976**, *80* (4), 465-473.
56. Perullini, M.; Aldabe Bilmes, S. A.; Jobbágy, M., Cerium Oxide Nanoparticles: Structure, Applications, Reactivity, and Eco-Toxicology. In *Nanomaterials: A Danger or a Promise? A Chemical and Biological Perspective*, Brayner, R.; Fiévet, F.; Coradin, T., Eds. Springer London: London, 2013; pp 307-333.
57. Xu, C.; Qu, X., Cerium oxide nanoparticle: a remarkably versatile rare earth nanomaterial for biological applications. *NPG Asia Materials* **2014**, *6* (3), e90-e90.
58. Gangopadhyay, S.; Frolov, D. D.; Masunov, A. E.; Seal, S., Structure and properties of cerium oxides in bulk and nanoparticulate forms. *Journal of Alloys and Compounds* **2014**, *584*, 199-208.
59. Baranchikov, A. E.; Polezhaeva, O. S.; Ivanov, V. K.; Tretyakov, Y. D., Lattice expansion and oxygen non-stoichiometry of nanocrystalline ceria. *CrystEngComm* **2010**, *12* (11), 3531-3533.
60. Tsunekawa, S.; Sivamohan, R.; Ohsuna, T.; Takahashi, H.; Tohji, K., Ultraviolet Absorption Spectra of CeO₂ Nano-Particles. *Materials Science Forum* **1999**, *315-317*, 439-445.
61. Stambouli, A. B.; Traversa, E., Solid oxide fuel cells (SOFCs): a review of an environmentally clean and efficient source of energy. *Renewable and Sustainable Energy Reviews* **2002**, *6* (5), 433-455.
62. Corma, A.; Atienzar, P.; García, H.; Chane-Ching, J.-Y., Hierarchically mesostructured doped CeO₂ with potential for solar-cell use. *Nature Materials* **2004**, *3* (6), 394-397.
63. Reinhardt, K.; Winkler, H., Cerium Mischmetal, Cerium Alloys, and Cerium Compounds. *Ullmann's Encyclopedia of Industrial Chemistry* **2000**.
64. Patil, S.; Kuiry, S. C.; Seal, S.; Vanfleet, R., Synthesis of Nanocrystalline Ceria Particles for High Temperature Oxidation Resistant Coating. *Journal of Nanoparticle Research* **2002**, *4* (5), 433-438.
65. Abbasi, Z.; Haghghi, M.; Fatehifar, E.; Saedy, S., Synthesis and physicochemical characterizations of nanostructured Pt/Al₂O₃-CeO₂ catalysts for total oxidation of VOCs. *Journal of Hazardous Materials* **2011**, *186* (2), 1445-1454.
66. Abbasi, Z.; Haghghi, M.; Fatehifar, E.; Saedy, S., Synthesis and Physicochemical Characterization of Nanostructured Pt/CeO₂ Catalyst Used for Total Oxidation of Toluene. *International Journal of Chemical Reactor Engineering* **2011**, *9* (1).

67. Orge, C. A.; Órfão, J. J. M.; Pereira, M. F. R.; Duarte de Farias, A. M.; Neto, R. C. R.; Fraga, M. A., Ozonation of model organic compounds catalysed by nanostructured cerium oxides. *Applied Catalysis B: Environmental* **2011**, *103* (1), 190-199.
68. Yuan, Z.-Y.; Idakiev, V.; Vantomme, A.; Tabakova, T.; Ren, T.-Z.; Su, B.-L., Mesoporous and nanostructured CeO₂ as supports of nano-sized gold catalysts for low-temperature water-gas shift reaction. *Catalysis Today* **2008**, *131* (1), 203-210.
69. Yabe, S.; Sato, T., Cerium oxide for sunscreen cosmetics. *Journal of Solid State Chemistry* **2003**, *171* (1), 7-11.
70. Ecco, L. G.; Fedel, M.; Deflorian, F.; Becker, J.; Iversen, B. B.; Mamakhel, A., Waterborne acrylic paint system based on nanoceria for corrosion protection of steel. *Progress in Organic Coatings* **2016**, *96*, 19-25.
71. Korsvik, C.; Patil, S.; Seal, S.; Self, W. T., Superoxide dismutase mimetic properties exhibited by vacancy engineered ceria nanoparticles. *Chemical Communications* **2007**, (10), 1056-1058.
72. Pirmohamed, T.; Dowding, J. M.; Singh, S.; Wasserman, B.; Heckert, E.; Karakoti, A. S.; King, J. E. S.; Seal, S.; Self, W. T., Nanoceria exhibit redox state-dependent catalase mimetic activity. *Chemical Communications* **2010**, *46* (16), 2736-2738.
73. Song, G.; Cheng, N.; Zhang, J.; Huang, H.; Yuan, Y.; He, X.; Luo, Y.; Huang, K., Nanoscale Cerium Oxide: Synthesis, Biocatalytic Mechanism, and Applications. *Catalysts* **2021**, *11* (9).
74. Asati, A.; Kaittanis, C.; Santra, S.; Perez, J. M., pH-Tunable Oxidase-Like Activity of Cerium Oxide Nanoparticles Achieving Sensitive Fluorogenic Detection of Cancer Biomarkers at Neutral pH. *Analytical Chemistry* **2011**, *83* (7), 2547-2553.
75. Celardo, I.; Pedersen, J. Z.; Traversa, E.; Ghibelli, L., Pharmacological potential of cerium oxide nanoparticles. *Nanoscale* **2011**, *3* (4), 1411-1420.
76. Li, M.; Shi, P.; Xu, C.; Ren, J.; Qu, X., Cerium oxide caged metal chelator: anti-aggregation and anti-oxidation integrated H₂O₂-responsive controlled drug release for potential Alzheimer's disease treatment. *Chemical Science* **2013**, *4* (6), 2536-2542.
77. Xu, C.; Lin, Y.; Wang, J.; Wu, L.; Wei, W.; Ren, J.; Qu, X., Nanoceria-Triggered Synergetic Drug Release Based on CeO₂-Capped Mesoporous Silica Host-Guest Interactions and Switchable Enzymatic Activity and Cellular Effects of CeO₂. *Advanced Healthcare Materials* **2013**, *2* (12), 1591-1599.
78. Limbach, L. K.; Bereiter, R.; Müller, E.; Krebs, R.; Gälli, R.; Stark, W. J., Removal of Oxide Nanoparticles in a Model Wastewater Treatment Plant: Influence of Agglomeration and Surfactants on Clearing Efficiency. *Environmental Science & Technology* **2008**, *42* (15), 5828-5833.
79. Singh, S.; Kumar, A.; Karakoti, A.; Seal, S.; Self, W. T., Unveiling the mechanism of uptake and sub-cellular distribution of cerium oxide nanoparticles. *Molecular BioSystems* **2010**, *6* (10), 1813-1820.
80. Safi, M.; Sarrouj, H.; Sandre, O.; Mignet, N.; Berret, J. F., Interactions between sub-10-nm iron and cerium oxide nanoparticles and 3T3 fibroblasts: the role of the coating and aggregation state. *Nanotechnology* **2010**, *21* (14), 145103.
81. Chen, J.; Patil, S.; Seal, S.; McGinnis, J. F., Nanoceria Particles Prevent ROI-Induced Blindness. In *Recent Advances in Retinal Degeneration*, Anderson, R. E.; LaVail, M. M.; Hollyfield, J. G., Eds. Springer New York: New York, NY, 2008; pp 53-59.
82. Karakoti, A.; Singh, S.; Dowding, J. M.; Seal, S.; Self, W. T., Redox-active radical scavenging nanomaterials. *Chemical Society Reviews* **2010**, *39* (11), 4422-4432.

83. Rzigalinski, B. A.; Carfagna, C. S.; Ehrich, M., Cerium oxide nanoparticles in neuroprotection and considerations for efficacy and safety. *Wiley Interdiscip Rev Nanomed Nanobiotechnol* **2017**, *9* (4), 10.1002/wnan.1444.
84. Nalabotu, S. K.; Kolli, M. B.; Triest, W. E.; Ma, J. Y.; Manne, N. D. P. K.; Katta, A.; Addagarla, H. S.; Rice, K. M.; Blough, E. R., Intratracheal instillation of cerium oxide nanoparticles induces hepatic toxicity in male Sprague-Dawley rats. *Int J Nanomedicine* **2011**, *6*, 2327-2335.
85. Park, E.-J.; Choi, J.; Park, Y.-K.; Park, K., Oxidative stress induced by cerium oxide nanoparticles in cultured BEAS-2B cells. *Toxicology* **2008**, *245* (1), 90-100.
86. Zhang, H.; He, X.; Zhang, Z.; Zhang, P.; Li, Y.; Ma, Y.; Kuang, Y.; Zhao, Y.; Chai, Z., Nano-CeO₂ Exhibits Adverse Effects at Environmental Relevant Concentrations. *Environmental Science & Technology* **2011**, *45* (8), 3725-3730.
87. Lee, S. S.; Song, W.; Cho, M.; Puppala, H. L.; Nguyen, P.; Zhu, H.; Segatori, L.; Colvin, V. L., Antioxidant Properties of Cerium Oxide Nanocrystals as a Function of Nanocrystal Diameter and Surface Coating. *ACS Nano* **2013**, *7* (11), 9693-9703.
88. Modena, M. M.; Rühle, B.; Burg, T. P.; Wuttke, S., Nanoparticle Characterization: What to Measure? *Advanced Materials* **2019**, *31* (32), 1901556.
89. Laborda, F.; Bolea, E.; Cepriá, G.; Gómez, M. T.; Jiménez, M. S.; Pérez-Arategui, J.; Castillo, J. R., Detection, characterization and quantification of inorganic engineered nanomaterials: A review of techniques and methodological approaches for the analysis of complex samples. *Analytica Chimica Acta* **2016**, *904*, 10-32.
90. Brar, S. K.; Verma, M., Measurement of nanoparticles by light-scattering techniques. *TrAC Trends in Analytical Chemistry* **2011**, *30* (1), 4-17.
91. Gallego-Urrea, J. A.; Tuoriniemi, J.; Hassellöv, M., Applications of particle-tracking analysis to the determination of size distributions and concentrations of nanoparticles in environmental, biological and food samples. *TrAC Trends in Analytical Chemistry* **2011**, *30* (3), 473-483.
92. Tiede, K.; Boxall, A. B. A.; Tiede, D.; Tear, S. P.; David, H.; Lewis, J., A robust size-characterisation methodology for studying nanoparticle behaviour in 'real' environmental samples, using hydrodynamic chromatography coupled to ICP-MS. *Journal of Analytical Atomic Spectrometry* **2009**, *24* (7), 964-972.
93. v. d. Kammer, F.; Baborowski, M.; Tadjiki, S.; v. Tümpling jr, W., Colloidal Particles in Sediment Pore Waters: Particle Size Distributions and Associated Element Size Distribution in Anoxic and Re-oxidized Samples, Obtained by FFF-ICP-MS Coupling. *Acta hydrochimica et hydrobiologica* **2003**, *31* (4-5), 400-410.
94. Mehn, D.; Caputo, F.; Rösslein, M.; Calzolari, L.; Saint-Antonin, F.; Courant, T.; Wick, P.; Gilliland, D., Larger or more? Nanoparticle characterisation methods for recognition of dimers. *RSC Advances* **2017**, *7* (44), 27747-27754.
95. Proulx, K.; Wilkinson, K. J., Separation, detection and characterisation of engineered nanoparticles in natural waters using hydrodynamic chromatography and multi-method detection (light scattering, analytical ultracentrifugation and single particle ICP-MS). *Environmental Chemistry* **2014**, *11* (4), 392-401.
96. Telgmann, L.; Lindner, U.; Lingott, J.; Jakubowski, N., Analysis and Speciation of Lanthanoides by ICP-MS. *Physical Sciences Reviews* **2016**, *1* (11).
97. Meermann, B.; Nischwitz, V., ICP-MS for the analysis at the nanoscale – a tutorial review. *Journal of Analytical Atomic Spectrometry* **2018**, *33* (9), 1432-1468.
98. Thomas, R., A beginner's guide to ICP-MS. *Spectroscopy* **2001**, *16* (4), 38-42.

99. Thomas, R., *Practical guide to ICP-MS: a tutorial for beginners*. CRC press: 2008.
100. Beauchemin, D., Environmental analysis by inductively coupled plasma mass spectrometry. *Mass Spectrometry Reviews* **2010**, *29* (4), 560-592.
101. Dean, J. R., *Practical inductively coupled plasma spectrometry*. John Wiley & Sons: 2019.
102. The 30-Minute Guide to ICP-MS. *PerkinElmer* **2004**.
103. Al-Hakkani, M. F., Guideline of inductively coupled plasma mass spectrometry “ICP–MS”: fundamentals, practices, determination of the limits, quality control, and method validation parameters. *SN Applied Sciences* **2019**, *1* (7), 791.
104. Mermet, J.-M.; Poussel, E., Couplage plasma induit par haute fréquence-spectrométrie de masse. *Techniques de l'Ingénieur* **1999**, *4*, P2.
105. Miller, P. E.; Denton, M. B., The quadrupole mass filter: basic operating concepts. *Journal of chemical education* **1986**, *63* (7), 617.
106. Jakubowski, N.; Moens, L.; Vanhaecke, F., Sector field mass spectrometers in ICP-MS. *Spectrochimica Acta Part B: Atomic Spectroscopy* **1998**, *53* (13), 1739-1763.
107. Nu instruments, AttoM high resolution ICP-MS system manual Issue 1.0.1. **2010**.
108. Kawaguchi, H.; Fukasawa, N.; Mizuike, A., Investigation of airborne particles by inductively coupled plasma emission spectrometry calibrated with monodisperse aerosols. *Spectrochimica Acta Part B: Atomic Spectroscopy* **1986**, *41* (12), 1277-1286.
109. Degueldre, C.; Favarger, P. Y., Colloid analysis by single particle inductively coupled plasma-mass spectroscopy: a feasibility study. *Colloids and Surfaces A: Physicochemical and Engineering Aspects* **2003**, *217* (1), 137-142.
110. Degueldre, C.; Favarger, P. Y., Thorium colloid analysis by single particle inductively coupled plasma-mass spectrometry. *Talanta* **2004**, *62* (5), 1051-1054.
111. Degueldre, C.; Favarger, P. Y.; Bitea, C., Zirconia colloid analysis by single particle inductively coupled plasma–mass spectrometry. *Analytica Chimica Acta* **2004**, *518* (1), 137-142.
112. Degueldre, C.; Favarger, P. Y.; Wold, S., Gold colloid analysis by inductively coupled plasma-mass spectrometry in a single particle mode. *Analytica Chimica Acta* **2006**, *555* (2), 263-268.
113. Laborda, F.; Bolea, E.; Jiménez-Lamana, J., Single Particle Inductively Coupled Plasma Mass Spectrometry: A Powerful Tool for Nanoanalysis. *Analytical Chemistry* **2014**, *86* (5), 2270-2278.
114. Donovan, A. R.; Adams, C. D.; Ma, Y.; Stephan, C.; Eichholz, T.; Shi, H., Detection of zinc oxide and cerium dioxide nanoparticles during drinking water treatment by rapid single particle ICP-MS methods. *Analytical and Bioanalytical Chemistry* **2016**, *408* (19), 5137-5145.
115. Fréchette-Viens, L.; Hadioui, M.; Wilkinson, K. J., Quantification of ZnO nanoparticles and other Zn containing colloids in natural waters using a high sensitivity single particle ICP-MS. *Talanta* **2019**, *200*, 156-162.
116. Hadioui, M.; Merdzan, V.; Wilkinson, K. J., Detection and Characterization of ZnO Nanoparticles in Surface and Waste Waters Using Single Particle ICPMS. *Environmental Science & Technology* **2015**, *49* (10), 6141-6148.
117. Azimzada, A.; Farner, J. M.; Hadioui, M.; Liu-Kang, C.; Jreije, I.; Tufenkji, N.; Wilkinson, K. J., Release of TiO₂ nanoparticles from painted surfaces in cold climates: characterization using a high sensitivity single-particle ICP-MS. *Environmental Science: Nano* **2020**, *7* (1), 139-148.

118. Hadioui, M.; Knapp, G.; Azimzada, A.; Jreije, I.; Frechette-Viens, L.; Wilkinson, K. J., Lowering the Size Detection Limits of Ag and TiO₂ Nanoparticles by Single Particle ICP-MS. *Analytical Chemistry* **2019**, *91* (20), 13275-13284.
119. Azimzada, A.; Jreije, I.; Hadioui, M.; Shaw, P.; Farner, J. M.; Wilkinson, K. J., Quantification and Characterization of Ti-, Ce-, and Ag-Nanoparticles in Global Surface Waters and Precipitation. *Environmental Science & Technology* **2021**, *55* (14), 9836-9844.
120. Van Koetsem, F.; Geremew, T. T.; Wallaert, E.; Verbeken, K.; Van der Meeren, P.; Du Laing, G., Fate of engineered nanomaterials in surface water: Factors affecting interactions of Ag and CeO₂ nanoparticles with (re)suspended sediments. *Ecological Engineering* **2015**, *80*, 140-150.
121. Auffan, M.; Masion, A.; Labille, J.; Diot, M. A.; Liu, W.; Olivi, L.; Proux, O.; Ziarelli, F.; Chaurand, P.; Geantet, C.; Bottero, J. Y.; Rose, J., Long-term aging of a CeO(2) based nanocomposite used for wood protection. *Environ Pollut* **2014**, *188*, 1-7.
122. Jreije, I.; Azimzada, A.; Hadioui, M.; Wilkinson, K. J., Measurement of CeO₂ Nanoparticles in Natural Waters Using a High Sensitivity, Single Particle ICP-MS. *Molecules* **2020**, *25* (23), 5516.
123. Ramirez Arenas, L.; Ramseier Gentile, S.; Zimmermann, S.; Stoll, S., Coagulation of TiO₂, CeO₂ nanoparticles, and polystyrene nanoplastics in bottled mineral and surface waters. Effect of water properties, coagulant type, and dosage. **2020**, *92* (8), 1184-1194.
124. Bolea, E.; Jimenez, M. S.; Perez-Arategui, J.; Vidal, J. C.; Bakir, M.; Ben-Jeddou, K.; Gimenez-Ingalaturre, A. C.; Ojeda, D.; Trujillo, C.; Laborda, F., Analytical applications of single particle inductively coupled plasma mass spectrometry: a comprehensive and critical review. *Analytical Methods* **2021**, *13* (25), 2742-2795.
125. Hineman, A.; Stephan, C., Effect of dwell time on single particle inductively coupled plasma mass spectrometry data acquisition quality. *Journal of Analytical Atomic Spectrometry* **2014**, *29* (7), 1252-1257.
126. Montañó, M. D.; Badiei, H. R.; Bazargan, S.; Ranville, J. F., Improvements in the detection and characterization of engineered nanoparticles using spICP-MS with microsecond dwell times. *Environmental Science: Nano* **2014**, *1* (4), 338-346.
127. Pace, H. E.; Rogers, N. J.; Jarolimek, C.; Coleman, V. A.; Higgins, C. P.; Ranville, J. F., Determining transport efficiency for the purpose of counting and sizing nanoparticles via single particle inductively coupled plasma mass spectrometry. *Analytical chemistry* **2011**, *83* (24), 9361-9369.
128. Bi, X.; Lee, S.; Ranville, J. F.; Sattigeri, P.; Spanias, A.; Herckes, P.; Westerhoff, P., Quantitative resolution of nanoparticle sizes using single particle inductively coupled plasma mass spectrometry with the K-means clustering algorithm. *Journal of Analytical Atomic Spectrometry* **2014**, *29* (9), 1630-1639.
129. Hendriks, L.; Gundlach-Graham, A.; Günther, D., Performance of sp-ICP-TOFMS with signal distributions fitted to a compound Poisson model. *Journal of Analytical Atomic Spectrometry* **2019**, *34* (9), 1900-1909.
130. Tuoriniemi, J.; Cornelis, G.; Hassellöv, M., A new peak recognition algorithm for detection of ultra-small nano-particles by single particle ICP-MS using rapid time resolved data acquisition on a sector-field mass spectrometer. *Journal of Analytical Atomic Spectrometry* **2015**, *30* (8), 1723-1729.
131. Shaw, P.; Donard, A., Nano-particle analysis using dwell times between 10 μ s and 70 μ s with an upper counting limit of greater than 3×10^7 cps and a gold nanoparticle detection limit of less than 10 nm diameter. *Journal of Analytical Atomic Spectrometry* **2016**, *31* (6), 1234-1242.

132. Schwertfeger, D. M.; Velicogna, J. R.; Jesmer, A. H.; Scroggins, R. P.; Princz, J. I., Single Particle-Inductively Coupled Plasma Mass Spectroscopy Analysis of Metallic Nanoparticles in Environmental Samples with Large Dissolved Analyte Fractions. *Analytical Chemistry* **2016**, *88* (20), 9908-9914.
133. Hadioui, M.; Leclerc, S.; Wilkinson, K. J., Multimethod quantification of Ag⁺ release from nanosilver. *Talanta* **2013**, *105*, 15-19.
134. Hadioui, M.; Peyrot, C.; Wilkinson, K. J., Improvements to Single Particle ICPMS by the Online Coupling of Ion Exchange Resins. *Analytical Chemistry* **2014**, *86* (10), 4668-4674.
135. Lecompte, Y.; Bohand, S.; Laroche, P.; Cazoulat, A. In *Intérêt et limites du couplage plasma induit par haute fréquence-spectrométrie de masse (ICP-MS) pour le diagnostic urinaire d'une contamination interne par un radionucléide*, Annales de Biologie Clinique, 2013; pp 269-281.
136. May, T. W.; Wiedmeyer, R. H., A table of polyatomic interferences in ICP-MS. *ATOMIC SPECTROSCOPY-NORWALK CONNECTICUT-* **1998**, *19*, 150-155.
137. Wilschefski, S. C.; Baxter, M. R., Inductively Coupled Plasma Mass Spectrometry: Introduction to Analytical Aspects. *Clin Biochem Rev* **2019**, *40* (3), 115-133.
138. Abad-Álvaro, I.; Peña-Vázquez, E.; Bolea, E.; Bermejo-Barrera, P.; Castillo, J. R.; Laborda, F., Evaluation of number concentration quantification by single-particle inductively coupled plasma mass spectrometry: microsecond vs. millisecond dwell times. *Analytical and Bioanalytical Chemistry* **2016**, *408* (19), 5089-5097.
139. Jreije, I.; Azimzada, A.; Hadioui, M.; Wilkinson, K. J., Measurement of CeO₂ Nanoparticles in Natural Waters Using a High Sensitivity, Single Particle ICP-MS. **2020**, *25* (23), 5516.
140. Shigeta, K.; Traub, H.; Panne, U.; Okino, A.; Rottmann, L.; Jakubowski, N., Application of a micro-droplet generator for an ICP-sector field mass spectrometer – optimization and analytical characterization. *Journal of Analytical Atomic Spectrometry* **2013**, *28* (5), 646-656.
141. Wei, X.; Zheng, D.-H.; Cai, Y.; Jiang, R.; Chen, M.-L.; Yang, T.; Xu, Z.-R.; Yu, Y.-L.; Wang, J.-H., High-Throughput/High-Precision Sampling of Single Cells into ICP-MS for Elucidating Cellular Nanoparticles. *Analytical Chemistry* **2018**, *90* (24), 14543-14550.
142. Sanchez-Garcia, L.; Bolea, E.; Laborda, F.; Cubel, C.; Ferrer, P.; Gianolio, D.; da Silva, I.; Castillo, J. R., Size determination and quantification of engineered cerium oxide nanoparticles by flow field-flow fractionation coupled to inductively coupled plasma mass spectrometry. *J Chromatogr A* **2016**, *1438*, 205-15.
143. Speed, D.; Westerhoff, P.; Sierra-Alvarez, R.; Draper, R.; Pantano, P.; Aravamudhan, S.; Chen, K. L.; Hristovski, K.; Herckes, P.; Bi, X.; Yang, Y.; Zeng, C.; Otero-Gonzalez, L.; Mikoryak, C.; Wilson, B. A.; Kosaraju, K.; Tarannum, M.; Crawford, S.; Yi, P.; Liu, X.; Babu, S. V.; Moinpour, M.; Ranville, J.; Montano, M.; Corredor, C.; Posner, J.; Shadman, F., Physical, chemical, and in vitro toxicological characterization of nanoparticles in chemical mechanical planarization suspensions used in the semiconductor industry: towards environmental health and safety assessments. *Environmental Science: Nano* **2015**, *2* (3), 227-244.
144. Sahu, T.; Bisht, S.; Das, K.; Kerkar, S., Nanoceria: Synthesis and Biomedical Applications. *Current Nanoscience* **2013**, *9* (5), 588-593.
145. Cornelis, G.; Ryan, B.; McLaughlin, M. J.; Kirby, J. K.; Beak, D.; Chittleborough, D., Solubility and batch retention of CeO₂ nanoparticles in soils. *Environ Sci Technol* **2011**, *45* (7), 2777-82.

146. Dan, Y.; Ma, X.; Zhang, W.; Liu, K.; Stephan, C.; Shi, H., Single particle ICP-MS method development for the determination of plant uptake and accumulation of CeO₂ nanoparticles. *Anal Bioanal Chem* **2016**, *408* (19), 5157-67.
147. Clar, J. G.; Platten, W. E., 3rd; Baumann, E. J., Jr.; Remsen, A.; Harmon, S. M.; Bennett-Stamper, C. L.; Thomas, T. A.; Luxton, T. P., Dermal transfer and environmental release of CeO₂ nanoparticles used as UV inhibitors on outdoor surfaces: Implications for human and environmental health. *Sci Total Environ* **2018**, *613-614*, 714-723.
148. Scifo, L.; Chaurand, P.; Bossa, N.; Avellan, A.; Auffan, M.; Masion, A.; Angeletti, B.; Kieffer, I.; Labille, J.; Bottero, J. Y.; Rose, J., Non-linear release dynamics for a CeO₂ nanomaterial embedded in a protective wood stain, due to matrix photo-degradation. *Environ Pollut* **2018**, *241*, 182-193.
149. Keller, A. A.; Lazareva, A., Predicted Releases of Engineered Nanomaterials: From Global to Regional to Local. *Environmental Science & Technology Letters* **2013**, *1* (1), 65-70.
150. Tan, Z.-Q.; Yin, Y.-G.; Guo, X.-R.; Amde, M.; Moon, M. H.; Liu, J.-F.; Jiang, G.-B., Tracking the Transformation of Nanoparticulate and Ionic Silver at Environmentally Relevant Concentration Levels by Hollow Fiber Flow Field-Flow Fractionation Coupled to ICPMS. *Environmental Science & Technology* **2017**, *51* (21), 12369-12376.
151. Proulx, K.; Hadioui, M.; Wilkinson, K. J., Separation, detection and characterization of nanomaterials in municipal wastewaters using hydrodynamic chromatography coupled to ICPMS and single particle ICPMS. *Analytical and Bioanalytical Chemistry* **2016**, *408* (19), 5147-5155.
152. Laborda, F.; Bolea, E.; Jimenez-Lamana, J., Single particle inductively coupled plasma mass spectrometry: a powerful tool for nanoanalysis. *Anal Chem* **2014**, *86* (5), 2270-8.
153. Birbaum, K.; Brogioli, R.; Schellenberg, M.; Martinoia, E.; Stark, W. J.; Gunther, D.; Limbach, L. K., No evidence for cerium dioxide nanoparticle translocation in maize plants. *Environ Sci Technol* **2010**, *44* (22), 8718-23.
154. Roh, J. Y.; Park, Y. K.; Park, K.; Choi, J., Ecotoxicological investigation of CeO(2) and TiO(2) nanoparticles on the soil nematode *Caenorhabditis elegans* using gene expression, growth, fertility, and survival as endpoints. *Environ Toxicol Pharmacol* **2010**, *29* (2), 167-72.
155. Hadioui, M.; Peyrot, C.; Wilkinson, K. J., Improvements to single particle ICPMS by the online coupling of ion exchange resins. *Anal Chem* **2014**, *86* (10), 4668-74.
156. Abad-Alvaro, I.; Pena-Vazquez, E.; Bolea, E.; Bermejo-Barrera, P.; Castillo, J. R.; Laborda, F., Evaluation of number concentration quantification by single-particle inductively coupled plasma mass spectrometry: microsecond vs. millisecond dwell times. *Anal Bioanal Chem* **2016**, *408* (19), 5089-97.
157. US Research Nanomaterials, I. Cerium oxide nanopowder/nanoparticles. <https://www.us-nano.com/inc/sdetail/214>.
158. Thorp, J.; Lamberti, G.; Casper, A., St. Lawrence River Basin. 2005; pp 982-1028.
159. O'Brien, N.; Cummins, E., Nano-Scale Pollutants: Fate in Irish Surface and Drinking Water Regulatory Systems. *Human and Ecological Risk Assessment: An International Journal* **2010**, *16* (4), 847-872.
160. Gottschalk, F.; Sun, T.; Nowack, B., Environmental concentrations of engineered nanomaterials: review of modeling and analytical studies. *Environ Pollut* **2013**, *181*, 287-300.
161. Peters, R. J. B.; van Bommel, G.; Milani, N. B. L.; den Hertog, G. C. T.; Undas, A. K.; van der Lee, M.; Bouwmeester, H., Detection of nanoparticles in Dutch surface waters. *Science of The Total Environment* **2018**, *621*, 210-218.

162. Oriekhova, O.; Stoll, S., Stability of uncoated and fulvic acids coated manufactured CeO₂ nanoparticles in various conditions: From ultrapure to natural Lake Geneva waters. *Science of The Total Environment* **2016**, *562*, 327-334.
163. Ramirez, L.; Ramseier Gentile, S.; Zimmermann, S.; Stoll, S., Behavior of TiO₂ and CeO₂ Nanoparticles and Polystyrene Nanoplastics in Bottled Mineral, Drinking and Lake Geneva Waters. Impact of Water Hardness and Natural Organic Matter on Nanoparticle Surface Properties and Aggregation. **2019**, *11* (4), 721.
164. Montaña, M. D.; Lowry, G. V.; von der Kammer, F.; Blue, J.; Ranville, J. F., Current status and future direction for examining engineered nanoparticles in natural systems. *Environmental Chemistry* **2014**, *11* (4).
165. Praetorius, A.; Gundlach-Graham, A.; Goldberg, E.; Fabienke, W.; Navratilova, J.; Gondikas, A.; Kaegi, R.; Günther, D.; Hofmann, T.; von der Kammer, F., Single-particle multi-element fingerprinting (spMEF) using inductively-coupled plasma time-of-flight mass spectrometry (ICP-TOFMS) to identify engineered nanoparticles against the elevated natural background in soils. *Environmental Science: Nano* **2017**, *4* (2), 307-314.
166. Markus, A. A.; Krystek, P.; Tromp, P. C.; Parsons, J. R.; Roex, E. W. M.; Voogt, P.; Laane, R., Determination of metal-based nanoparticles in the river Dommel in the Netherlands via ultrafiltration, HR-ICP-MS and SEM. *Sci Total Environ* **2018**, *631-632*, 485-495.
167. Sharma, V. K.; Filip, J.; Zboril, R.; Varma, R. S., Natural inorganic nanoparticles--formation, fate, and toxicity in the environment. *Chem Soc Rev* **2015**, *44* (23), 8410-23.
168. Vitalij K. Percharlsky; Karl A. Gschneidner, J., Rare-earth element. In *Encyclopaedia Britannica*, Encyclopaedia Britannica, inc.: 2019.
169. Castor, S. B., Rare Earth Elements. *Industrial Minerals & Rocks* **2006**, 769-792.
170. US Research Nanomaterials, I. Lanthanum oxide nanopowder/nanoparticles. <https://www.us-nano.com/inc/sdetail/965>.
171. Azimzada, A.; Farner, J. M.; Jreije, I.; Hadioui, M.; Liu-Kang, C.; Tufenkji, N.; Shaw, P.; Wilkinson, K. J., Single- and Multi-Element Quantification and Characterization of TiO₂ Nanoparticles Released From Outdoor Stains and Paints. *Frontiers in Environmental Science* **2020**.
172. Pace, H. E.; Rogers, N. J.; Jarolimek, C.; Coleman, V. A.; Higgins, C. P.; Ranville, J. F., Determining transport efficiency for the purpose of counting and sizing nanoparticles via single particle inductively coupled plasma mass spectrometry. *Anal Chem* **2011**, *83* (24), 9361-9.
173. Shaw, P.; Donard, A., Nano-particle analysis using dwell times between 10 μ s and 70 μ s with an upper counting limit of greater than 3×10^7 cps and a gold nanoparticle detection limit of less than 10 nm diameter. *Journal of Analytical Atomic Spectrometry* **2016**, *31* (6), 1234-1242.
174. Markus, A. A.; Krystek, P.; Tromp, P. C.; Parsons, J. R.; Roex, E. W. M.; Voogt, P. d.; Laane, R. W. P. M., Determination of metal-based nanoparticles in the river Dommel in the Netherlands via ultrafiltration, HR-ICP-MS and SEM. *Science of The Total Environment* **2018**, *631-632*, 485-495.
175. Mitrano, D. M.; Ranville, J. F.; Bednar, A.; Kazor, K.; Hering, A. S.; Higgins, C. P., Tracking dissolution of silver nanoparticles at environmentally relevant concentrations in laboratory, natural, and processed waters using single particle ICP-MS (spICP-MS). *Environmental Science: Nano* **2014**, *1* (3), 248-259.
176. Kaur, I.; Ellis, L.-J.; Romer, I.; Tantra, R.; Carriere, M.; Allard, S.; Mayne-L'Hermite, M.; Minelli, C.; Unger, W.; Potthoff, A.; Rades, S.; Valsami-Jones, E., Dispersion of Nanomaterials in Aqueous Media: Towards Protocol Optimization. *JoVE* **2017**, (130), e56074.

177. Bihari, P.; Vippola, M.; Schultes, S.; Praetner, M.; Khandoga, A. G.; Reichel, C. A.; Coester, C.; Tuomi, T.; Rehberg, M.; Krombach, F., Optimized dispersion of nanoparticles for biological in vitro and in vivo studies. *Particle and Fibre Toxicology* **2008**, *5* (1), 14.
178. DeLoid, G. M.; Cohen, J. M.; Pyrgiotakis, G.; Demokritou, P., Preparation, characterization, and in vitro dosimetry of dispersed, engineered nanomaterials. *Nat Protoc* **2017**, *12* (2), 355-371.
179. Hartmann, N. B.; Jensen, K. A.; Baun, A.; Rasmussen, K.; Rauscher, H.; Tantra, R.; Cupi, D.; Gilliland, D.; Pianella, F.; Riego Sintes, J. M., Techniques and Protocols for Dispersing Nanoparticle Powders in Aqueous Media—Is there a Rationale for Harmonization? *Journal of Toxicology and Environmental Health, Part B* **2015**, *18* (6), 299-326.
180. Taurozzi, J. S.; Hackley, V. A.; Wiesner, M., Preparation of nanoparticle dispersions from powdered material using ultrasonic disruption. *NIST special publication* **2012**, *1200* (2), 1200-2.
181. Taurozzi, J. S.; Hackley, V. A.; Wiesner, M., Reporting guidelines for the Preparation of Aqueous nanoparticle dispersions from dry materials. *NIST special publication* **2012**, *1200*, 1.
182. Zhang, M.; Yang, J.; Cai, Z.; Feng, Y.; Wang, Y.; Zhang, D.; Pan, X. J. E. S. N., Detection of engineered nanoparticles in aquatic environments: current status and challenges in enrichment, separation, and analysis. **2019**, *6* (3), 709-735.
183. Heithmar, E. M.; Pergantis, S. A., *Characterizing concentrations and size distributions of metal-containing nanoparticles in waste water*. US Environmental Protection Agency, Office of Research and Development ...: 2010.
184. Gondikas, A. P.; Kammer, F. v. d.; Reed, R. B.; Wagner, S.; Ranville, J. F.; Hofmann, T., Release of TiO₂ nanoparticles from sunscreens into surface waters: a one-year survey at the old Danube recreational Lake. *Environmental Science & Technology* **2014**, *48* (10), 5415-5422.
185. Loosli, F.; Le Coustumer, P.; Stoll, S., TiO₂ nanoparticles aggregation and disaggregation in presence of alginate and Suwannee River humic acids. pH and concentration effects on nanoparticle stability. *Water Research* **2013**, *47* (16), 6052-6063.
186. Klein, J. J. M. d.; Quik, J. T. K.; Bäuerlein, P. S.; Koelmans, A. A., Towards validation of the NanoDUFLOW nanoparticle fate model for the river Dommel, The Netherlands. *Environmental Science: Nano* **2016**, *3* (2), 434-441.
187. Phalyvong, K.; Sivry, Y.; Pauwels, H.; Gélabert, A.; Tharaud, M.; Wille, G.; Bourrat, X.; Ranville, J. F.; Benedetti, M. F., Assessing CeO₂ and TiO₂ Nanoparticle Concentrations in the Seine River and Its Tributaries Near Paris. **2021**, *8* (271).
188. Surette, M. C.; Nason, J. A., Nanoparticle aggregation in a freshwater river: the role of engineered surface coatings. *Environmental Science: Nano* **2019**, *6* (2), 540-553.
189. Mozhayeva, D.; Engelhard, C., Separation of Silver Nanoparticles with Different Coatings by Capillary Electrophoresis Coupled to ICP-MS in Single Particle Mode. *Analytical Chemistry* **2017**, *89* (18), 9767-9774.
190. Azimzada, A.; Farner, J. M.; Jreije, I.; Hadioui, M.; Liu-Kang, C.; Tufenkji, N.; Shaw, P.; Wilkinson, K. J., Single- and Multi-Element Quantification and Characterization of TiO₂ Nanoparticles Released From Outdoor Stains and Paints. *Frontiers in Environmental Science* **2020**, *8* (91).
191. Ladner, D. A.; Steele, M.; Weir, A.; Hristovski, K.; Westerhoff, P., Functionalized nanoparticle interactions with polymeric membranes. *Journal of Hazardous Materials* **2012**, *211-212*, 288-295.

192. Olabarrieta, J.; Monzón, O.; Belaustegui, Y.; Alvarez, J.-I.; Zorita, S., Removal of TiO₂ nanoparticles from water by low pressure pilot plant filtration. *Science of The Total Environment* **2018**, *618*, 551-560.
193. Van Koetsem, F.; Verstraete, S.; Wallaert, E.; Verbeken, K.; Van der Meeren, P.; Rinklebe, J.; Du Laing, G., Use of filtration techniques to study environmental fate of engineered metallic nanoparticles: Factors affecting filter performance. *Journal of Hazardous Materials* **2017**, *322*, 105-117.
194. Gubala, V.; Johnston, L. J.; Liu, Z.; Krug, H.; Moore, C. J.; Ober, C. K.; Schwenk, M.; Vert, M., Engineered nanomaterials and human health: Part 1. Preparation, functionalization and characterization (IUPAC Technical Report). *Pure and Applied Chemistry* **2018**, *90* (8), 1283-1324.
195. Gubala, V.; Johnston, L. J.; Krug, H. F.; Moore, C. J.; Ober, C. K.; Schwenk, M.; Vert, M., Engineered nanomaterials and human health: Part 2. Applications and nanotoxicology (IUPAC Technical Report). *Pure and Applied Chemistry* **2018**, *90* (8), 1325-1356.
196. Stark, W. J.; Stoessel, P. R.; Wohlleben, W.; Hafner, A., Industrial applications of nanoparticles. *Chemical Society Reviews* **2015**, *44* (16), 5793-5805.
197. Abou El-Nour, K. M. M.; Eftaiha, A.; Al-Warthan, A.; Ammar, R. A. A., Synthesis and applications of silver nanoparticles. *Arabian Journal of Chemistry* **2010**, *3* (3), 135-140.
198. Auffan, M.; Masion, A.; Labille, J.; Diot, M. A.; Liu, W.; Olivi, L.; Proux, O.; Ziarelli, F.; Chaurand, P.; Geantet, C.; Bottero, J. Y.; Rose, J., Long-term aging of a CeO₂ based nanocomposite used for wood protection. *Environ Pollut* **2014**, *188*, 1-7.
199. Fréchette-Viens, L.; Hadioui, M.; Wilkinson, K. J., Practical limitations of single particle ICP-MS in the determination of nanoparticle size distributions and dissolution: case of rare earth oxides. *Talanta* **2017**, *163*, 121-126.
200. Thorp, J. H.; Lamberti, G. A.; Casper, A. F., St. Lawrence river basin. In *Rivers of North America*, Elsevier Inc.: 2005; pp 982-1028.
201. Azimzada, A.; Jreije, I.; Hadioui, M.; Shaw, P.; Farner, J. M.; Wilkinson, K. J., Quantification and Characterization of Ti-, Ce-, and Ag-Nanoparticles in Global Surface Waters and Precipitation. *Environmental Science & Technology* **2021**.
202. Maillette, S.; Peyrot, C.; Purkait, T.; Iqbal, M.; Veinot, J. G. C.; Wilkinson, K. J., Heteroagglomeration of nanosilver with colloidal SiO₂ and clay. *Environmental Chemistry* **2017**, *14* (1), 1-8.
203. Lead, J. R.; Wilkinson, K. J., Aquatic Colloids and Nanoparticles: Current Knowledge and Future Trends. *Environmental Chemistry* **2006**, *3* (3), 159-171.
204. Cuss, C. W.; Glover, C. N.; Javed, M. B.; Nagel, A.; Shotyk, W., Geochemical and biological controls on the ecological relevance of total, dissolved, and colloidal forms of trace elements in large boreal rivers: review and case studies. *Environmental Reviews* **2019**, *28* (2), 138-163.
205. Hincapié, I.; Caballero-Guzman, A.; Hiltbrunner, D.; Nowack, B., Use of engineered nanomaterials in the construction industry with specific emphasis on paints and their flows in construction and demolition waste in Switzerland. *Waste Management* **2015**, *43*, 398-406.
206. Hischier, R.; Nowack, B.; Gottschalk, F.; Hincapie, I.; Steinfeldt, M.; Som, C., Life cycle assessment of façade coating systems containing manufactured nanomaterials. *Journal of Nanoparticle Research* **2015**, *17* (2), 68.
207. van Broekhuizen, P.; van Broekhuizen, F.; Cornelissen, R.; Reijnders, L., Use of nanomaterials in the European construction industry and some occupational health aspects thereof. *Journal of Nanoparticle Research* **2011**, *13* (2), 447-462.

208. Clar, J. G.; Platten, W. E.; Baumann, E. J.; Remsen, A.; Harmon, S. M.; Bennett-Stamper, C. L.; Thomas, T. A.; Luxton, T. P., Dermal transfer and environmental release of CeO₂ nanoparticles used as UV inhibitors on outdoor surfaces: Implications for human and environmental health. *Science of The Total Environment* **2018**, *613-614*, 714-723.
209. Kaiser, J.-P.; Roesslein, M.; Diener, L.; Wick, P., Human Health Risk of Ingested Nanoparticles That Are Added as Multifunctional Agents to Paints: an In Vitro Study. *PLOS ONE* **2013**, *8* (12), e83215.
210. Hwang, D. K.; Moon, J. H.; Shul, Y. G.; Jung, K. T.; Kim, D. H.; Lee, D. W., Scratch Resistant and Transparent UV-Protective Coating on Polycarbonate. *Journal of Sol-Gel Science and Technology* **2003**, *26* (1), 783-787.
211. Scifo, L.; Chaurand, P.; Bossa, N.; Avellan, A.; Auffan, M.; Masion, A.; Angeletti, B.; Kieffer, I.; Labille, J.; Bottero, J.-Y.; Rose, J., Non-linear release dynamics for a CeO₂ nanomaterial embedded in a protective wood stain, due to matrix photo-degradation. *Environmental Pollution* **2018**, *241*, 182-193.
212. Tsuzuki, T.; Wang, X., Nanoparticle Coatings for UV Protective Textiles. *Research Journal of Textile and Apparel* **2010**, *14* (2), 9-20.
213. Faure, B.; Salazar-Alvarez, G.; Ahniyaz, A.; Villaluenga, I.; Berriozabal, G.; De Miguel, Y. R.; Bergström, L., Dispersion and surface functionalization of oxide nanoparticles for transparent photocatalytic and UV-protecting coatings and sunscreens. *Science and Technology of Advanced Materials* **2013**, *14* (2), 023001.
214. Auffan, M.; Masion, A.; Labille, J.; Diot, M.-A.; Liu, W.; Olivi, L.; Proux, O.; Ziarelli, F.; Chaurand, P.; Geantet, C.; Bottero, J.-Y.; Rose, J., Long-term aging of a CeO₂ based nanocomposite used for wood protection. *Environmental Pollution* **2014**, *188*, 1-7.
215. Keller, A. A.; Wang, H.; Zhou, D.; Lenihan, H. S.; Cherr, G.; Cardinale, B. J.; Miller, R.; Ji, Z., Stability and Aggregation of Metal Oxide Nanoparticles in Natural Aqueous Matrices. *Environmental Science & Technology* **2010**, *44* (6), 1962-1967.
216. Van Koetsem, F.; Verstraete, S.; Van der Meeren, P.; Du Laing, G., Stability of engineered nanomaterials in complex aqueous matrices: Settling behaviour of CeO₂ nanoparticles in natural surface waters. *Environmental Research* **2015**, *142*, 207-214.
217. Van Hoecke, K.; De Schampelaere, K. A. C.; Van der Meeren, P.; Smagghe, G.; Janssen, C. R., Aggregation and ecotoxicity of CeO₂ nanoparticles in synthetic and natural waters with variable pH, organic matter concentration and ionic strength. *Environmental Pollution* **2011**, *159* (4), 970-976.
218. Montañó, M. D.; Lowry, G. V.; von der Kammer, F.; Blue, J.; Ranville, J. F., Current status and future direction for examining engineered nanoparticles in natural systems. *Environmental Chemistry* **2014**, *11* (4), 351-366.
219. Azimzada, A.; Tufenkji, N.; Wilkinson, K. J., Transformations of silver nanoparticles in wastewater effluents: links to Ag bioavailability. *Environmental Science: Nano* **2017**, *4* (6), 1339-1349.
220. Collin, B.; Tsyusko, O. V.; Starnes, D. L.; Unrine, J. M., Effect of natural organic matter on dissolution and toxicity of sulfidized silver nanoparticles to *Caenorhabditis elegans*. *Environmental Science: Nano* **2016**, *3* (4), 728-736.